




NOS Strategic Petroleum Reserve Support Project: Final Report

Volume Two — Measurements and Data Quality Assurance

March 1981



U.S. DEPARTMENT OF COMMERCE
National Oceanic and Atmospheric Administration
National Ocean Survey



Digitized by the Internet Archive
in 2012 with funding from
LYRASIS Members and Sloan Foundation

<http://archive.org/details/nosstrategicpetr00frey>



NOS Strategic Petroleum Reserve Support Project: Final Report

Volume Two — Measurements and Data Quality Assurance

Edited by:
Henry R. Frey and Gerald F. Appell

Submitted by:
Wesley V. Hull
Associate Director
Office of Oceanography
National Ocean Survey

Submitted to:
Charles A. Burroughs
Program Manager
NOAA Brine Disposal Analysis Program
Environmental Data and Information Service

Supported by:
Interagency Agreement EL-78-I-01-7146
between
National Oceanic and Atmospheric Administration
and
Strategic Petroleum Reserve Office
U.S. Department of Energy
and cooperatively by
NOAA National Ocean Survey

March 1981

U.S. DEPARTMENT OF COMMERCE

Malcolm Baldrige, Secretary

National Oceanic and Atmospheric Administration

James P. Walsh, Acting Administrator

National Ocean Survey

R. Adm. H.R. Lippold, Jr., Director

We dedicate this work to R. L. ("Bob") Charnell and N. P. ("Pat") Laird, NOAA oceanographers of the Pacific Marine Environmental Laboratory, who were lost at sea off Hawaii during December 1978.

This publication is issued by the National Ocean Survey (NOS) to acquaint readers with the results of scientific and engineering tasks carried out during the NOS Strategic Petroleum Reserve Support Project. This publication does not constitute an endorsement of any commercial product or intend to be an opinion beyond scientific or engineering results obtained by the National Ocean Survey. Moreover, the fact that all instruments of any one class were not selected for use in the described project is not a reflection on the quality of the instruments not selected.

No reference shall be made to the National Ocean Survey, or to this publication furnished by the National Ocean Survey, in any advertising or sales promotion which would indicate or imply that the National Ocean Survey recommends or endorses any proprietary product mentioned herein, or which has as its purpose an interest to cause directly or indirectly the advertised product to be used or purchased because of this National Ocean Survey publication.

CONTENTS

Figures	iv
Tables	vii
Abbreviations used	viii
Authors' affiliations	x
1. Summary	1
2. Introduction	9
3. Measurement systems	17
4. Current meter evaluation	31
5. Instrument inspection and acceptance tests and calibrations	53
6. Field data quality control	71
7. Uncertainty estimates	77
8. Gulf at-sea performance experiment	125
9. Current measurement uncertainty analysis	141
10. Data processing and validation	169
Acknowledgments	181
References	183
Appendixes	
A. Supplemental data for current meter evaluation	A-1
B. Instrument transfer functions	B-1
C. A model of Grundy 9021 speed and direction errors for horizontal dynamics	C-1

FIGURES

1.	The West Hackberry and Weeks Island proposed brine disposal sites and three intermediate trackline CTD/DO stations	2
2.	Grundy 9021 current meters on a subsurface platform being deployed by the NOAA Ship FERREL	4
3.	Measurement configuration	13
4.	Meteorological measurement system at station 28	21
5.	Water level gage on subsurface platform	23
6.	Wave gage on subsurface platform	24
7.	Platform/mooring system	27
8.	Photo control platform	29
9.	J-mooring	30
10.	David Taylor-Naval Ship Research and Development Center (DT-NSRDC) Number 1 Tow Carriage	32
11.	Photodiode sensor externally mounted to obtain rotor speed from rotor blade passings	33
12.	SN52 rotor calibration data	33
13.	Residual errors of SN52 rotor calibration data using equation 1	35
14.	Residual errors of SN03 rotor calibration data using equation 1	35
15.	Residual errors of SN52 rotor calibration data using equation 2	36
16.	Residual errors of SN52 rotor calibration data fitted to T&EL first-order equation 3	36
17.	Residual errors of SN52 rotor calibration data fitted to T&EL second-order equation	38
18.	Horizontal directivity response of SN52 rotor at 11 cm/s	39
19.	Horizontal directivity response of SN52 rotor at 21 cm/s	40
20.	T&EL submerged jet facility	41
21.	Compass calibration setup	45

FIGURES--Continued

22.	Residual errors of SN51 compass calibration data using equation 6	46
23.	Vertical planar motion mechanism (VPMM)	47
24.	Residual errors of SN24 temperature calibration data using equation 7	50
25.	Residual errors of SN24 conductivity calibration data using equation 8	50
26.	Error distributions from initial calibrations of 36 Grundy 9021 current meters	56
27.	Error distributions from recalibration of 21 Grundy 9021 current meters	58
28.	Residual error of Grundy Model 9400 conductivity sensor based on T&EL transfer function	66
29.	Residual error of Grundy Model 9400 temperature sensor based on T&EL transfer function	67
30.	Residual error of Grundy Model 9400 depth sensor based on T&EL transfer function	68
31.	Field check system onboard the NOAA Ship FERREL	72
32.	Graphic description of Sensor Measurement Uncertainty (SMU)	85
33.	GASP Experiment configuration	127
34.	NBIS acoustic current meter and platform used in GASP Experiment	128
35.	Wind speed and direction, oscillating current speed, and wave height during the first 20 days of GASP Experiment	132
36.	Currents measured at 3-m level with a Grundy Model 9021 current meter during the GASP Experiment	133
37.	Sixty consecutive 1-s velocity samples illustrate typical 1-hr burst-mode data obtained with NBIS (732) instrument at 3-m level	133
38.	Flow signal-to-noise (S/N) ratio for the first 20 days of the GASP Experiment	134
39.	East-north scatter plots of 1-hr flow vectors for nine current meters during the GASP Experiment	136/ 137

FIGURES--Continued

40.	Progressive vector diagrams of currents during GASP Experiment	138
41.	Scatter diagrams of 1-hr vector averaged speeds for instrument pairs at the 3-m level	139
42.	GASP Experiment data plotted as 20-day vector- averaged speeds and directions	140
43.	Laboratory rod blockage data	149
44.	Laboratory versus predicted values of current meter direction variation	154
45.	Platform blockage under steady and dynamic flow conditions	158
46.	Fouling speed decrease versus time for three fouling levels	160
47.	Sample speed and direction difference plots from GASP Experiment	165
48.	Speed and direction TMU's.	168
A-1.	Block diagram of instrumentation used for rotor evaluation	A-2
A-2.	Data collection flow chart for regression analysis of rotor calibration data	A-4
A-3.	Block diagram of instrumentation used for system thrupt verification	A-8
A-4.	Data collection flow chart for speed system thrupt verification	A-9
A-5.	Block diagram of instrumentation used in the dynamics evaluation	A-16
A-6.	Data collection flow chart for dynamics test	A-19

TABLES

1.	Summary of total measurement uncertainties (TMU)	7
2.	Total measurement uncertainties (TMU) for current speed and direction	8
3.	Measurement station positions	14
4.	Alinement accuracy data	42
5.	Distance constant data	43
6.	Data quality levels	74
7.	Laboratory standards	78
8.	Speed measurement uncertainty for NBIS, MMI, and Grundy current meters during the GASP Experiment	129
9.	Direction measurement uncertainty for NBIS, MMI, and Grundy current meters during the GASP Experiment	129
10.	Statistical summary of current meter observations during the first 20 days of the GASP Experiment	130
11.	G, α , and β for the range of laboratory speeds V_o and oscillation periods $T = 1/f$	152
12.	Comparison of predicted and laboratory measured speed errors	153
13.	Speed and direction errors due to pitch and yaw misalignment	163
14.	Predicted speed and direction errors during the GASP Experiment	164
15.	Speed and direction error summary	167
A-1.	Instrumentation used in the current meter evaluation	A-1
A-2.	Rotor calibration data	A-3
A-3.	Regression analysis of rotor calibration data	A-5
A-4.	Horizontal cosine response of SN52 rotor	A-7
A-5.	Compass calibration data	A-10
A-6.	Conductivity/temperature tests with SN24	A-13
A-7.	Dynamics test data	A-17

ABBREVIATIONS USED

ASCII	American standard code for information interchange
AMI	Applied Microsystems, Incorporated
BCD	Binary coded decimal
BPI	Bits per inch (magnetic tape packing density)
CCIW	Canada Centre for Inland Waters
CEAS	Center for Environmental Assessment Services (NOAA)*
Cl	Chlorinity
CL	Confidence level
CM	Current meter
CTD	Conductivity - temperature - depth
DO	Dissolved oxygen
DOE	Department of Energy
DQA	Data quality assurance
DQL	Data quality level
DT-NSRDC	David Taylor - Naval Ship Research and Development Center
ECU	Estimated Calibration Uncertainty
EDL	Engineering Development Laboratory (NOAA)*
FM	Frequency modulation
FSR	Full scale reading
GASP	Gulf At-Sea Performance (Experiment)
GCLW	Gulf Coast Low Water
HP	Hewlett - Packard
I&A	Inspection and acceptance
IAPSO	International Association of Physical Sciences of the Ocean
IC	Integrated circuit
ID	Identification
I/O	Input/output
LED	Light emitting diode
LSD	Least significant digit

NOAA organizations as of March 1, 1980

MMI	Marsh - McBirney, Incorporated
MSD	Most significant digit
N/A	Not applicable
NAVOCEANO	U.S. Naval Oceanographic Office
NBS	National Bureau of Standards
NBIS	Neil Brown Instrument Systems, Incorporated
NMFS	National Marine Fisheries Service (NOAA)*
NOAA	National Oceanic and Atmospheric Administration
NODC	National Oceanographic Data Center (NOAA)*
NOS	National Ocean Survey (NOAA)*
NSTL	National Space Technology Laboratories
NSWC	U.S. Naval Surface Weapons Center
OMT	Office of Marine Technology (NOAA)*
OOE	Office of Ocean Engineering (NOAA)*
OSI	Optimum Systems, Incorporated
PMEL	Pacific Marine Environmental Laboratory (NOAA)*
ppm	Parts per million
ppt	Parts per thousand
PVC	Polyvinyl chloride
RL	Rejection level
RMS	Root-mean-square
ROM	Read only memory
RSE	Residual Standard Error
SMU	Sensor Measurement Uncertainty
SN	Serial number
S/N	Signal to noise
SPR	Strategic Petroleum Reserve
T&EL	Test and Evaluation Laboratory (NOAA)*
TMU	Total Measurement Uncertainty
TSU	Total Systematic Uncertainty
UNESCO	United Nations Educational, Scientific, and Cultural Organization
VPMM	Vertical planar motion mechanism
YSI	Yellow Springs Instruments Company

AUTHORS' AFFILIATIONS

NOS Office of Oceanography

Marine Environmental Services Division

Rockville, Maryland

Henry R. Frey, NOS Project Manager and Principal Investigator

Michael W. Szabados, NOS Project Oceanographer

NOS Office of Marine Technology

Test and Evaluation Laboratory

Washington, D.C.

Gerald F. Appell, OMT Project Integrator and DQA Manager

Michael A. Basileo

Philip J. Bowen

David R. Crump

Algis N. Kalvaitis

Thomas N. Mero

NOS Office of Marine Technology

Engineering Development Laboratory

Riverdale, Maryland

Charles M. Roman*

Bobby J. Taylor

Woods Hole Oceanographic Institution

Woods Hole, Massachusetts

James R. McCullough

MAR, Incorporated

Rockville, Maryland

Stephen H. Koeppen

* currently with Applied Technology Group, NOS Office of Oceanography

1. SUMMARY

by Henry R. Frey and Gerald F. Appell

The Department of Energy (DOE), which is implementing the Strategic Petroleum Reserve (SPR), is storing crude oil in underground salt domes beneath Louisiana and Texas. Because the present capacity of existing caverns in the salt domes is insufficient for large volumes of oil, additional salt must be dissolved to form expanded storage; the leachate must then be piped into the Gulf of Mexico. This brine solution may be potentially hazardous to the area's shrimp and demersal fish. At DOE's request, the National Ocean Survey (NOS) collected 12 months of oceanographic and meteorological data to develop physical oceanographic characterizations of the sites, particularly those properties that govern the advection and diffusion of salt brine discharges.

These data were collected at two proposed brine disposal sites on the Louisiana inner continental shelf from June 1978 to June 1979. The Environmental Data and Information Service (EDIS), which is managing NOAA's Brine Disposal Analysis Program being conducted for DOE, will synthesize the information from NOS and also the chemical and biological studies of the area by NOAA's National Marine Fisheries Service.

Since DOE needed information as soon as possible, the field work schedule was accelerated. The NOS SPR Support Project Manager designed the field experiment and set the scientific requirements. NOS assessed the instrument technology, selected the instruments, and evaluated the Grundy Model 9021 current meter. Inspection and acceptance tests, calibrations, development of quality control hardware and procedures, and training of personnel were also carried out.

1.1. MEASUREMENTS

The NOAA Ship FERREL, based at the NOS Atlantic Marine Center, conducted 18 cruises for the NOS SPR Support Project. While the

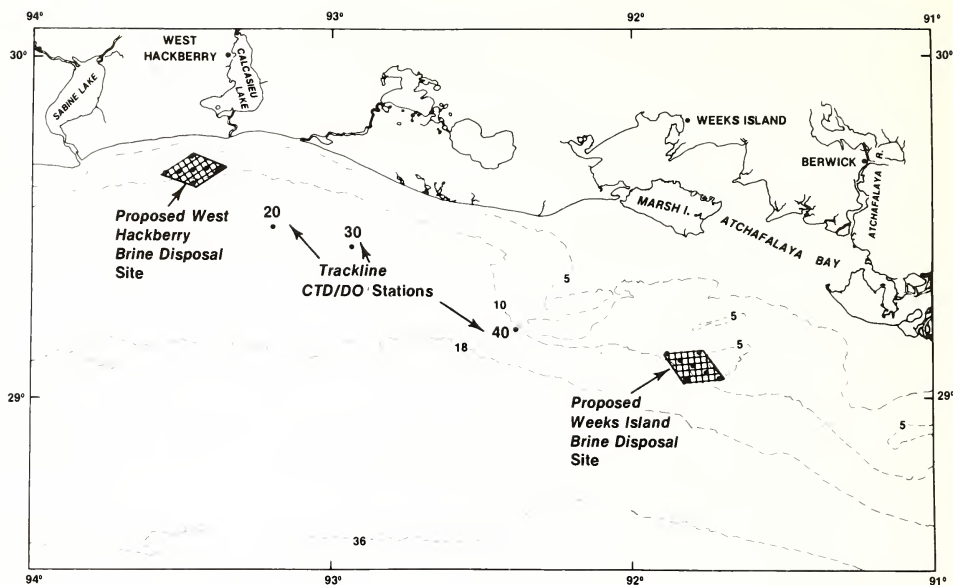


Figure 1.--The West Hackberry and Weeks Island proposed brine disposal sites and three intermediate trackline CTD/DO stations.

FERREL was in port for routine maintenance during December 1978 and January 1979, the NOAA Research Vessel VIRGINIA KEY conducted two cruises for the project. The NOAA Ship MT. MITCHELL made hydrographic surveys of both sites as an adjunct task.

Time-series oceanographic measurements obtained at the proposed West Hackberry and Weeks Island brine disposal sites (figure 1) included current speed and direction, water temperature and conductivity, wave heights, and water levels. Measurements of currents, conductivity, and temperature were made 1 m and 3 m above the sea floor. These measurements were made also at 2 m and 4 m for a more detailed vertical profile of the currents in February at the Weeks Island site and in April at the West Hackberry site. Time-series meteorological measurements of wind speed and direction, air temperature, and barometric pressure were obtained at offshore oil production platforms.

Conductivity-temperature-depth (CTD) profiles and water samples were obtained monthly. The water samples were analyzed for salinity and dissolved oxygen. During October 1978, sea surface currents were observed at the West Hackberry site by using aerial photography to track aluminum powder patches. During April and May 1979, a 32-day experiment--the Gulf At-Sea Performance (GASP) Experiment--was conducted at the West Hackberry site. The main objective of this experiment was to obtain the field data needed to correlate the response of the Grundy Model 9021 current meter with laboratory tests and with an error prediction model.

Rather than use compliant moorings, subsurface platforms were designed to assure a constant vertical separation of 2 m between the current meters, minimize contamination of the current data by wave dynamics, and provide rigid mounting for the wave and water level gages. Figure 2 shows a platform equipped with two Grundy current meters being deployed.

The following instruments were used in the project:

- Grundy Model 9021 current meters measured current speed and direction, water temperature, and conductivity. They also had an acoustic link.
- Aanderaa meteorological stations measured wind speed and direction, barometric pressure, and air temperature.
- Aanderaa Model WLR-5 water level recorders measured differential water levels.
- Applied Microsystems, Inc., Model 750A wave gages measured wave heights.
- A micro-Winkler dissolved oxygen apparatus was installed in the FERREL's wet lab. Just before the project started, NOS obtained a Grundy Model 9400 CTD system and a Guildline Model 8400 Autosol salinometer for its ongoing programs; these instruments satisfied the CTD and water sample salinity requirements.

1.2. DATA QUALITY ASSURANCE

The application of data quality assurance (DQA) principles and the quality of oceanographic measurements were high priorities during the NOS Strategic Petroleum Reserve Support Project. An extensive DQA program was designed to determine the performance of each

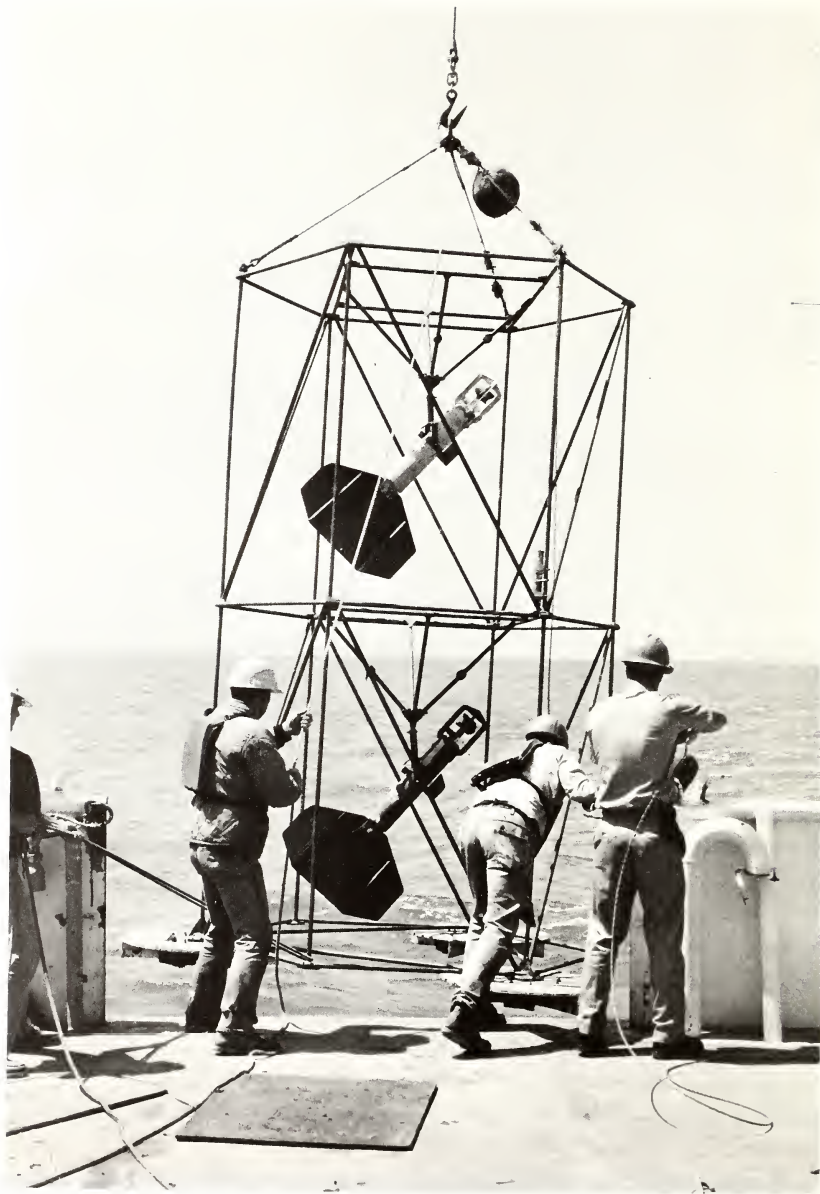


Figure 2.--Grundy 9021 current meters on a subsurface platform being deployed by the NOAA Ship FERREL.

instrument, assure continued performance during the survey, investigate system and environmental contamination, develop total measurement uncertainties, and maximize the usefulness of the oceanographic data.

An evaluation of the Grundy Model 9021 current meter was particularly emphasized to provide the performance information needed to define the accuracy of the time-series data set. NOS Test and Evaluation Laboratory (T&EL) engineers conducted current velocity tests at the David Taylor Naval Ship Research and Development Center (DT-NSRDC) tow tank facility at Carderock, Md. The performance tests included steady flow and dynamic response (using an oscillating mechanical driver to simulate wave-induced water motions). T&EL evaluated the water temperature and conductivity sensors and performed time base and environmental tests. The acoustic data link was evaluated at the Naval Surface Weapons Facility, White Oak, Md., in the Anacostia River, and at one of the survey sites. Evaluation of the current meter disclosed performance that caused all measurement uncertainties (current speed and direction, water temperature, and conductivity) to be larger than those specified by the manufacturer and those required for the survey. The design and assembly of the current meter needed to be improved to meet survey requirements.

Speed detection circuit reed switches bounced on initial instruments received by NOS and produced spurious counts. Attention to quality control and the addition of capacitors in the speed circuit solved the problem. The original compass malfunctioned when the combined pitch and roll exceeded 5 degrees. The manufacturer solved this problem by mounting the compasses in a gimbal assembly within a larger housing, but the assembly was found to need further redesign to meet specification. Because the thermistors used initially to sense temperature had a drift of 0.1°C over several hours, they were replaced with platinum resistance thermometers (by the manufacturer at no additional cost) to obtain the required accuracy. The conductivity circuitry exhibited temperature effects that exceeded specifications; this problem was solved by adding temperature compensating circuitry. T&EL developed the transfer function (calibration equation) used for processing speed data because the manufacturer's transfer function did not provide the required accuracy.

Instrument inspection and acceptance (I&A) tests and calibration procedures were developed for 36 current meters, 5 meteorological stations, 3 water level gages, 3 wave gages, and the CTD system, and also on the instrument quality control sensors (a Paroscientific Model 2100A pressure sensor, a Yellow Springs Instruments laboratory thermometer, and a Hewlett-Packard Model 5328 counter). These I&A tests revealed numerous deficiencies with most of the instrumentation that required adjustment, replacement of parts, or development of individual calibration equations. The survey would have been affected adversely by instrumentation problems without the benefit of these tests. Sensors that survived the 12-month field effort were recalibrated; interim calibrations were also performed on selected instruments.

Instrument quality control hardware and procedures were developed for shipboard use to detect malfunctions, provide quantitative operational guidance, and record a history of performance during the 12-month survey. A set of data quality levels was assigned to the various measurements; if the instruments' outputs remained within the data quality level, the instrument was deployed. A set of data rejection levels was also assigned to the various measurements; if the instruments' outputs exceeded these levels, they were not deployed until corrective maintenance (and recalibration, if necessary) was performed. Quality control measures could not always be performed in the field. Because of a shortage of current meters due to Tropical Storm DEBRA, post-deployment field checks were difficult to make, and the number of stations in the survey had to be reduced. Current speed and water conductivity measurement uncertainties increased because of severe marine fouling during the spring and summer.

A major concern was the relevance of laboratory test results of current velocity error sources to the actual field conditions. The GASP Experiment was performed to provide the independent field data necessary to correlate with tow tank tests and an error prediction model. Fortunately, the range of winds and currents observed during the 12-month survey was also encountered during the 32-day GASP Experiment.

All measurements can be traced to laboratory standards. Error sources were identified and analyzed to develop uncertainty statements. A Total Measurement Uncertainty (TMU) was computed for each

measurand. The TMU includes an Estimated Calibration Uncertainty (ECU), Sensor Measurement Uncertainty (SMU), and environmental error sources. A summary of representative TMU's is given in table 1. The qualifications described in section 7 of this report should be con-

Table 1. Summary of Total Measurement Uncertainties (TMU)

<u>Instrument/Parameter</u>	
Grundy Model 9021 Current Meter	
Temperature	$\pm 0.28^{\circ} \text{ C}$
Conductivity	$\pm 0.24 \text{ mS/cm}$
Time base	$\pm 66 \text{ s/month}$
Aanderaa Meteorological Station	
Wind speed at 5 m/s	$+ 1.1, - 1.6 \text{ m/s}$
Wind direction	$\pm 16 \text{ degrees}$
Air temperature	$+ 0.83, - 0.43^{\circ} \text{ C}$
Air pressure	$+ 0.5, - 8.2 \text{ mbar}$
Applied Microsystems Model 750A Wave Gage	
Pressure	$\pm 0.029 \text{ dbar}$
Aanderaa Model WLR-5 Water Level Gage	
Pressure (SN 360)	$+ 0.083, - 0.048 \text{ dbar}$
Differential water level (SN 360)	$+ 0.13, - 0.14 \text{ m}$
Grundy Model 9400 CTD System	
Temperature (1/78-12/78)	$+ 0.20, - 0.04^{\circ} \text{ C}$
Conductivity	$+ 0.06, - 0.36 \text{ mS/cm}$
Pressure	$+ 1.10, - 0.85 \text{ dbar}$
Guildline Model 8400 Autosol	
Salinity	$+ 0.023, - 0.005 \text{ ppt}$
Micro-Winkler Titration Apparatus	
Dissolved oxygen	$\pm 0.03 \text{ ml/l}$
Beckman RS-5 Salinometer	
Temperature	$\pm 0.83^{\circ} \text{ C}$
Conductivity	$\pm 0.90 \text{ mS/cm}$
Salinity	$\pm 1.56 \text{ ppt}$

considered before using the TMU's, which, for each measurement, are intended to bound errors for 95 percent of the "typical" field measurements.

Special emphasis was placed on developing current measurement uncertainties (table 2). Sources of current measurement errors include the calibration uncertainties and environmentally induced effects such as flow blockage by platform members, fouling of rotors, misalignment of current meters with the flow direction, and dynamic current (principally wave) effects. MAR, Inc., provided the current measurement uncertainty analysis using data from laboratory evaluations, the GASP Experiment, and 12 months of field effort. A mathematical model of the dynamic errors was developed and tested via GASP Experiment and laboratory data. A complete discussion of the current measurement uncertainties is presented in section 9 and appendix C.

The quality of data acquired during this 12-month survey is represented in the TMU's and is traceable to accepted standards by the methodology and procedures described in this report.

Current meter, meteorological station, water level gage, wave gage, CTD, and water sample (salinity and dissolved oxygen) data have been processed, validated, and archived at the National Oceanographic Data Center (NODC). Instructions for obtaining the project data from NODC are described in section 10. Analysis and interpretation of the data are presented in volume one of this report, Oceanography on the Louisiana Inner Continental Shelf (Frey et al. 1981).

Table 2. Grundy Model 9021 Total Measurement Uncertainties (TMU)
for current speed and direction

Grundy 9021

Speed TMU	at 5 cm/s:	+2.1, -3.0 cm/s
	at 40 cm/s:	+0.7, -6.3 cm/s
Speed TMU	at 5 cm/s:	+2.0, -3.3 cm/s
(during fouling season)	at 40 cm/s:	+0.0, -8.3 cm/s
Direction TMU	at 5 cm/s:	\pm 13.9 degrees
	at 10-40 cm/s:	\pm 10.0 degrees

2. INTRODUCTION

by Henry R. Frey and Gerald F. Appell

This volume of the final report on the National Ocean Survey (NOS) Strategic Petroleum Reserve (SPR) Support Project describes the measurements and quality of physical oceanographic and related meteorological data collected during the project, including statements of total measurement uncertainties and the availability of data. The analysis and interpretation of the oceanographic data are given in NOS Strategic Petroleum Reserve Support Project: Final Report--Volume One, Oceanography on the Louisiana Inner Continental Shelf (Frey et al. 1981). The results do not purport to represent baseline conditions of the area, but rather characterize the important physical oceanographic features which will affect brine discharges.

2.1. STRATEGIC PETROLEUM RESERVE

The Department of Energy (DOE) is implementing the Strategic Petroleum Reserve by storing crude oil in underground salt domes beneath Texas and Louisiana, near the Gulf Coast. Since the present capacity of existing caverns in the salt domes is insufficient for large volumes of oil, additional salt must be dissolved and the resulting brine solution dispensed by a pipeline into the Gulf of Mexico. The diffusion of the brine solution into the receiving waters of the inner continental shelf may pose a potential hazard to the area's shrimp and demersal fish population. The National Environmental Policy Act of 1969 and subsequent Federal legislation require that the likelihood of environmental damage be assessed and that the extent of possible damage be documented before the planned action is permitted. DOE is directing the Strategic Petroleum Reserve under the National Energy Policy and Conservation Act of 1975.

2.2. NOS SPR SUPPORT PROJECT

As part of the Brine Disposal Analysis Program conducted for DOE and managed by the NOAA Environmental Data and Information Service

(EDIS), NOS collected oceanographic and related meteorological data to obtain characterizations of two proposed brine disposal sites off Louisiana from June 1978 to June 1979. To determine instrument performance and to develop total measurement uncertainties, NOS designed a strategy for assuring data quality that advanced the state-of-the-art.

The NOS SPR Support Project was a cooperative, reimbursable project carried out in collaboration with EDIS under an interagency agreement with DOE. In response to requests from EDIS and DOE, preliminary planning for the NOS SPR Support Project began in August 1977, and the project itself began on November 15, 1977, by an amendment to the agreement between NOAA and DOE. Although the NOS Office of Marine Surveys and Maps was responsible for the project initially, responsibility was transferred to the NOS Office of Oceanography during a reorganization in January 1979. The NOS Office of Marine Technology (OMT) provided engineering and technological support through the OMT Test and Evaluation Laboratory (T&EL) and Engineering Development Laboratory (EDL). As an adjunct cooperative task, the Office of Marine Surveys and Maps provided hydrographic surveys of the two proposed disposal sites conducted by the NOAA Ship MT. MITCHELL. The Circulatory Surveys Branch of the Marine Environmental Services Division processed and analyzed most of the oceanographic and meteorological data. NOS contracted Optimum Systems, Inc., (OSI) of Rockville, Md., to assist in developing software and in processing the data.

The Southeast Fisheries Center at Galveston, Tex., a component of the NOAA National Marine Fisheries Service (NMFS), has completed a companion study to characterize the chemical and biological features of the two sites. EDIS will synthesize the physical, chemical, and biological data collected by NOS and NMFS into environmental assessments of brine disposal. These environmental assessments will then be used by DOE and EPA as decision making documents in assessing the likelihood and extent of possible environmental damage.

2.3. EXPERIMENTAL DESIGN

The field experiment for oceanographic and meteorological observations was designed by the NOS SPR Support Project Manager and

carried out by the Commanding Officer of the NOAA Ship FERREL, which is based at the NOS Atlantic Marine Center. The FERREL conducted 18 cruises during the 12 months of field work. While the FERREL was in port for routine maintenance from December 1978 to January 1979, the NOAA Atlantic Oceanographic and Meteorological Laboratory made available the NOAA Research Vessel VIRGINIA KEY for two cruises, which the NOS Project Manager supervised.

The proposed brine disposal sites, known as West Hackberry and Weeks Island after the inland locations of the salt domes (figure 1), are about 185 km apart. The proposed locations for the pipeline diffusers are 29°40.00' N, 93°28.00' W for the West Hackberry site and 29°05.70' N, 91°47.60' W, for the Weeks Island site. The West Hackberry site is approximately 11 km south of Holly Beach, La., between the Sabine Pass and the Calcasieu Pass. The Weeks Island site is about 42 km due south of Marsh Island and 93 km southwest of Berwick, La., the staging point for the NOS field study. The two sites differ significantly in bottom type: sediments at the West Hackberry site consist of silt and clay with less than 40 percent sand, while the sediments at the Weeks Island site consist of more than 70 percent sand. The center of the West Hackberry site is 9.1 m deep at Gulf Coast Low Water (GCLW), and the center of the Weeks Island site is 7.6 m deep at GCLW.

The experimental design was based on preliminary information which indicated that (1) meteorological data at each site were needed to help analyze and interpret the oceanographic data; (2) over the same relative distance, alongshore events in the currents would be more coherent than events occurring in the transshore* direction; (3) current meter data might be significantly contaminated by waves and swell on the shallow Louisiana shelf; (4) the locations of the diffuser sites might be subject to change; and (5) *in situ* equipment would be particularly subject to damage or loss because of commercial fishing, crew boat and supply ship traffic, other vessel activities, and storms.

*Transshore is defined in this report as meaning normal to the shore.

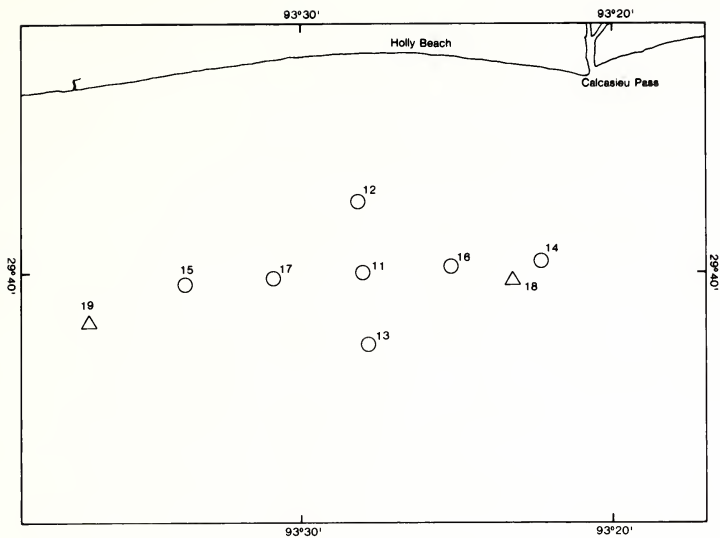
The geometry of the instrument arrays at the two sites was nearly identical except for the relative positions of the meteorological instruments, which were mounted on existing oil production platforms. The arrays are shown in figure 3, and the station positions are listed in table 3. An alongshore section, parallel to the local isobaths, extended 9.3 km to each side of the center station, while a transhore section extended 3.7 km shoreward and 3.7 km offshore of the center station.

Subsurface platforms, designed specifically for the project by EDL, were situated at the center of the array and at the extreme alongshore and transhore stations. The subsurface platforms were equipped with two current meters positioned 1 m and 3 m above the bottom. The current meters had sensors that recorded temperature and conductivity, as well as current speed and direction. Each center subsurface platform was equipped also with a water level gage and a wave gage. Meteorological instruments, which recorded wind speed and direction, barometric pressure, and air temperature, were mounted on oil production platforms (designated in figure 3 by the symbol Δ) that were within 5.2 km of the extreme alongshore stations.

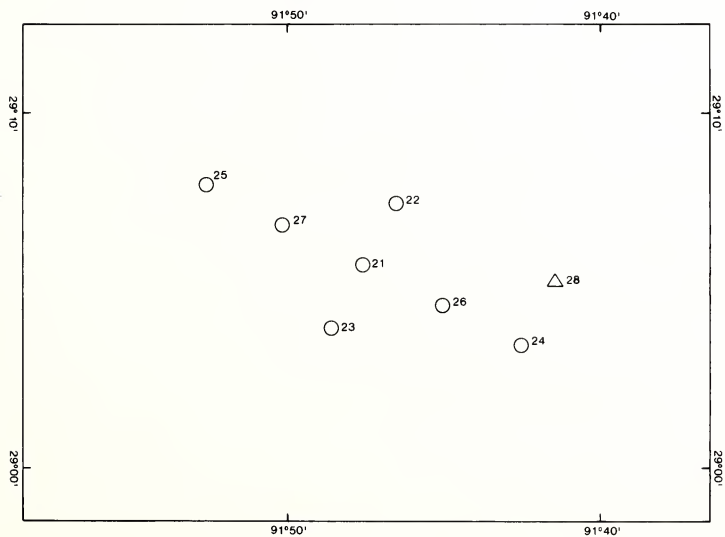
In addition to the data collected from the *in situ* time-series recording instruments, conductivity-temperature-depth/dissolved oxygen (CTD/DO) data were collected approximately once a month at the five subsurface platform positions and at two stations halfway between the center and the extreme alongshore stations. The CTD data were obtained with a profiling instrument; DO data were obtained from water samples collected 1 m below the surface, at midwater, and 1 m above the bottom. These water samples were also analyzed for salinity onboard the FERREL, and the results were compared with those from the CTD instrument. In addition to the data collected within each site, the FERREL collected data at three stations along the trackline between the two sites. CTD profiles were obtained monthly together with DO samples 1 m below the surface and 1 m above the bottom at the trackline stations.

2.4. INSTRUMENT DATA QUALITY ASSURANCE STRATEGY

An instrument data quality assurance (DQA) strategy was implemented to enable NOS to provide Total Measurement Uncertainties (TMU's) for the NOS SPR Support Project data. The DQA was essential



A. West Hackberry Site



B. Weeks Island Site

Figure 3.--Measurement configuration.

Table 3. Measurement station positions

Station	Relative position	North latitude	West longitude	Depth (GCLW) (m)
West Hackberry station positions				
11	Center	29°40.00'	93°28.00'	9.8
12	North	29°41.99'	93°28.14'	7.9
13	South	29°38.00'	93°27.86'	11.0
14	East	29°40.33'	93°22.29'	9.4
15	West	29°39.65'	93°33.70'	9.8
16	E. intermediate	29°40.18'	93°25.19'	9.4
17	W. intermediate	29°39.79'	93°30.99'	9.8
18	E. meteorological	29°39.79'	93°23.20'	-19.5*
19	W. meteorological	29°38.62'	93°36.74'	-15.8*
Weeks Island station positions				
21	Center	29°05.70'	91°47.60'	7.9
22	North	29°07.49'	91°46.55'	5.8
23	South	29°03.94'	91°48.63'	11.0
24	East	29°03.43'	91°42.56'	7.0
25	West	29°07.95'	91°52.61'	8.2
26	E. intermediate	29°04.56'	91°45.06'	7.0
27	W. intermediate	29°06.82'	91°50.12'	8.2
28	E. meteorological	29°05.26'	91°41.43'	-14.0*
Trackline station positions				
20		29°30.00'	93°11.70'	11.9
30		29°26.40'	92°56.26'	14.6
40		29°12.20'	92°22.93'	11.0

*Height above sea surface at GCLW.

so that the data could be defended in licensing hearings and to assure that the data set is as useful as possible for analysis by NOS and the oceanographic community. T&EL not only possessed the necessary expertise but also could act as an independent auditor of instrument performance. EDL provided field quality control equipment and procedures, integrated logistics support, and training for the ship's personnel.

The overall strategy for DQA involved

1. determining the accuracy requirements, sampling intervals, averaging periods, spatial resolution, and other measurement requirements;

2. matching these measurement requirements with instrument technology and selecting instruments for the project;

3. evaluating the current meters in detail;
4. calibrating the sensors before, during, and after the project;
5. selecting acceptance and rejection levels for each instrument for quality control in the field;
6. providing the FERREL with equipment and procedures to make field checks;
7. determining the training needed for new measurement systems onboard the FERREL;
8. analyzing the field check data once a month and recommending ways to maintain data quality; and
9. developing TMU's for all measurands.

Owing to the magnitude and complexity of the field work, the NOS Project Manager assigned highest priority to the DQA strategy associated with the measurement of current speed and direction. More than half of the experiment resulted in time-series data for current speed and direction and water temperature. All other measurands were considered of equal priority.

2.5. DATA PROCESSING QUALITY ASSURANCE STRATEGY

NOS headquarters in Rockville, Md., received the data obtained during the NOS SPR Support Project in various forms, including

1. 9-track tapes of current meter, meteorological station, and water level gage data translated from binary to decimal form on the FERREL;
2. 9-track tapes of wave gage data translated from binary to decimal form by Applied Microsystems, Inc.;
3. 9-track tapes of continuous CTD profile data recorded in frequencies through a digital data logger on the FERREL;
4. water chemistry log sheets indicating surface temperature, salinity, and DO values determined onboard the FERREL from water samples;
5. log sheets of discrete-depth CTD values determined with a Beckman RS-5 salinometer onboard the VIRGINIA KEY during the FERREL's winter in port;
6. log sheets of discrete-depth CTD values determined with the FERREL's CTD profiler by recording output frequencies when the data logger was inoperative;

7. copies of the FERREL's Deck Log and Daily Weather Log for days when the ship was offshore;
8. deployment and recovery logs and file header information; and
9. cruise reports from the Commanding Officer to the NOS Project Manager.

All time-series records were converted to engineering units by using calibration equations, and the parameters were examined for consistency. Data files were checked for the absence of data or the loss of data caused by glitches, bit drops, parity errors, and record-length transcribing errors. The records were then checked for time errors using instrument start/stop and deployment/recovery times; time-series records that contained timing errors were omitted from the analyses, except when noted. Header information was examined and corrected, when necessary, by examining all pertinent supporting data.

All data log sheets were scrutinized for computational errors after values were determined to be consistent. If the log sheets indicated times that were not consistent with the ship's Deck Log, other supporting documentation was examined. Salinity values from the recording CTD profiler were compared with those from water sample analysis.

3. MEASUREMENT SYSTEMS

by Henry R. Frey, Gerald F. Appell, and Bobby J. Taylor

The design of the field measurement effort was described in section 2.3; this section describes the measurement systems used to carry out the experimental design.

The current measurement system in use by the NOAA Ship FERREL prior to the NOS SPR Support Project was designed principally to measure tidal currents in protected estuaries and was inadequate to measure currents on the exposed continental shelf where waves and swell can cause severe contamination of current meter data. A new current measurement system that would satisfy project requirements was procured and made ready for operation. Meteorological stations, wave gages, and water level gages were also procured. A recently acquired CTD system and a precision laboratory salinometer, part of ship's scientific equipment for estuarine surveys, were installed. The FERREL's wet laboratory was refurbished, and a micro-Winkler dissolved oxygen measurement system was installed. Hardware and procedures were developed to check and verify all project measurement sensors onboard the ship.

It was necessary to take special precautions to minimize the contamination of the current meter data by waves and swell because the stations were relatively shallow with depths from 5.8 to 11.0 m; this problem was addressed in part by using rigid subsurface instrument platforms which could be deployed and recovered by the FERREL. It was hypothesized that the subsurface platforms would produce less noise than compliant moorings in the current meter signals. Conventional J-moorings were used as a backup measure during the winter months. Recording meteorological stations were mounted on oil production platforms at the peripheries of the sites.

3.1. GRUNDY MODEL 9021G CURRENT METERS

At the time of selection, the Plessey Model 9021G Current Meter was the only instrument available in sufficient numbers that

would satisfy project requirements; 30 were required initially, and 6 more were procured during the field phase of the project. (The Plessey Environmental Systems Company was acquired by Grundy Limited during February 1979, and its name was changed to Grundy Environmental Systems Company.) The Grundy Model 9021G Current Meter measures and records current speed and direction, temperature, and conductivity and is equipped with an acoustic link for data transmission through the water. The standard instrument is rated to 2,000-m depth.

The Grundy meters sense speed with a Roberts-type rotor, direction with a gimbaled magnetic compass, temperature with a platinum resistance thermometer, and conductivity with an inductive transformer. Measurements were made at preselected intervals and were recorded serially on 6.4-mm magnetic tape with a reel-to-reel system in 10-bit binary code. Timing was controlled by a continuously operating crystal oscillator. The circuitry and the recording system were powered by rechargeable batteries. Acoustic telemetry was used principally to check the operation of current meters after deployment and, occasionally, to observe real-time data. The data sampling interval was initially selected at 5 min. During October 1979, the interval was changed to 10 min after it was determined, by examining scatter in the direction data, that the increased interval would not affect data quality.

Current speed is measured by counting the pulses caused by magnets imbedded in the rotor as the magnets pass reed switches. The reed switch pulses are accumulated over the sampling interval; thus, the current speed is averaged over the sampling interval. Reverse flows, which cause the rotor to reverse rotation, result in counts being subtracted from the cumulative count during the sampling interval. However, because the forward flow response of the rotor is greater than the reverse flow response, the instrument's ability to cancel out wave dynamics is imperfect.

Current direction is not averaged but is recorded instantaneously at the end of the sampling interval. A relatively large vane is affixed to the current meter housing to provide alignment torque. (The instrument is suspended from a swivel mounting assembly.) The usual method of deployment for the Grundy current

meter is attachment to an asymmetrical A-frame supported by a mooring line; in this mode of operation, the frame provides additional alinement torque. In the application reported here, the current meters were suspended from mounting points on subsurface platforms, without the typical A-frame support.

Measurements of water temperature and conductivity obtained concurrently with current speed and direction measurements add important additional information about the circulation features which govern the advection and dispersion of brine discharges. The temperature and conductivity data make it possible to infer the source of water types which are advected past the instruments, to compute stratification stability and Richardson numbers between vertically displaced instruments, and to provide time-series temperature and conductivity statistics for biological analysis. It is beneficial that the temperature and conductivity sensors are an integral part of the current meter; separate instruments would have to be mounted far enough apart to minimize the flow blockage of the current sensors, and the separation would cause ambiguities in interpreting the data. The measurement of time-series conductivity with an inductive sensor is made exceedingly difficult by the severe biological fouling which occurs along the Louisiana coast.

3.2. AANDERAA METEOROLOGICAL STATIONS

The two proposed brine disposal sites are situated where wind stress effects on currents are known to exceed tidal and density effects for a significant fraction of time. Wind speed and direction measured over water as time-series data at the sites were determined to be essential parameters for a full understanding of the circulation. Barometric pressure data were required both to estimate uncertainties in measuring waves and water levels with pressure-type sensors and to correlate variations with extreme meteorological events. A survey of available instruments conducted at the beginning of the project indicated that the only remote recording meteorological station available as a complete integral unit was the Aanderaa Automatic Weather Station.

The Aanderaa system was designed with its own internal power supply for automatic operation at remote locations. The system

procured for the NOS SPR Support Project included a canister base that housed a data logger, an electrical connector board for patching sensors, and a protected aneroid pressure transducer. An aluminum mast affixed to the top of the canister base supported wind speed and direction sensors at about 3 m above the base. A shield protected an air temperature sensor on the aluminum mast from direct solar radiation. Photographs of the meteorological station are shown in figure 4.

Recording intervals were controlled with a quartz clock. The intervals were set initially at 5 min. During July 1978, the interval was increased to 10 min, and the number of words was reduced from 12 to 6 to accommodate a data translation problem. The Aanderaa meteorological stations operated at 10-min sampling intervals for periods up to 70 days.

The wind speed sensor consists of a 3-cup rotor whose revolutions are sensed by a magnetic reed switch inside a housing. Wind direction was sensed by a vane coupled magnetically to a potentiometer inside a housing; the sensor housings were oriented toward true north. Air pressure was sensed by a potentiometer-type aneroid pressure transducer. Platinum resistance temperature sensors were employed. (Water temperatures were observed for the first 4 months of the study, but the observations were abandoned because of severe operational difficulties.)

3.3 AANDERAA MODEL WLR-5 WATER LEVEL RECORDER

Pressure-type water level gages were mounted at each site's center instrument platform to provide data for determining harmonic constituents, ranges, and times of high and low water with respect to reference stations and to satisfy project requirements for studying nontidal effects. Only two digital magnetic tape recording instruments met requirements of the preselection survey; both were foreign-made. The Aanderaa Model WLR-5 Water Level Recorder with a 20-m depth range was selected and procured. The Aanderaa water level gage uses a quartz pressure transducer and averages over a preselected time interval to eliminate wave-induced fluctuations. The data are recorded on a 6.4-mm magnetic tape as four 10-bit binary words in serial form. The instrument is self-contained and operates on an internal battery power supply.

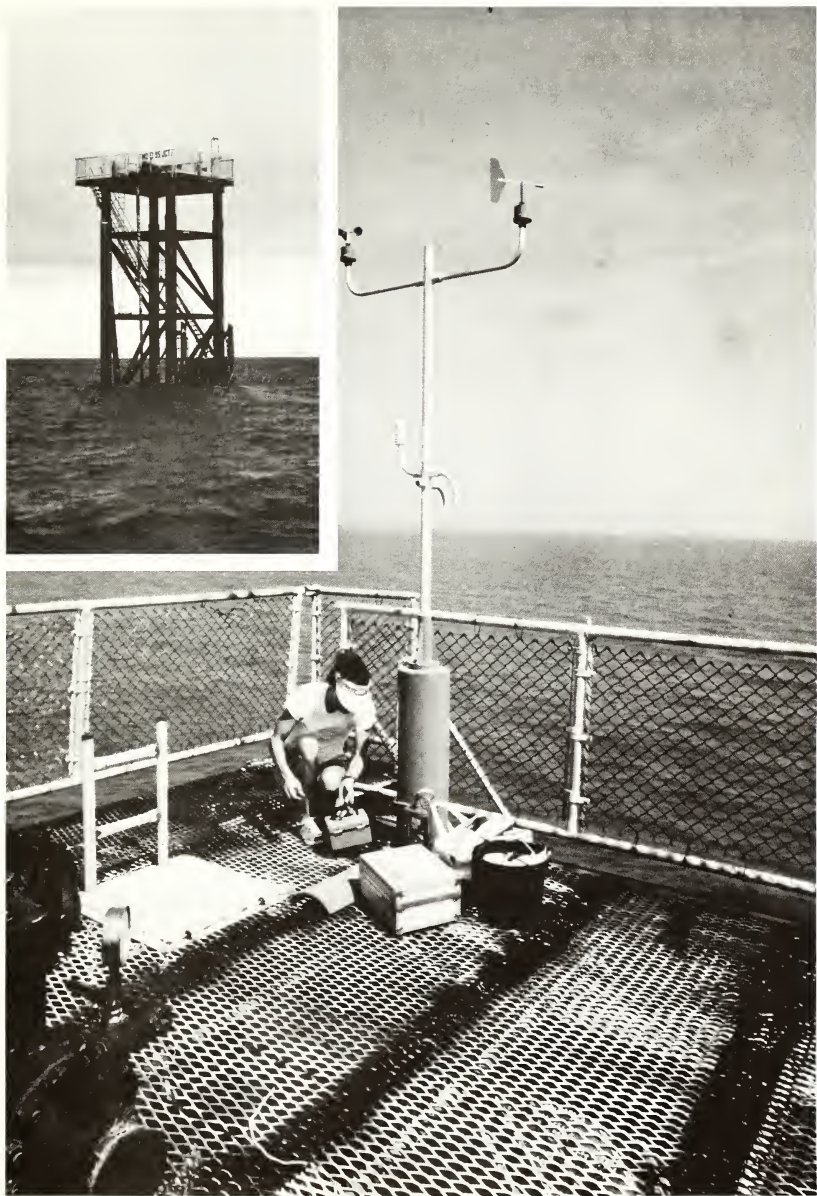


Figure 4.--Meteorological measurement system at station 28.

Three Aanderaa water level gages were procured for the project; they sampled every 5 min with a 56-s integration time. The sampling interval was increased to 10 min during October 1978. The water level gages were positioned vertically as shown in figure 5.

3.4. APPLIED MICROSYSTEMS MODEL 750A WAVE HEIGHT RECORDER

Wave gages were used to obtain data both for the oceanographic characterization and for DQA purposes. In addition to the statistical characterization of the wave field, wave measurements also provide information needed to assess wave induced errors in current meter data. A pressure-type wave gage, rather than a surface-piercing wave staff or a surface-following wave buoy, was selected so that it could be mounted on a subsurface platform near the current meters.

A survey of instruments available at the beginning of the project indicated that, although two were available, only one could be obtained in sufficient time to meet the project schedule. The Applied Microsystems Model 750A water level gage with a wave gage option was procured.

The Applied Microsystem Model 750A wave height recorder uses a quartz pressure transducer to sense water level fluctuations. A 12.7-cm, reel-to-reel magnetic tape recorder provides 366 m of 6.4-mm tape for data storage. The instrument uses a quartz clock for sample interval timing and as a time base for the tape motor advance rate. The wave height recorder is completely self contained and operates on internal battery power.

The pressure transducer senses every 4 hr, and its FM output is integrated for 112.5 s, to produce a water level measurement of 20 bits. This is followed by 966 10-bit wave samples; each sample is integrated for 0.439 s. The latter process continues for 7.5 min. The system then shuts itself down for 4 hr, and the procedure is then repeated; record lengths up to 40 days could be obtained in this manner.

Three Applied Microsystems gages were procured with 20-m depth ranges. The wave gages were deployed with the Aanderaa water level gages at the center stations. These gages were mounted horizontally and strapped to a horizontal frame member at the midsection of the platform as shown in figure 6.

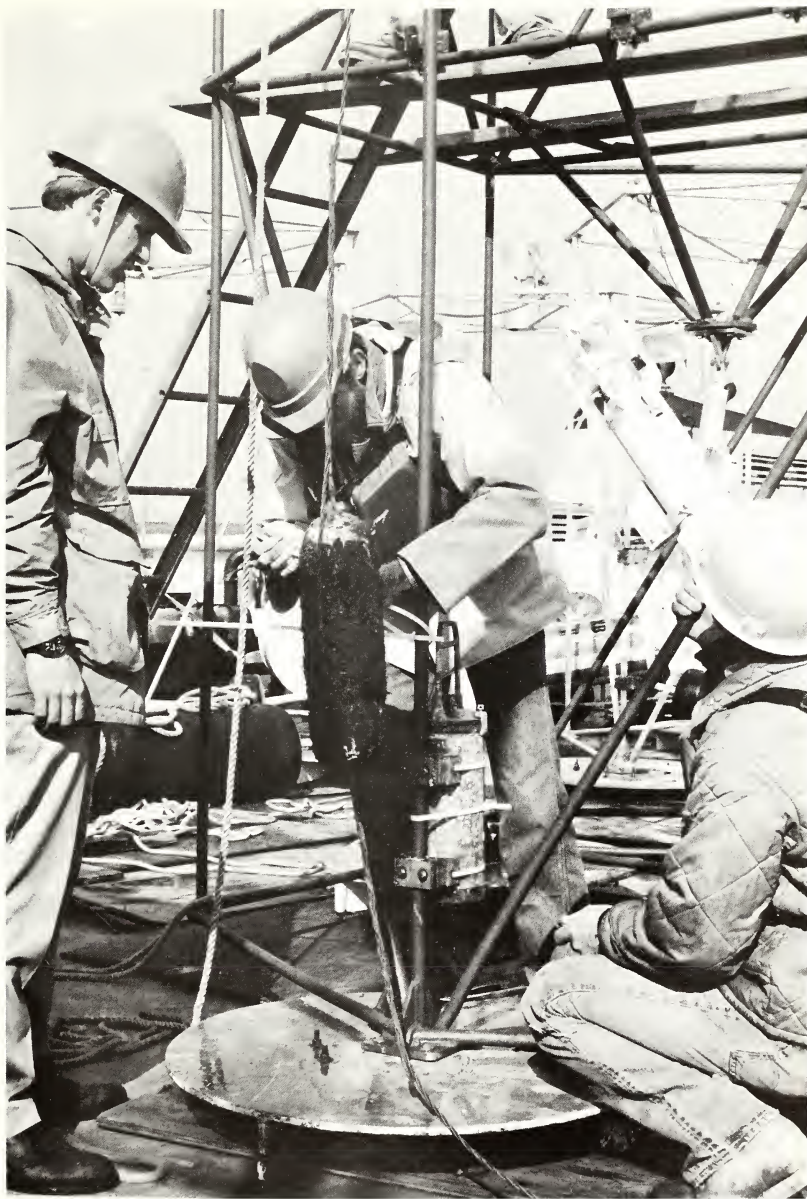


Figure 5.--Water level gage on subsurface platform.



Figure 6.--Wave gage on subsurface platform.

3.5. GRUNDY MODEL 9400 CTD SYSTEM

A profiling system for obtaining quasi-continuous measurements of conductivity and temperature with depth (CTD) consisted of a Grundy Model 9400-1 Underwater Unit, Model 7400 Electric Winch, and Model 8428-3C Data Logger. This system had been procured for the ongoing NOS estuarine survey program just prior to the beginning of the NOS SPR Support Project and was integrated onboard the FERREL in time to serve as the primary CTD measurement system for the project.

The underwater unit (or profiler) consists of the conductivity, temperature, and depth sensors and a signal mixer module mounted on a stainless steel frame; the sensors and mixer module are housed individually. The outputs from the sensors are frequency modulated in the mixer module and transmitted to the ship via a single-conductor cable.

An electric winch on the starboard boat deck of the FERREL was in plain view of the bridge wing where winch operations could be observed readily by the watch officer and where data contamination by ship's discharges would be minimized. The winch operated at a speed of 33 cm/s. The single-conductor cable terminated in the FERREL's monitor room, which housed the CTD data logger and tape recorder. Analog FM signals for each measurand were processed by the Grundy Model 8428 Data Logger and recorded on 9-track magnetic tape by a Kennedy Model 9832 tape recorder.

The Model 9400 unit uses a platinum resistance thermometer to sense temperature, an inductive transformer to sense conductivity, and a bonded strain gage to sense pressure. An optional dissolved oxygen (DO) sensor was ordered from the manufacturer but was rejected when it failed repeatedly to meet specifications. The manufacturer of the CTD system was unable to provide an acceptable electrochemical DO sensor during the course of the project.

3.6. BECKMAN MODEL RS-5 PORTABLE SALINOMETER

During the winter import period of the NOAA Ship FERREL, the NOAA Research Vessel VIRGINIA KEY was used for the field work. It was not possible to transfer the Grundy CTD system from the FERREL to the VIRGINIA KEY for this period of time, and a Beckman instrument was used in its place. The Beckman RS-5 instrument was lowered

from the VIRGINIA KEY's winch wire; depths were determined from a meter wheel.

The Beckman Model RS-5 Portable Salinometer is a battery-operated field instrument that uses an electrodeless toroidal sensor for conductivity measurements and a thermistor sensor for temperature measurements. The sensors are potted into a PVC assembly at the end of steel-reinforced electrical cable. Both the conductivity and temperature observations are made by zeroing bridge circuitry and recording the data manually. The instrument has an internal circuit to compute salinity from conductivity and temperature; this internal circuit was not used to compute salinity for the NOS SPR Support Project; salinity was computed independently of the instrument.

3.7. GUILDLINE MODEL 8400 AUTOSAL

A Guildline Model 8400 Autosol, part of the FERREL's scientific instrument inventory for estuarine surveys, was used to determine salinity values of water samples. The Autosol uses a square-wave, potential comparator technique to compare the conductivity of sea water continuously at a precisely defined constant temperature with an integral reference conductance (standard resistor). The instrument readout includes both binary coded decimal (BCD) output and digital display of the ratio of sample conductivity to standard seawater conductivity; resolution is equivalent to or better than 0.002 ppt. The ratio can be converted to salinity either by computation or by the use of tables.

The Autosol was located in the wet laboratory of the FERREL which was insulated and air conditioned. Water samples were drawn from 1.7-liter Niskin bottles; the bottles were positioned 1 m below the surface, at midwater, and 1 m above the bottom.

3.8. MICRO-WINKLER DISSOLVED OXYGEN APPARATUS

A modification of the Winkler technique for the determination of DO (Carpenter 1965) was selected. A titration apparatus was assembled at T&EL and integrated aboard the FERREL. The apparatus consisted of a microburette, sample flask, magnetic stirrer, and digital counter assembly. Titration of the seawater sample was accomplished by determining the amount of reagent required to complete the titra-

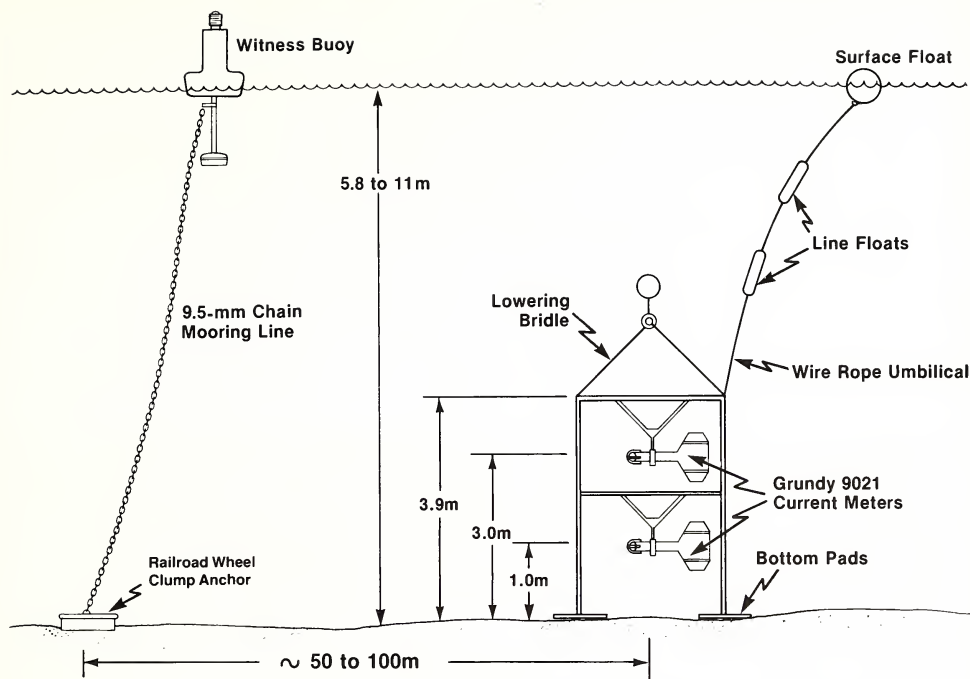


Figure 7.--Platform/mooring system.

tion to the nearest 0.0001 ml. For detailed procedures, refer to the Instruction Manual for Obtaining Oceanographic Data (U.S. Naval Oceanographic Office 1968). Water samples for the determination of DO were obtained with 1.7-liter Niskin bottles. (See section 3.7.)

3.9. PLATFORMS AND MOORINGS

The platforms and moorings required for the project were developed by EDL. Subsurface instrument platforms with witness moorings, photo-control platforms, and J-moorings comprised this task.

3.9.1. Subsurface Platforms

The compound platform/mooring system (figure 7) consisted of a bottom-resting platform that supported the recording instruments (current meters, wave gages, and water level gages) and separate witness moorings.

The platforms were constructed from 5086 T-6, 2.5-cm diameter, marine grade extruded aluminum rods. Each supported two Grundy Model 9021 current meters, one 1 m above the bottom and one 3 m above the bottom and had provisions for attaching wave gages, water level gages, and pingers. The platforms were nonmagnetic to avoid current meter compass deviations. A wire-rope umbilical and lifting bridle were used for deployment and retrieval.

3.9.2. Witness Moorings

The witness moorings, used to identify the platform positions to vessels, are shown in figure 7. Three witness moorings were normally used to mark each platform position. The moorings consisted of Rolyan Model 1428-L buoys, modified by adding padeyes and radar reflectors and equipped with buoy lights, a 9.5-mm chain mooring line, and a railroad wheel clump anchor. The U.S. Coast Guard deployed special purpose buoys to mark the center of each site.

3.9.3. Photo-Control Platforms

The photo-control platforms, designed to meet requirements for the sea surface current observations, are shown in figure 8. The mooring arrangement used an aluminum frame fitted with painted styrofoam, a mast supporting a pennant daymark and a buoy light, and a taut line mooring. The two-part taut line mooring consisted of a combination of synthetic line and chain designed to produce the restoring forces necessary to maintain the platforms within a 3-m position uncertainty. The stretch of the synthetic line allowed the platform to rise and fall with changes in water level. Railroad wheel clump anchors moored the platforms to the bottom.

3.9.4. J-Moorings

Current meters on J-moorings were deployed during the FERREL's winter repair period as a backup measure in the event of storm damage to platforms. The J-mooring configuration is shown in figure 9. A 70-cm subsurface buoy supported the mooring line and a Grundy current meter. The current meter was attached to the mooring line using a standoff supplied by the manufacturer. Lead weights were used to anchor the J-moorings to avoid instrument compass deviations. A witness mooring identical to that shown in figure 7 was attached to the instrument mooring with a wire-rope ground line.

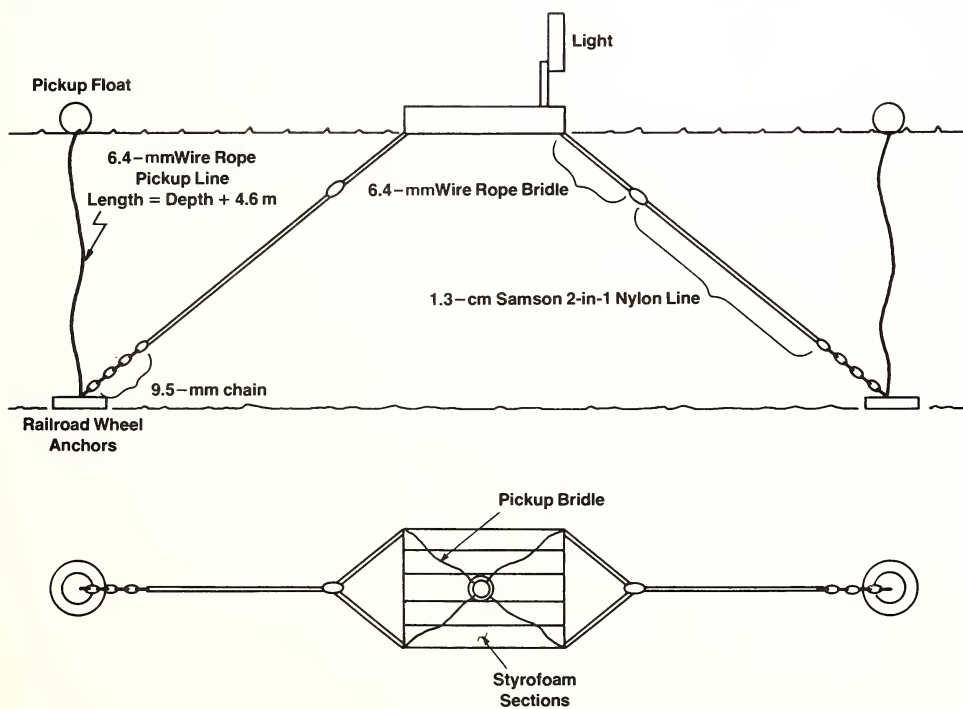


Figure 8.--Photo control platform.

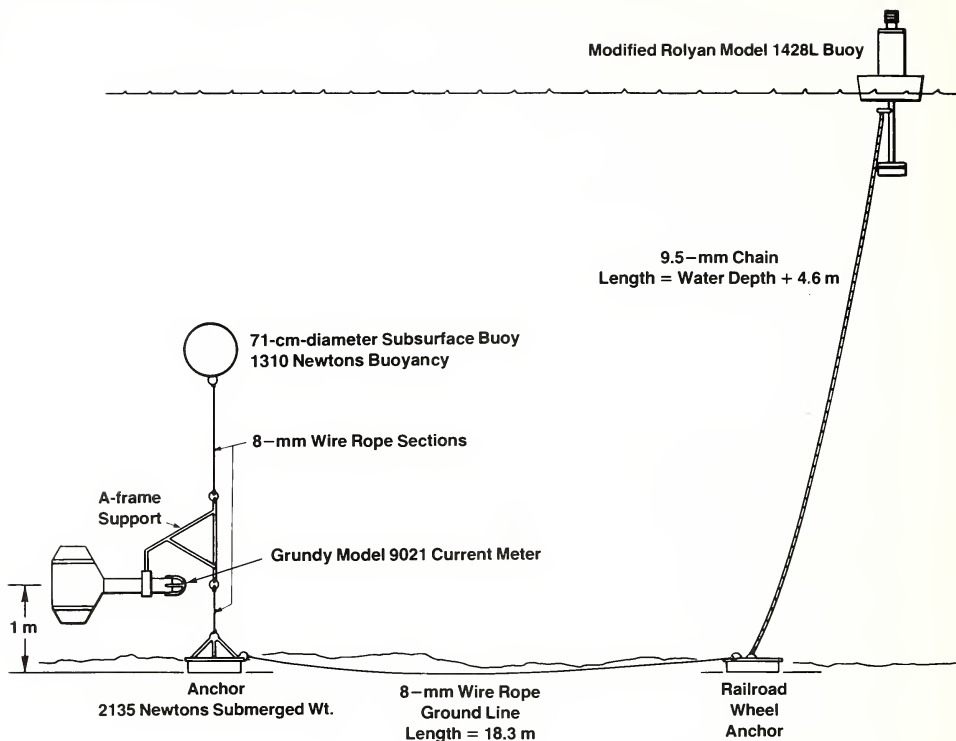


Figure 9.--J-mooring.

4. CURRENT METER EVALUATION

by Gerald F. Appell, David R. Crump, and Thomas N. Mero

An evaluation program was established by T&EL for the Grundy Model 9021 current meter to determine its performance characteristics. The current meter was first marketed in February 1977; it had a minimum of field use and no independently published performance information at the beginning of the NOS SPR Support Project. The evaluation revealed serious problems that would have caused all measurands to fail specification compliance; it provided test data that required the manufacturer to improve his product in order to meet specifications and pass acceptance testing. Appendix A contains test data, test procedures, and a failure mode analysis. Test results provided guidance in preparing inspection and acceptance testing, calibration procedures, and a data quality control plan.

4.1 RESPONSE TO STEADY FLOW

Performance tests of the meter's current velocity response characteristics were conducted at the David Taylor-Naval Ship Research and Development Center (DT-NSRDC) Number 1 Tow Carriage Facility. Test fixtures were designed and fabricated to mount current meters to the tow carriage as they would be mounted on the platforms described in section 3. The Grundy swivel-gimbal assembly was attached directly to the platforms instead of using the Grundy-designed, A-frame mooring system.

The tow carriage (figure 10) is an electrohydraulically powered vehicle weighing 22,500 kg. It rides on steel rails atop a basin 335 m long, 13.5 m wide, with depths of 3.3 and 6.7 m. Test velocities can be maintained to within ± 0.1 cm/s over a range of 2.5 to 500 cm/s. Tow carriage speed is monitored by an HP5328A universal counter and a magnetic pickup that senses the pulses generated from a steel gear coupled to a precision wheel. An

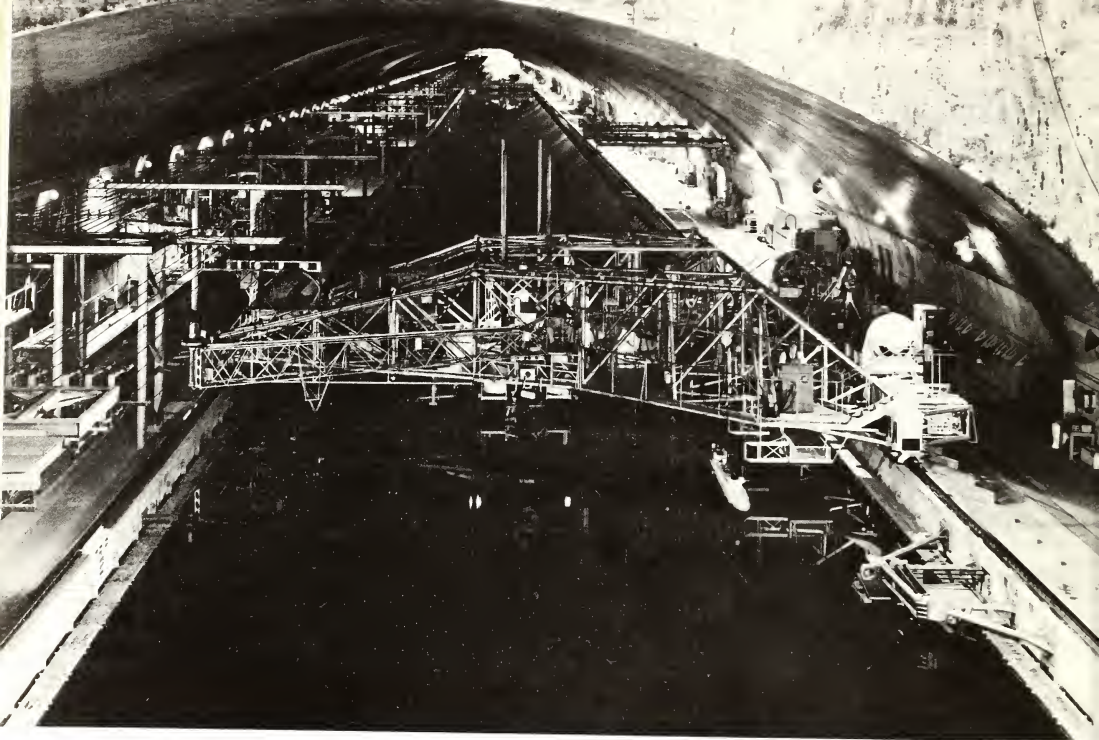


Figure 10.--David Taylor-Naval Ship Research and Development Center (DT-NSRDC) Number 1 Tow Carriage. Both static and dynamic tests of the Grundy Model 9021 were simulated using Tow Carriage No. 1.

HP9825 calculator converts the pulses sampled during a test run to speed (cm/s).

Test results were obtained with an external photodiode sensor (figure 11) that was used to determine the time between two consecutive rotor blade passings. The time interval measurements were converted to rotor revolutions (r/min). Direct monitoring of rotor revolutions allowed us to analyze rotor characteristics without the effect of the instrument's internal averaging. It also provided rapid data sampling and sufficient data quantity for statistical analysis.

4.1.1. Rotor Calibration

The rotor calibration (figure 12) shows the average speed of the rotor as a function of the average tow carriage speed. Each

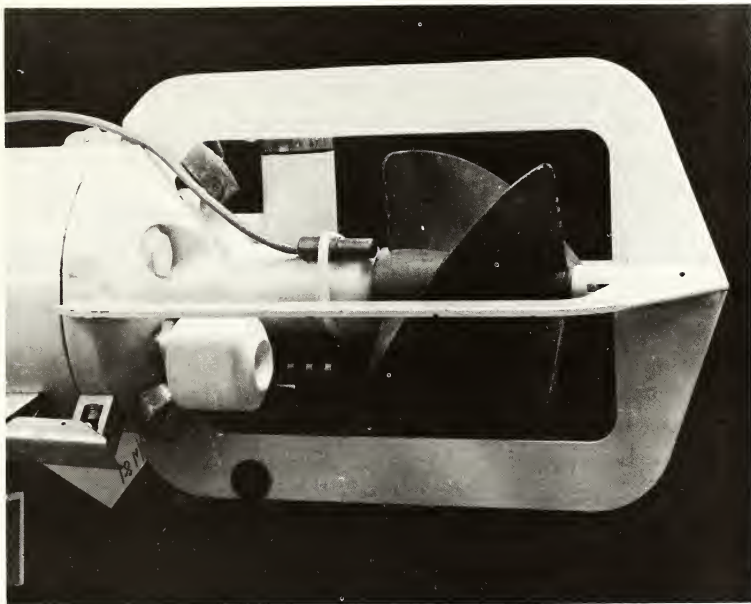


Figure 11.--Photodiode sensor externally mounted to obtain rotor speed from rotor blade passings.

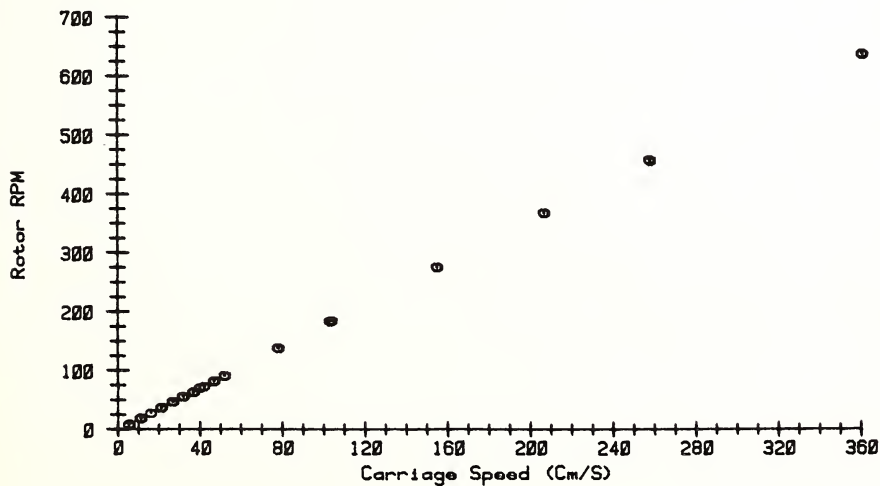


Figure 12.--SN52 rotor calibration data.

test point represents the average of 30 s of consecutive digital samples for each independent test run; the number of samples per test run is thus proportional to the tow speed.

Test data were converted to velocity using the equation provided in the manufacturer's manual,

$$V = 0.527 N + 1.2, \quad (1)$$

where V is the indicated flow speed (cm/s) and N is the rotor rotation rate (r/min).

Residual errors were computed as the difference between the speed indicated by the manufacturer's equation and the true speed of the tow carriage. The results are plotted in figure 13. A demonstration current meter provided by Grundy was also calibrated; this instrument (SN03) did not have the optional conductivity and temperature sensors or acoustic transducer. The results obtained using the same procedures, plotted to the identical equation, are displayed in figure 14. We concluded from the data that the hydrodynamic blockage of the optional sensors reduced the rotor gain by approximately 3 percent. In response to these findings, the manufacturer provided a second equation for use with instruments having the optional sensors:

$$V = 0.543 N + 1.2. \quad (2)$$

Figure 15 shows the results when equation (2) was applied to the data in figure 12. Figure 16 is an error plot obtained from using the equation,

$$V = 0.564 N + 0.1, \quad (3)$$

that was computed by T&EL from the data of figure 12 using a first-degree regression analysis. The data indicated a concave appearance to the residual errors; thus, a second-degree fit was performed by T&EL. The equation,

$$V = 0.00002 N^2 + 0.552 N + 0.8, \quad (4)$$

corrects the high speed drop in the linear equation and produces the residuals of figure 17.

4.1.2. Directivity Response to Steady Flow

Directivity response is defined as the current meter's output response to flow vectors with angles of attack that vary in relation to the meter's heading. This information is important to the

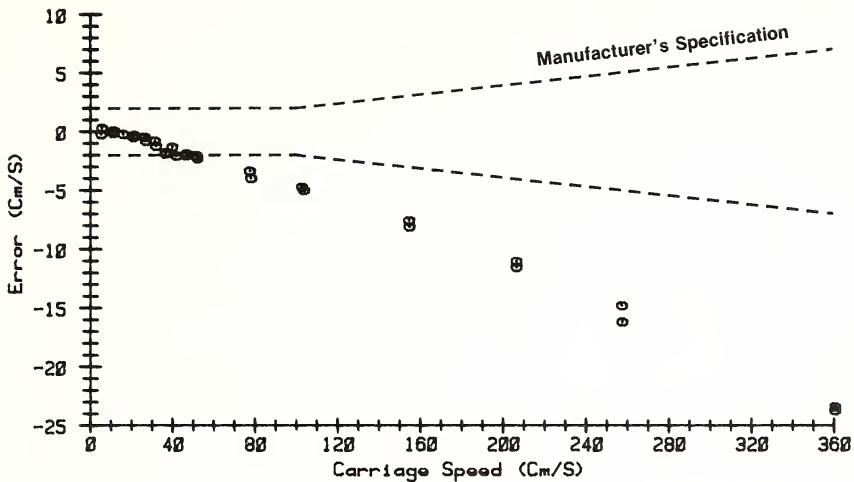


Figure 13.--Residual errors of SN52 rotor calibration data using equation 1. (A blockage effect of the optional measurement transducers biased data outside manufacturer's specifications.)

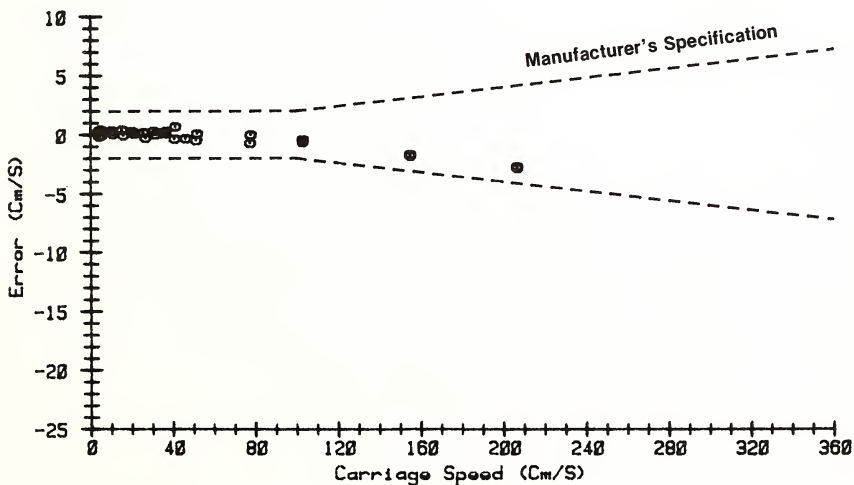


Figure 14.--Residual errors of SN03 rotor calibration data using equation 1. (SN03 does not have optional measurement transducers.)

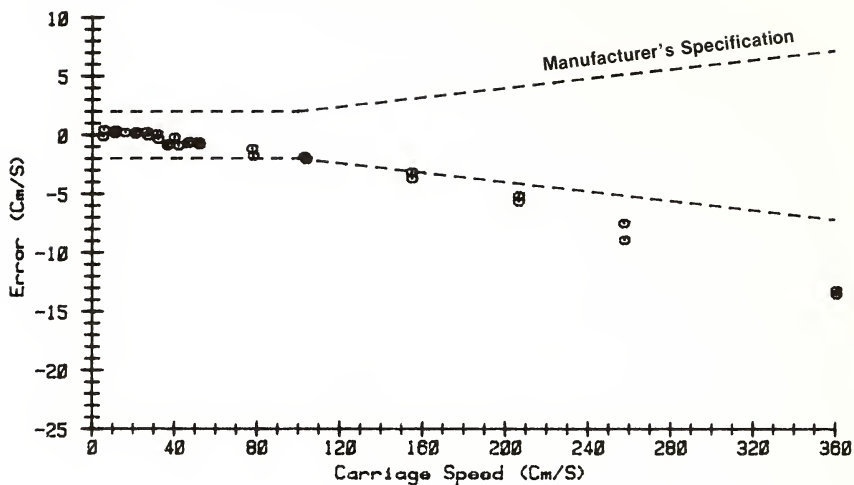


Figure 15.--Residual errors of SN52 rotor calibration data using equation 2.

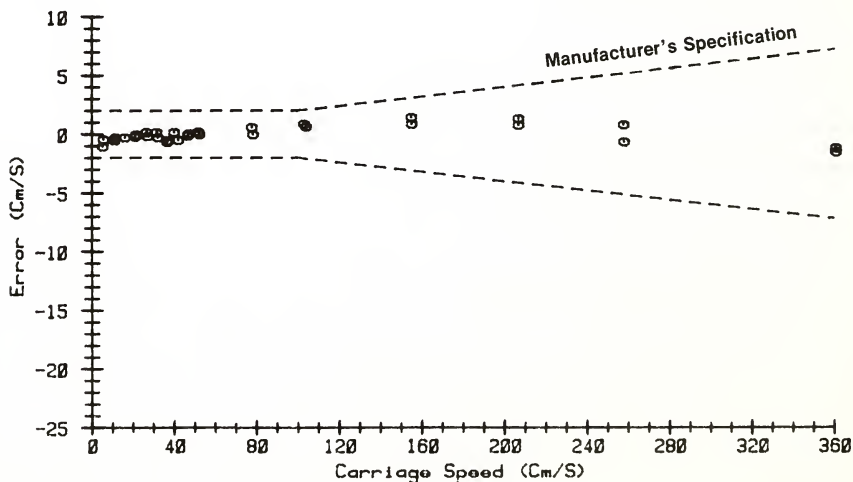
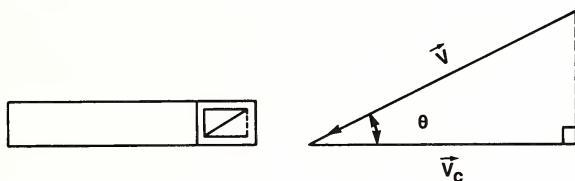


Figure 16.--Residual errors of SN52 rotor calibration data fitted to T&EL first-order equation 3.

determination of meter accuracy because the previously derived rotor calibration equation may not apply when the flow vector angle is changed. Under ideal response conditions, the meter should measure the magnitude of the velocity in the direction it is heading. If the meter heading is not the same as the resultant flow vector heading, the current meter response characteristic should be determined. If the meter response follows a cosine relationship, then the component of the resultant flow vector is measured according to the trigonometric relationship, $|\vec{V}_c| = |\vec{V}| \cos \theta$, where \vec{V} is the resultant flow vector, V_c is the vector component at the measured direction, and θ is the angle between the resultant flow vector heading and measured meter heading:



Test results are shown in the polar plots of figures 18 and 19. The outer circle represents the constant tow carriage speed; the inner circles represent a cosine relationship to the tow carriage velocity (the component of net velocity) at each test angle. Each data point represents the measured flow speed (V_c) at the angle of attack (θ) between the true flow heading and the meter heading. Equation 4 was used to compute flow speed. The data indicate a good agreement with the cosine relationship about the forward axis of the current meter with considerable distortion in the reverse or rear axis. Blockage caused by the instrument housing and other assemblies accounts for reduction in sensitivity about the axis.

In a steady flow environment, the meter will align into the flow and equation 4 would apply. However, in areas where tidal flows predominate and tide reversals cause periods of low currents, the vane may not align the meter to the true current heading. In this case, flows may be measured from other than the true current heading and may average to indicate a reverse current. The accuracy during these conditions is low because of the angle uncertainties and the

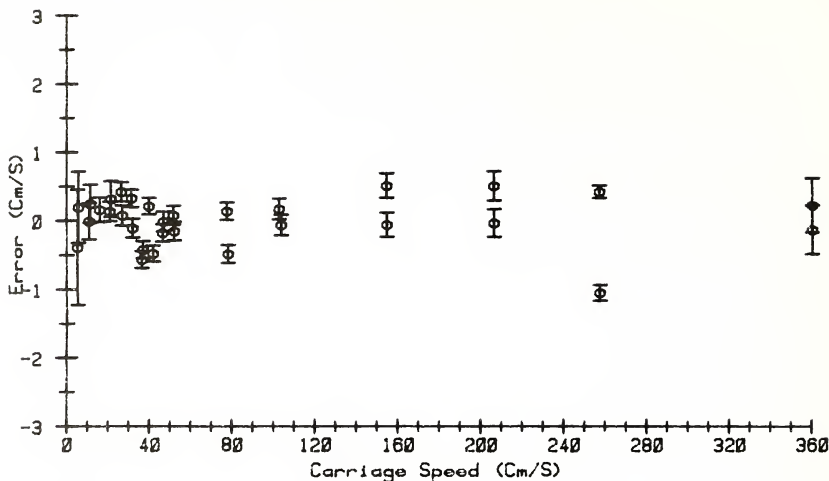


Figure 17.--Residual errors of SN52 rotor calibration data fitted to T&EL second-order equation 4; 95-percent confidence levels are included.

directivity response characteristics. In general, this condition could occur when flow falls below 5 cm/s. Significant speed errors may result from the use of equation 4. The manufacturer provides the following equation for use in reverse flows:

$$V = 0.829 (1023-N). \quad (5)$$

However, because of the uncertainty in the true current direction when the vane is "wandering," using the reverse direction equation is of little real value. Dynamic flow conditions can also create currents that change direction faster than the vane can totally respond and can even reverse rotor direction.

4.1.3. Steady Flow Speed Data Verification

Rotor speed throughput was verified with the T&EL submerged jet facility (figure 20). This facility is a continuous-flow, submerged-jet water tunnel for analyzing the characteristics of current meters. The dimensions of the test section are 76 cm by 1,137 cm by 168 cm; the jet is 38 cm in diameter. Current velocities can be set in the range between 0.5 to 250 cm/s.

The data taken by the external photodiode sensor were compared to the internally recorded data. Agreement between the two speed

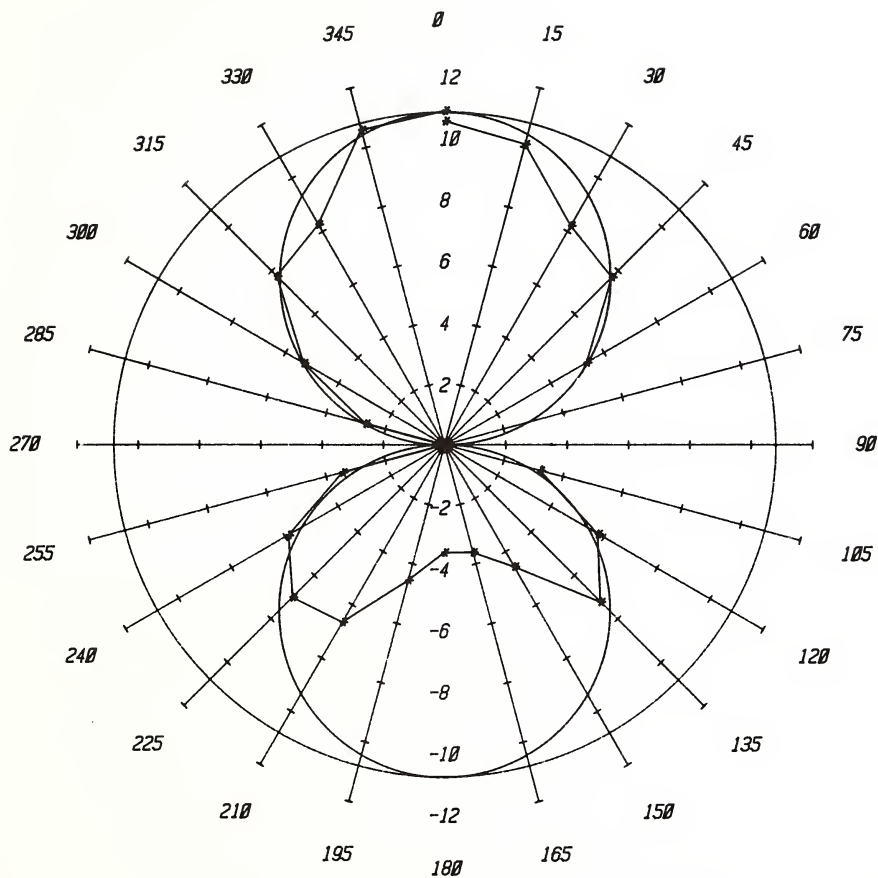


Figure 18.--Horizontal directivity response of SN52 rotor at 11 cm/s. The outer circle represents the tow carriage speed of 11 cm/s, and the inner circles show the cosine function speeds at each test angle. Test points plotted are the Grundy output speeds using equation 4.

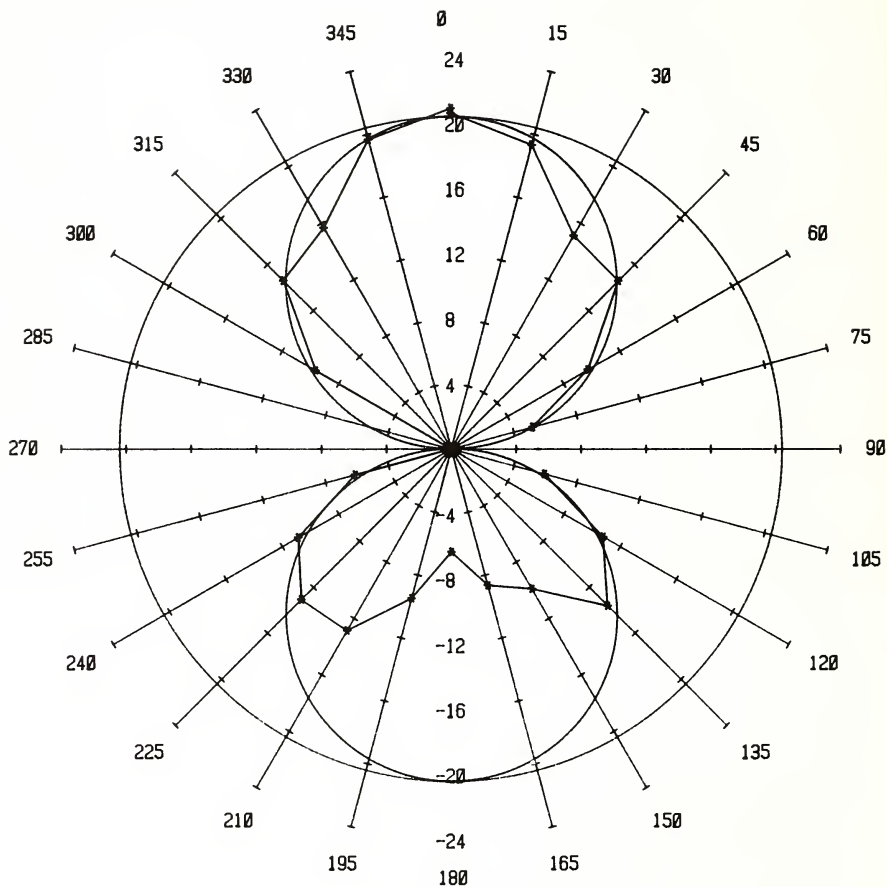


Figure 19.--Horizontal directivity response of SN52 rotor at 21 cm/s. The outer circle represents the tow carriage speed of 21 cm/s, and the inner circles show the cosine function speeds at each test angle. Test points plotted are the Grundy output speeds using equation 4.

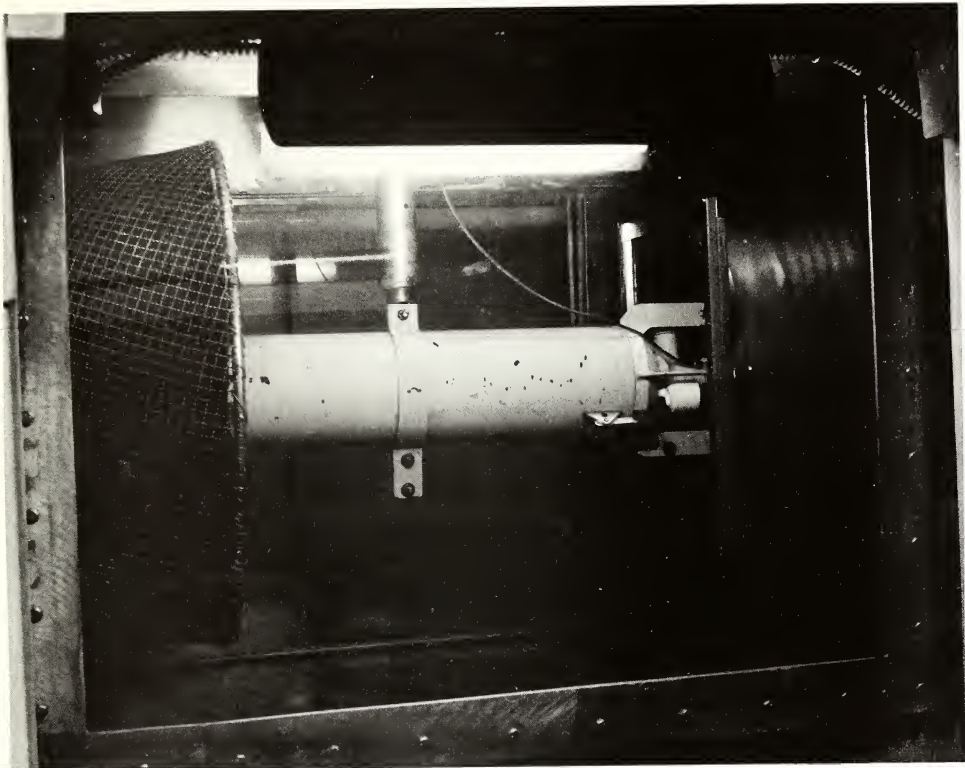


Figure 20.--T&EL submerged jet facility.

measurement systems should be within ± 1 r/min (the measurement resolution of the instrument) or approximately ± 0.5 cm/s. In several cases, the internally recorded speed data averaged 2.5 cm/s (5 r/min) less than those indicated by the rotor at various flow speeds. The DT-NSRDC tow facility tests indicated similar discrepancies with current meter measured speeds as low as 8 cm/s from the true reading. We determined that contact bounce from the reed switches sensing the rotor magnets caused the current meter to interpret the secondary pulses as a current reversal. As a result, the pulses were subtracted from the net count.

The Grundy circuit was designed with a 1-ms time constant to filter the effect of switch bounce; however, secondary closures were observed after almost 5 ms on some meters. Filter capacitors

with 5-ms time constants were installed on all units. Also, a screening program was established to reject reed switches with abnormal bounce characteristics. The new filters reduce the high-speed measuring capability from 600 to 500 cm/s. Tests of 30 modified Grundy 9021 current meter speed circuits revealed that 10 percent of the averaged data points were outside the ± 0.5 cm/s resolution; however, all the data points were within ± 0.9 cm/s.

4.1.4. Steady Flow Direction Characteristics

Current direction is determined via two devices, a vane-swivel assembly that aligns the current meter into the flow and a magnetic compass that determines the heading of the meter's horizontal axis with respect to magnetic north. Vane alignment tests were performed on the DT-NSRDC tow carriage, and compass performance tests were conducted at the Hyde Airfield, Clinton, Md.

Vane alignment of the meter with the flow vector depends on the hydrodynamic force exerted on the vane surface by water flow; the flow creates a restoring torque to maintain alignment. Flows greater than 5 cm/s create sufficient restoring torque on the vane to align the system to within the estimated test method uncertainty of ± 2 degrees. At flows of about 2 cm/s, the vane did not respond to the true flow direction, resulting in a large direction uncertainty. Table 4 lists the test results.

Table 4.--Alignment accuracy data; Grundy Model 9021 SN52, DT-NSRDC, December 28, 1977

Carriage speed (cm/s)	9021 compass (degrees)	Vane alignment error (degrees)
2.1	306	19
5.1	292	5
10.5	285	-2
26.9	286	0

Heading Reference: 287.5 degrees (magnetic)

Alinement response time is expressed in terms of a distance constant that is defined as the distance traveled by the water past the instrument to produce a 180-degree direction change. This constant is a function of the alinement torque provided principally by the vane. At flow speeds above the vane threshold (+5 cm/s), the distance constant remains about the same. The test results listed in table 5 indicate an average distance constant of 358 cm; for a 180-degree change in current direction, sufficient time is required for 358 cm of water to travel past the current meter to maintain alinement.

Table 5.--Distance constant data, Grundy Model 9021 SN52, DT-NSRDC, December 28, 1977

Carriage speed (cm/s)	Vane response time (s)	Distance (cm)
6.1	60	366
10.2	35	357
20.3	17	345
25.9	14	363

The Grundy Model 9021 current meters contained the Model 213 DIGICOURSE, Inc., compass. This compass consists of a fluid damped, grey coded disk with light emitting diodes (LED's) providing digital output indicative of the magnetic heading. The disk is pivoted on bearings which give it freedom to respond to the Earth's magnetic field and which also allow freedom in the vertical (pitch and roll) axis up to a maximum of ± 5 degrees of arc. When that angle is exceeded, the disk's freedom is restricted and it can no longer respond to the Earth's magnetic field. Tests indicated that 5 degrees of pitch or roll could easily be exceeded in the presence of orbital, wave-generated flow conditions. Also, tow basin tests and initial field deployments indicated that swivel-clamp assembly positioning was extremely critical in establishing the current meter balancing. It was apparent that, even under ideal conditions, a pitch-roll

attitude of ± 5 degrees could not be established and maintained consistently.

Grundy replaced the Model 213 with a Model 215 compass. The Model 215 contains a Model 213 compass mounted in a gimbal assembly within a larger housing. The gimbal was designed to maintain the Model 213 unit within a ± 5 -degree vertical attitude while limiting total vertical excursion of the housing to ± 40 degrees. All NOS units were equipped with the Model 215 DIGICOURSE compass.

Calibrations were performed on the Model 215 compass mounted in the Grundy current meter. Data were taken with the meter level in the horizontal plane and at various tilt angles. Magnetic north heading was referenced to a Lutz compass, and angular increments were measured by an enscribed ring (figure 21). Data analysis indicated that the gimbal assemblies did not provide sufficient tilt freedom. The compass would not indicate incremental angle changes when tilted greater than 10 degrees from level. By redesigning the gimbal bearing assemblies and using nonrestrictive conductor wire, DIGICOURSE resolved the problem. However, the ± 40 -degree specification was reduced and a ± 30 -degree vertical excursion was assured. DIGICOURSE redesigned the gimbal assembly again when it was discovered that the gimbals were subject to shock failure.

Figure 22 shows the results of a representative compass calibration performed on a Model 213 compass mounted within a Grundy 9021G. The recorded data are represented by a 10-bit word with 0 being a northern-going current and 512 being a southern-going current. Therefore, the conversion for computing direction is

$$D = 0.3516 N, \quad (6)$$

where D is the magnetic heading in degrees and N is the digital output for the compass word. Additional tests were performed on Model 215 compasses at vertical angles up to 30 degrees, and no additional deviations were noted from the calibration of figure 22. The bias error shown in figure 22 can be removed by alining the compass during current meter calibration. In its redesigned configuration, the DIGICOURSE Model 215 performed to within acceptable limits.

4.2 DYNAMIC RESPONSE

The response of the Grundy Model 9021 current meter to a dynamic environment was evaluated through a series of simulation



Figure 21.--Compass calibration setup.

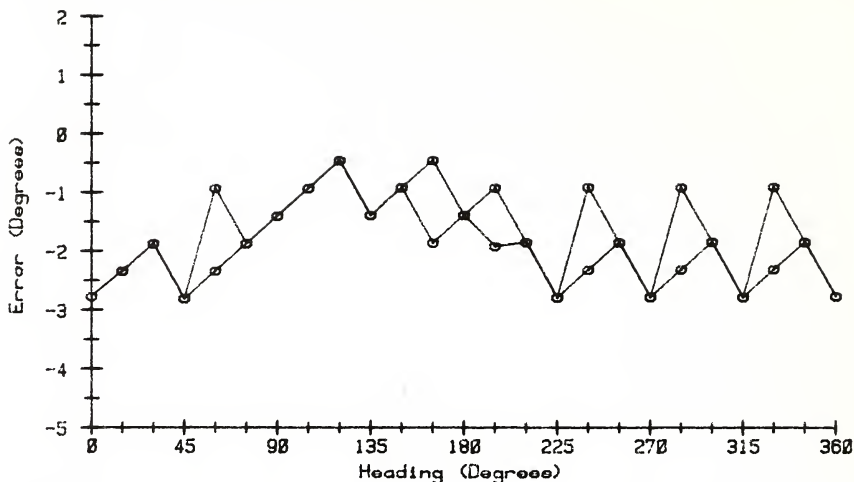


Figure 22.--Residual errors of SN51 compass calibration data using equation 6.

tests using the T&EL-designed Vertical Planar Motion Mechanism (VPMM) at the DT-NSRDC tow facility. The VPMM was developed primarily to evaluate current sensors in a controlled dynamic environment (Kalvaitis 1978). Three distinct modes of dynamics can be generated: circular, vertical, and horizontal (figure 23). Test objects up to 2-m long and weighing 80 kg can be tested at carriage speeds up to 77 cm/s. Peak-to-peak amplitudes of 0.15 to 1.22 m can be adjusted in 0.15-m increments. The attack angle of the dynamic motion, referenced to the tow direction, is variable from 0 to 90 degrees in 15-degree increments. Periods of motion ranging from 4.5 to 12 s can be generated by a 3-hp servo controlled motor. Oscillatory motions generated are monitored by a position monitor attached to the motor's drive shaft and a digital timer. An HP9825 calculator is used for digital sampling of the instrumentation for computing fixture period or instantaneous velocity. Tests were conducted under orbital and horizontal mode dynamics to predict performance in a midwater and near-bottom shallow water environment (appendix A).

Appendix A lists the results of vector averaging of the test data. The vector analysis was performed by computing north and east vector components (V_n and V_e) for each sample of average speed and instantaneous direction. The mean of 30 accumulated V_n and V_e

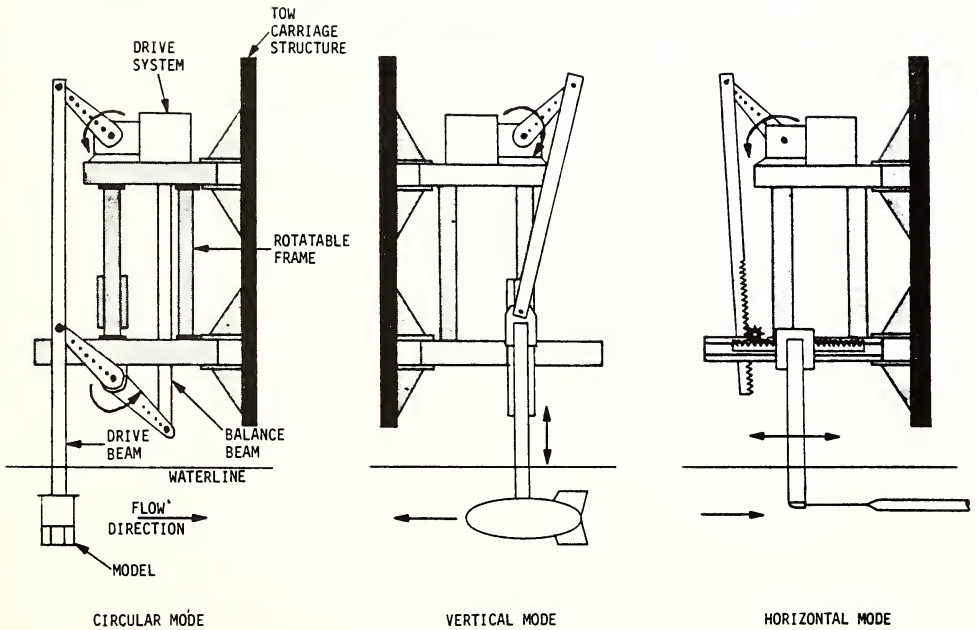


Figure 23.--Vertical planar motion mechanism (VPMM).

components was determined and then used to compute the resultant vector magnitude and direction translated to polar coordinates. The data are displayed in increasing signal-to-noise (S/N) ratios. (Signal to noise is the ratio of the tow carriage speed to the angular velocity of the VPMM.) The magnitude of the error between the tow carriage velocity and the vector-averaged instrument velocity is a function of the S/N ratio. As the S/N ratio approaches 1, the speed and direction errors approach the experiment measurement uncertainty.

The horizontal dynamics data provide a description of performance in shallow water with meter placement near the bottom and within the platform. Orbital data are representative of a near-surface deployment. We anticipate midwater performance, in elliptical dynamics, to be represented closer by the horizontal rather than the orbital errors. Performance of the Grundy 9021 on a mooring line, under the same environmental conditions, may or may not be similar.

4.3 TEMPERATURE AND CONDUCTIVITY

Performance of the meter's conductivity and temperature measurement capability was tested using T&EL facilities. Thirty samples from the current meter were collected at each test point along with a standard temperature measurement taken at the beginning and end of each test point. Two water samples were also collected and processed on a laboratory salinometer prior to each test point. Three temperature cycles were performed with the bath salinity at 35, 20, and 5 ppt.

We encountered problems in the first instrument tested that used a semiconductor temperature sensor. Tests revealed a serious drift problem occurring at a rate of 0.1°C over several hours. Grundy replaced the semiconductor sensor with a platinum resistance transducer. Temperature tests on this transducer revealed that errors were well within manufacturer's specifications of $\pm 0.1^{\circ}\text{C}$ using their calibration equation,

$$T = 0.03613 N - 2, \quad (7)$$

where T is temperature in $^{\circ}\text{C}$ and N is the BCD output. Figure 24 depicts the performance of the meter tested. No measurable drift in the sensor was detected during the course of the evaluation. Platinum transducers were installed in all NOS current meters.

Initial conductivity tests found that the electronic circuitry and conductivity head exhibited a temperature effect. Grundy modified

the circuitry by adding temperature compensation to reduce the effect. Temperature compensation of the conductivity circuitry was provided on all current meters procured for the project. Conductivity measurements were within the manufacturer's specification of ± 0.08 mS/cm using the Grundy calibration equation,

$$C = 0.05859 N, \quad (8)$$

where C is conductivity in mS/cm and N is the BCD output. Figure 25 represents the instrument performance for three temperature/conductivity cycles.

4.4 RECORDING SYSTEM ACCURACY

The meter was in a fully operational mode and recording data internally during most laboratory tests to evaluate the system characteristics. T&EL developed and constructed a tape translator that could read the tapes and print a hard copy of the data. Data were checked on all meters for proper recording of the data pulses and intelligence of all taped signals. In all cases, taped data matched printer/verifier data, and taped signals exhibited the proper characteristics.

4.5 ENVIRONMENTAL TEMPERATURE AND VIBRATION TESTS

We conducted environmental temperature tests in accordance with MIL-STD-810C (U.S. Department of Defense 1975), with the high temperature restricted to 40°C, the low storage temperature restricted to -30°C, and low operational temperature limited to -5°C. During the operational phases of the test, the meter was recording internally on a 30-s sequence and externally through the printer/verifier. Battery voltage and time base accuracy were monitored continually through all phases of the test.

The time base deviated by ± 10 ppm during the high temperature tests and by ± 6 ppm during the low temperature phase (both within the manufacturer's specified time base accuracy of ± 23 ppm).

The 12-V battery voltage dropped 0.5 V during high temperature tests and 0.7 V during the low temperature tests. The variations are considered to be within the normal operating characteristics of a lead-acid battery.

The system electronics, data thruput, and recorder were not adversely affected by the test conditions.

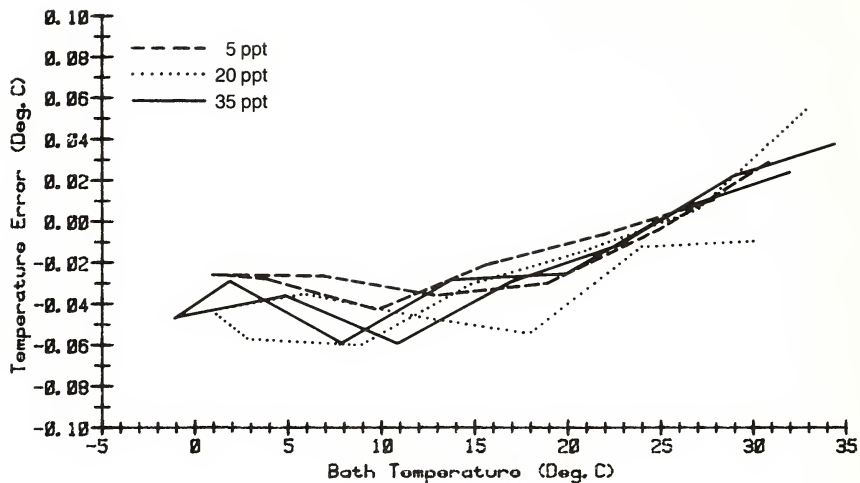


Figure 24.--Residual errors of SN24 temperature calibration data using equation 7.

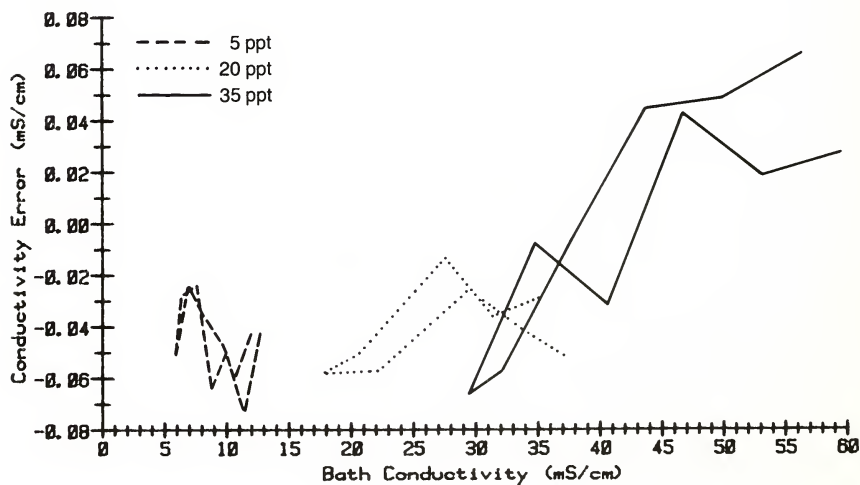


Figure 25.--Residual errors of SN24 conductivity calibration data using equation 8.

We performed vibration tests in accordance with the procedures of MIL-STD-167-1 (U.S. Department of Defense 1974). The meter was in a fully operational mode and sampled every 30 s. Data on all parameters were measured externally with the printer/verifier and recorded internally on magnetic tape. The vibration tests produced no observable mechanical problems or resonance modes. The system functioned normally, and tape transport and recorded data were not affected.

4.6. ACOUSTIC TRANSDUCER

Tests were performed at the Naval Surface Weapons Center Acoustic Facility, White Oak, Md., to evaluate the performance of the acoustic transducer. Additional tests were performed in the Anacostia River and at the proposed West Hackberry brine disposal site in the Gulf of Mexico.

Tests to determine signal transmit and receive characteristics and levels verified that operation was within manufacturer's specifications. The deepwater version was tested operationally in the Anacostia River with the Grundy Model 5621 Acoustic Receiver. Acoustic interference from various sources prevented reception of intelligent data that could be printed on the printer/verifier. A shallow-water circuit modification to reduce power and keep the reference carrier on between words resulted in slight improvement, and intermittent transmission could be obtained. *In situ* tests in the Gulf of Mexico, from the NOAA Ship FERREL in approximately 10 m of water, also revealed that signals could be received only when the receiver hydrophone was within about 30 m of the current meter and ship noise was low.

4.7. INSTRUMENT TRANSFER FUNCTIONS

The recorded meter output contains six serially coded, 10-bit binary words for each sample sequence. The Grundy Model 8220 printer/verifier converts the six serial output words to their respective BCD equivalents. The order of output and the respective transfer functions, where N is the BCD output, are

Word 1 - Instrument serial number = serial number
2 - Current direction (degrees) = $0.3516N$
3 - Current speed (cm/s) = $0.00002N^2 + 0.552N + 0.8$
4 - Temperature ($^{\circ}$ C) = $0.03613N - 2$
5 - Sequence count = count
6 - Conductivity (mS/cm) = $0.05859 N$

4.8. DISCUSSION

T&EL provided the second-order equation,

$$V = 0.00002 N^2 + 0.552 N + 0.8, \quad (4)$$

to compute flow speed over the range of 3 to 360 cm/s. Use of this equation gave a residual standard error (RSE) of 0.4 cm/s in the test data. The manufacturer's equation results in an RSE of 2.0 cm/s for the same set of test data. The rotor threshold on meter SN52 was approximately 2 cm/s. Flows below 5 cm/s have an uncertainty greater than 40 percent of indicated flow, and reverse flow indications generally occur during these low-speed conditions. The reed switch pulse detection circuit caused problems during laboratory testing. Reed switches may continue to be a source of reliability problems in the field.

The current measurement performance of the Grundy Model 9021 current meter in a steady flow environment is closely represented by the manufacturer's specifications using the transfer functions we recommend in section 4.7. The Grundy 9021 was not designed for use in a highly dynamic environment, and we recommend that it be used only when the expected signal-to-noise condition is greater than 1. As will be discussed in section 8, the signal-to-noise ratio observed *in situ* exceeded 1 more than 95 percent of the time.

The temperature and conductivity measurands were within the manufacturer's claims, when all adjustments and modifications were made. Biofouling of the conductivity cell can seriously degrade measurements, and future procurements should specify antifoulant protection provided by the manufacturer.

Environmental tests indicate that the instrument performs under the range of conditions specified by the manufacturer. Construction and assembly of the instrument is such that no degradation is expected during normal marine deployments.

In shallow water, less than about 15 m deep, the acoustic link is not functional for reliable transmission of data; however, the acoustic link does indicate instrument operation.

The design of the swivel/clamp and tail vane assembly results in the center of buoyancy and center of gravity being located sufficiently apart to cause difficulty in balancing the meter in water. The design also adds to the complexity of the hydrodynamic response in the presence of dynamic motions.

5. INSTRUMENT INSPECTION AND ACCEPTANCE TESTS AND CALIBRATIONS

by Thomas N. Mero

I&A tests and calibrations were conducted by T&EL to provide data quality control for project instruments--36 Grundy 9021 recording current meters, 5 Aanderaa meteorological stations, 3 Aanderaa water level recorders, and 3 Applied Microsystems wave height recorders. Instruments used as standards in the field quality control checkouts, including a Paroscientific Model 2100A pressure sensor, a Yellow Springs Instruments Model 777 thermometer, and a Hewlett-Packard Model 5328A counter, were also calibrated.

In addition to the initial I&A tests and calibrations, selected instruments were returned to T&EL during the field effort for recalibration. At the completion of the field effort, all instruments were returned to T&EL for post-survey calibration and/or operational checks. The Grundy Model 9400 CTD system, also used in the project, was calibrated prior to the survey, after 6 months of operations, and at the conclusion of the field effort.

5.1. GRUNDY MODEL 9021 RECORDING CURRENT METERS

Thirty-six Grundy Model 9021 recording current meters were checked to verify proper operation and were calibrated prior to acceptance. Following acceptance, the instruments were delivered to the NOAA Ship FERREL for use at sea.

5.1.1. Inspection and Acceptance Testing

I&A test procedures were developed for the Grundy current meter to verify that each instrument performed in accordance with manufacturer's specifications prior to acceptance and use by NOS; these procedures were designed to check the operation of the instrument and the recording system and to check the accuracy of each parameter measured.

The instruments were repaired, adjusted, and modified, as required, to bring performance within the manufacturer's specification.

As part of the I&A tests, the design and operation of the instruments were checked for obvious defects. Two problems were encountered with the physical instrument design which required corrective action. In the first problem, leads from the temperature and conductivity sensors would occasionally disconnect from the electronics when the instrument was placed in its pressure housing; these leads were secured prior to acceptance. In the second problem, a potentiometer located on the CTD analog board also was vulnerable to damage during assembly. To eliminate this problem, Grundy substituted a smaller potentiometer in the remaining instruments.

During operational checks, data-recording errors in six current meters were detected. The errors were traced to a defective integrated circuit (IC) in the tape-deck electronics. The manufacturer determined that improper operation of the printer/verifier during final checkout caused the IC failure. Circuit boards were repaired by T&EL personnel.

A review of calibration data on the current speed measurement subsystem disclosed data throughput errors in four current meters. In each case, instrument electronics recorded low rotor speeds; reed switch bounce was determined to be the cause, and new reed switch assemblies were installed.

The performance of the magnetic compass was measured with the current meter in a level position and also at a 25-degree tilt (pitch) angle. Initial tests on the first 11 current meters detected sticking compasses in a majority of the instruments. DIGICOURSE, the compass manufacturer, determined that a modification of the compass gimbal assembly was required. To accommodate ship cruise schedules, the compasses were modified and reinstalled at the DIGICOURSE plant in New Orleans, La., where T&EL personnel performed the acceptance tests on the 11 instruments. Additional modified compasses, shipped to T&EL, were damaged in transit. The manufacturer made a second gimbal modification to minimize further shock damage. All the remaining instruments were equipped with compasses containing the second modification.

Calibration of the temperature sensors revealed two sensors that were out of specification. It was determined that a secondary

temperature standard used by the manufacturer had drifted, resulting in the calibration errors. T&EL adjusted and recalibrated the temperature sensors prior to acceptance.

Calibration of the conductivity sensors found six sensors out of specification. The conductivity heads of four of these sensors needed demagnetization and related adjustments. The remaining two sensors were returned to Grundy for repairs.

A time-base check, to verify the accuracy of the instrument's internal clock, found three clocks out of specification. One was adjusted, a capacitor was added to the clock board on the second, and the clock board was replaced entirely on the third.

5.1.1.2. Calibration Data Analysis

The Total Systematic Uncertainty (TSU) of the test setup for each parameter is determined by using three times the standard deviation whenever sufficient data were available or by using the worst-case uncertainty estimate when sufficient data were not available. The error from each test point for all 36 instruments was combined, and the Residual Standard Error (RSE) was computed for the ensemble of instruments. The 95-percent confidence level for the transfer function was computed using the appropriate multiplier selected from Student's "t" table (section 7.3.1, equation 11). The TSU was then combined with the 95-percent confidence limits of the instruments' transfer function to form the Estimated Calibration Uncertainty (ECU). Along with the error analysis, histograms are presented (figure 26) that indicate the error distribution for all 36 instruments tested.

Current Speed Data Summary

Total Systematic Uncertainty (TSU):	± 1.6 cm/s
Residual Standard Error (RSE) based on computed transfer function (36 instruments):	± 0.51 cm/s
Error distribution of 36 units:	(See figure 26a.)
Estimated Calibration Uncertainty (ECU): ECU = TSU + 1.96 RSE = ± 2.6 cm/s	± 2.6 cm/s

Current Direction Data Summary

Total Systematic Uncertainty (TSU):	± 1.5 degrees
-------------------------------------	-------------------

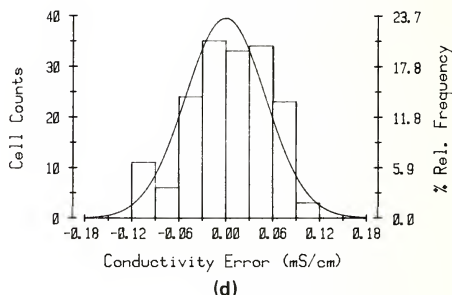
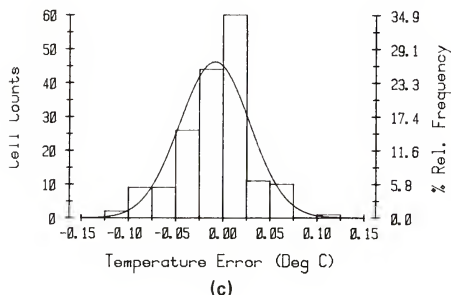
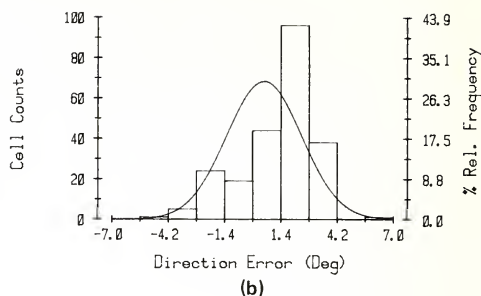
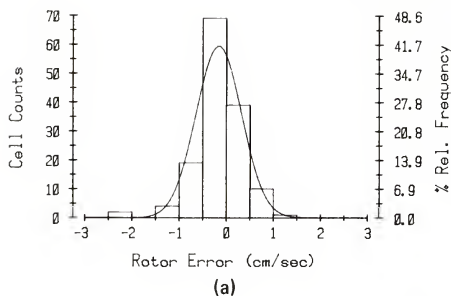


Figure 26.--Error distributions from initial calibration of 36 Grundy 9021 current meters.

Residual Standard Error (RSE) based on manufacturer's transfer function:

± 1.9 degrees

Error distribution of 36 instruments:

(See figure 26b.)

Estimated Calibration Uncertainty (ECU):

$ECU = TSU + 1.96 (RSE) = \pm 5.2$ degrees

± 5.2 degrees

Temperature Data Summary

Total Systematic Uncertainty (TSU):

$\pm 0.008^{\circ} C$

Residual Standard Error (RSE) based on manufacturer's transfer function:

$\pm 0.039^{\circ} C$

Error distribution of 36 instruments:

(See figure 26c.)

Estimated Calibration Uncertainty (ECU):

$ECU = TSU + 1.98 (RSE) = \pm 0.085^{\circ} C$

$\pm 0.085^{\circ} C$

Conductivity Data Summary

Total Systematic Uncertainty (TSU):

± 0.015 mS/cm

Residual Standard Error (RSE) based on manufacturer's transfer function:	$\pm 0.053 \text{ mS/cm}$
Error distribution of 36 instruments:	(See figure 26d.)
Estimated Calibration Uncertainty (ECU): ECU = TSU + 1.98 (RSE) = $\pm 0.12 \text{ mS/cm}$	$\pm 0.12 \text{ mS/cm}$

5.1.3. Mid-Survey Calibration

As part of the instrument data quality control program, 17 current meters were returned to T&EL during the survey for recalibration. The procedures developed for the I&A tests were followed for each recalibration. Most of the instruments returned for recalibration required some repairs and/or adjustments. Each instrument's measurement accuracy was adjusted to within manufacturer's specification before calibration; the new accuracy data, therefore, could not be used to assess prior field performance but served as beginning points for the remainder of the field effort.

5.1.4. Post-Survey Calibration

The 27 current meters that were recovered at the completion of the survey were returned to T&EL for post-survey calibration. Twenty-one were fully operational and were calibrated according to existing procedures. No adjustments were made by T&EL personnel prior to the calibration of the instruments.

The current speed test results, shown in figure 27a, indicated no significant change in accuracy from the initial data. Checks on the compasses found four units with gimbal problems and errors outside of manufacturer's specifications. (Direction errors are shown in figure 27b.) The recalibration of the temperature, shown in figure 27c, found 14 of the 21 units performing to within $\pm 0.10^\circ \text{ C}$. The remaining units exhibited larger offset errors but did not indicate any positive or negative trends in sensor drift. Because of the painting of conductivity cells, adjustments made onboard the FERREL, and possible sensor drift, only two instruments performed within the manufacturer's conductivity specification of 0.12 mS/cm . Errors on a majority of the conductivity sensors were less than $\pm 1.0 \text{ mS/cm}$, as shown in figure 27d. Unfortunately, the conductivity electronics were adjusted in the field prior to shipment to T&EL; therefore the data shown do not represent actual field measurement errors.

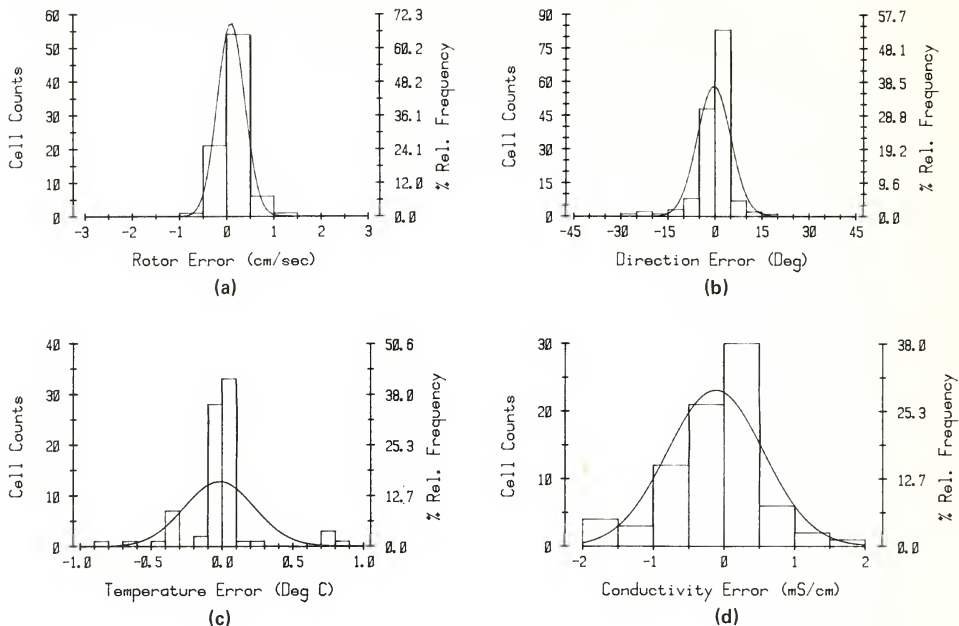


Figure 27.--Error distributions from recalibration of 21 Grundy 9021 current meters.

Refer to sections 7 and 9 for further analyses of uncertainties associated with Grundy Model 9021 measurements.

5.2. AANDERAA METEOROLOGICAL STATIONS

Five Aanderaa meteorological stations were subjected to I&A tests and calibrations prior to acceptance and use. At the completion of the field effort, the systems were returned to T&EL, where operational checks were conducted along with calibrations of the air pressure and temperature sensors.

5.2.1. Inspection and Acceptance Tests

The data logger and the four sensors composing each Aanderaa meteorological station were subjected to separate I&A testing. Five data loggers (Model DL-1) were inspected for defects in workmanship and shipping damage. When no deficiencies were encountered, the systems were checked for proper operation. The quartz clock failed

on one data logger during testing; the manufacturer was consulted, and a replacement clock was installed. A data tape was recorded on each data logger during testing and subsequently verified on T&EL's translator. The instrument's internal clock frequency was also checked; it performed within specifications for each data logger.

Four wind speed sensors (Model 2593) were tested in the National Weather Service's wind tunnel at Sterling, Va. A calibration check indicated speed measurement accuracies within manufacturer's specifications of ± 2 percent for all four sensors. A fifth sensor arrived after the Sterling tests and was sent to the FERREL for tests using the shipboard checkout hardware.

Five wind direction sensors (Model 2053) were tested in the laboratory for measurement accuracy. All sensors performed within the manufacturer's specifications of ± 5 degrees.

Ten temperature sensors (Model 1289A) were tested over their operating range. All performed within specified accuracies of $\pm 0.05^{\circ}\text{C}$ when a zero correction was applied and within $\pm 0.1^{\circ}\text{C}$ without the zero correction. The zero correction was not necessary to meet NOS survey requirements.

Six air pressure sensors (Model 2056) were calibrated upon arrival at T&EL. Use of the manufacturer's transfer function resulted in measurement errors outside of the specification of ± 0.6 percent of full-scale reading (FSR). A second-order transfer function with a temperature term was computed by T&EL to provide the required accuracy.

5.2.2. Calibration Data Summary

ECU's for the meteorological measurands were computed in a manner similar to that described for the current meter measurands (section 5.1.2).

Wind Speed (4 sensors)

Total Systematic Uncertainty (TSU):	$\pm 0.15 \text{ m/s}$
Residual Standard Error (RSE):	$\pm 0.22 \text{ m/s}$
Estimated Calibration Uncertainty (ECU):	
$\text{ECU} = \text{TSU} + 2.1 (\text{RSE}) = \pm 0.62 \text{ m/s}$	$\pm 0.62 \text{ m/s}$

Wind Direction (5 sensors)

Total Systematic Uncertainty (TSU):	± 1.0 degree
Residual Standard Error (RSE):	± 2.5 degrees
Estimated Calibration Uncertainty (ECU):	
ECU = TSU + 1.96 (RSE) = ± 6.0 degrees	± 6.0 degrees

Temperature (10 sensors)

Total Systematic Uncertainty (TSU):	$\pm 0.008^{\circ}$ C
Residual Standard Error (RSE):	$\pm 0.11^{\circ}$ C
Estimated Calibration Uncertainty (ECU):	
ECU = TSU + 1.96 (RSE) = $\pm 0.23^{\circ}$ C	$\pm 0.23^{\circ}$ C

Air Pressure (6 sensors)

Total Systematic Uncertainty (TSU):	± 0.1 mbar
Estimated Calibration Uncertainty (ECU):	

<u>Sensor SN</u>	<u>ECU</u>
65	± 1.7 mbar
76	± 1.5 mbar
79	± 1.4 mbar
89	± 0.7 mbar
95	± 1.2 mbar
96	± 0.7 mbar

5.2.3. Mid-Survey Calibration

During the survey, two air pressure sensors were returned to T&EL for an interim calibration. An ECU was computed for each sensor based on the derivation of a new transfer function.

<u>Sensor SN</u>	<u>ECU</u>
65	± 1.3 mbar
89	± 0.9 mbar

5.2.4. Post-Survey Calibration

At the conclusion of the survey, all the meteorological stations were returned to the laboratory. Each sensor underwent operational checks, and calibrations were performed on temperature and air pressure sensors.

The operational checks of the data loggers found problems with encoder adjustments and supply spool tension; the data loggers

were returned to the manufacturer for repairs. One wind speed sensor did not operate, and the dampening fluid in two direction sensors had leaked. These sensors were also returned to Aanderaa for repairs. One temperature probe was inoperative when returned. Eight of the nine remaining probes performed to within $\pm 0.13^{\circ}\text{C}$, and one indicated a drift of -0.17°C . Calibration of the air pressure sensors revealed significant drift in two sensors, but these sensors may have been damaged during shipment.

The following are the ECU's determined from the post-survey calibrations.

Temperature (9 sensors)

Estimated Calibration Uncertainty (ECU): $\pm 0.18^{\circ}\text{C}$

Air Pressure (6 sensors)

<u>Sensor SN</u>	<u>ECU</u>
65	+ 1.1 mbar
76	+ 1.0 mbar
79	+ 1.3 mbar
89	+ 0.7 mbar
95	+ 1.1 mbar
96	+ 1.7 mbar

Uncertainties for the air pressure sensors are based on new transfer functions. Section 7 addresses sensor drift.

5.3. AANDERAA MODEL WLR-5 WATER LEVEL RECORDERS

T&EL performed I&A tests and calibrations on three Aanderaa Model WLR-5 water level recorders prior to acceptance and survey use. One instrument was returned to T&EL for calibration following 5 months of survey operations. At the completion of the survey, the three instruments were returned for calibration.

5.3.1. Inspection and Acceptance Tests

A visual inspection was made to assure acceptable design and construction as well as to check for any shipping damage which may have occurred. After no deficiencies were found, the instruments were subjected to operational checks. The selected sample interval

for one unit was found to be incorrect; it would sample at intervals equal to the selected interval plus the instrument integration time. The manufacturer provided a replacement circuit board, which was installed by T&EL personnel. The recording system of each instrument was verified using T&EL's tape translator.

Following the operational checks, a pressure calibration was performed on each instrument. One unit leaked during the initial test at low pressure; a manufacturer's representative replaced the transducer fitting to resolve this problem. All three instruments failed to meet specifications when the manufacturer's transfer function was used; new transfer functions were computed by T&EL for each sensor.

5.3.2. Calibration Data Analysis

Total Systematic Uncertainty (TSU): $\pm 0.3 \times 10^{-2}$ dbar

Estimated Calibration Uncertainty (ECU):

ECU = TSU + worst-case, 95-percent confidence limits:

<u>Instrument SN</u>	<u>ECU</u>
360	$\pm 1.2 \times 10^{-2}$ dbar
361	$\pm 0.7 \times 10^{-2}$ dbar
362	$\pm 1.2 \times 10^{-2}$ dbar

5.3.3. Mid-Survey Calibration

In October 1978, SN 361 was returned to T&EL for calibration. This instrument was selected based upon field-check data that indicated sensor drift. The calibration procedure used for the I&A tests was followed, and a new transfer function was computed.

The calibration indicated an ECU for this sensor of $\pm 0.9 \times 10^{-2}$ dbar. No change was made in the sensor equation used for processing survey data.

5.3.4. Post-Survey Calibration

At the completion of the survey, the three instruments were recalibrated.

The following are the ECU's established from post-survey calibration:

<u>Instrument SN</u>	<u>ECU</u>
360	$\pm 1.1 \times 10^{-2}$ dbar
361	$\pm 0.7 \times 10^{-2}$ dbar
362	$\pm 1.0 \times 10^{-2}$ dbar

These uncertainty estimates are based upon new transfer functions. Section 7 addresses sensor drift.

5.4. APPLIED MICROSYSTEMS MODEL 750A WAVE HEIGHT RECORDERS

Three Applied Microsystems (AMI) Model 750A wave height recorders underwent I&A tests and calibrations prior to acceptance and use. One instrument was returned to T&EL for calibration following 5 months of survey operations. At the completion of the survey, all three units were recalibrated.

5.4.1. Inspection and Acceptance Tests

A visual inspection of the instruments showed no deficiencies. Operational checks found faulty magnetic tape takeup reel tension in one instrument; the manufacturer was consulted, and the tension of all three instruments was adjusted. One instrument time base was found to be outside of specification. Although a spare time-base board was installed, it was also outside of specification. The manufacturer suggested that a component be replaced in both boards; this corrected the problem. Magnetic tapes were verified using T&EL's tape translator.

Following the operational checks, a pressure calibration was performed on each instrument. Measurement errors that resulted from using the manufacturer's transfer function were outside of specifications for all three instruments. T&EL computed new transfer functions, based on test data, for each instrument. The computed transfer functions provided accuracy within manufacturer's specifications.

5.4.2. Calibration Data Summary

Total Systematic Uncertainty (TSU): $\pm 0.7 \times 10^{-2}$ dbar

Estimated Calibration Uncertainty (ECU):

ECU = TSU + worst-case, 95-percent confidence limit:

<u>Instrument SN</u>	<u>ECU</u>
131	$\pm 1.9 \times 10^{-2}$ dbar
132	$\pm 1.9 \times 10^{-2}$ dbar
133	$\pm 1.4 \times 10^{-2}$ dbar

5.4.3. Mid-Survey Calibration

In October 1978, instrument SN 133 was returned for calibration. This instrument was selected because field-check data indicated sensor drift.

No operational problems were encountered. The calibration indicated a sensor uncertainty of $\pm 1.1 \times 10^{-2}$ dbar.

5.4.4. Post-Survey Calibration

At the completion of the survey, the AMI systems were calibrated at T&EL. All instruments were operational when returned.

The ECU's based on the post-survey calibration are as follows:

<u>Instrument SN</u>	<u>ECU</u>
131	$\pm 1.5 \times 10^{-2}$ dbar
132	$\pm 1.3 \times 10^{-2}$ dbar
133	$\pm 1.0 \times 10^{-2}$ dbar

These uncertainties are based on new transfer functions. Section 7 addresses sensor drift.

5.5. GRUNDY MODEL 9400 CTD SYSTEM

The Grundy Model 9400 CTD system with an optional DO sensor was calibrated before the survey to establish its measurement capability. The system was recalibrated after 8 months of survey operation and at the conclusion of the survey.

5.5.1. Initial Calibration

I&A tests and calibrations were performed on each sensor of the system. Operational checks were also performed on the Grundy Model 8428 data logger that was used to record the Model 9400 data.

The conductivity sensor (Model 6500) calibration sequence consisted of two temperature cycles of 13 test points each in a 35-ppt salinity bath. Use of the manufacturer's transfer function resulted in measurement errors greater than ± 0.12 mS/cm. Further testing indicated that temperature effects on the conductivity cell and electronics were the major source of the errors. Wire-loop conductance measurements were taken at five temperatures to define the magnitude of the sensor temperature coefficient. A multiple-regression analysis was performed on the wire-loop data to provide an equation for conductance as a function of sensor output frequency and temperature. This equation was combined with the average cell constant of the sensor (computed from the original bath data) to produce a sensor calibration equation for conductivity as a function of sensor output and temperature.

The temperature sensor (Model 4500) calibration was performed simultaneously with the conductivity cycle. Use of the manufacturer's transfer function resulted in an average offset error of -0.05° C. To improve the sensor accuracy, a least-squares curve fit was performed to provide a new sensor transfer function.

The depth sensor (Model 4600) calibration consisted of pressure cycles performed at three temperatures. Because sensor errors that resulted from using the manufacturer's transfer function were within specified accuracy, a computed transfer function was not required. Problems were encountered early in the testing when a leak was detected in the sensor's electronics housing. The sensor "O"-ring seal was replaced and testing continued.

Tests were conducted to determine the performance of the DO sensor (Model 5175). After significant drift was encountered during the first series of tests, the sensor was returned to the manufacturer for repair. Upon its return to T&EL, a second series of tests was performed. Serious drift and operational problems were again encountered, and the DO sensor (supplied to Grundy from another manufacturer) along with its support electronics were returned to Grundy to obtain a credit for its cost.

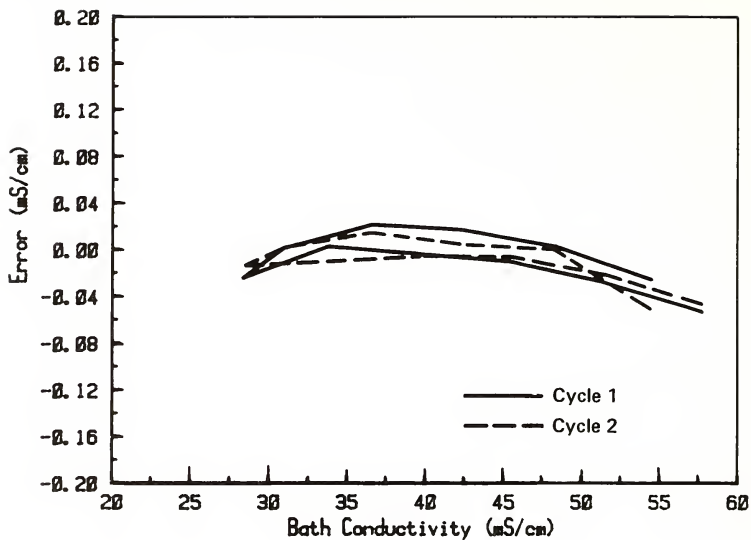


Figure 28.--Residual error of Grundy Model 9400 conductivity sensor based on T&EL transfer function.

5.5.2. Calibration Data Summary

(Residual errors are shown in figures 28 through 30.)

Conductivity Sensor

Total Systematic Uncertainty (TSU):	± 0.013 mS/cm
Residual Standard Error (RSE) based on computed transfer functions:	± 0.023 mS/cm
Residual error plot:	(See figure 28.)
Estimated Calibration Uncertainty (ECU):	
ECU = TSU + 2.04 (RSE) = ± 0.060 mS/cm	± 0.060 mS/cm

Temperature Sensor

Total Systematic Uncertainty (TSU):	$\pm 0.006^{\circ}$ C
Residual Standard Error (RSE) based on computed transfer function:	$\pm 0.012^{\circ}$ C
Residual error plot:	(See figure 29.)
Estimated Calibration Uncertainty (ECU):	
ECU = TSU + 2.03 (RSE) = $\pm 0.03^{\circ}$ C	$\pm 0.03^{\circ}$ C

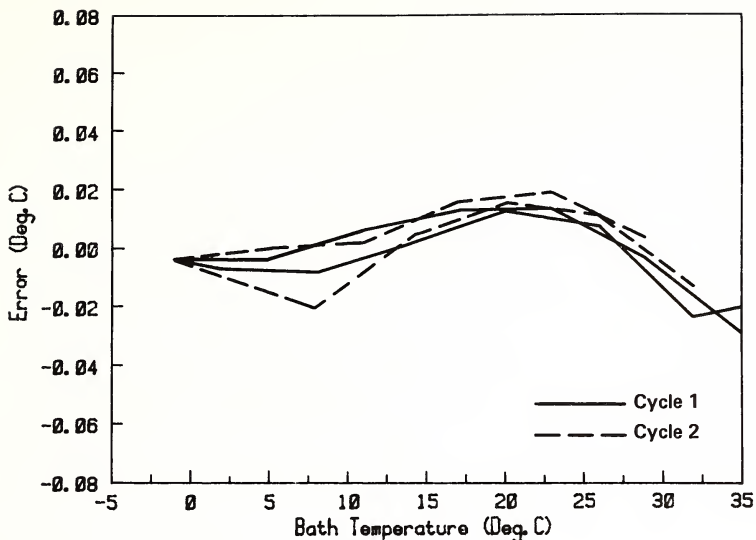


Figure 29.--Residual error of Grundy Model 9400 temperature sensor based on T&EL transfer function.

Depth (Pressure) Sensor

Total Systematic Uncertainty (TSU):	± 0.17 dbar
Residual Standard Error (RSE):	± 0.32 dbar
Residual error plot:	(See figure 30.)
Estimated Calibration Uncertainty (ECU):	
ECU = TSU + 2.05 (RSE) = ± 0.83 dbar	± 0.83 dbar

5.5.3. Mid-Survey Calibration

Following 8 months of survey operations, the Grundy Model 9400 system was returned to T&EL for calibration. The procedure and transfer function established during the initial calibration were applied for these tests. The following are the derived calibration uncertainties for each sensor (based on the RSE). Because no significant sensor drift was detected, new transfer functions were not required.

Conductivity Sensor

Estimated Calibration Uncertainty (ECU):	± 0.11 mS/cm
--	------------------

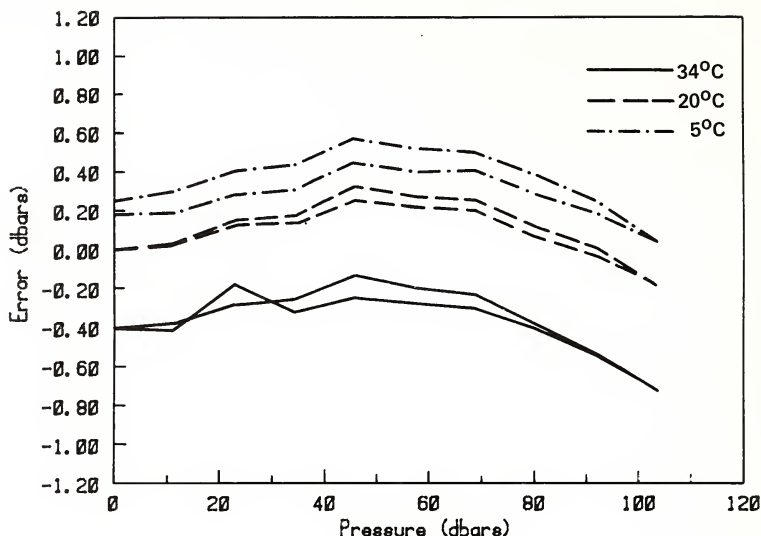


Figure 30.--Residual error of Grundy Model 9400 depth sensor based on T&EL transfer function.

Temperature Sensor

Estimated Calibration Uncertainty (ECU): $\pm 0.04^{\circ} \text{C}$

Depth (Pressure) Sensor

Estimated Calibration Uncertainty (ECU): $\pm 1.1 \text{ dbar}$

5.5.4. Post-Survey Calibration

At the conclusion of the survey, the CTD system was returned to T&EL. The calibration of the temperature sensor indicated a calibration shift that resulted in an offset error of 0.13°C . The depth sensor was not operational when the system arrived at T&EL. (Refer to section 7 for ECU values for the conductivity and temperature sensors.)

5.6. INSTRUMENT FIELD-CHECK TEST STANDARDS

The standards used for the instrument field checks were calibrated at T&EL before and after the survey; an additional mid-survey calibration was performed on the pressure standard,

assuring the traceability of the field-check measurements that were conducted on the FERREL.

5.6.1. Paroscientific Pressure Sensor

A Paroscientific Model 2100A absolute pressure transducer was used as part of the instrument field checkout hardware. This sensor was calibrated three times during the project. The initial calibration determined that the manufacturer's transfer function did not provide the required accuracy; therefore, a transfer function was generated by T&EL for each calibration.

The estimated uncertainties, as determined from the calibrations, are described below:

Total Systematic Uncertainty (TSU): $\pm 0.7 \times 10^{-2}$ dbar

Estimated Calibration Uncertainty (ECU):

ECU = TSU + worst-case, 95-percent confidence limit:

May 1978	ECU = $\pm 1.6 \times 10^{-2}$ dbar
December 1978	ECU = $\pm 1.6 \times 10^{-2}$ dbar
August 1979	ECU = $\pm 1.8 \times 10^{-2}$ dbar

5.6.2. Yellow Springs Instruments (YSI) Model 777 Thermometer

A YSI thermometer was calibrated for use as the shipboard temperature standard. Adjustments were required to achieve the required accuracy of $\pm 0.05^{\circ}$ C. A second calibration at the end of the survey found the accuracy still within the $\pm 0.05^{\circ}$ C with no adjustment necessary.

5.6.3. Hewlett-Packard (HP) Model 5328A Counter

The HP5328A counter was used on the FERREL for time-base checks and rotor spin-down tests. T&EL calibrated the counter before and after the survey and encountered no significant drift problems.

5.7. INSTRUMENT TRANSFER FUNCTION

T&EL performed I&A tests and calibrations on five different types of oceanographic instruments with 13 sensors, not including time bases. Not one of the instrument models would have performed within the

accuracy requirements set for the project, that were no more demanding than the manufacturer's specifications, had the appropriate transfer functions not been developed. Instrument transfer functions are listed in appendix B.

The T&EL-derived transfer functions were used to process the following data: Grundy Model 9021 current speed, Aanderaa air pressure, Aanderaa water pressure (water level), Applied Microsystems water pressure (wave height), Grundy Model 9400 conductivity and temperature, and Paroscientific Model 2100A pressure (pressure sensor checkout). The manufacturers' transfer functions were used for all other sensors.

6. FIELD DATA QUALITY CONTROL

by Gerald F. Appell, Algis N. Kalvaitis, Thomas N. Mero, and
Charles R. Roman

An essential element of the DQA effort was field data quality control aboard the NOAA Ship FERREL. A field check system was designed and built by EDL and installed onboard the FERREL. Requirements for the system were set by T&EL with guidance from the NOS Project Manager. Field checks provided the capability to (1) monitor instrument performance in the field and detect sensor drift, (2) determine the optimal calibration cycle for sensors, (3) provide a traceable link for the uncertainty estimates, and (4) provide a history of instrument performance during the 12-month period. The tests also provided information on sensor malfunctions so that corrective action could be taken prior to deployment.

6.1. FIELD CHECK SYSTEM

The field check equipment was designed to provide information on each instrument's performance. Engineering was concentrated in the design of mechanical fixtures for interfacing the field check equipment to the different instrumentation. Most of the equipment was rack-mounted for ease of operation and storage. Figure 31 shows the field check equipment installed in the electronics shop aboard the FERREL.

Rotors on the current meters and wind speed sensors were checked for bearing quality using a spindown test. Throughput verification of the speed measurement was performed by driving the rotor with an air jet to a measured rpm value and comparing this value with the instrument output. These checks provided assurance that the rotors and measurement circuits performed within established quality levels.

The current meter compass check verified that gimbal sticking problems were not occurring and that the compass was free to respond. This was a quality check to assure that the compass was functioning.



Figure 31.--Field check system onboard the NOAA Ship FERREL. Equipment rack is at far left; temperature bath is in foreground; rotor check hood is installed on a Grundy 9021 current meter for speed throughput and rotor spindown tests.

Conductivity and temperature checks were performed as follows: A Vishay Model 40 decade resistance box was used as part of a wire-loop check of the conductivity cells on the current meters and the Grundy Model 9400 profiling CTD. This method provided system throughput verification of conductivity but could not check for external cell contamination that could affect the cell calibration constant. A bath check was designed to determine calibration changes due to marine fouling and antifoulant coatings applied on the cells. The bath used was a 38-liter insulated container filled with seawater. Comparison checks were made using the Grundy Model 9400 CTD. The same bath was used to check all temperature sensors at both ambient and ice-point temperatures. A Yellow Springs Instruments Model 777 temperature probe was used as the comparison standard.

Time-base checks on all instruments were made using an HP5328A universal counter as the standard.

Pressure measuring sensors were checked shipboard using a Paroscientific, Inc., Model 600 Digiquartz Pressure Measurement System as a standard. Dry nitrogen gas was used to generate pressure, and a Volumetrics Model BCE-1 Precision Control Console was used to regulate the pressure. A vacuum capability was also provided to check the barometric pressure transducers from the meteorological stations.

Field check results were documented through shipboard field check logs, printer/verifier output records, and spindown X-Y plotter graphs. Documented results were sent to T&EL for DQA analysis after each cruise. The shipboard standards were maintained and calibrated by T&EL.

6.2. FIELD CHECK PROCEDURES

Detailed procedures outlining each of the above tests were produced by EDL. The procedures are described in an unpublished report (National Ocean Survey 1978); copies are on file at the NOS Office of Oceanography and also at the NOS Test and Evaluation Laboratory.

Table 6.--Data quality levels

INSTRUMENT PARAMETER	FIELD STANDARD	DATA QUALITY LEVEL (DQL)	REJECTION LEVEL (RL)
Grundy Model 9021			
Current Meter			
speed throughput	Note 1	+ 5 counts	+ 10 counts
direction	Note 1	Template	Template
temperature	Note 2	512 counts \pm 40 counts	512 counts \pm 100
conductivity	Note 3	+ 0.20 C	+ 1.00 C
time base	Note 4	\pm 1 count	\pm 5 counts
	Note 1	60 s \pm 0.001 s	\pm 0.01 s
Aanderaa Model WLR-5			
Water Level Gage			
pressure	Note 5	\pm 3 mbar	\pm 15 mbar
time base	Note 1	488.2813 μ s \pm 4 ns	\pm 20 ns
AMI Model 750A			
Wave Gage			
pressure	Note 5	+ 3 mbar	+ 15 mbar
time base	Note 1	429.1534 μ s \pm 0.8 ns	\pm 20 ns
Aanderaa Meteorological			
Sensors			
speed throughput	Note 1	+ 1 count	+ 4 counts
direction	Note 1	Template	Template
temperature	Note 6	+ 5 degrees	+ 10 degrees
pressure	Note 3	+ 0.10 C	+ 1.00 C
time	Note 5	+ 3 mbar	+ 15 mbar
	Note 1	61.03516 μ s \pm 1 ns	10 ns
Grundy Model 9400 CTD			
temperature	Note 3	+ 0.20 C	+ 1.00 C
conductivity	Note 4	\pm 2.0 Hz	+ 0.12 mS/cm
pressure	Note 5	\pm 55 mbar	\pm 1 m H ₂ O

* Accumulated 24-hr error at RL

- 1 - Hp Model 5328A Universal Counter
 2 - Magnetic source
 3 - YSI Model 777 Thermistor
 4 - Vishay Model 40 Decade Resistor
 5 - Paroscientific Model 245A Pressure Transducer
 6 - Angular index

6.3. DATA QUALITY AND REJECTION LEVELS

Table 6 shows the criteria developed to provide guidance to shipboard personnel. Field check results were matched to the criteria, so that decisions concerning instrument disposition could be made.

A data quality level (DQL) was established based upon the measurement capability of shipboard standards and field equipment plus the desired control of the parameter. Measurements taken with the field check equipment were compared within the DQL of the instrument being checked. The check results were documented and sent to T&EL for analysis; T&EL monitored instrument stability.

If the DQL was exceeded during field checks, instructions specified the action to be taken. In most cases the instrument would be used, and T&EL would be notified of the discrepancy. T&EL would either request additional shipboard instrument tests or have the instrument returned to T&EL for calibration.

When the DQL was exceeded by a wide margin, an instrument's measurement was considered unacceptable. The rejection level (RL) was provided as a guide to determine whether or not an instrument was acceptable for deployment. The establishment of an RL was based upon the need to avoid a judgment decision in the field. The RL signifies a malfunctioning sensor or one that is exhibiting a stability problem.

Instruments that exceeded the RL were not deployed but returned to T&EL, with appropriate documentation, for repair and recalibration.

6.4. TRAINING

A training program was established for ship's personnel to assure that field check equipment and project instruments were operated and maintained properly aboard the FERREL.

T&EL and EDL representatives provided training at Berwick, La., in the operation of field check equipment, quality control operations, and documentation. Trial deployments were conducted in the Atchafalaya River and at one of the project test sites to develop the proper deployment and recovery procedures. T&EL representatives also provided training in laboratory techniques for micro-Winkler dissolved oxygen analysis and on the operation of the Guildline Model

8400 Autosal Laboratory Salinometer; this training was conducted first in Washington, D.C., and after installation of the laboratory gear aboard the FERREL.

Representatives from Grundy Environmental Systems, Inc., Aanderaa Instruments, Ltd., and Applied Microsystems, Inc., provided training in operation, care, and maintenance of each of their respective instruments.

6.5. SUMMARY OF INSTRUMENT FIELD PERFORMANCE AND MEASUREMENT QUALITY CONTROL

The field check results and observations of instrument field performance provided the basis for establishment of measurement history from pre-survey calibration through post-survey calibration. This measurement traceability was used in sections 7 and 9 to justify the measurement uncertainties established.

Field check results of the current meter speed measurement were useful as a guide for maintenance and repair actions. Rotor balance adjustments and bearing, reed switch, and rotor replacements were all part of the activities required to maintain the current speed measurement quality control. Shipboard bath checks indicated that conductivity measurements were being seriously degraded by barnacle fouling. This resulted in a series of corrective actions to provide fouling protection and restore quality control to the conductivity measurement. Other field checks indicated that, after corrective actions, most sensors measured within the established RL and, of these sensors, approximately 95 percent measured within the DQL.

Diver observation of the current meter attitude within the platforms revealed that the meters were not level. *In situ* measurements indicated a ± 15 -degree uncertainty in vertical attitude during June and July 1978. Diver adjustments and changes in procedures decreased the uncertainty to ± 10 degrees during the remainder of the survey.

7. UNCERTAINTY ESTIMATES

by Algis N. Kalvaitis, Philip J. Bowen, and Michael A. Basileo

One of the most important characteristics of a data set is its accuracy, or closeness of the measured value to the true value. Strictly speaking, the actual error of a measured value is unknowable, both in magnitude and direction. Limits to the error can be estimated, however, by knowledge of the measurement process and sensitivities to controlled and uncontrolled factors. The information contained in the uncertainty analysis determines the ultimate worth of the data. The usefulness of a reported value whose accuracy is totally unknown is very limited.

The estimation of measurement uncertainty is a necessary process in any DQA effort and should be continuously refined as error estimates are updated. In the initial planning stages, preliminary error analyses were conducted to determine if the original scientific and engineering data requirements had been satisfied. This section describes the final uncertainty estimates for each parameter along with the rationale, methodology, and analysis with which they were derived.

7.1. TRACEABILITY OF MEASUREMENTS

The traceability from the field data to recognized standards is the foundation for a measurements program and the basis for the uncertainty estimates. A standard is defined as a quantity with attributes known to a fundamental level of uncertainty. For the NOS/SPR Support Project, the standards were located at various laboratories, including T&EL, and onboard the NOAA Ship FERREL. The laboratory standards (table 7) were used in the calibration and testing of the meteorological and oceanographic instruments. These standards are traceable to the National Bureau of Standards (NBS) or to other internationally recognized standards. Measurement traceability in the field was maintained through the use of a multiparameter suite

Table 7. Laboratory Standards

<u>Parameter</u>	<u>Standard</u>	<u>Estimated Uncertainty</u>	<u>Location of Facility</u>
Temperature	NBS-calibrated platinum resistance thermometer and Mueller bridge verified by triple point of water cell.	+ 0.003 ^o C	T&EL, Washington, D.C.
Pressure	Dead-weight piston gage calibrated by NBS.	+ 0.1 mbar (air) + 0.003 dbar (water)	T&EL, Washington, D.C.
Water Speed	Tow carriage speed derived from measurements of distance and time which are traceable to NBS. Residual flows or stray currents excluded from uncertainty estimate.	+ 0.10 cm/s	DT-NSRDC Carderock, Md.
Air Speed	Wind tunnel with speeds monitored by a Pitot static tube calibrated at NBS.	+ 0.5 m/s	NWS, Sterling, Va.
Magnetic Direction	Compass rose and/or magnetometer calibrated at NBS, and precision compass.	+ 1 degree of arc	Geomagnetic Center, Corbin, Va.
Conductivity	Guildline Autosol and IAPSO standard seawater. T&EL secondary seawater standards.	+ 0.006 mS/cm	T&EL, Washington, D.C.

of shipboard standards that was used to verify instrument condition prior to deployment. The shipboard standards were calibrated a minimum of two times at T&EL during the survey operation. The shipboard standards and hardware are described in section 6.

7.2. ERROR IDENTIFICATION

The initial step in estimating the measurement uncertainties was to list the error sources which might have contaminated the data. Possible error sources were divided into the following major groups: instrument characteristics; calibration, sampling, environmental influences, and analytical uncertainties; and human errors.

7.2.1. Instrument Characteristics

The instruments and sensors exhibit characteristics which introduce error sources. These uncertainties are the result of several limitations inherent in the instrument design.

Input variations to or within the instrument, generally voltage, may cause errors. Data may be degraded in transmission from one instrument component to another, e.g., from sensor to recorder. Errors in instrument output may be introduced by nonlinearities and

quantization noise in an analog-to-digital converter. Information carried by an electrical waveform may be distorted by filtering or by amplifier saturation (clipping). Errors in instrument output may also be caused by energy absorption (hysteresis) or the instability (drift) of the sensor or other component.

The accuracy of the measurement is limited by the resolution or readability of an analog signal or the number of significant digits in a digital output. Finally, the precision or degree of reproducibility among repeated measurements under constant input is seldom perfect.

7.2.2. Calibration Uncertainties

Calibration, or the act of comparing instrument outputs to a known reference quantity (standard), is a source of uncertainty. Calibration uncertainties also include the inability of a transfer function to describe instrument responses completely.

The uncertainty of the transfer or reference standard includes uncertainties in the process used to calibrate them. Operating characteristics of the facility may introduce uncertainties. An example is the inhomogeneity and drift rate of a temperature bath. The laboratory calibration may not simulate adequately the total environment in which the instrument operates. A current meter is calibrated in still water although the *in situ* flow field may be highly turbulent. Placement of an instrument in a facility may induce errors due to the relative sizes of instrument and facility (e.g., velocity blockage in water flow facilities and wind tunnels).

A transfer function mathematically describes a series of instrument outputs as a function of known inputs, generally over the full range. Departures in instrument response from the smoothed trend cannot be accounted for by the transfer function and will result in measurement uncertainties. In addition, the use of the single transfer function to represent a group of "identical" instruments will usually result in broadened uncertainty bands because the instruments are not necessarily identical.

7.2.3. Sampling Uncertainties

The measurement process often includes temporal and spatial limitations and, in some cases, an insufficient density and duration

of measurements to detect short-term phenomena or long-term trends.

The measurement system may introduce a change in the quantity being measured. For example, an anemometer may be in the lee of a platform that could distort significantly the local velocity field. Uncertainties as to precisely when or where a measurement was made can affect the validity of certain data. For example, a vertical or horizontal displacement of a sensor may introduce errors, particularly in large gradients. Also, an inadequate number of measurements or a long averaging interval may not indicate large departures from the mean.

A final uncertainty concerns the possible contamination of samples, either during sampling or storage. Every possible precaution should be exercised to avoid any contamination of data.

7.2.4. Environmental Influence Uncertainties

The ideal sensor should respond to a single physical parameter regardless of the environment in which the measurement is being made. Unfortunately, many sensors respond to more than the parameter of prime interest. For example, a pressure sensor is generally affected by temperature variations unless compensating corrections are applied.

The motions of a measurement platform, instrument, and/or the unsteadiness of the parameter being sensed can induce large errors. A particularly vulnerable parameter is current velocity. Both speed and direction records can be contaminated by an unsteady flow field and the accompanying imperfect response of the transducers under these conditions.

The orientation of the instrument may cause measurement difficulties. For example, a misalignment of a current speed sensor relative to the flow field will contribute uncertainties.

Fouling/corrosion may produce long-term drift or failure. A rotating element current meter may become totally immobilized by biofouling. Salt deposits on air temperature probes produce errors during crystalization and deliquescence phases.

The local environment may be affected by solar radiation or convection heating and by elevated wind speeds. Radiation from the measurement platform or water surface may result in heating the probe; convection currents from the platform may induce local heating of

the air and subsequent errors. Uncertainties in air pressure measurement will occur at elevated wind speeds due to a pressure change (Venturi effect) at the barometer inlet port. Water pressure transducers in high currents are similarly affected.

7.2.5. Analytical Uncertainties

The processing of instrument data introduces uncertainties and should be taken into consideration. Significant figures of data sets may be rounded or truncated during the processing cycle and may result in errors. High-pass or low-pass filtering will mask the original measurements.

7.2.6. Human Errors

Human errors are those introduced by operators at any point in the data collection, transfer, analysis, and reporting chain. Human errors may be introduced during the data collection phase and consist of reading instruments incorrectly, transposing digits, recording incorrect values, etc. The human factor is important from the standpoint of following written procedures and performing any mathematical manipulation.

7.3. ERROR ANALYSIS

Quantitative estimates of some errors described in the previous section were obtained empirically through testing and calibration of the various sensor systems. The analyses are applicable, except where noted, to all instruments of a given model and are designed to bound typically occurring errors (at the 95-percent confidence level) rather than worst-case values. In this error analysis, the bases for determining Estimated Calibration Uncertainty (ECU), Sensor Measurement Uncertainty (SMU), and Total Measurement Uncertainty (TMU) are given.

7.3.1. Estimated Calibration Uncertainty (ECU)

Instrument characterization and calibration errors were determined from the calibration process and results. These errors define instrument performance under controlled conditions.

Calibration data were treated in one of two ways, depending on instrument type. One method was to use a single transfer function

to describe a group of sensors of the same model. The single equation was either furnished by the manufacturer or determined by the calibration process. The second method was to determine individual transfer functions for each sensor of a given model by using least-squares, curve fitting techniques. This approach was necessary for those sensors requiring a more complex transfer function because of significant nonlinearity or temperature dependence.

The departure of each sensor from its transfer function was determined by computing residuals. Residuals are the differences between the measured value (Y_m) of the physical parameter and that predicted (Y_p) by substituting sensor output at each calibration point into the transfer function. To arrive at a representative estimate of this departure, the Residual Standard Error (RSE) was computed:

$$RSE = \left[\sum (y_p - y_m)^2 / (n-k) \right]^{1/2} \quad (\text{Summation is for } i = 1 \text{ to } n.), \quad (9)$$

where $(y_p - y_m)$ is the residual,

n is the number of points,

and k is the number of fitted constants or

is equal to 1 for supplied transfer functions.

To arrive at a statistical boundary to the uncertainty of values predicted by the transfer function, confidence intervals can be computed. The confidence interval is the estimated range of values of a measurement which will contain the true value. Thus, for a 95-percent confidence interval, there is a 95-percent probability that the true value of the measurement is contained in the region bounded by the indicated value plus or minus the computed confidence interval.

For individual transfer functions obtained by least-squares fits to calibration data, confidence intervals were obtained with the following equation:

$$W_h = \pm (t) (RSE) (1 + [h]' ([X]' [X])^{-1} [h])^{1/2}, \quad (10)$$

where $[X]$ is the n by k matrix of independent variable data,
 $[X]'$ is the transpose of the data matrix (k by n),
 $[h]$ is the k by 1 vector of independent variables about
 which the confidence level is computed,
 $[h]'$ is the transpose of $[h]$ (1 by k),
 RSE is the residual standard error of the curve fit,
 t is the value of Student's "t" distribution for $(n-k)$
 degrees of freedom at the 0.95 level (Natrella 1963),
 and $\pm W_h$ is the 95-percent confidence interval about the fitted
 equation at $[h]$.

As can be seen from the above equation, the value of W_h depends
 somewhat on the value of the independent variables. Maxima occur at
 the ends of the calibration range; a minimum occurs at the center of
 the range. The values shown for 95-percent confidence intervals in
 this report represent the maximum values.

For the case where a single transfer function was used to
 describe a group of sensors, confidence intervals were computed
 using

$$W_h = \pm(t) (RSE), \quad (11)$$

where the variables are as previously defined, except that $(n-1)$
 degrees of freedom were used and RSE was computed using residuals
 from the supplied transfer function.

Generally speaking, the confidence limits were found to be two to
 three times the RSE, depending upon the number of degrees of freedom.

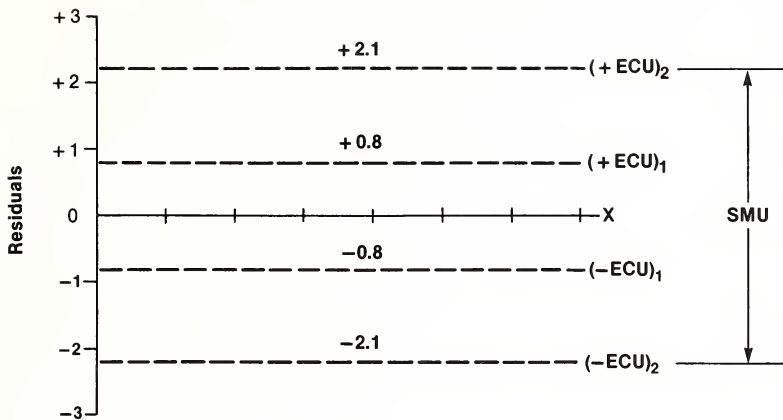
The ECU was computed by summing the systematic error components
 with the 95-percent confidence limit of the sensor transfer function.
 Systematic errors are defined as uncertainties associated with the
 calibration process, standards, and facilities. Values given for
 systematic errors in this report have been derived from calibration
 certificates for the measurement standards, measurement histories
 associated with the standards, prior measurements of facility capa-
 bilities, and prior experience with the measurement processes. The
 ECU thus represents the performance characteristics of the measurement
 systems under laboratory conditions.

7.3.2. Sensor Measurement Uncertainty (SMU)

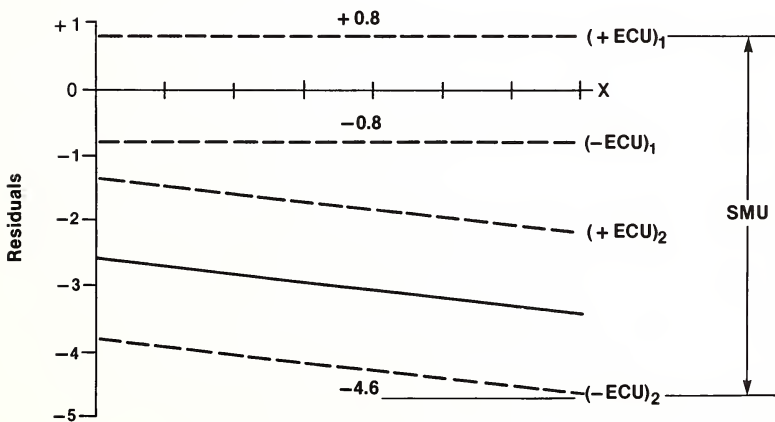
The SMU is computed to provide an estimate of measurement system error over a defined period of time. Transportation, deployment, and aging of electronic components can be expected to cause deviations from an initial laboratory calibration. The magnitude of this deviation can be estimated by performing another laboratory calibration at the end of the field data acquisition phase. Comparison of the pre- and post-survey calibrations is then used as the basis for determining the SMU for the time period between calibrations. Note that this approach is valid only if it can be assumed that, during the interval, the instrument response did not shift greatly and then return to the pre-survey value. For this project, field-check records and interim calibrations on selected instruments, along with prior knowledge of the performance characteristic of some of the instruments, were used to verify this assumption.

The uncertainty levels defined by the SMU represent 95th percentile errors for the defined time period; i.e., the levels are exceeded in only 5 percent of the data. Figure 32a portrays typical results for the case where uncertainty analysis has been applied to a group of sensors. The units on the ordinate are arbitrary for the purposes of this discussion. Assume the original calibration for the group of sensors yielded an ECU (systematic errors plus 95-percent confidence level) of ± 0.8 . After some period of field usage, the sensors were again calibrated with respect to the original transfer function. The ECU computed for the second calibration is shown as ± 2.1 . Because the results of the second calibration encompass totally those of the first calibration, the second ECU is used as the SMU for the interval between calibrations. While it is true that the group of sensors had smaller uncertainty at the beginning of the interval, lack of interim calibration data precluded any valid attempt at apportioning the apparent degradation as a function of time. The approach taken throughout the uncertainty analysis, therefore, is to define a single value for SMU that can be applied to the entire time interval.

Another example of typical results is shown in figure 32b. This type of behavior was generally observed when performing an uncertainty analysis for a single sensor. As shown, a net drift occurred between the two laboratory calibrations. In the analysis,



(a)



(b)

Figure 32.--Graphic description of Sensor Measurement Uncertainty (SMU).

the ECU for each calibration was computed along with the drift between calibrations. The value computed for SMU in these cases was the summation of the ECU from calibration 1, the maximum net drift and the ECU from calibration 2. The SMU computed in cases where net drift is significant would be asymmetrical; for example, in figure 32b, the SMU would be +0.8, -4.6.

In summary, the SMU represents an estimate of measurement system uncertainty that includes the changes in sensor performance caused by usage in the field environment. While typically greater than the ECU, the SMU does not usually address all possible factors pertinent to the uncertainty of data gathered in the field survey. The missing factors are addressed in the following section on Total Measurement Uncertainty.

7.3.3. Total Measurement Uncertainty (TMU)

A realistic estimate of instrument measurement capability in the marine environment may be described by incorporating other error components inherent in the measurement process. This estimate is termed the TMU and reflects a statistical determination of the overall error associated with the marine data. It includes the calibration uncertainties (ECU), instrument drift, and other error components associated with the *in situ* measurement process, such as biofouling or solar radiation. For the purposes of this analysis, the TMU is intended to bound errors for 95 percent of the "typical" field measurements, except those obtained during extreme events (wind speed > 20 m/s, current speed > 20 cm/s, and current speed/wave particle speed < 1). The TMU excludes errors induced by data smoothing operations such as filtering; also, estimates are not made of uncertainties introduced by an inadequate sampling scheme. In summary, the TMU is measurement-system dependent, laboratory-calibration dependent, and environmental-conditions dependent.

7.4. SPECIFIC ERROR ESTIMATES

The remainder of this section describes the treatment of the individual error components for each project instrument including the assumptions, rationale, and equations used in generating the error estimates. Estimates of synergistic effects on instrument performance have been excluded. Descriptions of the calibration

processes, including standards, along with environmentally induced uncertainties are included. The Grundy 9021 current speed and direction error estimates are discussed separately in section 9.

7.4.1. Grundy 9021 Water Temperature

The temperature sensors were initially calibrated at T&EL in early 1978 as received from the manufacturer. The instruments were adjusted, if necessary, to agree with the supplied transfer function by calibrating each unit in controlled baths at five nominal temperatures (-1°C , 7°C , 15°C , 23°C , and 31°C). Each calibration point consisted of 30 averaged measurements of sensor and standard. The systematic errors in the calibration process consist of the absolute error in the measurement standard (temperature bridge and platinum resistance thermometer) and bath gradients. The magnitude of these combined errors is estimated not to exceed $\pm 0.008^{\circ}\text{C}$.

A total of 36 sensors were calibrated, and the RSE was computed to be $\pm 0.039^{\circ}\text{C}$. To compute the uncertainties in the transfer function at the 95-percent confidence level, an appropriate multiplier was selected from Student's "t" table for 179 degrees of freedom:

$$95\text{-percent CL} = (\pm 0.039^{\circ}\text{C}) (1.98) = \pm 0.077^{\circ}\text{C}.$$

The ECU is a summation of the systematic and transfer function errors and represents the laboratory uncertainty of the 36 instruments as a group:

$$\text{ECU (36 units)} = (\pm 0.008) + (\pm 0.077) = \pm 0.085^{\circ}\text{C}.$$

Post-survey calibrations were performed on 20 operational instruments at four nominal temperatures: 7°C , 15°C , 23°C , and 30°C . Four instruments (SN's 24, 55, 61, and 62) had unreasonably high average residuals ($> 0.75^{\circ}\text{C}$) and were thus excluded from the error analysis. Inspection of field-check records indicated that SN 55 was within the DQL of $\pm 0.2^{\circ}\text{C}$ for all field checks performed (table 6); the TMU to be computed can thus be applied to field data acquired with SN 55. The RSE for the remaining 16 instruments was found to be $\pm 0.13^{\circ}\text{C}$. The arithmetic mean of the residuals was found to be -0.04°C , indicating little apparent bias. The computation of

95-percent confidence level for the post-survey calibrations, using the "t" statistic for 63 degrees of freedom, resulted in

$$95\text{-percent CL} = (\pm 0.13^{\circ} \text{ C}) (2.05) = \pm 0.27^{\circ} \text{ C}.$$

As a group, the 16 temperature sensors changed with respect to the initial calibrations in such a way as to broaden the 95-percent confidence level by a factor of nearly four. The SMU, representing meter performance during the survey, is the summation of systematic and 95-percent confidence limit values:

$$\text{SMU} = (\pm 0.008) + (\pm 0.27) = \pm 0.28^{\circ} \text{ C}.$$

Spatial errors may also contaminate the measurements. For example, if the current meter is in a ± 15 -degree tilt attitude ($\approx \pm 7.5$ cm vertical displacement of sensor) and in a temperature gradient of 2° C/m , spatially generated uncertainties of $\pm 0.15^{\circ} \text{ C}$ will be introduced if tilt is present. Since the attitude of the meter was not measured, this uncertainty is not treated in the analysis. Another potential error source is biofouling of the temperature sensor and the corresponding lengthening of its time constant. The time constant of a clean probe is ≈ 5 s, and the time constant of a fouled probe is unknown. Nevertheless, this effect is considered negligible since the variability scale of ocean temperature fluctuations is likely to be several orders of magnitude greater.

The TMU for *in situ* temperature measurement, using the Grundy 9021 current meter, is estimated to be

$$\text{TMU} = \pm 0.28^{\circ} \text{ C}.$$

Based on similarity of performance of all temperature sensors demonstrated during field checks, the above TMU can be applied to all temperature measurements made during the survey (except those made with SN's 24, 61, and 62).

7.4.2. Grundy 9021 Conductivity

The Grundy Model 9021 conductivity sensors were initially calibrated at T&EL as received from the manufacturer. The instruments

were adjusted, if necessary, to agree with the manufacturer's transfer function by calibrating each unit in controlled baths at five nominal conductivities: 17, 24, 28, 43, and 58 mS/cm. Each calibration point consisted of 30 averaged measurements of the conductivity sensor and the measurement standard. These conductivity calibrations were conducted concurrently with the temperature calibrations. The systematic errors in the calibration process consist of the uncertainties associated with the measurement standard (the Guildline 8400 Autosol), the temperature uncertainty, and bath drift. The magnitude of these combined errors is estimated not to exceed ± 0.015 mS/cm.

A total of 36 sensors were calibrated, and the RSE for the group was computed to be ± 0.053 mS/cm. To compute the uncertainties in the corresponding transfer function at the 95-percent confidence level, an appropriate multiplier was selected from Student's "t" table for 179 degrees of freedom; the RSE was multiplied by this value:

$$95\text{-percent CL} = (\pm 0.053 \text{ mS/cm}) (1.98) = \pm 0.10 \text{ mS/cm}.$$

The ECU is a summation of the systematic errors and the transfer function errors:

$$\text{ECU (36 units)} = (\pm 0.015) + (\pm 0.10) = \pm 0.12 \text{ mS/cm}.$$

This value represents the calibration uncertainty of the 36 instruments taken as a group.

Severe fouling of conductivity sensors during the summer of 1978 rendered much of the conductivity data untraceable to the laboratory calibrations (section 6.5). A detailed analysis of all available records has shown that valid uncertainty estimates can be made only for a limited number of meters over a limited time period. A group of 10 Grundy 9021 meters underwent laboratory calibrations at T&EL after antifoulant painting and some readjustment. Based on available records, no evidence of shipboard readjustment could be found on these 10 meters. For this group, the ECU was derived from the laboratory calibrations; the SMU was computed incorporating results of shipboard checks. It was necessary, in this case, to use field-check data as a basis for conductivity sensor degradation, or drift, since this was the only available information. The time period covered

by the uncertainty analysis generally spans November 1, 1978, to April 1, 1979. (After April 1, 1979, shipboard adjustment of the conductivity sensors invalidated traceability to the point where no reasonable estimate of data uncertainty could be derived.)

The RSE was computed for laboratory calibrations of the 10 meters and found to be ± 0.047 mS/cm. The 95-percent confidence limits for the transfer function were computed using a "t" statistic for 41 degrees of freedom:

$$95\text{-percent CL} = (\pm 0.047 \text{ mS/cm}) (2.02) = \pm 0.095 \text{ mS/cm}.$$

The ECU was computed by summing the estimated systematic error and the 95-percent CL:

$$\text{ECU} = (\pm 0.015) + (\pm 0.095) = \pm 0.11 \text{ mS/cm}.$$

There were 33 field checks performed on these meters during the time period of interest. Computation of RSE for the resultant 99 data points yielded ± 0.11 mS/cm. The computation of 95-percent confidence level for the field check resulted in using a "t" statistic for 98 degrees of freedom:

$$95\text{-percent CL} = (\pm 0.11 \text{ mS/cm}) (1.98) = \pm 0.22 \text{ mS/cm}.$$

The arithmetic mean of the residuals was found to be zero indicating no apparent bias. As a group, the 10 meters drifted from the laboratory calibration in such a way as to approximately double the 95-percent confidence limits. The SMU, representing the meter performance over the time period of interest, was computed from the systematic and field-check components:

$$\text{SMU} = (\pm 0.015) + (\pm 0.22) = \pm 0.24 \text{ mS/cm}.$$

As with temperature measurement using the Grundy Model 9021 (section 7.4.1), spatial conductivity errors may be present in the data due to a vertical dislocation of the cell in a conductivity gradient. Biofouling inside the cell has been shown to result in a -8 to -12 mS/cm error. This error analysis, however, does not apply

to data collected during the fouling season nor does it consider any spatial uncertainties of the sensor in a conductivity gradient. The TMU, using the qualified Grundy Model 9021 current meter and data records, is therefore estimated to be

$$\text{TMU} = \pm 0.24 \text{ mS/cm.}$$

7.4.3. Grundy 9021 Time Base

The time-base oscillators for the Grundy 9021 current meters were initially calibrated at T&EL at the beginning of the survey. The systematic errors in the calibration process were estimated not to exceed ± 1 ppm. The calibration consisted of a one-point check. All values were adjusted to within the manufacturer's specification of ± 23 ppm. The RSE after adjustment was computed to be ± 11 ppm.

To compute the uncertainties at the 95-percent confidence level, an appropriate multiplier was selected from Student's "t" table for 35 degrees of freedom:

$$95\text{-percent CL} = (\pm 11 \text{ ppm}) (2.02) = 22 \text{ ppm.}$$

The ECU was computed by summing the systematic errors and the 95-percent CL errors:

$$\text{ECU (36 units)} = (\pm 1) + (\pm 22) = \pm 23 \text{ ppm.}$$

During the course of the survey, 16 of the above sensors were again checked by T&EL; based on these checks, an RSE of ± 12 ppm was determined. The computation of the 95-percent CL, using the "t" statistic for 15 degrees of freedom, resulted in

$$95\text{-percent CL} = (\pm 12 \text{ ppm}) (2.13) = \pm 26 \text{ ppm.}$$

The SMU was computed by summing the systematic and 95-percent CL values:

$$\text{SMU (interim)} = (\pm 1) + (\pm 26) = \pm 27 \text{ ppm.}$$

During the survey, field checks and adjustments were performed on the time-base oscillators. Field-check records, which recorded oscillator deviation after adjustment, were available for 34 instruments. The number of checks per instrument varied from 1 to 10; the total number of points was 203. The RSE of the field check was found to be ± 11 ppm. The conclusion drawn is that redeployed meters were approximately equivalent to laboratory calibrated meters with respect to time-base uncertainty.

A final (end point) calibration check was performed by T&EL at the end of the survey on 21 sensors, and an RSE of ± 11 ppm was computed. The computation of the 95-percent CL, using the "t" statistic for 20 degrees of freedom, resulted in

$$95\text{-percent CL} = (\pm 11 \text{ ppm}) (2.09) = \pm 23 \text{ ppm}.$$

The SMU at the end of the survey is therefore

$$\text{SMU (final)} = (\pm 1) + (\pm 23) = \pm 24 \text{ ppm}.$$

A potential source of error is oscillator shift caused by temperature change. Tests performed at T&EL showed a change of 4 ppm over a temperature range of -5°C to $+40^{\circ}\text{C}$. Water temperatures during the survey cover a narrower range (approximately $+8^{\circ}\text{C}$ to $+34^{\circ}\text{C}$); a 95-percent range would be narrower yet. Since data are not available on the temperature effect over the narrower range, no additional uncertainty will be added. Thus, the TMU equals the SMU and represents the time-base accuracy during the survey. The differences between the three sets of laboratory checks are not felt to be significant; hence, the average value of the three 95-percent confidence levels (± 24 ppm) will be combined with the systematic error:

$$\text{TMU} = (\pm 1) + (\pm 24) = \pm 25 \text{ ppm} = \pm 66 \text{ s/month}.$$

7.4.4. Aanderaa Wind Speed

The cup anemometers on the Aanderaa meteorological stations were calibrated initially in the National Weather Service Test and Evaluation Division wind tunnel in Sterling, Va. One sensor was calibrated at 10 points spanning from approximately 2.5 to 26 m/s

in ascending order; each point consisted of 100 measurements. After the calibration data were analyzed and found to be in close agreement (0.7 percent) with the manufacturer's equation, it was decided to perform calibration checks at two air speeds (13 and 26 m/s) on the remaining three anemometers. These checks were also within 1 percent of reading of the transfer function provided; the RSE was computed to be ± 0.22 m/s. The systematic errors in the calibration process consist of the absolute error in the measurement of the tunnel speed by means of the Pitot tube, the velocity blockage by the anemometer in the test section, and uniformity of the tunnel velocity profile. The magnitude of these combined errors is estimated not to exceed ± 0.15 m/s.

To compute the uncertainties in the transfer function at the 95-percent confidence level, an appropriate number from Student's "t" table for 15 degrees of freedom was selected; the RSE of ± 0.22 m/s was multiplied by this value:

$$95\text{-percent CL} = (\pm 0.22 \text{ m/s}) (2.13) = \pm 0.47 \text{ m/s.}$$

The ECU was computed by summing the systematic errors and the transfer function errors:

$$\text{ECU (4 units)} = (\pm 0.15) + (\pm 0.47) = \pm 0.62 \text{ m/s.}$$

At the end of the survey, the anemometers were checked by T&EL. With the exception of SN 46 that was found to be inoperative, it was determined that performance had not degraded. The SMU, representing anemometer performance over the period of interest, was therefore equal to the original uncertainty estimate (ECU) of ± 0.62 m/s (excluding SN 46).

Meteorological measurements were conducted from four oil production rigs that served as platforms for the Aanderaa meteorological stations, designated as stations 18, 19, 28, and 29. The platforms and their ancillary hardware might have significantly affected the wind measurements. For example, station 19 was positioned approximately 2 m from a 1-m-diameter, 6-m-high horn/light tower that distorted the wind field. A similar configuration was investigated empirically by Gill et al. (1967), who found errors

in wind speed from -20 percent to +9 percent. Because of the small size of the platform superstructure, any flow-field distortion induced by the platform is considered minimal. The station 28 anemometer, although in an unobstructed location, was mounted on a larger platform having a relatively small frontal area that should induce minimal wind field distortion. Because of the uncertainties in the estimates of distortion induced by platforms (Mollo-Christensen 1979), the error estimates generated for station 19 (albeit conservative) are applicable to station 28. Stations 18 and 29 are excluded from this analysis: Instrument problems with station 29 resulted in no data return, and distortion estimates cannot be provided for station 18 because of the lack of information available for similarly configured complex shapes. It should be realized that the velocity field will be affected by a 1-m-diameter, 2.5-m-high crane within 1 m of the meteorological tower and by the larger platform. Mollo-Christensen (1979) suggests that the magnitude of flow interference for complicated objects such as drilling platforms is better quantified by full-scale comparison field tests or wind tunnel testing of models rather than by computations. The values of -20 percent to +9 percent wind field distortion will be applied to the error analysis for platforms 19 and 28.

Turbulence has also been shown to induce errors in wind measurement, particularly when using cup anemometers, according to MacCready (1966) and Lindley (1975). Dynamic response characteristics of the cups may introduce errors from +3 percent to +10 percent when turbulence is present. Another factor that should be considered is that wind-speed measurements are generally referenced to a height above water level, the standard height being 10 m. The elevations of the anemometers above mean sea level were as follows: West Hackberry East (station 18), 19.1 m; West Hackberry West (station 19), 15.6 m; and Weeks Island East (station 28), 14.6 m. An analysis of the uncertainties in transposing the measurements to the standard height is beyond the scope of this study but should be considered by other investigators.

The TMU for the wind speed data was computed as follows:

$$TMU = SMU + W (\epsilon_V^2 + \epsilon_T^2)^{\frac{1}{2}},$$

where W = wind speed,

ϵ_V = uncertainty attributed to wind field
distortion introduced by platform,

and ϵ_T = uncertainty induced by turbulence on
anemometer cups.

Positive component at $W = 5$ m/s:

$$TMU = + 0.62 + 5 (0.09^2 + 0.03^2)^{\frac{1}{2}} = + 0.62 + 0.49 = + 1.1 \text{ m/s.}$$

Negative component at $W = 5$ m/s:

$$TMU = - 0.62 - 5 (0.20) = - 1.6 \text{ m/s.}$$

Note that, because the *in situ* turbulence intensity was not measured and the cup anemometer was not tested dynamically to quantify the effect, the minimum uncertainty of +3 percent was assumed.

As can be seen from the above equation, TMU is dependent upon wind speed. Values of TMU were also computed at 10, 15, and 20 m/s, using the same method shown above for 5 m/s. Results of the computations are summarized below:

Wind Speed	TMU
<u>(m/s)</u>	<u>(m/s)</u>
5	+1.1, -1.6
10	+1.6, -2.6
15	+2.0, -3.6
20	+2.5, -4.6

The TMU values represent the uncertainties associated with wind speed measurements made during the survey, excluding measurements made with SN 46. Because field checks were not performed on the anemometers, information on when proper operation ceased is not available. It may, however, be possible to deduce this from data records.

7.4.5. Aanderaa Wind Direction

The wind direction vanes on the Aanderaa meteorological stations were calibrated initially at T&EL at the beginning of the survey. Each calibration consisted of 24 points equally distributed over 15-degree intervals. Each point consisted of two measurements. The systematic errors in the calibration process were estimated not to exceed ± 1 degree.

Using the manufacturer's transfer function, the computed RSE was ± 2.5 degrees. To quantify the uncertainties in the transfer function at the 95-percent CL, an appropriate value was selected from Student's "t" table for 119 degrees of freedom; the RSE was multiplied by this number:

$$95\text{-percent CL} = (\pm 2.5 \text{ degrees}) (1.98) = \pm 5.0 \text{ degrees.}$$

The ECU was computed by summing the systematic and transfer function errors:

$$\text{ECU (5 units)} = (\pm 1.0) + (\pm 5.0) = \pm 6.0 \text{ degrees.}$$

An additional spare sensor (SN 2153) was shipped directly to the FERREL and thus did not undergo initial calibration. Based on similarity of performance demonstrated by the initial five sensors, the computed ECU is assumed to apply also to the sixth unit.

At the end of the survey, the vanes were checked by T&EL. It was found that the damping fluid had leaked from two of the direction sensors (SN's 374 and 2153); performance had not otherwise degraded for the group. While the lack of fluid could have an effect on the noise level in the direction data, there should be no effect on mean accuracy. The group of direction sensors was thus assumed to have no accuracy degradation. The SMU, representing vane performance over the period of interest, was therefore equal to the original estimated ECU of ± 6.0 degrees.

As with wind-speed measurements, the wind-field distortion induced by the measurement platform introduced direction errors. Again, platform 19 was used in this analysis to illustrate the effect. According to Gill et al. (1967), direction uncertainties of up to ± 10 degrees may occur 95 percent of the time. Another source of

error is alinement of the wind-vane orientation mark with true north. This operation consisted of using the FERREL's gyroscope, in combination with a visual sighting along one side of the platform, to determine its orientation relative to north and then transposing these measurements to the vane orientation mark. It is estimated that the uncertainty in this procedure was ± 3 degrees.

Another potential uncertainty is the vane threshold, or minimum wind speed, to which the vane responds. In other words, the vane may not be alined with the wind field. Although tests were not performed, the vane threshold is 0.3 m/s according to the manufacturer. Wind-direction measurements at low wind speed should be treated as suspect. Because winds exceed that value greater than 95 percent of the time, this is not considered a problem.

The TMU was derived by summing quadratically the wind-field distortion error and alinement error and adding this value to the SMU:

$$TMU = \pm 6 + (10^2 + 3^2)^{\frac{1}{2}} = \pm 16 \text{ degrees.}$$

This value represents the estimated uncertainty of wind-direction measurement for the group of vanes used during the survey. This analysis is applicable for wind-direction measurements from stations 19 and 28 but not for 18. (See section 7.4.4 for explanation concerning exclusions.)

7.4.6. Aanderaa Air Temperature

The air temperature sensors on the Aanderaa meteorological stations were initially calibrated at T&EL at the beginning of the survey. The calibrations consisted of 18 test points over the range of -8°C to $+40^{\circ}\text{C}$; at each point, five samples of sensor output were acquired and averaged. The manufacturer's transfer function was used to convert sensor data to temperature. The systematic errors in the calibration process consist of the absolute error in the temperature bridge and platinum thermometer and bath gradients. The magnitude of these combined errors is estimated not to exceed $\pm 0.008^{\circ}\text{C}$.

A total of 10 sensors were calibrated. The RSE was computed to be $\pm 0.11^{\circ}\text{C}$. Uncertainties in the combined transfer function at the 95-percent confidence level were computed by selecting an appropriate

multiplier from Student's "t" table for 179 degrees of freedom; the RSE was multiplied by this value:

$$95\text{-percent CL} = (\pm 0.11^{\circ} \text{ C}) (1.98) = \pm 0.22^{\circ} \text{ C}.$$

The ECU was computed by summing the systematic errors and the transfer function errors:

$$\text{ECU (10 sensors)} = (\pm 0.008) + (\pm 0.22) = \pm 0.23^{\circ} \text{ C}.$$

Post-survey calibrations were performed on 10 probes during October 1979. These sensors were checked at five nominal temperatures: 0° C , 10° C , 20° C , 30° C , and 40° C . Inspection of the results indicated that one sensor, SN 690, was inoperative; this sensor was excluded from the error analysis. The RSE for the remaining instruments was found to be $\pm 0.086^{\circ} \text{ C}$; the mean of the residuals was -0.037° C , indicating no significant bias. The corresponding uncertainty at the 95-percent CL in the transfer function for 45 degrees of freedom, using the "t" statistic, resulted in

$$95\text{-percent CL} = (\pm 0.086^{\circ} \text{ C}) (2.02) = \pm 0.17^{\circ} \text{ C}.$$

The post-survey ECU represents the laboratory performance of the nine sensors at the end of the survey; it was computed by summing the systematic and 95-percent CL values and was found to be $\pm 0.18^{\circ} \text{ C}$. Because this uncertainty band is completely contained within the initial ECU, the SMU is equal to the initial ECU for the entire survey:

$$\text{SMU (9 sensors)} = \pm 0.23^{\circ} \text{ C}.$$

In the field environment, temperature measurements may be contaminated by radiation effects, self heating of the probe, deliquescence effects, and convection heating. Radiation errors are often present when making air-temperature measurements. These effects are minimized by using radiation screens over the probe; nevertheless, midday solar radiation, low-Sun elevations, and night-time radiation

losses can introduce errors of -0.2°C to $+0.6^{\circ}\text{C}$ according to McTaggart-Cowan and McKay (1976). This particular intercomparison was conducted on land using similarly configured shields; solar reflectivity from the water surface could exacerbate these errors in the marine environment.

Another source of uncertainty is the self-heating of the probe caused by the power-dissipation characteristics of the platinum-resistance probe design. This error is computed to be less than $+0.05^{\circ}\text{C}$ and is based on the dissipation constant of the probe. This uncertainty would not occur during the in-water calibrations and must be taken into consideration when making measurements of air temperature.

Convection currents from the platform and structure, which are at above-ambient air temperatures during the day, may produce errors at wind speeds less than 0.5 m/s . This effect is excluded from the analysis because 95 percent of the Gulf winds are greater than that magnitude. A final, although somewhat unlikely, error source is the deposition and subsequent dissolving of salt on the temperature probe during changes in relative humidity. Holmes (1975) conducted laboratory tests and estimated the deliquescence-induced error at between 0.2°C and 1.0°C . This error is also excluded as it is questionable whether salt deposition could occur on the sensors located at 14 to 22 m above sea level.

The TMU is computed from the combination of the SMU with the radiation and self-heating errors:

$$\text{TMU (positive)} = + 0.23 + [(0.6)^2 + (0.05)^2]^{\frac{1}{2}} = + 0.83^{\circ}\text{C}.$$

$$\text{TMU (negative)} = - 0.23 + (-0.2) = - 0.43^{\circ}\text{C}.$$

The TMU represents the estimated uncertainty in air-temperature measurements made during the survey, excluding measurements made with SN 690. Because field checks were not performed on these sensors, information on when proper operation ceased is not available. It may, however, be possible to deduce this from field data records.

7.4.7. Aanderaa Air Pressure

The six air pressure sensors used in the Aanderaa meteorological stations were initially calibrated at T&EL at the beginning of the survey. Each calibration consisted of three cycles (0° C, 25° C, and 48° C) of 13 points each. The same calibration procedure was followed for the subsequent interim and post-survey calibrations. The systematic error associated with the calibration process was estimated not to exceed ± 0.1 mbar.

In all cases, the calibration data were fitted to the function,

$$p = A_0 + A_1 X + A_2 X^2 + B\theta, \quad (12)$$

where x is the sensor output, θ is the sensor temperature, and p is the air pressure in mbar.

The 95-percent confidence limit computed about each of the six fitted transfer functions ranged from ± 0.6 to ± 1.6 mbar. Because of the small population (six fitted equations), attempts at statistically determining a representative single value for the 95-percent confidence limit resulted in an overly conservative estimate (i.e., larger than the highest value). A value of ± 1.6 mbar was therefore selected for use in the uncertainty computation.

The ECU was computed by summing the systematic and transfer function errors:

$$\text{ECU (6 units)} = (\pm 0.1) + (\pm 1.6) = \pm 1.7 \text{ mbar.}$$

Two sensors were scheduled for recalibration, one after 3 months and the second after 6 months to identify drift errors occurring during the course of the survey. After 3 months the mean drift of SN 89 was -0.8 mbar (less than the calibration uncertainty). The conclusion was drawn that the sensor drift errors would be small and, consequently, the recalibration schedule for the second sensor was allowed to slip. In March 1979, recalibration of SN 65 yielded a large mean drift of -1.8 mbar; by then, however, it was too late to complete recalibrations of all the remaining sensors.

Post-survey calibrations were completed on all six sensors in July 1979. Analysis of results for SN 65 indicated that a significant shift had occurred between March 1979 and July 1979, apparently due

to internal damage. Available records indicate that SN 65 was not used after March 1979. The results of the interim recalibration performed that month will be used as final calibration data for the sensor. Transfer functions were fitted to the data from the six recalibrations. The 95-percent confidence limits about each of the equations ranged from ± 0.6 to ± 1.5 mbar. A value of ± 1.5 mbar was selected to represent the 95-percent confidence limit for the recalibration, and the ECU for the recalibrations is then ± 1.6 mbar.

The drift error for each sensor was determined by comparing the initial and final calibration equations at nine points over a range of pressures and temperatures. The resulting drift errors are minimized by restricting the pressure and temperature ranges to those actually encountered during the survey. It is estimated that 95 percent of the survey observations of air pressure fall within the range of 1,000 to 1,034 mbar. The temperature range of 0° C to 48° C provides for both the expected environmental range and the temperature rise of the pressure sensors due to insolation. For the group of six sensors, the drift error range was -1.0 to -3.9 mbar with a mean drift of -2.3 mbar. As with the computation of the ECU, the attempt to determine statistically a single value representative of the group of sensors again leads to an overly conservative estimate. The range value, -3.9 mbar, is selected as the smallest value that can describe the group performance. The SMU is the sum of this drift error and the two ECU's calculated for the initial and final calibrations:

$$\text{SMU} = +1.7, -5.5 \text{ mbar.}$$

The TMU is the sum of the calibration and drift errors (SMU) and the additional errors related to field deployment such as uncertainties due to the temperature, wind speed, and elevation.

There are two temperature related errors to consider, the error in the measured air temperature and the difference between this measured temperature and the actual temperature of the pressure sensors. The measured air temperature was used in the calibration equation (12) for computation of air pressure. The TMU of the measured temperature was -0.43° C, $+0.83^{\circ}$ C (section 7.4.6), corresponding to a negligible pressure uncertainty of +0.02 to -0.03 mbar.

The differential temperature uncertainty is a result of insolation. The air-pressure sensors are mounted inside a canister 26 cm in diameter and 90 cm high. Cooling is achieved by convection away from the cylindrical surface; but the bottom of the canister is open so that, depending on the mounting (i.e., open grate or solid plate), a variable amount of direct air exchange is possible.

To estimate the insolation effects, one station was placed on the roof of Building 160 in the Washington Navy Yard. An additional air temperature probe was mounted in contact with the pressure sensor. Comparison of temperatures showed a maximum lag of 2.8°C at sunrise and a maximum rise of 11.5°C with cloud cover of 10 percent or less and with a wind speed of 1.5 m/s. Additional observations at higher wind speeds indicated that the temperature rise is reduced by half to 5.8°C at 4.5 m/s. These measurements are inexact; it is difficult to find repeated conditions of cloud cover and wind vector in the limited data. For this reason, a conservative estimate is made of the effects of insolation. A typical wind speed of 5 m/s was assumed from the survey data records, and the temperature uncertainty is estimated to be in the range of -3°C to $+10^{\circ}\text{C}$. The corresponding pressure uncertainty is $+0.1$ to -0.4 mbar.

As part of the same test, the data from the roof-mounted station were examined for depression of the air pressure reading with wind speed. The comparison instrument was a recording barometer operating inside the building. The measured average wind speed ranged from 0.2 to 7.9 m/s or about half the range indicated on available charts of survey data. A comparison of wind speed and pressure difference showed no correlation (correlation coefficient < 0.1), and the wind depression effect is considered zero.

During the survey, the air-pressure sensors were mounted on towers at elevations ranging from 13.0 to 20.6 m. The air-pressure readings are greater at sea level by approximately 0.11 mbar/m so that the uncertainty due to uncompensated elevation errors is -1.3 , -2.3 mbar.

The TMU is the sum of the SMU, the temperature effects, and the uncertainties due to elevation:

$$\text{TMU} = \begin{bmatrix} +1.7 \\ -5.5 \end{bmatrix} + \begin{bmatrix} +0.1 \\ -0.4 \end{bmatrix} + \begin{bmatrix} -1.3 \\ -2.3 \end{bmatrix} = \begin{bmatrix} +0.5 \\ -8.2 \end{bmatrix} \text{ mbar.}$$

7.4.8. Applied Microsystems Wave Height

The absolute pressure transducers used in the three Applied Microsystems, Inc., water level gages were initially calibrated at T&EL prior to the beginning of the survey. Each calibration consisted of three cycles (10° C, 20° C, 30° C) of 13 points each. The systematic error associated with the calibration process was estimated not to exceed ± 0.007 dbar. The optimum fitted transducer response function was

$$p = A_1 X + A_2 X^2 + B_1 \theta + C_1 X\theta, \quad (13)$$

where $X = 1 - T_0/T$,

p is the pressure in dbar,

θ is the temperature in °C,

T_0 is the period of the output signal at zero pressure,

and T is the period at pressure equal to p .

The same calibration procedure was followed for the subsequent interim and post-survey calibrations. The maximum value of the 95-percent confidence limits computed about each of the pre-survey transfer functions ranged from ± 0.007 to ± 0.012 dbar. The pre-survey ECU was obtained by summing the transfer function and systematic errors:

<u>SN</u>	<u>ECU (Initial)</u>
131	± 0.019 dbar
132	± 0.019 dbar
133	± 0.014 dbar

The pressure transducer installed in SN 133 was recalibrated after 5 months; the mean drift was -0.027 dbar. The conclusion was drawn that this drift was not excessive and no additional interim calibrations were scheduled.

Post-survey calibrations were completed in November 1979. The 95-percent confidence limits computed about each of the post-survey transfer functions ranged from ± 0.003 to ± 0.008 dbar. The ECU for the final calibrations was computed by summing the 95-percent confidence limit and systematic errors:

<u>SN</u>	<u>ECU (Initial)</u>
131	+ 0.015 dbar
132	+ 0.013 dbar
133	+ 0.010 dbar

The drift error for each transducer was determined by comparing the initial and final calibration equations. The resulting drift errors can be minimized by restricting the comparison to the pressure and temperature ranges actually encountered during the survey. The absolute pressure range is estimated to be 12 to 19 dbar, based on the bottom depths at stations 11 and 21, the gage mounting height of 2 m, the maximum expected wave height of 3 m, the maximum tidal excursion of 0.9 m, and the barometric range of 1,000 to 1,034 mbar. The temperature range observed was 10° C to 30° C. Over these limited ranges, the drift error for each transducer is nearly constant; the largest standard deviation of the mean drift error is less than ± 0.002 dbar. The mean drift error for each of the three transducers is given below:

<u>SN</u>	<u>MEAN DRIFT</u>
131	-0.059 dbar
132	-0.085 dbar
133	-0.038 dbar

The drift error for the frequency-counter oscillators in the water level gages is negligible; the internal oscillators were maintained within specification.

The SMU includes the systematic errors, the net drift between calibrations, and the respective 95-percent confidence level values:

$$SMU(131) = \begin{bmatrix} +0.007 \\ -0.007 \end{bmatrix} + \begin{bmatrix} \\ -0.059 \end{bmatrix} + \begin{bmatrix} +0.012 \\ -0.008 \end{bmatrix} = \begin{bmatrix} +0.019 \\ -0.074 \end{bmatrix} \text{ dbar.}$$

The SMU for the remaining two sensors was computed in similar fashion; results are summarized below:

<u>SN</u>	<u>SMU</u>
131	+0.019, -0.074 dbar
132	+0.019, -0.098 dbar
133	+0.014, -0.048 dbar

The TMU is the sum of the calibration and drift errors (SMU) and the additional errors related to the environment, such as uncertainties due to temperature or water current. A constant monthly water temperature was assumed in the processing of field data so that there are errors due to both variability and offset of the measured monthly temperature. The temperature was measured by Grundy Model 9021 current meters positioned 1 m above and below the AMI wave gages. The TMU of the measured temperature at the current meter is $\pm 0.28^{\circ}\text{C}$ (section 7.4.1). The spatial temperature error between the current meter and the wave gage is estimated to be $\pm 2.0^{\circ}\text{C}$ or less, based on measured vertical temperature profiles. The monthly mean temperature and standard deviation were calculated from a tabulation of daily means. The effect of temperature variance with any given day was found to be negligible; the principal variation was due to the within-month trend. The error term representing the variability in the monthly mean is estimated to be twice the computed monthly standard deviation and ranges from $\pm 0.6^{\circ}\text{C}$ to $\pm 4.0^{\circ}\text{C}$. The temperature sensor error, the spatial temperature error, and the maximum value of the monthly variability are combined to obtain the random component of the measured temperature error (e_r):

$$e_r = \pm (0.28^2 + 2.0^2 + 4.0^2)^{\frac{1}{2}} = \pm 4.5^{\circ}\text{C}.$$

The difference between the assumed monthly temperatures and the measured monthly means ranged from -1.0°C to $+10.7^{\circ}\text{C}$. The total temperature error, computed by summing this bias with the random component (e_r), is then -5.5°C , $+15.2^{\circ}\text{C}$. The temperature sensitivity ($\Delta p/\Delta \theta$) was determined by differentiation of equation (13). The resultant expression was evaluated over the range of 12 to 19 dbar for each sensor, yielding the following pressure uncertainties:

<u>SN</u>	<u>ERROR</u>
131	+0.004, -0.013 dbar
132	0.000, -0.002 dbar
133	+0.002, -0.006 dbar

The estimate of pressure deviation induced by water velocity at the pressure port is based on a mean velocity range of 0 to 20 cm/s

at the sensor level with a signal-to-noise ratio of 1 (instantaneous velocity of 40 cm/s). Tow tank measurements (Muir 1978) with an instrument of similar dimensions resulted in a pressure deviation proportional to the square of the velocity with the proportionality constant dependent upon the sensor geometry and attitude. The reported velocity range was 1 to 6 m/s. Extrapolation of Muir's results to 0.4 m/s indicates that the pressure error due to water velocity would be less than ± 0.01 dbar.

The actual averaging error is dependent upon the periods and relative amplitudes of the spectral components of the measured data. An estimate was made of this error based on sine waves with a maximum height of 3.0 m, a sensor depth of 5 m, and an integrating time of 112.5 s. Over the wave period range of 3 to 8 s, the peak averaging error is ± 0.014 dbar.

The environmental error, e_e , is the root-sum-square of the error due to water velocity and the averaging error:

$$e_e = \pm (0.010^2 + 0.014^2)^{\frac{1}{2}} = \pm 0.017 \text{ dbar.}$$

The TMU for the total pressure measured in the water level mode is the sum of the SMU, the temperature related error, and the environmental error, e_e :

$$\text{TMU (SN 131)} = \begin{bmatrix} +0.019 \\ -0.074 \end{bmatrix} + \begin{bmatrix} +0.004 \\ -0.013 \end{bmatrix} + \begin{bmatrix} +0.017 \\ -0.017 \end{bmatrix} = \begin{bmatrix} +0.040 \\ -0.104 \end{bmatrix} \text{ dbar.}$$

The computed TMU for each of the three sensors is given below:

<u>SN</u>	<u>TMU (Water Level Mode)</u>
131	+0.040, -0.104 dbar
132	+0.036, -0.117 dbar
133	+0.033, -0.071 dbar

The TMU for the wave measurement mode is substantially less. Differential pressures corresponding to wave heights are computed by subtracting the mean pressure from each of the subsequent samples in the wave measuring interval. In this mode, both the drift errors and the temperature errors are negligible. The remaining components

of the TMU are the calibration uncertainty (the ECU less the systematic error) and environmental errors, e_e :

$$\text{TMU (SN 131)} = (\pm 0.012) + (\pm 0.017) = \pm 0.029 \text{ dbar.}$$

The larger of the two ECU values has been used and, for all three sensors, was obtained from the initial calibration. The TMU computed for each of the sensors is summarized below:

<u>SN</u>	<u>TMU (Wave-Measurement Mode)</u>
131	$\pm 0.029 \text{ dbar}$
132	$\pm 0.029 \text{ dbar}$
133	$\pm 0.024 \text{ dbar}$

In addition to providing a time base for the pressure sensors, the internal oscillators control the instrument sampling interval. As previously discussed, the oscillators in all three instruments were within specification for pressure measurements. Based on field-check records, the measured oscillator deviations were less than $\pm 0.9 \text{ ppm}$. This corresponds to a time-base error of $\pm 2.5 \text{ s/month}$.

7.4.9. Aanderaa Total Pressure and Water Level

The Aanderaa Model WLR-5 water level recorders were initially calibrated at T&EL prior to the beginning of the survey. Each calibration consisted of three cycles (10° C , 20° C , and 30° C) of 13 points each. The optimum fitted transducer response function was

$$p = A_1 X + A_2 X^2 + B_1 \theta + C_1 X\theta, \quad (13)$$

where $X = 1 - T_0/T$,

p is the pressure in dbar,

θ is the temperature in $^\circ \text{C}$,

T_0 is the period of the output signal at zero pressure,

and T is the period at pressure equal to p .

The same calibration procedure was followed for the subsequent interim and post-survey calibrations. The maximum value of the 95-percent confidence limits, computed about each of the pre-survey transfer functions, ranged from ± 0.004 to ± 0.009 dbar. The systematic error associated with the calibration process was estimated not to exceed ± 0.003 dbar.

The pre-survey ECU was obtained by summation of the transfer function and systematic errors:

<u>SN</u>	<u>ECU (Initial)</u>
360	± 0.012 dbar
361	± 0.007 dbar
362	± 0.012 dbar

One recorder, SN 361, was recalibrated after 5 months. Based on this calibration, it was assumed that the sensor drift error was not excessive, and no additional interim calibrations were scheduled.

Post-survey calibrations were completed in August 1979. The 95-percent confidence limits, computed about each of the post-survey transfer functions, ranged from ± 0.004 to ± 0.008 dbar. The ECU for the final calibrations was computed by summing the 95-percent confidence limit and the systematic errors:

<u>SN</u>	<u>ECU (Final)</u>
360	± 0.011 dbar
361	± 0.007 dbar
362	± 0.010 dbar

The drift error for each recorder was determined by comparing the initial and final calibration equations. The resulting drift errors were minimized by restricting the comparison to the pressure and temperature ranges actually encountered during the survey. The absolute pressure range was estimated to be 14 to 21 dbar based on the recorder depths at stations 11 and 21, the maximum wave height of 3 m, the tidal excursion of 0.9 m, and the barometric range of 1,000 to 1,034 mbar. The temperature range observed was 10° C to

30° C. Over these limited ranges, the drift errors for the three recorders are listed below:

<u>SN</u>	<u>DRIFT ERROR</u>
360	+ 0.038 dbar
361	- 0.035 dbar
362	- 0.022 dbar

The drift of the frequency-counter oscillators in the recorders was negligible; the internal oscillators were maintained within specification.

The SMU includes the systematic errors, the net drift between calibrations, and the respective 95-percent confidence limit values:

$$\text{SMU (SN 360)} = \begin{bmatrix} +0.003 \\ -0.003 \end{bmatrix} + \begin{bmatrix} +0.038 \\ \end{bmatrix} + \begin{bmatrix} +0.009 \\ -0.008 \end{bmatrix} = \begin{bmatrix} +0.050 \\ -0.011 \end{bmatrix} \text{ dbar}$$

The SMU for the remaining two recorders was computed in a similar fashion; the results are summarized below:

<u>SN</u>	<u>SMU</u>
360	+0.050, -0.011 dbar
361	+0.007, -0.042 dbar
362	+0.012, -0.032 dbar

The TMU is the sum of the calibration and drift errors (SMU) plus the additional errors related to the operating environment, such as uncertainties due to temperature, water current, and averaging interval. A constant water temperature was assumed in the processing of field data so that there are errors resulting from both variability and offset of the measured monthly mean temperature. The random variability (e_r) of the measured temperature was $\pm 4.5^\circ \text{C}$ (section 7.4.8, AMI Water Level/Wave Gage error analysis). The difference between the assumed monthly temperature and the measured monthly means ranged from -2.0°C to $+17.7^\circ \text{C}$. The total temperature error, computed by summing this bias with the random component is then -6.5 to $+22.2^\circ \text{C}$. The temperature sensitivity ($\Delta p / \Delta \theta$) was determined by differentiation of equation (13) and was evaluated over the pressure

range of 14 to 21 dbar. The resulting pressure uncertainty due to temperature is summarized below:

<u>SN</u>	<u>ERROR</u>
360	+0.002, -0.006 dbar
361	+0.005, -0.015 dbar
362	0 dbar

The estimated pressure uncertainty due to water velocity is ± 0.01 dbar (section 7.4.8).

The actual sample averaging error is dependent upon the periods and relative amplitudes of the spectral components of the measured data. The averaging error was estimated based on sine waves with a 95-percentile wave height of 3 m at the surface, a sensor depth of 5 m, and an integrating time of 56 s. Over the wave period interval of 3 to 8 s, the peak estimated averaging error is ± 0.029 dbar.

The environmental error (e_e) is the root-sum-square of the errors due to water velocity and sample averaging,

$$e_e = \pm (0.010^2 + 0.029^2)^{\frac{1}{2}} \text{ dbar} = \pm 0.031 \text{ dbar.}$$

For total pressure measurements from the recorder, the TMU is the sum of the SMU, the temperature-induced errors (e_r), and the environmental errors (e_e):

$$\text{TMU (SN 360)} = \begin{bmatrix} +0.050 \\ -0.011 \end{bmatrix} + \begin{bmatrix} +0.002 \\ -0.006 \end{bmatrix} + \begin{bmatrix} +0.031 \\ -0.031 \end{bmatrix} = \begin{bmatrix} +0.083 \\ -0.048 \end{bmatrix} \text{ dbar.}$$

The computed TMU (total pressure) for all three recorders is summarized below:

<u>SN</u>	<u>TMU (Total Pressure)</u>
360	+0.083, -0.048 dbar
361	+0.043, -0.088 dbar
362	+0.043, -0.063 dbar

In addition to total pressure measurement, recorder data were used to compute differential water levels over 24-hr intervals. For this method of water level computation, the significant error sources are the averaging error; the variations of water density, barometric pressure, temperature, and water velocity at the sensor port over the interval; and the sensor calibration uncertainties.

The averaging error and water velocity error are ± 0.029 dbar and ± 0.010 dbar, respectively, as previously computed. Of the observed diurnal temperature ranges, 95 percent were less than $\pm 1.4^\circ \text{C}$ corresponding to a pressure uncertainty of less than ± 0.001 dbar; thus, the effect of temperature variation on the measured pressures is negligible.

The differential water-column height over the interval is computed from pressure measurements as follows:

$$h_2 - h_1 = (P_{m_2} - P_{a_2})/(\rho_2 g) - (P_{m_1} - P_{a_1})/(\rho_1 g), \quad (14)$$

where h is water column height, P_m is the absolute pressure at the sensor, P_a is the atmospheric pressure, ρ is the mean water column density, and g is the local gravity (assumed constant over the interval).

Equation (14) can be rearranged to isolate those terms related to variation in P_a and ρ and thus facilitate computation of uncertainties due to expected variations:

$$h_2 - h_1 = (P_{m_2} - P_{m_1})/(\rho_2 g) \pm \Delta \rho h_1 / \rho_2 \pm \Delta P_a / (\rho_2 g). \quad (15)$$

In equation (15), $(\Delta \rho h_1 / \rho_2)$ and $(\Delta P_a / \rho_2 g)$ are, respectively, the uncompensated effects of diurnal variations in density and atmospheric pressure.

Based on survey data, the maximum density change over the intervals analyzed was $\pm 0.00089 \text{ g/cm}^3$ and the maximum height (h_1) was 9.1 m. Then,

$$\Delta \rho h_1 / \rho_2 = (\pm 0.00089 / 1.015) (9.1) \text{ m} = \pm 0.008 \text{ m}.$$

It is estimated from the barometric pressure records that 95 percent of the diurnal variations of atmospheric pressure are less than ± 11 mbar, so that

$$\Delta P_a / (\rho_2 g) = \pm 0.11 \text{ m.}$$

The total environmental error (e_e) (in equivalent height) is the root-sum-square of the averaging error, the errors due to water current and to diurnal variations in water column density, and barometric pressure:

$$e_e = \pm (0.029^2 + 0.01^2 + 0.11^2 + 0.008^2)^{1/2} = \pm 0.114 \text{ m.}$$

If the atmospheric pressure (P_a) and mean water column density (ρ) could be assumed constant at the times of the two measurements, equation (14) would reduce to

$$h_2 - h_1 = (P_{m_2} - P_{m_1}) / (\rho_2 g). \quad (16)$$

The uncertainty of the computed differential water level due to the errors in the measured quantities (P_{m_1} , P_{m_2} , and ρ) is, from differentiation of equation (16),

$$d(h_2 - h_1) = (\Delta P_{m_1} + \Delta P_{m_2}) / (\rho_2 g) - (\Delta \rho / \rho_2) (h_2 - h_1). \quad (17)$$

The fractional density ($\Delta \rho / \rho_2$) in equation (17) is primarily the difference between the density ρ_2 used in reduction of field data (1.025 g/cm^3) and the range of measured densities (1.010 to 1.023 g/cm^3). The density error due to the errors in measured conductivity and temperature is comparatively small and can be neglected. With a tidal range of 0.9 m , the density-error term is

$$-(\Delta \rho / \rho_2) (h_2 - h_1) = - \left\{ \begin{bmatrix} +0.015 \\ +0.002 \end{bmatrix} \right\} \left\{ \frac{1}{1.015} \right\} \left\{ 0.9 \right\} \text{ m} = \begin{bmatrix} -0.013 \\ -0.002 \end{bmatrix} \text{ m.}$$

The remaining uncertainty ($\Delta P_{m_1} + \Delta P_{m_2}$) in equation (17) is due to the pressure sensor calibration uncertainty. Both ΔP_{m_1} and

ΔP_{m_2} are equal to the 95-percent confidence limits about the fitted calibration equation. Because this is a pressure difference computation, the systematic errors of the calibration process are not included:

$$(\Delta P_{m_1} + \Delta P_{m_2}) = (2) (95\text{-percent confidence limits})$$

For SN 360, the 95-percent confidence limits were ± 0.009 dbar. The calibration uncertainty term is then

$$(\Delta P_{m_1} + \Delta P_{m_2}) / (\rho_2 g) = \pm 0.018 \text{ m.}$$

The calibration uncertainties for the three sensors are as follows:

<u>SN</u>	<u>Calibration Uncertainty</u>
360	$\pm 0.018 \text{ m}$
361	$\pm 0.008 \text{ m}$
363	$\pm 0.018 \text{ m}$

The TMU in differential water-column height computation is the sum of the instrument calibration errors, the error due to density offset, and the environmental error:

$$\text{TMU (SN 360)} = \begin{bmatrix} +0.018 \\ -0.018 \end{bmatrix} + \begin{bmatrix} -0.002 \\ -0.013 \end{bmatrix} + \begin{bmatrix} +0.114 \\ -0.114 \end{bmatrix} = \begin{bmatrix} +0.130 \\ -0.145 \end{bmatrix} \text{ m.}$$

The computed TMU's for all three recorders are given below:

<u>SN</u>	<u>TMU (Differential Water Level)</u>
360	+0.13, -0.14 m
361	+0.12, -0.14 m
362	+0.13, -0.14 m

In addition to providing a time base for the pressure sensors, the internal oscillators control the instrument sampling interval. As previously discussed, the oscillators in all three instruments were within specification for pressure measurements. Based on

field-check records, the measured oscillator deviations were less than ± 0.9 ppm. This corresponds to a time-base error of ± 2.5 s/month.

7.4.10. Grundy 9400 Temperature

The temperature sensing portion of the CTD profiling system was initially calibrated at T&EL in January 1978. The calibration consisted of 39 points over a range of -1° C to $+35^{\circ}$ C. The systematic errors in the calibration process consist of the absolute error in the temperature bridge and platinum thermometer and also bath gradients. The magnitude of these combined errors is estimated not to exceed $\pm 0.006^{\circ}$ C.

A transfer function was fitted to the calibration data using the method of least squares; the resultant RSE was found to be $\pm 0.012^{\circ}$ C. Uncertainties in the transfer function at the 95-percent confidence level were computed by selecting an appropriate multiplier from Student's "t" table for 38 degrees of freedom; the RSE was multiplied by this value:

$$95\text{-percent CL} = (\pm 0.012^{\circ} \text{ C}) (2.03) = \pm 0.024^{\circ} \text{ C}.$$

The ECU was computed by summing the systematic and transfer function errors:

$$\text{ECU} = (\pm 0.006) + (\pm 0.024) = \pm 0.030^{\circ} \text{ C}.$$

An interim calibration was performed in December 1978, consisting of 26 points over the range of -1° C to 34° C. Substituting calibration data into the equation fitted during the January calibration resulted in a mean of the residuals equal to -0.012° C, indicating an apparent net drift. The standard deviation of the residuals was $\pm 0.012^{\circ}$ C; computation of the 95-percent confidence level for the interim calibration, using the "t" statistic for 25 degrees of freedom, yielded

$$95\text{-percent CL} = (\pm 0.012^{\circ} \text{ C}) (2.06) = \pm 0.024^{\circ} \text{ C}.$$

It is interesting to note that an ECU computed for the interim calibration is identical to the initial ECU ($\pm 0.030^{\circ}\text{C}$), indicating that sensor scatter has not changed but is now centered around a slightly different point (0.012°C lower). The SMU for the temperature sensor performance from January through December 1978 includes the systematic errors, the net drift between calibrations, and the respective 95-percent confidence level values:

$$\text{SMU (interim)} = \begin{bmatrix} +0.006 \\ -0.006 \end{bmatrix} + \begin{bmatrix} \\ -0.012 \end{bmatrix} + \begin{bmatrix} +0.024 \\ -0.024 \end{bmatrix} = \begin{bmatrix} +0.030 \\ -0.042 \end{bmatrix}^{\circ}\text{C}.$$

A final calibration consisting of 26 points over the range of 0°C to 30°C was performed in July 1979. Substituting these data into the January 1978 equation resulted in a mean of the residuals equal to $+0.13^{\circ}\text{C}$, indicating a significant net drift. The standard deviation of the residuals was equal to $\pm 0.010^{\circ}\text{C}$. The 95-percent confidence levels about the mean were computed using the "t" statistic for 25 degrees of freedom:

$$95\text{-percent CL} = (\pm 0.010^{\circ}\text{C}) (2.06) = \pm 0.021^{\circ}\text{C}.$$

An ECU computed for the final calibration ($\pm 0.027^{\circ}\text{C}$) again shows similarity of sensor performance. The SMU (final) represents the temperature measurement performance from December 1978 to the end of the survey and includes the systematic errors, the net drift between interim calibration and final calibration, and the respective 95-percent CL values:

$$\text{SMU (final)} = \begin{bmatrix} +0.006 \\ -0.006 \end{bmatrix} + \begin{bmatrix} +0.13 \\ \end{bmatrix} + \begin{bmatrix} +0.024 \\ -0.021 \end{bmatrix} = \begin{bmatrix} +0.16 \\ -0.03 \end{bmatrix}^{\circ}\text{C}.$$

In the field environment, data can be affected by the rate of change of temperature due to the time constant of the temperature sensor. The effect depends on the combination of profiling rate and local temperature gradients. A profiling speed of 0.25 m/s was used for the Grundy 9400 system; according to listed specifications, the temperature probe has a time constant of 0.35 s . The

"95-percent temperature gradient" (i.e., 5 percent of the actual gradients were steeper) selected was -2° C/m. Given that temperature measurements were only conducted during descent, the resultant error due to time response will be $+0.17^{\circ}$ C.

The TMU for water temperature measurements was computed by summing the SMU and the environmental errors due to gradients:

$$\text{TMU (1/78 - 12/78)} = \begin{bmatrix} +0.030 \\ -0.042 \end{bmatrix} + \begin{bmatrix} +0.17 \\ \end{bmatrix} = \begin{bmatrix} +0.20 \\ -0.04 \end{bmatrix} \text{ } ^{\circ} \text{C}$$

$$\text{TMU (12/78 - 7/79)} = \begin{bmatrix} +0.16 \\ -0.03 \end{bmatrix} + \begin{bmatrix} +0.17 \\ \end{bmatrix} = \begin{bmatrix} +0.33 \\ -0.03 \end{bmatrix} \text{ } ^{\circ} \text{C}$$

7.4.11. Grundy 9400 Conductivity

The conductivity sensing portion of the CTD profiling system was calibrated initially at T&EL in January 1978. The calibration consisted of 34 points over a range of 28 to 58 mS/cm. The systematic errors in the calibration process consist of the uncertainties associated with the working standard (Guildline 8400 Autosol) as well as temperature uncertainty and bath drift. The magnitude of these combined errors is estimated not to exceed ± 0.013 mS/cm.

A transfer function was fitted to the calibration data using multiple regression techniques; the resultant RSE was found to be ± 0.023 mS/cm. Uncertainties in the transfer function at the 95-percent confidence level were computed by selecting an appropriate multiplier from Student's "t" table for 33 degrees of freedom; the RSE was multiplied by this value:

$$95\text{-percent CL} = (\pm 0.023 \text{ mS/cm}) (2.04) = \pm 0.047 \text{ mS/cm}.$$

The ECU was computed by summing the systematic and transfer function errors:

$$\text{ECU} = (\pm 0.013) + (\pm 0.047) = \pm 0.060 \text{ mS/cm}.$$

An interim calibration was performed in December 1978, consisting of 25 points over the range of 27 to 57 mS/cm. Substituting calibration data into the equation derived during the January cali-

bration resulted in a mean of the residuals equal to -0.032 mS/cm, indicating an apparent net drift. The standard deviation of the residuals was equal to ± 0.031 mS/cm. The 95-percent confidence levels about the mean were computed using the "t" statistic for 24 degrees of freedom:

$$95\text{-percent CL} = (\pm 0.031 \text{ mS/cm}) (2.06) = \pm 0.063 \text{ mS/cm}.$$

The SMU represents conductivity measurement performance from January through December 1978; it includes the systematic errors, the net drift between calibrations, and the respective 95-percent confidence level values:

$$\text{SMU (interim)} = \begin{bmatrix} +0.013 \\ -0.013 \end{bmatrix} + \begin{bmatrix} \\ -0.032 \end{bmatrix} + \begin{bmatrix} +0.047 \\ -0.063 \end{bmatrix} = \begin{bmatrix} +0.06 \\ -0.11 \end{bmatrix} \text{ mS/cm}.$$

A final calibration was performed in July 1979, consisting of 26 points over the range of 29 to 59 mS/cm. Substituting these data into the January 1978 equation resulted in a mean of the residuals equal to $+ 0.01$ mS/cm; this is not considered a significant drift. The RSE was found to be ± 0.022 mS/cm; the 95-percent confidence levels were computed using the "t" statistic for 25 degrees of freedom:

$$95\text{-percent CL} = (\pm 0.022 \text{ mS/cm}) (2.06) = \pm 0.045 \text{ mS/cm}$$

The ECU for the final calibration was ± 0.058 mS/cm. Since this uncertainty band is completely contained within the interim SMU, the final SMU is equal to the interim SMU, resulting in a single value for the duration of the survey:

$$\text{SMU (1/78 - 7/79)} = + 0.06, - 0.11 \text{ mS/cm}.$$

Because the transfer function for the conductivity sensor includes a temperature sensitivity term, there is the potential for additional conductivity uncertainty induced by the uncertainty of the temperature measuring system. The magnitude of the tempera-

ture coefficient, however, is small enough (0.0068 mS/cm per °C) so that this error source can be neglected.

In the field environment, data can be affected by the rate of change of conductivity due to the time constant of the conductivity sensor. The effect depends on the combination of profiling rate and local conductivity gradients. A profiling speed of 0.25 m/s was used for the Grundy 9400 system; according to listed specifications, the conductivity sensor has a time constant of 0.1 s. The "95-percent conductivity gradient" (i.e., 5 percent of the actual gradients were steeper) selected was +10 mS/cm per meter. Given that conductivity was measured only during descent, the resultant error due to time response will be -0.25 mS/cm.

The TMU for conductivity measurements was computed by summing the SMU and the environmental errors due to gradients:

$$\text{TMU (1/78 - 7/79)} = \begin{bmatrix} +0.06 \\ -0.11 \end{bmatrix} + \begin{bmatrix} \\ -0.25 \end{bmatrix} = \begin{bmatrix} +0.06 \\ -0.36 \end{bmatrix} \text{ mS/cm.}$$

7.4.12. Grundy 9400 Depth

The depth (pressure) sensing portion of the CTD profiling system was initially calibrated at T&EL in January 1978. The calibration consisted of three cycles (5° C, 24° C, and 34° C) of 19 points each over a range of 0 to 100 dbar.* The systematic errors in the calibration process consist of the uncertainties associated with the standard (dead-weight piston gage) and are estimated not to exceed ± 0.17 dbar.

The manufacturer's transfer function was used to convert sensor output to indicated pressure; the resultant RSE was ± 0.32 dbar. Uncertainties in the transfer function at the 95-percent confidence level were computed by selecting an appropriate multiplier from Student's "t" table for 56 degrees of freedom; the RSE was multiplied by this value:

$$95\text{-percent CL} = (\pm 0.32 \text{ dbar}) (2.05) = \pm 0.66 \text{ dbar.}$$

*All pressures are gage pressure.

The ECU is the sum of the systematic and transfer function errors:

$$\text{ECU} = (\pm 0.17) + (\pm 0.66) = \pm 0.83 \text{ dbar}.$$

An interim calibration was performed in December 1978, consisting of three cycles (5°C , 20°C , and 34°C) of 21 points each over the range of 0 to 100 dbar. Substituting calibration data into the manufacturer's transfer function yielded an average residual of $+0.35$ dbar, indicating an apparent net drift. The standard deviation of the residuals was ± 0.30 dbar; computation of the 95-percent confidence level for the interim calibration, using the "t" statistic for 62 degrees of freedom, resulted in

$$95\text{-percent CL} = (\pm 0.30 \text{ dbar}) (2.00) = \pm 0.60 \text{ dbar}.$$

An ECU computed for the interim calibration (± 0.77 dbar) indicated sensor scatter comparable to the initial calibration. The SMU, which represents pressure sensor performance from January through December 1978, includes the systematic errors, the net drift between calibrations, and the respective 95-percent confidence level values:

$$\text{SMU (interim)} = \begin{bmatrix} +0.17 \\ -0.17 \end{bmatrix} + \begin{bmatrix} +0.35 \\ \end{bmatrix} + \begin{bmatrix} +0.60 \\ -0.66 \end{bmatrix} = \begin{bmatrix} +1.12 \\ -0.83 \end{bmatrix} \text{ dbar}.$$

The 9400 pressure sensing system developed operational problems in the field after the December 1978 calibration. When the system was returned in July 1979, the pressure sensor was found to be inoperative; thus, a final calibration was not performed. A check of field records indicated that the system was operational during the last cruise of the survey; it is suspected that the damage occurred during shipment. Since field checks were not performed, it is not possible to quantify pressure measurement uncertainty after December 1978.

In the field environment, data can be affected by the rate of change of pressure (i.e., the lowering rate) due to the time constant of the sensor. For the profiling speed used (0.25 m/s) and the reported sensor time constant (0.1 s), an error of -0.025 dbar will be induced.

The TMU for pressure measurements was computed by summing the SMU and the error due to sensor time constant:

$$\text{TMU (1/78 - 12/78)} = \begin{bmatrix} +1.12 \\ -0.83 \end{bmatrix} + \begin{bmatrix} -0.025 \\ -0.025 \end{bmatrix} = \begin{bmatrix} +1.10 \\ -0.85 \end{bmatrix} \text{ dbar}$$

7.4.13. Guildline 8400 Salinity

Shipboard measurements of salinity were conducted on the FERREL using the Guildline Model 8400 Autosol, SN 43.163. This instrument was initially calibrated at the NOS Northwest Regional Calibration Center in March 1978 using IAPSO standard seawater (C1 = 19.376 ppt) as a standard. The calibration report indicated that the instrument accuracy was within ± 0.003 ppt. It is estimated that additional uncertainties incurred during salinity measurements due to sample handling, cell rinsing, etc., did not exceed ± 0.002 ppt. The ECU for salinity measurements made with the Guildline Autosol is the sum of the two error components:

$$\text{ECU} = (\pm 0.003) + (\pm 0.002) = \pm 0.005 \text{ ppt.}$$

The Autosol was standardized before each set of shipboard salinity measurements; thus, the effects of drift were removed and the above ECU is valid for the duration of the survey.

To obtain measurement results in terms of salinity, it is necessary to convert the Autosol reading (proportional to conductivity ratio) to salinity using sample-temperature correction factors and the UNESCO salinity/conductivity relationships. During measurements, the sample-temperature correction step was inadvertently omitted. Salinity computations were thus made using a conductivity ratio at 21°C instead of the ratio at 15°C for which the tables and equations were developed. This process induces a bias in the salinity values that is positive below 35 ppt. The magnitude of the bias computed was $+0.02$ ppt at 20 ppt, decreasing to 0 ppt at 35 ppt. It is estimated that 95 percent of the salinities measured fell within the range of 21 to 35 ppt; the resultant bias would thus span $+0.018$ ppt to 0 ppt. The TMU is the sum of the ECU and the error due to computations:

$$\text{TMU} = \begin{bmatrix} +0.005 \\ -0.005 \end{bmatrix} + \begin{bmatrix} +0.018 \end{bmatrix} = \begin{bmatrix} +0.023 \\ -0.005 \end{bmatrix} \text{ ppt.}$$

7.4.14. Dissolved Oxygen (Micro-Winkler Titration)

Measurements were conducted in the FERREL chemistry laboratory on water samples using a potassium-iodate solution traceable to NBS standard potassium-dichromate solution or a solution of potassium iodate prepared from analytical-reagent-quality (certified by American Chemical Society) potassium-iodate powder and distilled water. Titration apparatus and glassware were provided by T&EL; volumetric calibrations on flasks were performed at T&EL. Measurements were made using the modified Winkler titration described by Carpenter (1965). The uncertainties associated with the dissolved oxygen measurements are within ± 0.04 ppm.

No additional uncertainties have been attributed to either operator errors or degradation of required chemicals. Training was provided at T&EL in the DO measurement process for FERREL personnel; further, the shipboard Winkler apparatus was designed to minimize field-induced problems. A sufficient stock of chemicals was provided to replenish those suspected of being contaminated.

7.4.15. Beckman RS-5 *In Situ* Salinometer

The Beckman RS-5 Salinometer measures temperature, conductivity, and salinity and was initially calibrated in March 1978 at the Northwest Regional Calibration Center. It was found that all parameters were within the manufacturer's specified accuracies of $\pm 0.5^{\circ}\text{C}$, ± 0.5 mS/cm, and ± 0.5 ppt.

After survey use on the NOAA Research Vessel VIRGINIA KEY, the instrument was recalibrated at T&EL in February 1979. Results of calibrations for the three parameters are detailed below.

Temperature

The temperature sensing portion of the RS-5 was calibrated at four points between $+7^{\circ}\text{C}$ and $+20^{\circ}\text{C}$. Systematic errors in the calibration process consist of the absolute error in the temperature bridge and the platinum thermometer and bath gradients. The magnitude of the combined errors is estimated not to exceed $\pm 0.006^{\circ}\text{C}$.

The RSE, determined from calibration data, was $\pm 0.26^{\circ}$ C. The 95-percent confidence level was computed by selecting an appropriate multiplier from Student's "t" table for 3 degrees of freedom; the RSE was multiplied by this value:

$$95\text{-percent CL} = (\pm 0.26) (3.18) = \pm 0.83^{\circ} \text{ C.}$$

The ECU was computed by summing the systematic error and the 95-percent confidence level:

$$\text{ECU} = (\pm 0.006) + (\pm 0.83) = \pm 0.83^{\circ} \text{ C.}$$

Because the post-survey calibration uncertainties encompass the initial calibration results, the SMU will be equal to the post-survey ECU:

$$\text{SMU} = \pm 0.83^{\circ} \text{ C.}$$

In obtaining the field data, the sensor package was lowered to predetermined depths and allowed to stabilize prior to recording data. The uncertainty in vertical position (i.e., depth) of the sensor package was estimated to be within 0.3 m. It is also estimated that more than 95 percent of the data were gathered during well-mixed conditions. While the uncertainty in depth may be significant in terms of where the data were obtained, it has no impact on the uncertainty of the temperature data *per se*. The TMU is therefore equal to the SMU:

$$\text{TMU} = \pm 0.83^{\circ} \text{ C.}$$

Conductivity

Calibration of the RS-5 conductivity sensor was performed at five points over the range of 17 to 58 mS/cm. The systematic errors in the calibration process consist of the uncertainties associated with the working standard (Guildline 8400 Autosol), the temperature uncertainty, and bath drift. The magnitude of these combined errors is estimated not to exceed ± 0.013 mS/cm.

The RSE was found to be ± 0.32 mS/cm; the computation of

95-percent confidence level, using the "t" statistic for 4 degrees of freedom, resulted in

$$95\text{-percent CL} = (\pm 0.32) (2.78) = \pm 0.89 \text{ mS/cm.}$$

The ECU is the summation of the systematic error and the 95-percent confidence level:

$$\text{ECU} = (\pm 0.013) + (\pm 0.89) = \pm 0.90 \text{ mS/cm.}$$

As with temperature, the post-survey calibration uncertainties encompass the initial calibration results. Thus, the SMU is equal to the post-survey ECU:

$$\text{SMU} = \pm 0.90 \text{ mS/cm.}$$

Uncertainty of vertical position had no effect on conductivity uncertainty (see temperature section); the short deployment times resulted in no degradation due to biofouling of the conductivity sensor. The TMU is therefore equal to the SMU:

$$\text{TMU} = \pm 0.90 \text{ mS/cm.}$$

Salinity

Calibration of the salinity measurement from the RS-5 was performed at five points over the range of 16 to 35 ppt salinity. Systematic errors in the calibration process consist of the uncertainty of the working standard (Guildline 8400 Autosol) that is estimated not to exceed ± 0.003 ppt.

The RSE computed from the calibration data was ± 0.56 ppt. Computation of the 95-percent confidence level, using the "t" statistic for 4 degrees of freedom, yielded

$$95\text{-percent CL} = (\pm 0.56) (2.78) = \pm 1.56 \text{ ppt.}$$

The ECU was computed by summing the systematic error and the 95-percent confidence level:

$$\text{ECU} = (\pm 0.003) + (\pm 1.56) = \pm 1.56 \text{ ppt.}$$

The post-survey calibration uncertainties encompass the initial calibration results; thus the SMU is equal to the ECU:

$$\text{SMU} = \pm 1.56 \text{ ppt.}$$

As indicated in the sections on temperature and conductivity, no additional uncertainty due to environmentally induced factors was incurred. Thus, the TMU is equal to the SMU:

$$\text{TMU} = \pm 1.56 \text{ ppt.}$$

8. GULF AT-SEA PERFORMANCE EXPERIMENT

by Henry R. Frey, Gerald F. Appell, David R. Crump, and
James R. McCullough

The Gulf At-Sea Performance (GASP) Experiment was conducted by NOS at the West Hackberry site for 32 days beginning April 5, 1979. Objectives and results of the GASP Experiment related to DQA are discussed in this section; objectives and results related to the physical oceanographic characterization of the West Hackberry site are described in volume one of this report (Frey et al. 1981).

8.1. OBJECTIVES

The principal objective of the GASP Experiment was to obtain field data needed to correlate the response of the Grundy Model 9021 current meter with laboratory tests and an error prediction model. The results of the lab tests, error model, and GASP Experiment were analyzed to estimate the TMU's associated with current velocity measurements (section 9). The secondary objectives were (1) to test the hypothesis that current measurements from a subsurface platform in a shallow water environment would exhibit higher S/N ratios than those made from compliant moorings and (2) to determine the validity of combining prior current measurements, made by others at both sites using Endeco Model 105 instruments (U.S. Department of Energy 1978), with measurements obtained by NOS with the Grundy Model 9021 instruments. The design of the experiment was based on these objectives.

8.2. DESIGN OF THE EXPERIMENT

Analysis of 5 months of current measurements obtained previously by NOS at station 11 (West Hackberry center) indicated the principal current axis to be along 85 - 265 degrees true, approximately parallel to the local isobaths. The array of instruments was deployed in a single straight line along the principal axis to minimize effects of crossflow variations and, therefore, to avoid

the need to measure crossflow correlations. Both horizontal and vertical variations in the currents were monitored to determine the validity of the experiment. The primary level selected for obtaining DQA-related data was 3 m above the bottom.

The GASP Experiment configuration and instrument labeling code are given in figure 33. Grundy current meters were positioned at 1-m, 2-m, 3-m, and 4-m levels to observe vertical shear of the horizontal current and to test the platform vs. mooring hypothesis. Horizontal shear was monitored at the 3-m level with identical Neil Brown Instrument Systems (NBIS) vector-averaging acoustic current meters at each end of the array. Wave induced current fluctuations were measured with an NBIS burst-sampling acoustic current meter and a Marsh-McBirney, Incorporated (MMI) Model 585 burst-sampling electromagnetic current meter, both at the 3-m level. AMI wave gages were mounted on the platforms supporting the burst-sampling current meters. The two NBIS vector-averaging current meters (132 and 832) recorded data every 10 min. The burst-sampling current meters were positioned about 15 m inboard of the NBIS vector-averaging instruments and were set to sample at a 1-s rate for 1 min of each hour. As stated previously, Endeco current meters (633 and 613) were included to compare their performance with that of the Grundy current meters.

8.3. MEASUREMENT QUALITY CONTROL

Quality control of GASP Experiment data made possible the development of measurement uncertainties for each instrument and provided the basis for determining how closely measurements among instruments could be compared. The instruments were calibrated before deployment and after recovery from the GASP Experiment, except for the Grundy current meters that could not be withdrawn from the 12-month study to obtain individual calibrations. The measurement uncertainty of the Grundy current meters is based on the ensemble of 36 instrument uncertainties developed in section 9. The structural rod positions of the platforms used with the Grundy instruments were referenced to magnetic north during the GASP Experiment to examine platform blockage effects on current measurements. An NBIS acoustic current meter mounted on an instrument platform is shown in figure 34. Platforms used with the NBIS and MMI current meters had no structural members upstream and were designed to minimize data

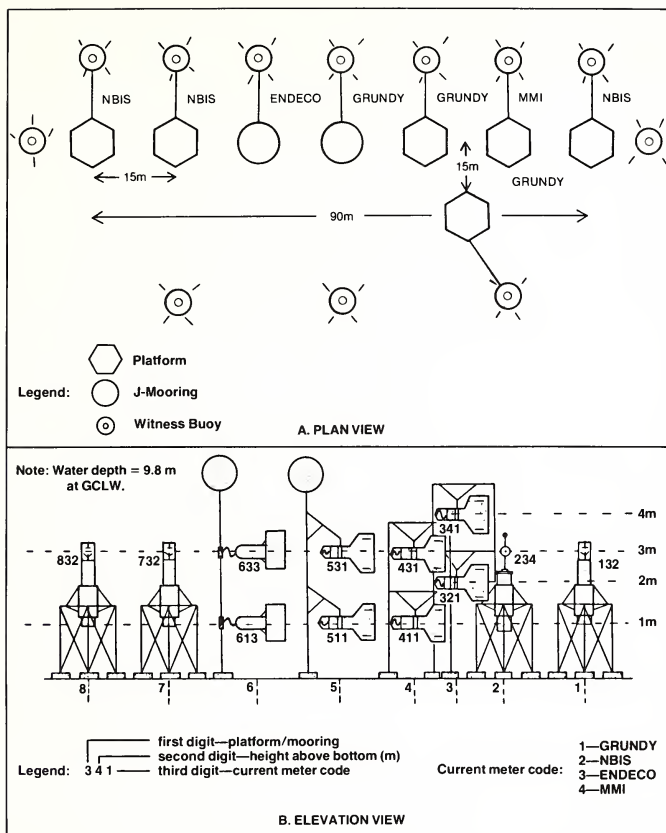


Figure 33.--GASP Experiment configuration.

contamination at the expense of vulnerability to damage; this was reduced by using 12 witness moorings surrounding the array. Individual instrument transfer functions based on the laboratory calibrations were developed for each of the NBIS and MMI current meters; field data processing was based on these transfer functions.

Speed calibrations were performed at the DT-NSRDC tow facility. A first-degree, least-squares analysis of the data from each current meter was applied to determine the transfer function for steady-flow conditions. Directivity tests were performed to quantify additional uncertainties due to noncosine responses. The MMI and NBIS burst-sampling instruments were also dynamically tested on the VPMM at

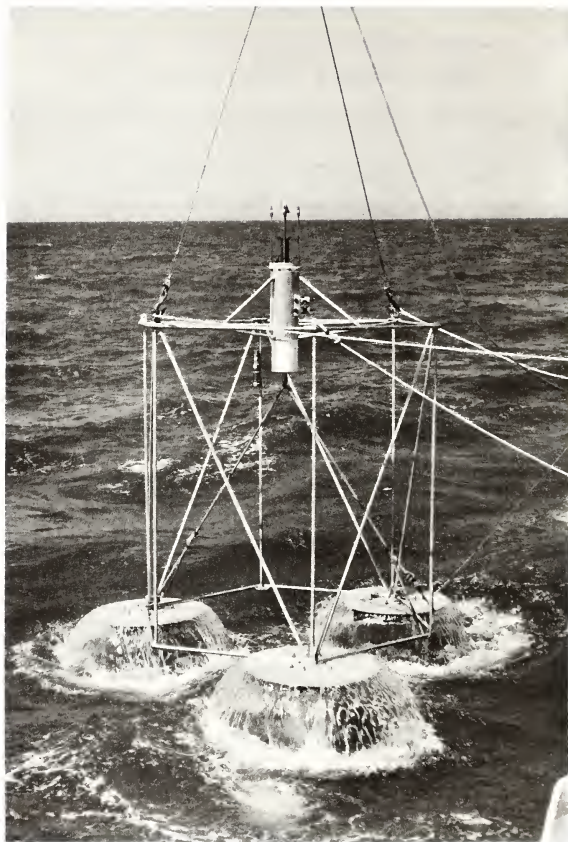


Figure 34.--NBIS acoustic current meter and platform used in GASP Experiment.

DT-NSRDC over the range of conditions imposed earlier on the Grundy Model 9021 instruments (section 4). The tests indicated that horizontal dynamics with S/N ratios greater than 1 produced no identifiable additional uncertainty in the determination of mean-flow components for these instruments. The TMU's listed in table 8 indicate the 95-percent level of estimated uncertainty associated with each speed measurement and were calculated for a speed of 16 cm/s, the approximate mean speed during the GASP Experiment. Additional environmental uncertainties for the NBIS and MMI meters were negligible.

Table 8.--Speed measurement uncertainty for NBIS, MMI, and Grundy current meters during the GASP Experiment

<u>Manufacturer</u>	<u>GASP Number</u>	<u>TMU (at 16 cm/s)</u>
NBIS	132	-3.5, +3.1 cm/s
MMI	234	-2.5, +2.5 cm/s
NBIS	732	-4.1, +3.8 cm/s
NBIS	832	-3.1, +2.8 cm/s
Grundy	(All)	-4.0, +1.8 cm/s

Direction measurement uncertainties include compass errors, flow directivity errors, dynamic errors, and environmentally induced errors. Compass calibrations were performed before the GASP Experiment and upon completion of the experiment. A first-degree, least-squares analysis of the data from each compass was applied to determine the transfer function. Flow directivity errors were determined during DT-NSRDC tow facility tests. Such errors are a function of the orthogonal speed errors. Dynamic flow errors in direction were determined during the VPMM tests at DT-NSRDC. Flow direction errors due to dynamics with S/N ratios greater than 1 were not observed. The direction measurement uncertainty for each instrument is identified in table 9 at the 95-percent confidence level and is represented at 16 cm/s, the mean speed during the GASP Experiment.

Table 9.--Direction measurement uncertainty for NBIS, MMI, and Grundy current meters during the GASP Experiment

<u>Manufacturer</u>	<u>GASP Number</u>	<u>TMU (at 16 cm/s)</u>
NBIS	132	- 1.8, + 7.3 degrees
MMI	234	- 4.0, + 4.0 degrees
NBIS	732	- 2.0, + 7.5 degrees
NBIS	832	- 1.6, + 7.1 degrees
Grundy	(All)	-10.9, +10.9 degrees

8.4. GENERAL CONDITIONS

A wide range of meteorological and oceanographic conditions existed during the 32-day GASP Experiment period; this was fortunate in that the conditions during the experiment were representative of the conditions experienced during the entire 12-month field effort.

For example, prefrontal southerly winds of 15 m/s drove 3-m level currents to over 80 cm/s; on the other hand, there were occasions when currents were within a few cm/s of zero. Prior to the GASP Experiment, the maximum observed current speed was also 80 cm/s, observed during Tropical Storm DEBRA on August 28, 1979; thus, the full range of current speeds observed during the entire 12-month field effort was encountered during the GASP Experiment.

8.4.1. Current Measurements

The test for horizontal homogeneity of the currents along the 3-m level of the array axis validated the experiment design. The mean speed and direction of the two instruments (132 and 832) at the array ends are shown in table 10. The 20-day, vector-averaged data indicate differences of 0.8 cm/s in speed and 0.4 degrees in direction (small fractions of the TMU's). The east and north components are in the ratio (132/832) of 1.05 and 1.01, respectively, while variances of the components are essentially indistinguishable. Because the NBIS current meters (132 and 832) were separated by approximately 90 m, an upper bound for the combined ocean and instrument mean shear is approximately $8 \times 10^{-5} \text{ s}^{-1}$.

The vertical shear of the horizontal currents, computed from the 20-day, vector-averaged data, is approximately $5 \times 10^{-2} \text{ s}^{-1}$, or about 10^3 times larger than the horizontal shear. Thus, separation in the vertical of 10 cm was as important as 100 m horizontal separation.

Table 10.--Statistical summary of current meter observations during the first 20 days of the GASP Experiment

Height above bottom (m)	GASP instrument number	Current meter type*	20-day vector averages (cm/s)				20-day vector speed (cm/s)	20-day vector direction (degrees)
			speed		standard			
			components		deviations			
			East	North	East	North		
4	341	R	-21.4	-3.1	14.8	8.1	21.6	261.8
3	132	A	-16.6	-3.1	13.8	8.9	16.9	259.4
3	234	E	-16.4	-1.2	14.0	9.3	16.5	265.9
3	431	R	-14.9	-2.6	12.9	7.4	15.2	260.2
3	732	A	-15.9	-2.8	14.1	9.4	16.1	260.2
3	832	A	-15.8	-3.1	13.7	9.0	16.1	259.0
2	321	R	-12.1	-2.1	13.1	9.5	12.3	260.1
1	411	R	- 5.9	-3.3	11.4	8.8	6.8	240.3
1	511	R	- 6.6	-1.4	12.0	8.9	6.8	258.2

*Current meter types:

R - rotor (Grundy) A - acoustic (NBIS) E - electromagnetic (MTI)

The data required to accomplish the principal objective of the GASP Experiment were obtained. Figure 35 shows wind speed and direction at 15.8 m above the sea surface, wave-induced speed fluctuations at the 3-m level, and maximum and significant surface wave heights. Figure 36 shows current speed and direction at the 3-m level with a storm occurring about midday on April 11, 1979. The mean currents exhibited a westward trend during most of the 32-day experiment.

8.4.2. Wave Climate and Flow Signal-to-Noise Ratio

Figure 37 shows a typical 1-min sample of 60 consecutive 1-s velocity measurements made each hour by the NBIS (732) acoustic meter. The scatter illustrates wave-induced flow; the large arrow is the mean for the burst. Because of limited current meter tape storage, the tape used was filled in 20 days, thus ending the record on April 26. Because of the short record on NBIS (732) and fouling on Grundy (431), only the first 20 days of the experiment were used for the comparative analysis. Since no *in situ* vector averaging was performed by the NBIS (732) instrument, 1-s samples were vector averaged after the experiment to estimate the hourly vector means. As seen in table 10, the hourly estimates made in this way and vector-averaged over 20 days appear to form unbiased estimates with only slightly greater variance than that of the *in situ* averaging instruments.

We define the flow signal-to-noise (S/N) ratio as the ratio of the mean flow to the standard deviation of the fluctuations in each 1-min burst. When the S/N is high, the mean flow is large compared with the fluctuations; when the ratio is below about 1.4, the fluctuations exceed the mean, and reversing flow is possible in each wave cycle. Figure 38 shows the S/N values for April 6 to April 26 as determined from the NBIS burst-sampling instrument (732). (Note that the ratio is typically in the range from 2 to 10 and only occasionally falls below the critical value of 1.4.) In addition, all values below 1.4 are associated with mean speeds of less than 10 cm/s. Similar conditions are indicated by the MMI burst-sampling instrument (234) for the same period and the balance of the experiment. Thus, during most of the experiment and during all of the energetic events, mean speeds exceeded the wave-induced fluctuations.

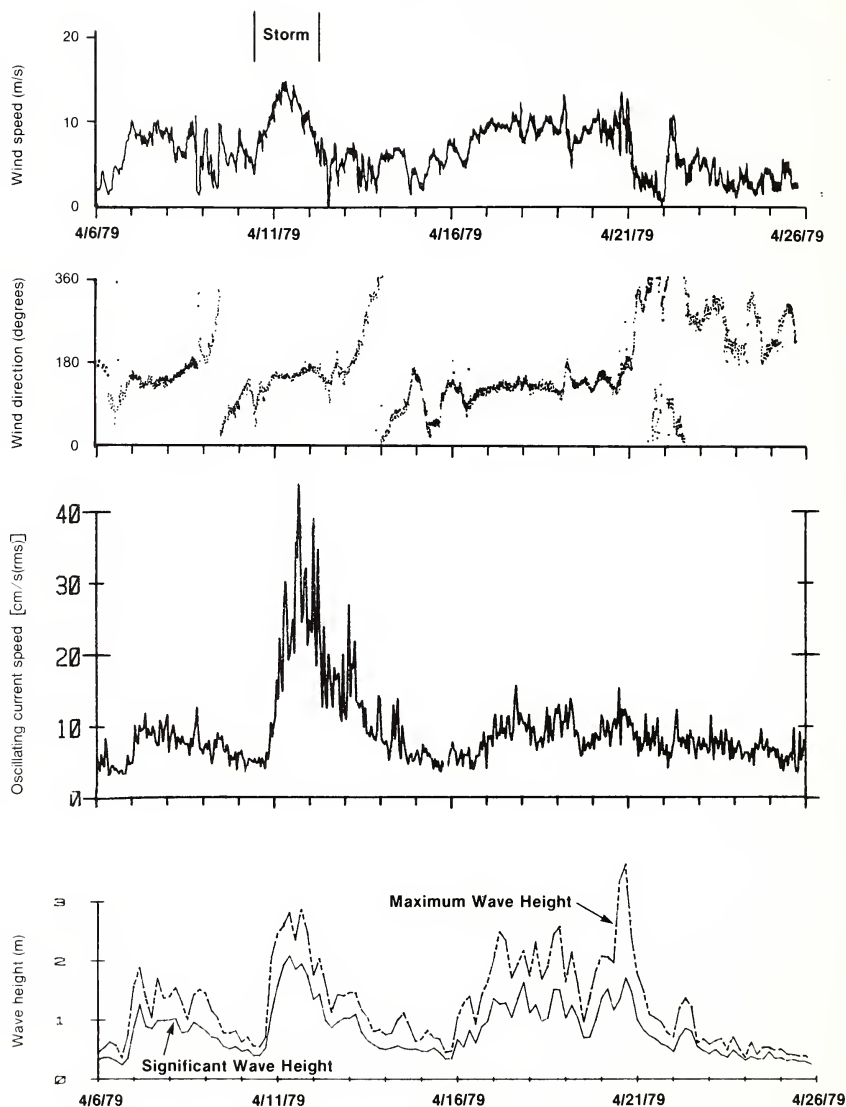


Figure 35.--Wind speed and direction (+16 m), oscillating current speed (+3 m), and wave height during the first 20 days of GASP Experiment. Note: Wind data have a 40-minute time discrepancy and are thus not archived.

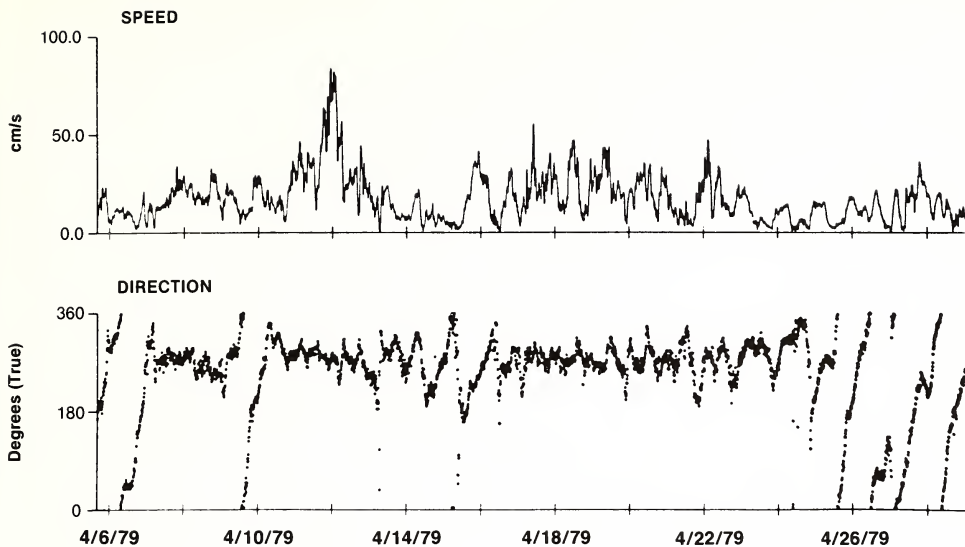


Figure 36.--Currents measured at 3-m level with a Grundy Model 9021 current meter during the GASP Experiment.

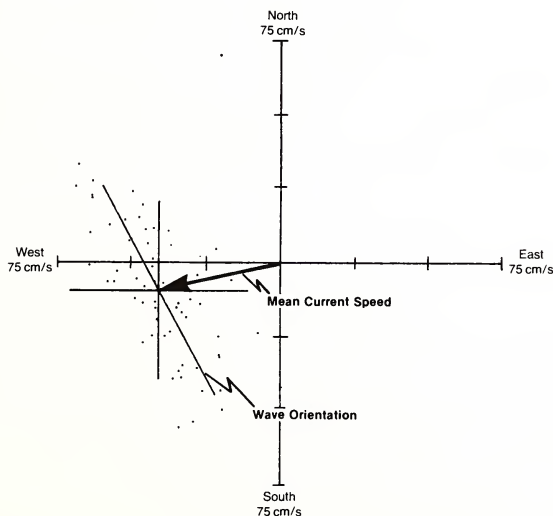


Figure 37.--Sixty consecutive 1-s velocity samples illustrate typical 1-hr burst-mode data obtained with NBIS (732) instrument at 3-m level. Scatter points represent the heads of instantaneous vectors (April 11, 1979, 2000 GMT, S/N = 1.6).

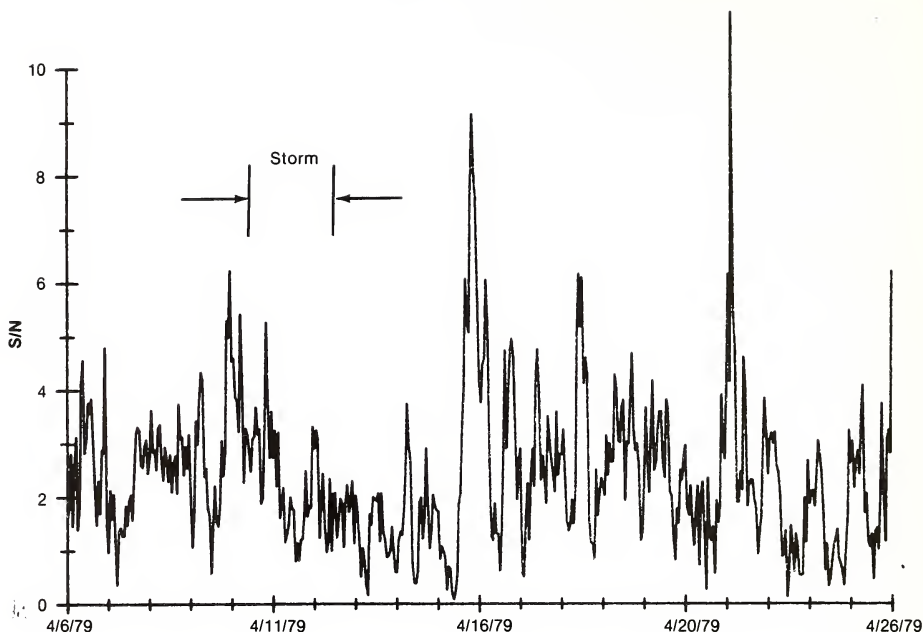


Figure 38.--Flow signal-to-noise (S/N) ratio for the first 20 days of the GASP Experiment. (Favorable current conditions ($S/N > 1$) predominate. Values shown for $S/N < 1$ occur at mean speeds < 10 cm/s.)

As shown earlier in section 4, such favorable conditions with nonreversing flow greatly increase the accuracy expected with large-vane-type current meters such as the Grundy Model 9021. Larger errors would be anticipated at lower S/N ratios, near or below 1.4.

8.4.3. Instrument Performance

The importance of vertical separation between GASP Experiment instruments precluded interpretation of data recorded by the Endeco Model 105 current meters. The Endeco instrument was moored with a 1.5-m rope tether and was, thus, free to move vertically (due to buoyant or hydrodynamic effects) up to twice this distance. Divers inspected the array of instruments immediately after deployment, after 15 days, and at the end of the 32-day experiment. During the midexperiment and final diving inspections, the Endeco (613) current

meter, clamped to its mooring at 1 m, was found buried in the bottom. Although both Endeco current meters operated and recorded data during the entire experiment, data from the 613 could not be used because the instrument was mounted too close to the bottom for its tether design; data from the 633 were not used because of unresolved inconsistencies in speed and direction.

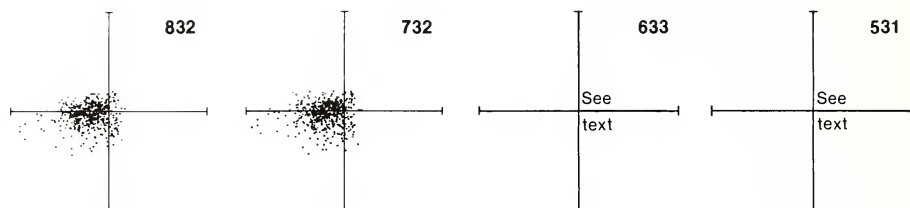
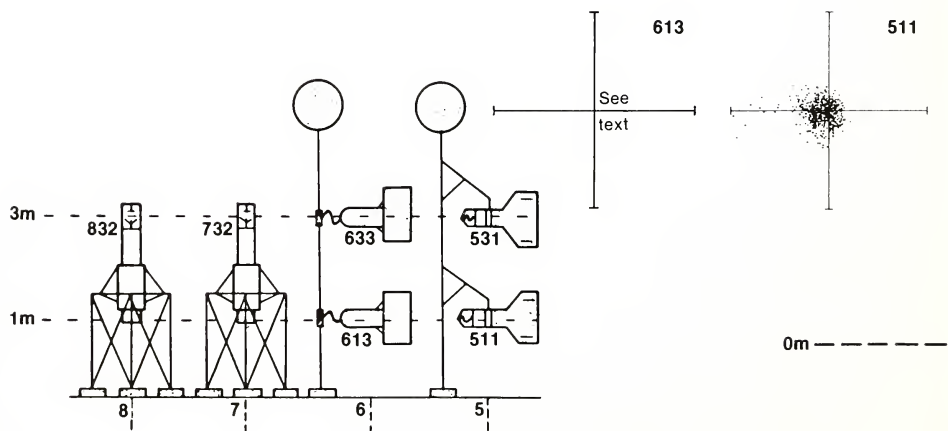
The uppermost Grundy current meter (531) on the subsurface mooring failed to record speed data during the entire GASP Experiment; thus, the differences in induced noise by platforms and compliant moorings remain untested. The wire rope on the subsurface mooring supporting the Grundy current meters parted 4 days before recovery, truncating the time series obtained with Grundy (511) at 1 m above the bottom.

Figure 39 shows the east-north scatter diagrams for the 1-hr, vector-averaged data during the initial 20-day period. The diagrams are arranged by relative depth and platform location corresponding to the diagram of figure 33. Both the mean and variance increase with height above the bottom. The similarity of the scatter diagrams suggests that few erratic sample errors were encountered and that directional biases (noted by Beardsley et al. [1977] with fixed-orientation, component-measurements current meters) were not present. Means and standard deviations for the data are given in table 10.

In figure 40, the low-frequency response and long-term directional variations of the nine current meters for the entire 32-day period are displayed as progressive vector diagrams. Directional differences of instruments 234 (+6.0 degrees) and 411 (-19.6 degrees) are apparent as are variations of mean speed with depth. The plots provide a compact overview of all the data. Note that the tides turn clockwise (increasing bearings with time) except at the 1-m level where the effect is less obvious.

Figure 41 shows the scatter diagrams from the 3-m level for the 1-hr vector-averaged speeds during the initial 20 days of the experiment in matrix form. Each frame (A-J) shows the hour-by-hour comparison of the instrument pair designated by the row and column headings. Frame A, for example, shows the correlation between the NBIS current meters (132 and 832) located at the extreme ends of the array. A 45-degree diagonal line representing perfect

----- 4m -----

 $2m$ 

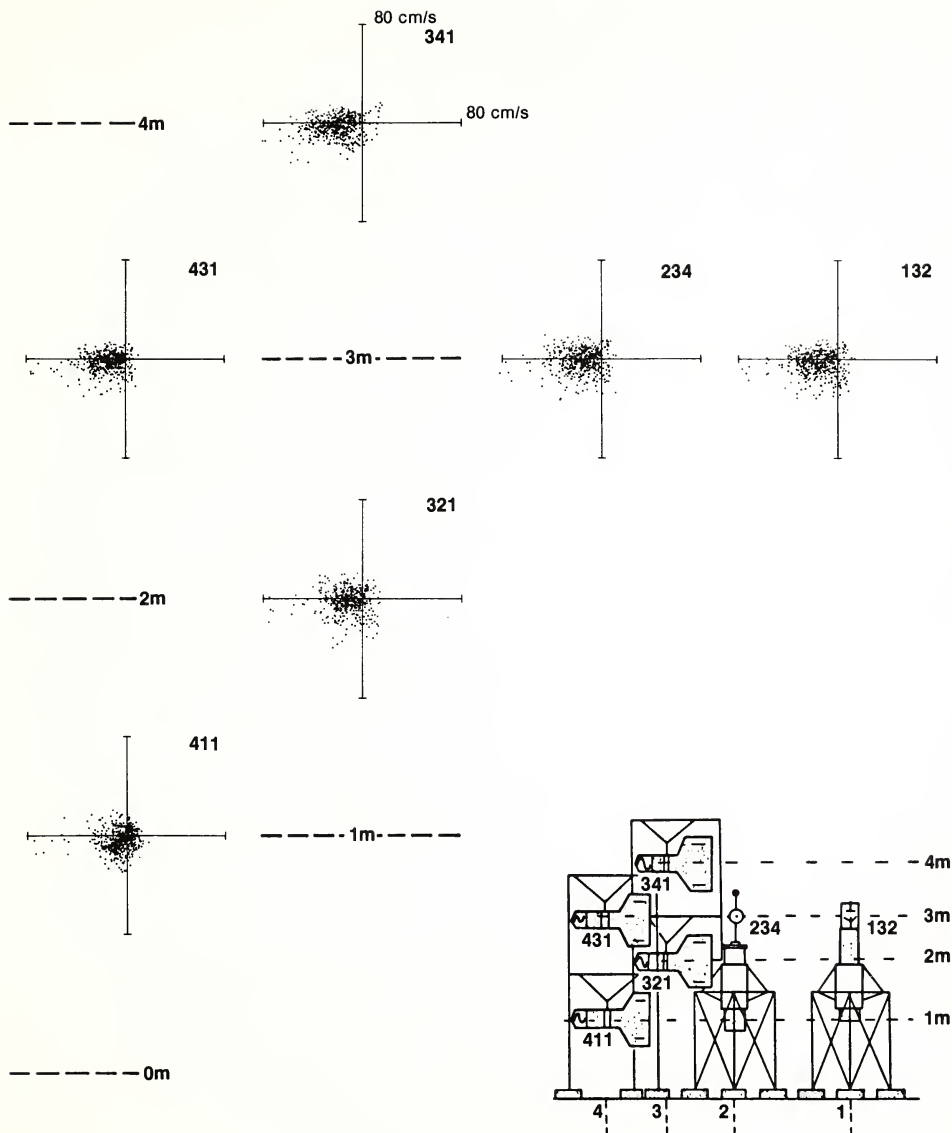


Figure 39.--East-north scatter plots of 1-hr flow vectors for nine current meters during the GASP Experiment. (Frames are arranged by depth and platform/mooring location. Note overall similarity and increasing mean and variance with height above bottom.)

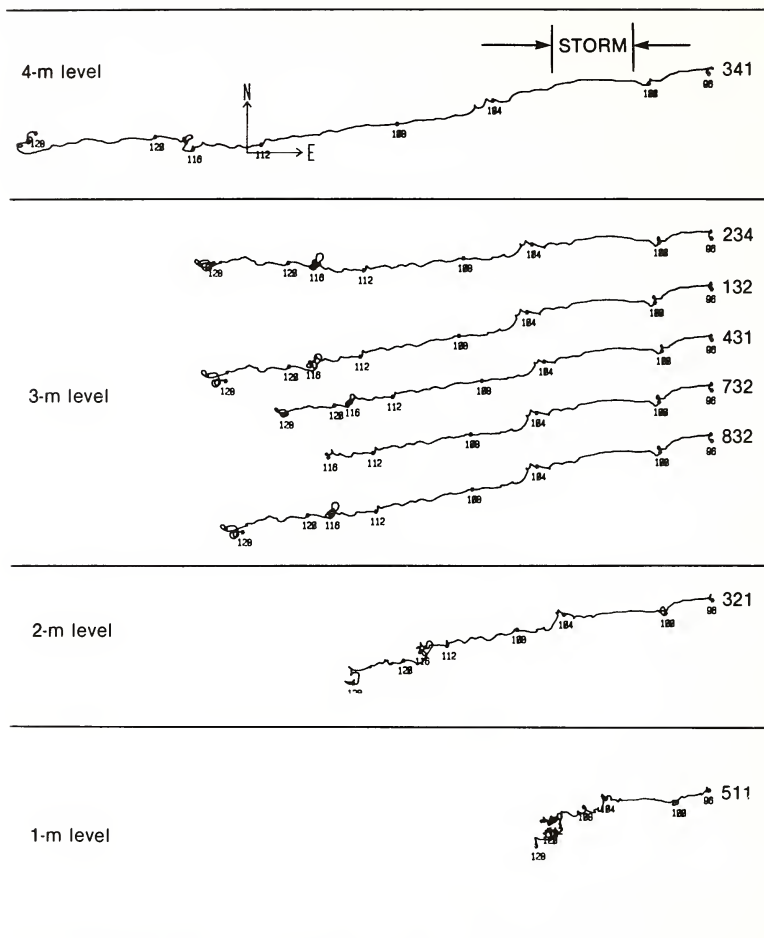


Figure 40.--Progressive vector diagrams of currents during GASP Experiment.

correlation has been added to each frame for reference. (Note that the smallest scatter (A) exists over the largest horizontal separation, suggesting that larger scatter is caused by instrument, depth, or sampling effects.) The slightly larger scatter associated with the MMI (234) and the NBIS (732) current meters are thought to be caused by the burst sampling (1 min per hr) used to estimate the hourly means. One prominent feature in this presentation is the relatively low readings at all speeds for the Grundy (431) instrument

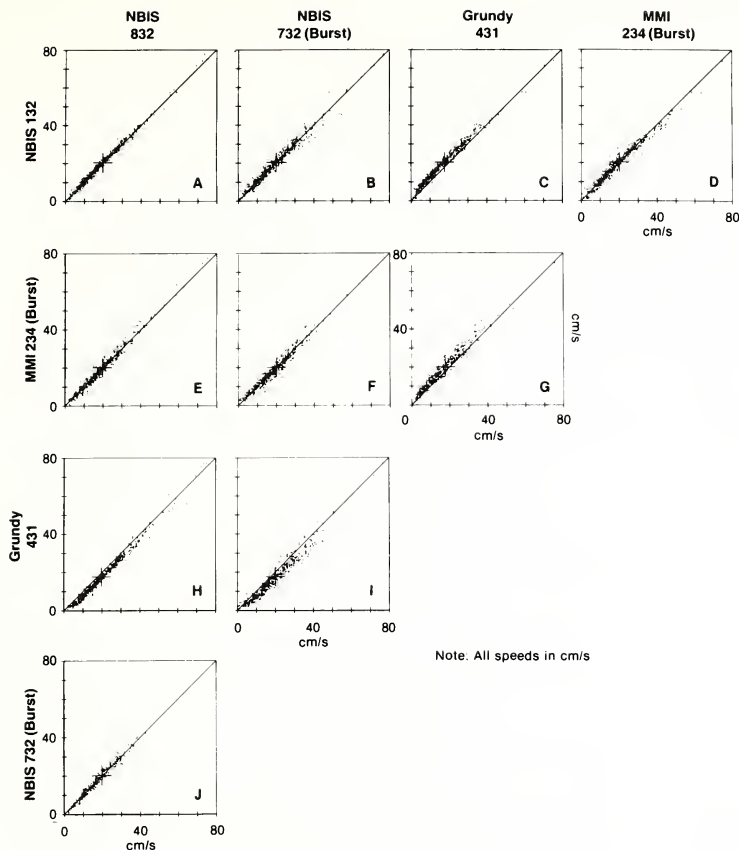


Figure 41.--Scatter diagrams of 1-hr vector averaged speeds for instrument pairs at the 3-m level. Frame A compares two acoustic instruments (132 and 832) at the extreme ends of the array. Burst instruments (234 and 732) show slightly greater scatter. The Grundy (431) reads consistently low at all speeds.

(frames C, G, H, and I). The effect appears to be a constant offset toward lower speed throughout the 20-day interval. Possible mechanisms include flow blockage by the platform rods, calibration uncertainties, instrument tilt, and cosine errors. The actual cause is not apparent from study of the field data, but the offset is contained in the TMU.

Figure 42 shows the 20-day vector mean speeds and directions (from table 10) as a function of depth. An arbitrary straight line (shear $\approx 5 \times 10^{-2} \text{ s}^{-1}$) has been added to the speeds for

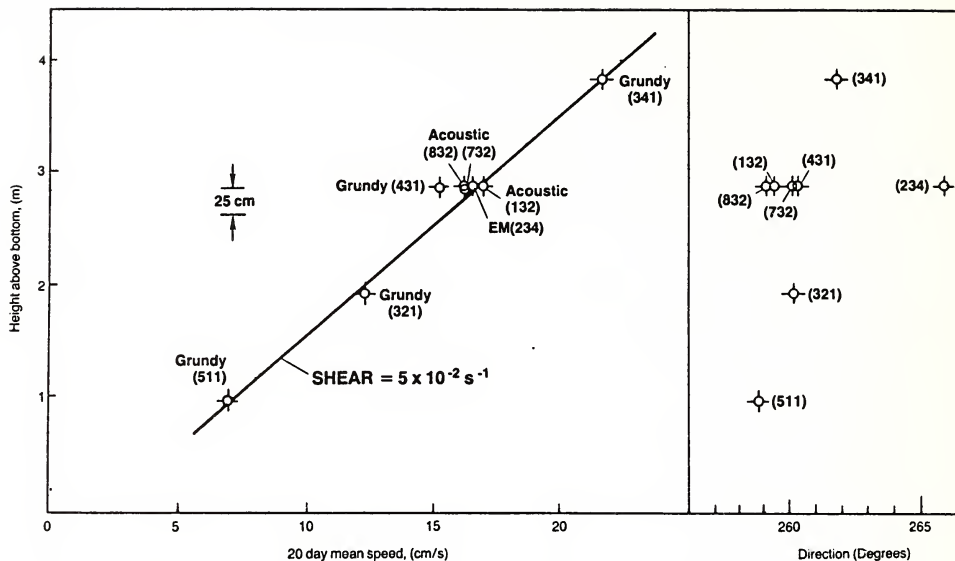


Figure 42.--GASP Experiment data plotted as 20-day vector-averaged speeds and directions. (The mean vertical shear of the horizontal currents is estimated at about $5 \times 10^{-2} \text{ s}^{-1}$.)

reference. All nine current meter means lie within $\pm 0.5 \text{ cm/s}$ of the line, except for the Grundy (431). The variation of the mean vector directions with depth (shown at the right-hand portion of figure 42) is less than ± 2 degrees, except for the MMI instrument (234).

8.5. CONCLUSIONS

The observed data show greater internal consistency than has been typical in similar at-sea experiments. [See for example Beardsley et al. (1977) and Halpern (1977).] Internal agreement among the GASP Experiment data is attributed to individual instrument calibration, rigid instrument platforms, favorable array design, and favorable flow conditions. The principal objective was accomplished; field data needed to correlate laboratory test data with an error prediction model were obtained, and TMU's associated with current velocity measurements were developed. A complete discussion of current-measurement TMU's is given in section 9.

9. CURRENT MEASUREMENT UNCERTAINTY ANALYSIS

by Stephen H. Koeppen

The measurement of current velocity was required to describe the circulation and to estimate brine dispersion at the proposed disposal sites. Because waves and swell are prevalent in the relatively shallow water in which the measurements were made, the currents observed by the instruments consisted of a steady flow component combined with an oscillating flow component. The oscillating component (dynamics) introduces errors into both the magnitude and direction of the mean current velocity measurement; this is caused by both the induced motion of the instrument and the nonlinear response of its sensors. Control of the dynamic induced errors was of prime concern in the design of the field experiment. Mounting of the current meters on platforms eliminated error components, which would otherwise have been induced by compliant moorings and subsequently interpreted as true velocities. The platforms, however, produced their own source of error--flow blockage; these and other sources of error and the derivation of their magnitude are considered in this section.

The establishment of a program to quantify current measurement uncertainties was initiated as the major part of the DQA effort. Extensive laboratory evaluations were conducted into the response characteristics of the Grundy Model 9021 under controlled, simulated field conditions (section 4). Quality assurance was provided by calibrating each rotor and compass during the initial I&A phase (section 5), and continued quality control was maintained by the shipboard field checks (section 6). A field experiment (section 8) was designed and implemented with the intention of providing quantitative field data to aid in the analysis of current measurement uncertainties. MAR, Inc., Rockville, Md., was contracted to provide the analysis and correlation of all data (Koeppen 1980); this was accomplished in collaboration with coinvestigators from NOS and the NOAA Office of Ocean Engineering (OOE).

The analysis presented here is separated from the uncertainties developed in section 7 because of the greater importance of the current velocity measurement to the circulation study. The determination of the 95-percent error bounds represented by an SMU was supplemented by a statistical analysis for the qualification of field error sources.

9.1. LABORATORY RESULTS

Sources of current measurement error include uncertainties in the calibration process and environmental effects such as

- platform blockage,
- rotor fouling,
- misalignment with flow direction, and
- dynamic current effects.

The purpose of the laboratory testing described in section 4 was to provide the data needed to quantify these errors. As in the calibration process, however, there are uncertainties in the laboratory measurements that contribute to uncertainties in the exact magnitude of the errors introduced by the environmental effects. These uncertainties lead to confidence limits about a mean or most probable error. In addition, these errors can vary as a function of time or from one current meter to another due to varying fouling levels, misalignment angles, etc., resulting in additional uncertainty over a period of time and over the current meters taken as a group.

The purpose of this section is to extract the data from the laboratory test results needed to quantify both calibration errors and environmental errors and, where appropriate, to estimate the 95-percent confidence limits of the laboratory measurement uncertainties. Additional uncertainties that vary over time and from one current meter to another are considered in section 9.2.

9.1.1. Steady Flow Measurements

As described in section 4, performance tests were carried out at the DT-NSRDC on a Grundy 9021, SN 52. These tests included rotor speed calibration, directivity response, vane alignment accuracy, and platform flow blockage. SN 52 was subsequently used as a "transfer standard" to calibrate the submerged jet facility at T&EL that was, in turn, used to calibrate the rotors on all

36 current meters before deployment. Compasses in all 36 units were also tested over their full range for deviations from the standard calibration equation provided by Grundy. Because of problems in the field with 15 of the current meters (section 5), the rotor and compass measurements were repeated for only 21 of the current meters after recovery. The errors associated with these performance tests and calibration measurements are discussed separately in the following paragraphs.

Rotor Speed Calibration:

Rotor calibration for the 36 units was a three-step process consisting of the tow tank calibration of SN 52, calibration of the T&EL submerged jet facility using SN 52 as a transfer standard, and calibration of the 36 current meter rotors in the submerged jet. The dominant systematic errors associated with each step and the resulting Estimated Calibration Uncertainty (ECU) for the 36 current meter rotors are discussed here.

The dominant systematic error in the first step, the tow tank calibration of Grundy SN 52, was determined to be the contribution of induced currents in the tow tank caused by the motion of the current meter through the water. This effect was minimized by waiting between successive tow carriage runs for the currents to dissipate; the error was estimated not to exceed ± 0.5 cm/s based on previous measurements of residual currents made at DT-NSRDC. Other systematic errors included the measurement error in the tow carriage speed, the effect of the finite tow channel cross-section on flow, and misalignment of the current meter with the tow direction; these errors were calculated but were found to be negligible compared to the induced current error.

A total of 31 tow carriage runs at speeds from 5 to 360 cm/s were performed. The Residual Standard Error (RSE), based on a second-order, least-squares fit to the data, was computed to be ± 0.35 cm/s. The 95-percent confidence limits (section 7) for 28 degrees of freedom were calculated to be

$$95\text{-percent CL} = \pm 0.89 \text{ cm/s.}$$

The ECU is the summation of the systematic and 95-percent CL errors:

$$\text{ECU (SN 52)} = (+ 0.5) + (+ 0.89) = + 1.4 \text{ cm/s.}$$

The dominant systematic error in the second of the three steps, the calibration of the T&EL submerged jet, was the error in the measurement standard used, i.e., the SN 52 ECU of ± 1.4 cm/s. The submerged jet turbine was calibrated over the range 3 to 40 cm/s at a total of 18 points. The RSE, based on a second-order, least-squares fit, was computed to be ± 0.08 cm/s. The 95-percent confidence limits for 15 degrees of freedom were found to be

$$95\text{-percent CL} = 0.20 \text{ cm/s.}$$

The ECU is the sum of the systematic error and the 95-percent CL:

$$\text{ECU (submerged jet)} = (+ 1.4) + (+ 0.20) = + 1.6 \text{ cm/s.}$$

The dominant systematic error in the third and final step, the laboratory calibration of the 36 current meters, was the uncertainty of the measurement standard used, i.e., the ECU of the submerged jet of ± 1.6 cm/s. The RSE for the group of current meters, based on measurements at four points in the range 5 to 40 cm/s for each current meter, was computed to be ± 0.51 cm/s. The RSE was multiplied by an appropriate value from Student's "t" table for 141 degrees of freedom (section 7.3.1, equation 11); the 95-percent confidence limits were found to be

$$95\text{-percent CL} = (+ 0.51 \text{ cm/s}) (1.96) = + 1.03 \text{ cm/s.}$$

The final ECU for the 36 current meters is the sum of the systematic error and 95-percent CL:

$$\text{ECU (36 Units)} = (+ 1.60) + (+ 1.03) = + 2.6 \text{ cm/s.}$$

This value represents the calibration uncertainty for the group of 36 current meters, using a common transfer function over the flow-speed range of 5 to 40 cm/s.

At the end of the survey, 21 of the original 36 current meters were again calibrated in the submerged jet. Since the RSE obtained was contained within the pre-survey RSE, the Sensor Measurement Uncertainty (SMU) for the group of 21 meters is equal to the original ECU of ± 2.6 cm/s. Based on the similarity of performance of all speed sensors that was demonstrated during field checks, this SMU was applied to all speed measurements made during the survey.

Compass Calibration:

Compasses in the current meters were calibrated using a Lutz compass as a standard. The systematic error in the calibration was the combined accuracy of the calibration fixture (approximately ± 0.5 degrees) and the accuracy of the Lutz compass (± 1.0 degree). Calibration measurements were made at 45-degree intervals for all 36 current meters before deployment and for 21 of the units after recovery. The RSE was computed to be 1.9 degrees for the pre-survey calibration of the 36 units.

Based on 287 degrees of freedom, the 95-percent confidence limits were found to be

$$95\text{-percent CL} = (\pm 1.9 \text{ degrees}) (1.96) = \pm 3.7 \text{ degrees.}$$

The ECU is the sum of the systematic and 95-percent CL errors:

$$\text{ECU (36 Units)} = (\pm 1.5) + (\pm 3.7) = \pm 5.2 \text{ degrees.}$$

This value represents the calibration uncertainty for the group of 36 current meter compasses using a common transfer function.

At the end of the survey, 21 of the original 36 current meters were calibrated. Eight of the 21 exhibited compass-sticking problems and were excluded from the calculation of the SMU (section 5). The RSE of the remaining 13 meters was found to be 2.9 degrees. Based on 103 degrees of freedom, the 95-percent confidence limits were found to be

$$95\text{-percent CL} = (\pm 2.9 \text{ degrees}) (2.00) = \pm 5.8 \text{ degrees.}$$

The SMU is represented by the broader 95-percent confidence limits of the post-survey calibration,

$$\text{SMU} = (\pm 1.5) + (\pm 5.8) = \pm 7.3 \text{ degrees.}$$

Because no obvious sticking problems were apparent in the field data, the SMU was applied to all direction measurements made during the survey.

Rotor Directivity Response:

The directivity response of the rotor is needed to predict speed errors resulting from both vertical and horizontal misalignment of the current meter with the direction of flow. Vertical misalignment (pitch) results from meter imbalance caused by clamping the suspension swivel assembly at a point offset from the balance point. Horizontal misalignment (yaw) occurs at lower speeds when the current meter vane produces insufficient alignment torque.

The directivity measurements described in section 4 were made at 15-degree intervals from 0 to 360 degrees at two different speeds. Based on the range of vertical and horizontal misalignment angles occurring during the survey, we needed to know the speed errors for a continuum of angles from 0 degrees to about 15 degrees. The laboratory data were interpolated between 0 and 15 degrees as follows: The data at 0, 15, and 30 degrees show a curvature and, because a true cosine response has a quadratic dependence at small angles, were interpolated according to

$$\Delta V/V_0 = -2.0 \times 10^{-4} \theta^2,$$

where $V = |\vec{V}|$ is the measured current speed, V_0 is the true current speed, $\Delta V = V - V_0$ is the speed error, and θ is the misalignment angle in degrees. The coefficient, -2.0×10^{-4} , was determined by averaging the four data points (two for each speed) at ± 15 degrees. The standard deviation in the coefficient was computed to be $\pm 0.71 \times 10^{-4}$. Based on 3 degrees of freedom, the 95-percent confidence limits of the coefficient were found to be

$$95\text{-percent CL} = \pm 1.1 \times 10^{-4}.$$

Thus, for a given misalignment angle θ , the 95-percent bounds on the percentage of error $\Delta V/V$ caused by misalignment are

$$\Delta V/V_0 \text{ (misalignment)} = (-0.020 \pm 0.011) \theta^2 \text{ percent.}$$

This result is used in section 9.2.4 where the speed error, caused by misalignment angles that vary among the group of 36 current meters because of varying pitch and yaw angles, is treated.

Vane Misalignment:

Vane misalignment (yaw) is a source of direction error as well as speed error. Consequently, we need to know the maximum vane misalignment angle, as a function of speed, over the speed range encountered in the field. Based on the fact that the test data at 2, 5, and 10 cm/s show an increase in misalignment angle with decreasing speed, an interpolation of inverse linear speed dependence for the range of 2 to 10 cm/s was tried and found to fit all three data points. The results are tabulated below:

<u>Speed (cm/s)</u>	<u>Maximum misalignment angle (degrees)</u>
2	± 20
3	± 10
4	± 7
5	± 5
6-7	± 4
8-9	± 3
10	± 2

At speeds above 10 cm/s, the misalignment angle is less than ± 2 degrees, or the estimated uncertainty of the test method. These misalignment angles are used in section 9.2.4, along with the directivity response, to determine speed and direction errors caused by combined pitch and yaw.

Platform Blockage:

Tests were performed at DT-NSRDC to determine the blockage effect caused by the 2.5-cm-diameter rods forming the platforms used to support the current meters. Figure 43 shows the results

of several tow carriage runs at different speeds as a function of the angle between the current meter direction and a single vertical rod. The distance from the rod to the current meter was the same distance as that used in the platforms, approximately 53 cm. Since the platforms contained rods spaced 30 degrees apart, the actual platform blockage effect is obtained from figure 43 by repeating the single-rod blockage at 30-degree intervals.

These data are used in section 9.2.2, which discusses the effects of ocean turbulence and dynamic currents on the blockage observed in the field.

9.1.2. Dynamic Effects Measurements

Dynamic testing of the Grundy 9021 on the T&EL Vertical Planar Motion Mechanism (VPPM) was described in section 4. In addition to the errors in the measurement of steady flow, dynamic wave particle currents introduce errors because of the time varying speed and direction of the current vector. These "dynamically induced" errors include

- scalar averaging errors,
- dynamic misalignment errors,
- rotor and compass dynamic response errors, and
- sampling errors.

Scalar speed averaging errors result because the Grundy current meter averages the scalar speed independently from direction, and the average magnitude of a time varying vector is not generally the same as the magnitude of the vector average. Dynamic misalignment errors occur when the current meter direction does not follow the instantaneous current direction because of inertial, hydrodynamic damping, and/or length-scale effects that cause errors in both speed and direction. These speed errors depend on the directivity response of the rotor and occur from dynamic misalignment in both pitch and yaw in the presence of orbital wave induced currents. Rotor dynamic response errors occur when currents vary faster than the rotor can respond. For such currents, the rotor may not perform a perfect speed average. Compass dynamic response errors can result from pitch and roll motions not removed by the compass gimbaling and yaw motions imparted to the compass card by the damping oil.

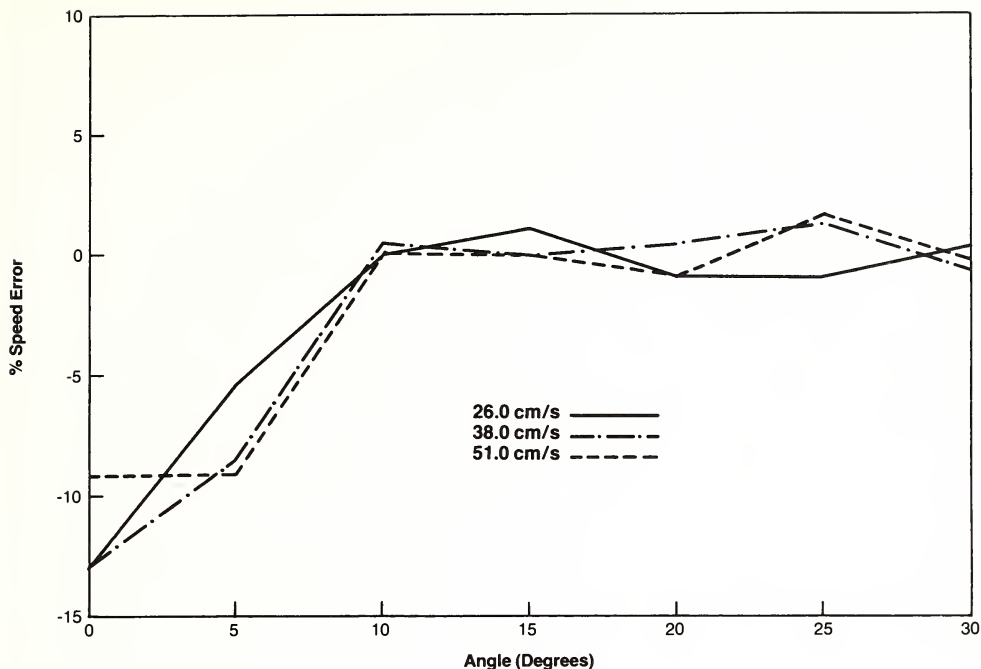


Figure 43.--Laboratory rod blockage data.

In addition to the above errors that can introduce biases into the measured speed and direction, sampling errors can be introduced because the measurement of a time varying quantity requires a sufficient number of samples to estimate accurately an average. Because (1) the 9021 averages speed over an instrument sample interval but gives only a single instantaneous sample of direction and (2) the sampling interval of 10 min used in the survey was much larger than the period of the dynamic current oscillations (≈ 5 s), sampling errors in direction are dominant in the survey data relative to sampling errors in speed. When a number of data samples are vector averaged, however, these direction sampling errors can result in both speed and direction errors in the vector average as a result of the nonlinear transformation from polar to Cartesian coordinates. The remainder of this section and section 9.2.5 are devoted to the determination of the dynamic speed and direction errors associated with a single 10-min sample from the 9021 current meter.

There are two basic approaches that can be taken to estimate the magnitude of the combined errors resulting from the above four error sources. One is a purely empirical approach based on laboratory and/or field data taken under controlled or at least known conditions. The other is to model each of the error sources for a particular current meter/mooring configuration and compare the model predictions with laboratory and field data. The latter approach, when feasible, is the more desirable since the model predictions often can be extended to conditions other than those for which data are available. The latter approach was taken and consisted of three steps.

First, the combined effect of scalar speed averaging errors and dynamic misalignment errors due to a horizontal, time varying current component was calculated using small-angle approximations. Horizontal (as opposed to orbital) dynamic currents were felt to be more representative of the near-bottom current conditions experienced during the survey. The resulting speed error depends on (1) relative angle between the mean and oscillating flow directions, (2) signal-to-noise ratio, (3) current meter angular motion attenuation factor, (4) current meter angular motion phase shift, and (5) rotor directivity response. Rotor dynamic response errors were assumed negligible; i.e., the rotor was assumed to perform a perfect speed average.

Next, the angular motion of the current meter in a sinusoidally varying current was calculated based on a second-order linear equation of motion. The justification for using linear theory was that the GASP Experiment data (section 8) indicated that signal-to-peak noise ratios greater than 1 were predominant during the survey. Because current direction variations are small for large S/N ratios, the small-angle approximations required for linear theory are justified. This calculation resulted in a phase shift and an amplitude attenuation factor relative to the angular motion of the actual instantaneous current vector.

Finally, the speed error and current meter angular motion predicted from the above model were compared to the laboratory dynamics test results for signal-to-peak noise ratios greater than 1. This comparison verified the model to within laboratory measurement uncertainties, resulting in a predictive model for speed and

direction errors as a function of signal-to-noise ratio, orientation of mean current relative to wave particle current direction, mean current speed, and frequency of the oscillatory current component.

The details of the first two of the above steps, the error model derivation, are given in appendix C. The results of the third step, the comparison of laboratory data with the model predictions, are presented in the following. Before getting into the comparison, however, we need to define exactly what is meant by an error since both the measured and the true speed and direction are time varying quantities. We define here an error, under dynamic conditions, to be the difference between a single 9021 sample of speed and direction and the magnitude and direction of the true mean (vector averaged) current. "Mean" or "average", in the context of dynamic currents, refers to an average over a large number of current oscillations. The model predictions are expressed in terms of a mean value and a sample-to-sample standard deviation (the square root of the variance) of these errors. The mean error was referred to earlier as a "bias" error, while the standard deviation is a quantitative measure of the "sampling" error.

As mentioned previously, the 9021 averages speed over an instrument sample interval while giving only a single instantaneous sample of direction at the end of the interval. Since averaging speed over 10 min includes a large number of current oscillations (120 for a 5-s oscillation period), a single sample of speed from the 9021 is (for all practical purposes) equal to its mean value, and the sample-to-sample variance in speed is essentially zero (neglecting, of course, time varying processes other than wave particle currents). On the other hand, a single sample of direction from the 9021 represents a true instantaneous sample of direction. The variance of this sample can be quite significant depending on the signal-to-noise ratio. In view of these facts, we have chosen to compare the model predictions for the mean speed error and the direction sampling error with the laboratory dynamics test results.

From appendix C, we find that the predicted mean fractional speed error due to dynamic effects is given by

$$\Delta\bar{V}/V_0 \text{ (dynamics)} = G(f, V_0) \sin^2\phi/2R^2, \quad (18)$$

where \bar{V} is the mean measured speed, i.e., the scalar averaged 9021 speed; V_0 is the true mean vector speed, i.e., the magnitude of the true vector averaged current; $\Delta\bar{V} = \bar{V} - V_0$ is the mean speed error; ϕ is the angle between the mean and oscillating current direction; f is the frequency of the oscillating current component; and R is the signal-to-RMS noise ratio, i.e., $R = \sqrt{2}$ times the signal-to-peak noise ratio as defined for the laboratory data presented in table A-7. R is convenient for use with field data since the current oscillations in the ocean are not perfectly sinusoidal and do not have a well defined peak value. The RMS value of the oscillating component, however, is easily measured and is equal to the square root of the sum of the variances in the north and east components of velocity at wave frequencies. The quantity $G(f, V_0)$ is given in equation (C-10) and depends on both the rotor directivity response and the frequency and speed dependence of the angular motion attenuation and the angular motion phase shift. For a current meter that measures the true instantaneous current speed, $G(f, V_0) = 1$. Table 11 gives values of $G(f, V_0)$ for the range of oscillation periods $T = 1/f$ and mean speeds V_0 of the laboratory data for $R > 1.4$ ($\approx \sqrt{2}$). Also given are the angular motion attenuation α and angular phase shift β .

Table 11.-- G , α , and β for the range of laboratory speeds V_0 and oscillation periods $T = 1/f$

V_0 (cm/s)	T (s)	$G(f, V_0)$	$\alpha(f, V_0)$	$\beta(f, V_0)$ (degrees)
26	8.4	0.0041	0.48	61
36	8.4	0.18	0.60	53
26	12.4	0.22	0.63	51
36	12.4	0.42	0.74	42

Table 12 compares several values of $\Delta\bar{V}$ as measured in the laboratory and as predicted by the above equation. The $\phi = 0$ degrees data were not included in the comparison since the predicted speed error is zero at $\phi = 0$ degrees.

Table 12.--Comparison of predicted and laboratory measured speed errors

No.	V_O (cm/s)	T (s)	ϕ (degrees)	R	$\overline{\Delta V}$ Theory (cm/s)	$\overline{\Delta V}$ Laboratory (cm/s)
1	26	9.1	45	1.78	+ 0.086	+ 0.21 \pm 1.4
2	36	12.4	45	1.67	+ 0.14	+ 1.0 \pm 1.4
3	26	11.3	45	2.20	+ 0.21	- 0.55 \pm 1.4
4	36	9.0	45	2.43	+ 0.33	- 0.22 \pm 1.4
5	36	11.4	45	3.08	+ 0.36	+ 0.76 \pm 1.4
6	36	11.9	90	1.61	+ 2.7	+ 1.7 \pm 1.4
7	26	8.4	90	1.64	+ 0.021	+ 0.10 \pm 1.4
8	26	12.2	90	2.38	+ 0.47	- 0.49 \pm 1.4
9	36	11.8	90	3.19	+ 0.68	- 0.29 \pm 1.4

The error bounds on the laboratory measured values are the 95-percent confidence limits based on the Grundy SN 52 ECU of ± 1.4 cm/s. It is seen that the predicted speed errors are generally quite small and agree with the laboratory measured values to within the measure-uncertainty.

If we define σ_θ to be the standard deviation (the square root of the variance) of the current meter direction θ , then (from appendix C) the predicted value of σ_θ in radians is given by

$$\sigma_\theta \text{ (dynamics)} = \alpha (f, V_O) \sin\phi/R. \quad (19)$$

Figure 44 shows predicted vs. laboratory measured values of σ_θ for the correspondingly numbered data sets of table 12. The points along the lower straight line fit indicate an additional attenuation of 0.37 not accounted for in the theory of appendix C, while the upper straight line indicates an additional factor of 0.83. We hypothesize that this is a result of the dynamic response effects of the 9021 compass. Since the compass incorporates oil damping, the compass card does not stay perfectly alined with north but is "dragged" back and forth by the oil as the current meter direction changes, resulting in an "apparent" smaller angular motion of the current meter. As the fre-

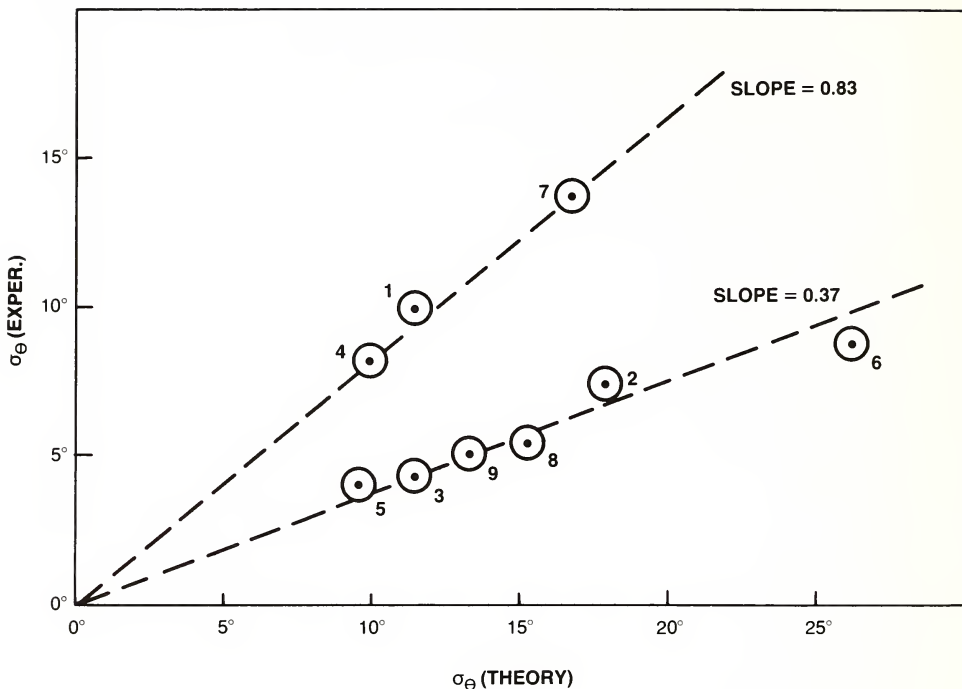


Figure 44.--Laboratory versus predicted values of current meter direction variation.

quency increases, the oil does not respond to the motions of the compass housing and the compass card becomes more and more stationary, resulting in a compass reading approaching that of the actual current meter motion. The fact that all the data points along the lower curve are for periods in the 11- to 12-s range, while those along the upper curve are all in the 8- to 9-s range, gives strong support to this explanation. While no published data could be found for the dynamics of the compass used in the 9021, data taken on another model of a DIGICOURSE marine compass indicate a frequency of maximum attenuation near 0.1 Hz centered in the range of oscillation frequencies of the laboratory data (Der 1977).

Two other effects, peculiar to the laboratory test apparatus that might be expected to affect the compass readout, are the magnetic influence of the tow carriage and the accelerations experienced by the current meter in simulating a time varying current.

Because the two groups of data points in figure 44 fit the individual straight lines so well, we feel that these additional effects are small.

Since figure 44 indicates that the compass attenuation factor is rapidly approaching 1 as the oscillation period decreases, we have assumed it will be close to 1 for $T = 5$ s (the approximate average oscillation period during the survey as determined from wave gage data). Consequently, we have taken equation (19) as the prediction of the RMS sampling error in direction.

In summary, a predictive model for the speed bias error and direction sampling error due to dynamic motion effects is derived that is applicable for signal-to-noise ratios greater than 1.4. The model predictions are consistent with laboratory data within experimental measurement uncertainties. This predictive model will be employed in section 9.2.5 using the results of the GASP Experiment for signal-to-noise ratio, current speed, current oscillation period, and angle between the mean and wave particle currents.

9.2. TOTAL MEASUREMENT UNCERTAINTY

As discussed in section 7, the Total Measurement Uncertainty (TMU) represents the 95-percent error bounds on the field data; that is, 95-percent of all measurements contain errors that are less than the TMU.

This section discusses the various sources of current measurement error enumerated at the beginning of section 9.1 which contribute to the TMU. Estimates of the uncertainty due to each of these error sources are made based on a combination of laboratory measurements, measurements made during the GASP Experiment, and field observations made during the 1-year survey. These uncertainties are combined in section 9.2.6 to form the TMU in current speed and direction.

Standard procedure, when combining errors from several independent sources, is to add systematic errors linearly and random errors quadratically. While systematic errors, by definition, are fixed and do not vary among different data samples, random errors vary between one data sample and another. Since we are not considering each current meter separately but developing a TMU for the 36 current meters as a group, random errors in this context

include both errors which vary among different current meters (pitch, fouling, and calibration errors) and errors which vary among different measurements with a given current meter (dynamic sampling errors and time-dependent fouling errors). Because random errors from different error sources will not all have their largest value simultaneously, adding them linearly would overestimate the expected total error. While quadratic addition, in a strict probabilistic sense, applies only to variances and not to the 95-percent error bounds about the mean (unless the individual errors are each normally distributed), it provides a reasonable estimate of the overall 95-percent error bounds when large numbers of independent errors are combined.

To perform the quadratic addition, it is necessary to know both the mean value of the error and the 95-percent confidence limits about the mean, for it is not the absolute error limits but the deviations about the mean error that are added quadratically. The aim of the following subsections is thus to estimate, for each error source, the mean error and the 95-percent confidence limits for both systematic and random errors. These errors are then combined in section 9.2.6 to form the TMU associated with a single sample of speed and direction.

9.2.1. Calibration Errors

Calibration errors are the speed errors in the steady-flow rotor calibration and the direction errors in the compass calibration. The random error component represents the variation among the 36 current meters from a common transfer function. From the Sensor Measurement Uncertainty of section 9.1.1, we summarize as follows:

Speed SMU:

Systematic error 95-percent CL = ± 1.60 cm/s

Random error 95-percent CL = ± 1.03 cm/s

Direction SMU:

Systematic error 95-percent CL = ± 1.5 degrees

Random error 95-percent CL = ± 5.8 degrees

9.2.2. Platform Blockage Errors

Laboratory data presented in section 9.1.1 showed an angularly dependent blockage effect of the rods comprising the platform used to support the current meters. In a dynamic ocean environment, an

oscillating current direction due to surface waves is present. Because the 9021 averages a large number of current speed oscillations over the 10-min sampling interval used in the survey, this angular dependence should be averaged out to some extent. In addition, turbulence present in the ocean tends to further smooth out the angular dependence.

To estimate the effect of an oscillating current direction on the angular dependence observed in the 10-min averaged 9021 speed data, we have used laboratory data to calculate the angular effect that would be observed for a sinusoidal current direction variation of ± 12 degrees. This is the peak-to-peak variation present under conditions of $\phi = 45$ degrees and signal-to-noise ratio of $R = 5.0$. [See equation (C-6).] The dominant angle ϕ between the mean and oscillating flow direction during the GASP Experiment was 45 degrees, while R was less than 5.0 approximately 95 percent of the time; that is, the current direction variation was $\geq \pm 12$ degrees approximately 95 percent of the time. Figure 45 shows a smoothed version of the steady-flow laboratory blockage data of figure 43 plus a ± 12 -degree sinusoidal average of the steady flow curve. The abscissa for the latter curve is the angle between a platform rod and the mean flow direction. It is seen that the ± 12 -degree sinusoidal average varies only about ± 0.5 percent from the actual mean angular blockage effect that was calculated from the data to be -4.5 percent. Because the platforms were oriented randomly during the survey, the angular mean represents an ensemble mean over the group of 36 current meters while the value of ± 0.5 percent represents a random component of uncertainty in the blockage effect.

In an effort to corroborate this result, data from the GASP Experiment were examined to see if the blockage effect could be observed. Data from the Grundy (431) were compared to data from the NBIS (132) that were free of blockage effects (section 8). Examination of speed-speed scatter plots as well as speed ratio versus direction data showed that the blockage predicted by the ± 12 -degree averaged curve of figure 45 agreed with the observed results to within the combined ECU of the Grundy and the NBIS current meters. In view of this, we have taken the ± 0.5 percent predicted by figure 45 as the random component of the blockage effect uncertainty at the 95-percent confidence level.

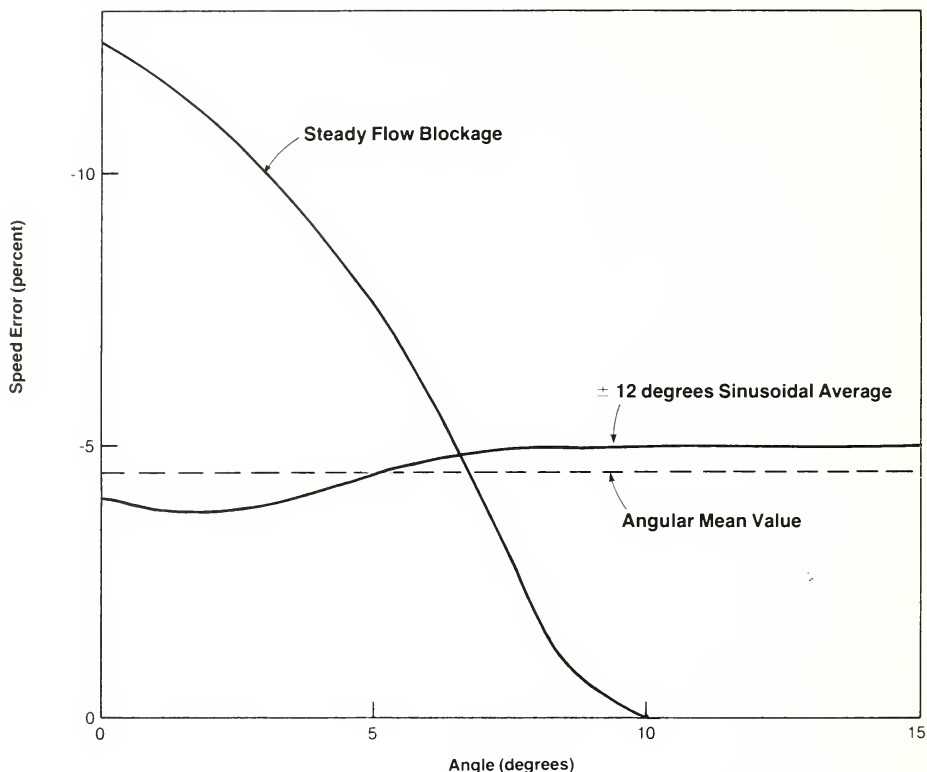


Figure 45.--Platform blockage under steady and dynamic flow conditions.

The systematic error in the blockage effect is the uncertainty in the calculation of the angular mean value from the blockage data. Based on the systematic speed uncertainty in the tow tank measurements of ± 0.5 cm/s discussed in section 9.1.1 and the standard deviation of 1.1 percent computed from the 21 data points of the blockage data, the 95-percent confidence limits were calculated to be ± 1.9 percent.

The resulting mean speed error and 95-percent confidence limits about the mean due to platform blockage are given as follows:

Mean error	=	- 4.5 percent
Systematic error 95-percent CL	=	± 1.9 percent
Random error 95-percent CL	=	± 0.5 percent

Direction errors were undetectable to within the laboratory measurement uncertainty and have been assumed negligible compared to other sources of direction error.

A factor not included in the above discussion is the effect of fouling on platform blockage since fouling changes the effective diameter of the rods. Since no data were available for a fouled rod, this was not taken into account. It is therefore possible that the above error estimate may not be valid during the September through November 1978 time frame when platform fouling was serious.

9.2.3. Rotor Fouling Errors

An accurate treatment of rotor fouling errors requires accurate field records of fouling conditions versus time as well as laboratory data on fouling effects over a range of fouling conditions. While the former were not available, laboratory speed measurements made on a "moderately" fouled rotor recovered during the fouling season showed a speed decrease of approximately 7 percent. These measurements, combined with the following discussion, allow an estimate of the error from fouling conditions that range about the "moderate" level defined by the 7-percent speed decrease.

Because of the absence of quantitative information on the fouling rates, we will assume (on the average) a linear increase in fouling rate with increased time of deployment. While this is undoubtedly too severe an assumption to apply during the first days after deployment, it will not have a significant impact on the results. Figure 46 shows fouling measured in speed decrease versus time for a hypothetical case of three current meters with fouling levels at recovery distributed about the moderate level of 7 percent. We will further assume that the fouling levels among the different current meters upon recovery vary uniformly about the moderate level of 7 percent, i.e., the speed decrease upon recovery varies uniformly in the interval $(1 - x) 7$ percent to $(1 + x) 7$ percent. It then can be shown that the ratio f of data collected during deployment at fouling levels less than the 7-percent level to the total number of data points is equal to

$$f = [\ln(1 + x) / x + 1] / 2 .$$

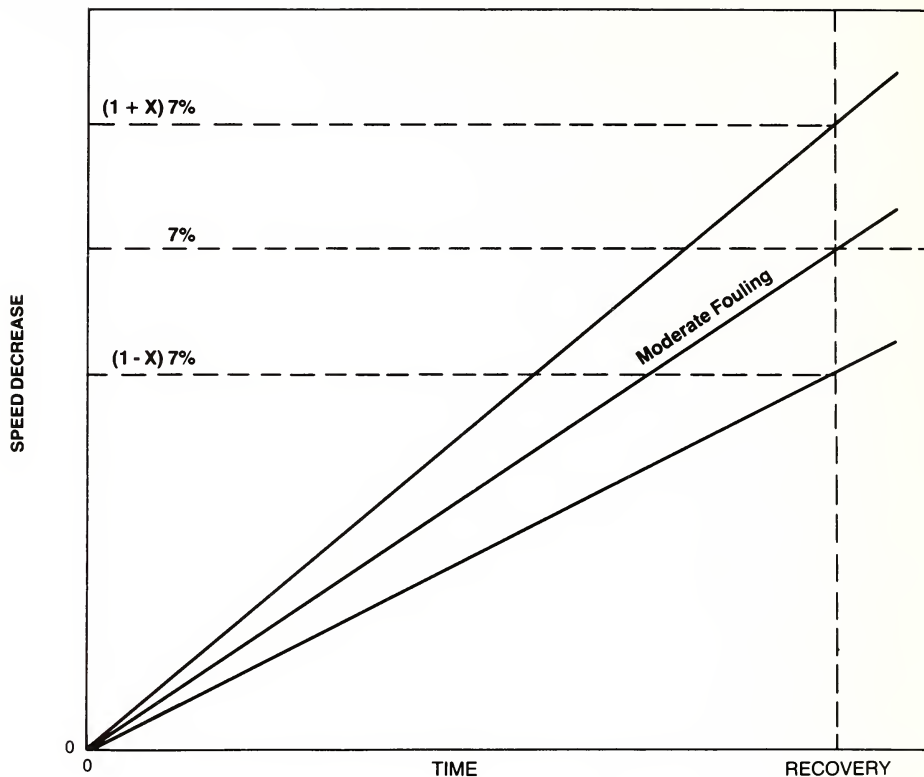


Figure 46.--Fouling speed decrease versus time for three fouling levels.

For example, if $x = 0.25$, then $f = 0.95$; i.e., 95 percent of the data will have a speed decrease error less than 7 percent. While the exact distribution of fouling levels is unknown, this illustration shows that the 95-percent confidence limits of 0- to 7-percent speed decrease account for fouling errors over a considerable range of fouling conditions about the "moderate" level. In addition, f is a slowly varying function of x so that the confidence value (f in percent) is not a sensitive function of the actual range of fouling conditions. In view of this, we take 0 to 7 percent as the approximate 95-percent confidence error bounds. We thus have the following figures for speed errors due to rotor fouling:

Mean error	=	- 3.5 percent
Systematic error 95-percent CL	=	0 percent
Random error 95-percent CL	=	\pm 3.5 percent

The random error component represents errors which are distributed both in time and among different current meters. Since the direction errors due to fouling were not measured, they are not accounted for but are estimated to be small relative to other sources of direction error.

The above treatment of fouling is not applicable to data where a barnacle became lodged between the impeller hub and the instrument housing causing a step decrease in sensitivity. Fortunately this latter type of occurrence is usually quite noticeable in the data. Data subsequent to such an occurrence can be considered to be unusable.

9.2.4. Misalignment Errors

Misalignment consists of both the pitch and yaw effects discussed in section 9.1.1. For the range of pitch and yaw angles of interest (θ_p and θ_y), the resultant overall misalignment angle θ is given approximately (to within 1 percent) by $\theta^2 = \theta_p^2 + \theta_y^2$. The resulting speed error, using the directivity response discussed in section 9.1.1, is

$$\Delta V/V_o = (-0.020 \pm 0.011) (\theta_p^2 + \theta_y^2) \text{ percent,}$$

where $\Delta V = V - V_o$, V , and V_o are the speed error, the measured speed, and true speed, respectively; θ_p and θ_y are measured in degrees, and ± 0.011 is the laboratory measurement uncertainty at the 95-percent confidence limit of the value of 0.020 for the coefficient. The direction error is simply $\pm \theta_y$. Since pitch angles vary from one current meter to another, this speed error is distributed among the current meters just as were fouling errors. We have accounted for this distribution of errors as follows:

During June through August 1978, static pitch angles were observed to be ≤ 15 degrees. During the rest of the survey, the current meters were balanced to ≤ 10 degrees pitch. If we make the assumption that pitch angles varied uniformly among different current meters from 0

degrees to a maximum pitch angle $\theta_{P \max} = 10$ or 15 degrees, then the mean and the 95-percent confidence limits of $\theta_P^2 + \theta_Y^2$ in the above equation for the speed error $\Delta V/V_0$ are given by

$$\overline{\theta_P^2} + \overline{\theta_Y^2} = \frac{1}{3} \theta_{P \max}^2 + \theta_Y^2$$

and

$$95\text{-percent CL} \approx \begin{cases} +\frac{2}{3} \theta_{P \max}^2 \\ -\frac{1}{3} \theta_{P \max}^2 \end{cases}$$

The mean represents an ensemble mean over the group of current meters, while the approximate 95-percent confidence limits are the range of variation in pitch angles among the group. We have assumed that yaw angles are the same function of speed for each current meter so that $\overline{\theta_Y^2} = \theta_Y^2$. The value $\frac{1}{3} \theta_{P \max}^2$ is the average of θ_P^2 from 0 degrees to the maximum pitch angle.

The calculation of the 95-percent confidence limits of $\Delta V/V_0$, as given by the above equation, is complicated by the fact that two sources of uncertainty are involved as a product, the systematic uncertainty in the coefficient and the random uncertainty in the misalignment angle. Because the uncertainty due to the coefficient is smaller than the uncertainty due to the variation in pitch angles, the uncertainty in $\Delta V/V_0$ is dominated by the random component. We have therefore neglected the systematic component. The resulting speed and direction errors due to misalignment are summarized below:

Speed:

Mean error	=	- 0.020 ($\theta_Y^2 + \frac{1}{3} \theta_{P \max}^2$) percent
Systematic error 95-percent CL	=	0
Random error 95-percent CL	=	- 0.020 x $\begin{cases} +\frac{2}{3} \theta_{P \max}^2 & \text{percent} \\ -\frac{1}{3} \theta_{P \max}^2 & \text{percent} \end{cases}$

Direction:

Mean error	=	0
Systematic error 95-percent CL	=	$\pm \theta_Y$
Random error 95-percent CL	=	0

The maximum pitch angle, $\theta_{p \max}$, is either 10 or 15 degrees, and θ_y is the vane misalignment angle which depends on the speed. The random speed error component represents errors which are distributed among different current meters due to varying pitch angles. It is not symmetrical about the mean because of the nonlinear (squared) dependence of the error on the pitch angle.

Table 13 gives the mean speed error and the 95-percent confidence limit for speed and direction errors using the results of section 9.1.1 for the speed dependence of θ_y . The results are shown for the two cases, $\theta_{p \max} = 10$ degrees and 15 degrees.

Table 13. Speed and direction errors due to pitch and yaw misalignment

Speed (cm/s)	Speed error (percent)				Direction error (degrees)
	Maximum pitch angle = 10 degrees		Maximum pitch angle = 15 degrees		
	Mean	95% CL	Mean	95% CL	
10-40	-0.75	+0.67 -1.10	-1.59	+1.51 -2.48	\pm 2
8	-0.85	"	-1.69	"	\pm 3
6	-0.99	"	-1.83	"	\pm 4
5	-1.17	"	-2.01	"	\pm 5

9.2.5. Dynamic Effects

The various dynamic effects contributing to speed and direction errors were discussed in section 9.1.2, where laboratory dynamics test results were compared with the predictions of the model developed in appendix C. One of the objectives of the GASP Experiment was to obtain field data necessary to correlate the dynamic response of the Grundy 9021 in the field with the laboratory test results and the error prediction model.

Table 14 gives the values of mean speed and direction errors, $\overline{\Delta V}$ and $\overline{\Delta \theta}$, and direction sampling error σ_θ predicted by the model of appendix C for several values of signal-to-noise ratio R and current speed V_0 during the GASP Experiment. Approximately 95 percent of the time, the signal-to-noise ratio was greater than 1.4, and the current speed ranged between 10 and 40 cm/s. The mean

Table 14.--Predicted speed and direction errors during the GASP Experiment

$T = 5 \text{ s}, \quad \phi = 45 \text{ degrees}$

R	V_o	$\overline{\Delta V}$	$\overline{\Delta \theta}$ (degrees)	σ_θ (degrees)
1.5	10	-0.3 cm/s	-0.2	3.3
1.5	26	-0.5 cm/s	-1.2	8.3
1.5	40	-0.2 cm/s	-2.5	12.0
2.5	10	-0.1 cm/s	-0.1	2.0
2.5	26	-0.2 cm/s	-0.4	5.0
2.5	40	-0.04 cm/s	-0.9	7.2

R = Signal-to-RMS noise ratio

$\overline{\Delta \theta} = \overline{\theta} - \theta_o$

V_o = Magnitude of vector averaged current

$\overline{\theta}$ = Mean 9021 direction

$\overline{\Delta V} = \overline{V} - V_o$

θ_o = Direction of vector averaged current

\overline{V} = Mean 9021 speed \approx single sample speed

σ_θ = Standard deviation of 9021 direction θ

signal-to-noise and current speed were approximately 2.5 and 16 cm/s, respectively. The $T = 5 \text{ s}$ oscillation period and the relative mean to oscillating current angle of $\phi = 45 \text{ degrees}$ were typical conditions. Because the 9021 averages a large number of wave particle current speed oscillations over a 10-min sampling interval, the sample-to-sample speed error is essentially constant and equal to its true mean value $\overline{\Delta V}$. Direction, on the other hand, is not averaged but is sampled only once per 9021 sampling interval. Consequently, the sample-to-sample direction error varies about its mean value $\overline{\Delta \theta}$ with a standard deviation σ_θ .

It is seen that both the mean speed and direction errors predicted are quite small and, in fact, are within the ECU of the Grundy current meter. The direction sampling error σ_θ , however, is reasonably large and quite possibly observable in the GASP Experiment data. In an effort to measure the direction sampling error σ_θ , data from the Grundy (431) at the 3-m level were compared with the NBIS (132) data. To eliminate any variance in the 9021 direction from sources other than wave particle currents, the

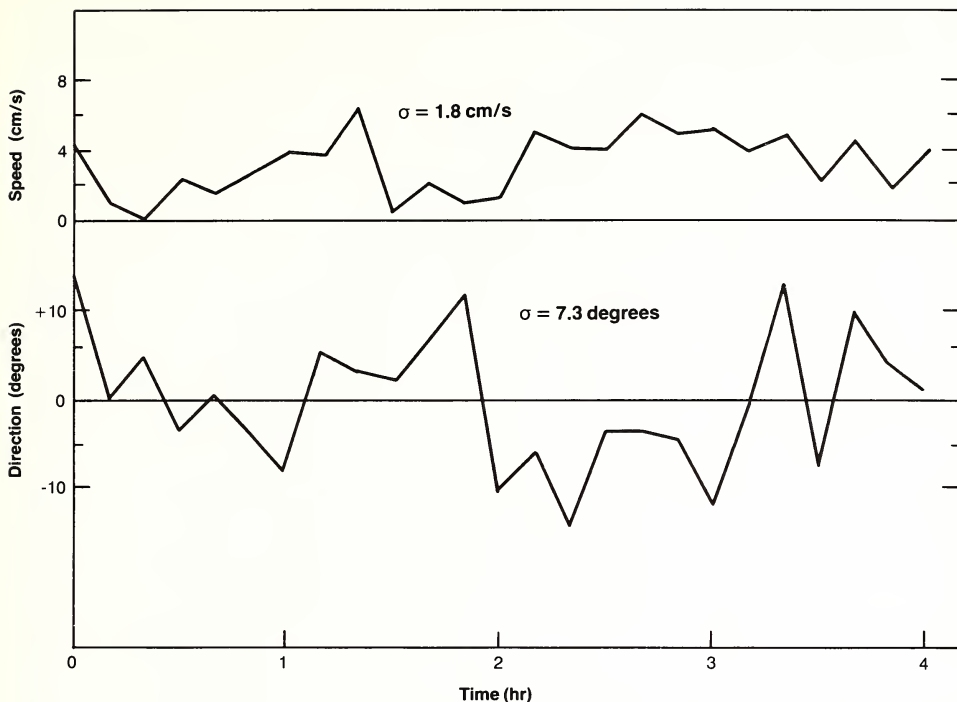


Figure 47.--Sample speed and direction difference plots from GASP Experiment; NBIS (132) - Grundy (431); Calendar day 98.

difference between the NBIS and Grundy directions was analyzed. Since the NBIS current meter is a true vector averaging device, its output at the end of a 10-min sampling interval should be free of sampling-induced errors and about equal to the mean vector speed and direction V_O and θ_O of table 14. If the current direction variations at the two instrument sites (due to processes other than wave particle currents) were the same, then we should expect the variance in the sample-to-sample direction difference, $\theta - \theta_O$, to be primarily caused by dynamic sampling errors in the Grundy direction θ .

Figure 47 shows a 10-min-interval, time-series plot of the speed and direction difference between the NBIS and the Grundy current meters for a 4-hr period at the beginning of calendar day 98 during the GASP Experiment. The speed difference was also calculated to check the variance from processes other than wave particle

currents. (The sample-to-sample speed difference should be essentially constant if dynamic effects alone are present, e.g., Grundy speed sampling error ≈ 0 .) The moderate sample-to-sample variance in the speed difference shown ($\sigma = 1.8$ cm/s) does indicate, however, that a source of variance other than wave dynamic effects is present.

The signal-to-noise ratio and mean speed during the 4-hr period shown were 2.9 and 26 cm/s, respectively. Examination of burst data from the NBIS (732) meter during this period showed the wave particle current direction to be approximately 45 degrees to the mean flow direction and the oscillation period to be ≈ 5 s. The value of σ predicted for these conditions is $\sigma_{\theta} = 4.3$ degrees. The difference data contain a source of variance other than dynamic effects, and this fact is consistent with the value $\sigma = 7.3$ degrees calculated from the direction difference data.

The consistency and correlation of both the laboratory data and the GASP Experiment data with the model predictions to within the laboratory and field measurement uncertainties have allowed us to use the error model predictions of table 14 to estimate the speed and direction errors caused by dynamic effects during the 1-year survey. Because the range of environmental conditions experienced during the GASP Experiment was similar to that encountered during the survey, we feel this is a valid procedure.

Since the errors in table 14 depend on both the speed and signal-to-noise ratio, the 95-percent confidence limits for the speed error were determined by quadratically adding the 95-percent CL due to the variation in S/N (1.5 to ∞) at the mean speed of 16 cm/s and the 95-percent CL due to speed variation (10 to 40 cm/s) at the mean S/N ratio of 2.5. This is the procedure discussed at the beginning of section 9.2 for combining the random errors of independent sources. S/N and speed were, by-and-large, independent during the GASP Experiment. Since the standard deviation in direction σ_{θ} is much larger than the variation in the mean direction error $\overline{\Delta\theta}$, the 95-percent CL for the direction error was taken to be $\pm \sqrt{2} \sigma_{\theta}$ (peak = $\sqrt{2}$ RMS) at the mean speed and S/N. The results for speed and direction errors caused by dynamic effects are as follows:

Speed:

Mean error	=	-1.0 percent
Systematic error 95-percent CL	=	0
Random error 95-percent CL	=	+1.2 percent
		-1.5 percent

Direction:

Mean error	=	-0.2 degrees
Systematic error 95-percent CL	=	0
Random error 95-percent CL	=	+4.6 degrees

The above errors apply to a single 10-min sample of speed and direction measured by the Grundy 9021.

9.2.6. Summary of Current Measurement Uncertainty

Table 15 summarizes the results of sections 9.2.1 through 9.2.5. These errors are combined to give the TMU shown in figure 48a, b, and c during the fouling and non-fouling seasons. The difference between the speed TMU's of the 10- and 15-degree maximum pitch cases were, at most, only a few tenths of a cm/s and, hence, have been combined into a single TMU. The mean direction error has been omitted from the TMU because it is so small. In combining the errors of table 15 to form the TMU's, the random error components have been added quadratically, the systematic components added linearly, and the two resulting numbers added linearly to give the combined uncertainty about the mean error.

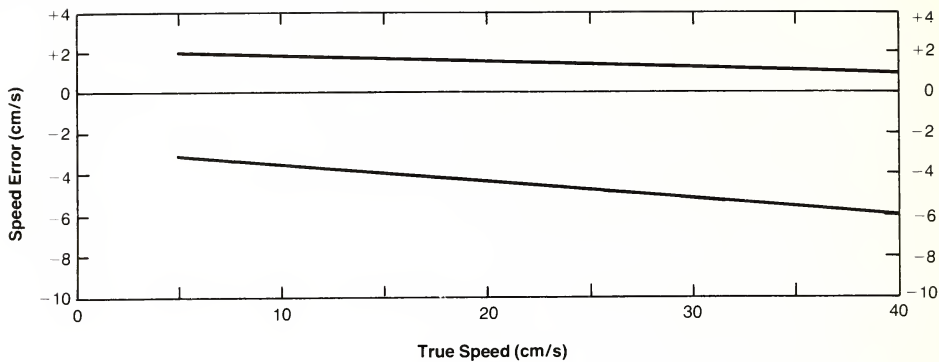
The TMU's shown represent the uncertainty associated with a single 10-min sample of speed and direction from the Grundy 9021.

Table 15.--Speed and direction error summary

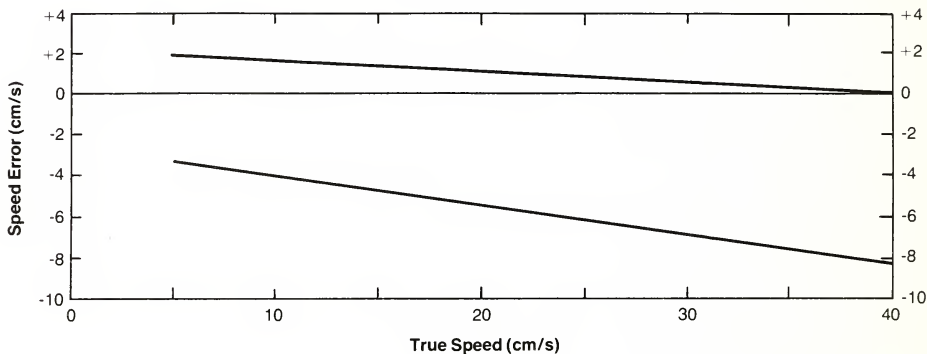
	Error source	Mean error	95% confidence limits about mean	
			Systematic component	Random component
SPEED	Calibration	----	+ 1.60 cm/s	+ 1.03 cm/s
	Blockage	- 4.5 percent	+ 1.9 percent	+ 0.5 percent
	Fouling*	- 3.5 percent	----	+ 3.5 percent
	Misalignment	Speed dependent** (table 13)	----	Speed dependent (table 13)
	Dynamics	- 1.0 percent	----	+1.2, -1.5 percent
DIRECTION	Calibration	----	+ 1.5 degrees	+ 5.8 degrees
	Blockage	----	----	----
	Fouling	----	----	----
	Misalignment	----	Speed dependent (table 13)	----
	Dynamics	- 0.2 degrees	----	+ 4.6 degrees

* Only applicable during fouling season

** Also depends on maximum pitch angle



(a) Speed TMU, non-fouling season



(b) Speed TMU, fouling season

Speed (cm/s)	Direction Error (degrees)
10-40	± 10.9
8-9	± 11.9
6-7	± 12.9
5	± 13.9

(c) Direction TMU

Figure 48.--Speed and direction TMU's.

10. DATA PROCESSING AND VALIDATION

by Michael W. Szabados and Henry R. Frey

The methods used during the processing and validation of data obtained during the NOS SPR Support Project are described in this section. This information, combined with the measurement and data quality assurance discussions in earlier sections, are supportive of the data sets archived at the National Oceanographic Data Center (NODC). Availability of the project's data sets from NODC is described in section 10.7. Instrument recording formats and transfer functions are given in appendix B.

The time-series data obtained with current meters, meteorological stations, and water level gages were translated from the 7.6-cm-diameter instrument tape reels to 9-track, 800-BPI, computer-compatible tapes onboard the NOAA Ship FERREL. The 9-track tapes were transmitted with supporting documentation to NOS headquarters at Rockville, Md. At the completion of the field effort, the original instrument tapes were transmitted to NOS headquarters. The wave gage tapes were forwarded with header information to the instrument manufacturer, Applied Microsystems, Incorporated, for translation to computer-compatible tapes.

Synoptic CTD data were recorded through a data logger onto 9-track tapes onboard the FERREL; these tapes were forwarded with header information to NOS headquarters for processing and analysis. Water chemistry log sheets listing sea surface temperature, dissolved oxygen, and salinity values were also forwarded to NOS headquarters.

Supporting documentation includes copies of letters of transmittal, 9-track tape file header information sheets, instrument deployment and recovery logs, ship's deck and daily weather logs (for days when the ship was at sea), cruise reports, and special situation reports. The aforementioned supporting documentation was sent to NOS headquarters and stored there. Instrument quality

control check logs were sent from the ship to T&EL for analysis, recommendations, and storage.

10.1. CURRENT METER DATA

Upon receipt at NOS headquarters, each current meter record was identified by station number, instrument serial number, height above the bottom, and deployment and recovery times. The data were processed on a CDC 6600 computer system using software developed by oceanographers in the Circulatory Surveys Branch (OA/C211), Marine Environmental Services Division, NOS. The initial processing step was accomplished with the Branch's Phase I Processing Program, which was modified to incorporate the processing step of their Phase II Processing Program. The Phase I Processing Program (1) converts binary to decimal (instrument units) data, (2) converts instrument units to engineering units through use of transfer functions, and (3) provides a printout of the complete header information and oceanographic data for each station.

The current meter data were subjected to various quality control checks during processing. Listings of the parameters (current speed and direction, water temperature and conductivity) were examined for apparent consistency. The data files were then scrutinized for absence or loss of data, spurious values ("glitches"), bit drops, parity errors, and the use of wrong word lengths (a potential problem during data tape translation). A rigorous time check was performed on each file, comparing the number of records in the file with the instrument start/stop and deployment/recovery times. Any file with a time registration problem or with irreparable data errors was so indicated in the data processing log; these files were not used for spectral or harmonic analyses; when used for statistical or descriptive purposes, however, the amount of time discrepancy was noted. The next step of processing involved file header checking and correction. Incorrect headers were corrected using the KORHED Program, discussed below.

Current meter files which passed quality control checks were subjected to a Phase III Processing Program. This program checks the data for errors and generates a corrected series by use of a Wiener predictor and interpolation scheme (Groves and Zettler 1964). The Wiener method assumes a stationary time series with accuracy repre-

sented by the mean-square discrepancy and with predictions based on linear operators.

Following the Phase III Processing Program, the KORHED Program was used to insert positions (longitude and latitude) on each data file header and to correct the station number, instrument serial number, depth, or start and stop times on those headers which may have been in error. A Display Program was used to copy the header information and the data onto 16-mm film; output from this step was useful in reviewing the data after completion of the processing.

Upon completion of current meter data processing, the NOS Project Manager applied additional and independent quality control checks. The final quality control checks, performed with the aid of supporting documentation and observations made during frequent field trips, included verification of instrument serial number, time registration, position (station number and height above bottom), and sensor quality levels (acceptance or rejection). Time-series plots of the data were examined for problems that may not have been disclosed in the supporting documentation, e.g., intermittent compass sticking, decrease in rotor response due to fouling, etc. The time-series plots were also viewed for oceanographic consistency, e.g. clockwise rotation of currents, decreases in conductivity measurements resulting from suspended sediments during storm events, and expected velocity shears.

The current meter data were reformatted and transmitted to the NOAA Program Manager during December 1979. The transmittal included 90 meter-months of current meter data.

10.2. METEOROLOGICAL DATA

As mentioned earlier, meteorological data arrived at NOS headquarters on 9-track tapes together with current meter and water level data. Information about each meteorological station record was logged to include station number, instrument serial number, and start and stop times. During processing, the data were subjected to the same quality control measures as described for the current meter data. Data files that passed the quality control criteria were processed in the same manner as the current meter data, except that the convention used for direction was "wind from." (The convention "current toward" was used for direction in the current meter data.)

The NOS Project Manager made quality control spot checks to assure correct position and time registration. The data were reformatted and transmitted to the NOAA Program Manager during December 1979. The transmittal included 9 meter-months of meteorological data.

10.3. WATER LEVEL GAGE DATA

Water level data were also subjected to the same quality control checks applied to current meter data. Data files that passed the quality control checks were processed in the same manner as the current meter data, except that the Wiener predictor and interpolation program were not used. The data were reformatted and forwarded to the NOAA Program Manager during February 1980. The tapes include 10.8 meter-months of water level data.

10.4. WAVE GAGE DATA

The 12.7-cm-diameter wave gage data tapes were sent directly from the FERREL to Applied Microsystems, Incorporated, for translation to 9-track computer-compatible tapes. The wave data were processed contractually by Optimum Systems, Incorporated (OSI), with technical guidance of the NOS Project Manager and Project Oceanographer. The 9-track tapes contained 80 words of header information in ASCII and data blocks of 768 words that required regrouping. The tapes were listed on OSI's IBM 370 system at Rockville, Md., and the number of files was verified against the supporting documentation. The starting point for each file of data was the first most significant digit (MSD) for time; this starting point was determined for each file, and the data were regrouped into blocks of 966 words. Transfer functions for the individual gages were applied to convert instrument units into engineering units (decibars). The data were converted again from pressure units (dbar) to heights (m). Each 966-word sample was padded with zeros to provide blocks of 1,000 words each. During this latter process, the heights were stored in millimeters.

Significant wave heights were determined from spectral analysis. Each record was padded with zeros at both ends to total 1,024 words; this was done to facilitate the use of the Fast Fourier Transform. In each frequency band, the center-point energy level was adjusted by the square of the corresponding hydrodynamic attenuation factor.

The total energy in each band was computed by integration within the band. The number of degrees of freedom for each band depended on the number of point energies within the band.

Bands with periods less than 4 s and more than 20 s were eliminated from the analysis. The short-period bands were eliminated because of the severe hydrodynamic attenuation caused by the water depth. The long-period bands were eliminated because of the restricted record lengths; the record length was a necessary compromise between data tape duration, interrecord intervals, and assumptions about the longest periods of peak energy.

Significant wave heights were calculated; these were equal to four times the RMS total energy. The calculated significant wave heights were recorded and forwarded to the NOAA Program Manager during December 1979. The wave data tapes included 14.7 meter-months of data.

10.5. CTD DATA

Information about each CTD cast recorded on the CTD 9-track data tape was included in all data transmittals from the FERREL to NOS headquarters. This information was used to cross reference the header files that were inserted on the tape prior to each CTD cast to indicate station identification, location, date, and time.

Initial processing was accomplished with a CTD Phase I Processing Program which (1) converts binary to instrument units to frequencies, (2) converts frequencies to engineering units through the use of transfer functions, (3) calculates salinity from conductivity and temperature using the UNESCO Equation (UNESCO 1971) and calculates sigma-t from salinity and temperature (Fofonoff 1958), and (4) provides a printout of the complete header information and data for each station and also an output tape with the parameters of depth, conductivity, temperature, salinity, and sigma-t.

The printouts were reviewed, noting the first and last good records of each down cast and any questionable data points. During December 1978, January 1979, and June 1979, CTD data were not recorded on magnetic tape but were recorded manually in the CTD log; these data were keypunched onto computer cards and processed using the Phase I CTD Program, starting with step 3.

The next step of processing involved editing those data points from the down cast that did not lie between the first and last good data points. In addition, spurious points noted during the first phase of processing were removed.

The CTD casts were graphically displayed in profiles of temperature, salinity, and sigma-t vs. depth using an XY-Plot Program. The profiles were scrutinized for effects of waves, swell, and ship's motion on depth readings; casts that indicated such motion were corrected. The data were then replotted and examined for proper editing. During the quality control checks of salinity data from the water samples, a problem with the salinity values (as determined by the CTD profiler) was revealed. The sign of a term in the conductivity/temperature-to-salinity equation was entered in error; the sign was corrected and the discrepancy was removed.

The validated CTD data were reformatted and forwarded to the NOAA Program Manager during January 1980. The data set includes 146 files of salinity, temperature, and sigma-t as a function of depth.

10.6. WATER CHEMISTRY DATA

Salinity and DO values, determined onboard the FERREL from 1.7-liter Niskin bottle water samples, were forwarded on data sheets to NOS headquarters. The values were examined for apparent consistency, and the computations were spot checked. As the water samples were obtained nearly simultaneously with the CTD casts, the recorded times of observations and salinity values were cross-checked; discrepancies in time were resolved by reference to the ship's deck log.

The data were reformatted on hard copy and forwarded to the NOAA Program Manager during October (West Hackberry site) and November (Weeks Island site) 1979. Water chemistry data for the trackline stations were forwarded during February 1980.

10.7. AVAILABILITY OF PROJECT DATA

Specific information about the status of the NOS SPR Support Project data set can be obtained by contacting

Program Data Manager (OA/D2X1)
SPR Brine Disposal Analysis Program
NOAA/EDIS/CEAS
3300 Whitehaven St., N.W.
Washington, DC 20235
Phone: (202) 634-7324
(FTS) 634-7324

The data can be obtained at a cost equal to the government's cost of reproduction. For further information, contact

NOAA/EDIS/NODC (OA/D761)
3300 Whitehaven St., N.W.
Washington, DC 20235
Phone: (202) 634-7500
(FTS) 634-7500

Data requests should specify the key words SPR-BRINE DISPOSAL ANALYSIS PROGRAM and BRINE and the desired work unit name, parameter name, and collection dates given in the following tabular presentation:

10.7.1. Work Units: Currents

Parameters: Current speed, current direction, water temperature, conductivity.

Collection dates: West Hackberry

<u>Station*</u>	<u>Period of record</u>	<u>Sensor depths (m) at GCLW</u>
1111	8/3/78 - 8/28/78 10/3/78 - 11/14/78 1/9/79 - 4/4/79 5/9/79 - 6/1/79	8.8
1112	8/3/78 - 8/29/78 10/3/78 - 12/7/78 12/7/78 - 1/9/79 1/31/79 - 3/13/79 4/5/79 - 4/29/79 5/9/79 - 6/1/79	6.8

* First two digits of station designation represent station numbers given in figure 3; third digit (1) designates current meter; fourth digit is a code for height above bottom (depth at GCLW).

Collection dates: West Hackberry--Continued

<u>Station*</u>	<u>Period of record</u>	<u>Sensor depths (m) at GCLW</u>
1113	4/5/79 - 5/8/79	7.8
1114	4/5/79 - 5/8/79	5.8
1115	4/4/79 - 5/4/79	8.8
1111J	11/14/78 - 12/7/78 1/9/79 - 1/31/79	8.8
1211	6/2/78 - 6/27/78	6.9
1212	7/26/78 - 8/17/78	4.9
1311	6/2/78 - 6/27/78 1/31/79 - 2/21/79 2/21/79 - 3/13/79 4/4/79 - 5/8/79	10.0
1312	6/2/78 - 8/15/78 10/31/78 - 11/14/78 1/31/79 - 2/21/79 2/21/79 - 6/1/79	8.0
1411	6/2/78 - 6/27/78 6/27/78 - 8/29/78 1/31/79 - 2/21/79	8.4
1412	6/2/78 - 6/27/78 7/26/78 - 8/14/78 1/31/79 - 2/21/79 2/21/79 - 3/13/79	6.4

* First two digits of station designation represent station numbers given in figure 3; third digit (1) designates current meter; fourth digit is a code for height above bottom (depth at GCLW).

Collection dates: West Hackberry--Continued

<u>Station*</u>	<u>Period of record</u>	<u>Sensor depths (m) at GCLW</u>
1511	6/27/78 - 7/24/78	8.8
	7/26/78 - 8/29/78	
	10/31/78 - 11/14/78	
	2/1/79 - 2/21/79	
	2/22/79 - 3/13/79	
	4/4/79 - 4/20/79	
1512	6/2/78 - 6/27/78	6.8
	6/27/78 - 8/29/78	
	10/31/78 - 11/14/78	
	1/9/79 - 2/21/79	
	2/22/79 - 4/4/79	
	4/4/79 - 4/20/79	

Collection dates: Weeks Island

<u>Station*</u>	<u>Period of record</u>	<u>Sensor depths (m) at GCLW</u>
2111	7/28/78 - 8/8/78	6.9
	9/1/78 - 9/15/78	
	9/16/78 - 10/2/78	
	10/2/78 - 10/30/78	
	10/30/78 - 1/21/79	
	1/29/79 - 3/12/79	
2112	7/1/78 - 7/28/78	4.9
	9/1/78 - 9/15/78	
	9/16/78 - 10/2/78	
	10/2/78 - 10/30/78	
	10/30/78 - 11/13/78	
	1/6/79 - 1/21/79	
	2/20/79 - 3/26/79	
	4/18/79 - 5/5/79	
	5/21/79 - 6/2/79	
2113	2/20/79 - 3/26/79	5.9
2114	3/12/79 - 3/26/79	3.9

* First two digits of station designation represent station numbers given in figure 3; third digit (1) designates current meter; fourth digit is a code for height above bottom (depth at GCLW).

Collection dates: Weeks Island--Continued

<u>Station*</u>	<u>Period of record</u>	<u>Sensor depths (m) at GCLW</u>
2111J	11/13/78 - 12/11/78	6.9
2211	6/30/78 - 8/11/78	4.8
2212	7/28/78 - 8/16/78	2.8
2311	6/12/78 - 7/28/78 10/30/78 - 1/21/79 1/29/79 - 4/17/79 5/21/79 - 6/3/79	10.0
2312	2/20/79 - 3/27/79 5/21/79 - 6/3/79	8.0
2411	7/1/78 - 8/8/78 2/22/79 - 3/13/79	6.0
2412	7/28/78 - 8/20/78 2/22/79 - 3/12/79	4.0
2511	6/30/78 - 7/28/78 10/30/78 - 12/10/78 1/6/79 - 1/21/79 2/11/79 - 5/7/79 5/21/79 - 6/3/79	7.2
2512	6/30/78 - 7/28/78 10/30/78 - 11/13/78 1/6/79 - 1/21/79 2/1/79 - 2/21/79 3/14/79 - 4/17/79 5/21/79 - 6/3/79	5.2

* First two digits of station designation represent station numbers given in figure 3; third digit (1) designates current meter; fourth digit is a code for height above bottom (depth at GCLW).

10.7.2. Work Unit: Meteorological

Parameters: Wind speed, wind direction, air temperature, air pressure.

Collection dates:
West Hackberry

7/26/78 - 9/31/78
1/31/79 - 2/21/79
4/25/79 - 6/1/79*
5/8/79 - 6/1/79*

Collection dates:
Weeks Island

10/2/78 - 12/10/78
1/29/79 - 2/22/79
2/23/79 - 3/12/79
3/28/79 - 4/17/79
5/21/79 - 6/2/79

* Two stations were deployed at West Hackberry during the period 5/8/79 - 6/1/79.

10.7.3. Work Unit: Wave Height

Parameter: Significant wave height

Collection dates:
West Hackberry

8/3/78 - 9/3/78
9/5/78 - 10/3/78
11/1/78 - 11/11/78
11/11/78 - 12/7/78
12/8/78 - 12/17/78
1/9/79 - 1/31/79
2/2/79 - 2/21/79
3/13/79 - 4/4/79
4/5/79 - 5/8/79

Collection dates:
Weeks Island

7/1/78 - 7/27/78
7/28/78 - 8/22/78
9/2/78 - 9/13/78
9/16/78 - 9/21/78
10/2/78 - 10/30/78
10/30/78 - 11/13/78
11/13/78 - 12/11/78
12/12/78 - 1/6/79
1/6/79 - 1/29/79
2/21/79 - 3/12/79
3/27/79 - 4/4/79
4/18/79 - 4/27/79
5/8/79 - 5/14/79
5/21/79 - 6/2/79

10.7.4. Work Unit: Water Levels

Parameters: Total pressure (decibars)

Collection dates:
West Hackberry

6/21/78 - 8/31/78
10/31/78 - 1/4/79
1/9/79 - 3/13/79
5/9/79 - 6/1/79

Collection dates:
Weeks Island

9/1/78 - 9/15/78
10/30/78 - 11/13/78
3/26/79 - 4/17/79
4/18/79 - 5/21/79

10.7.5. Work Unit: CTD

Parameters: Depth, temperature, salinity, sigma-t

Collection dates: 6/26/78 - 6/2/79

10.7.6. Work Unit: Water Chemistry and Physics

Parameters: Salinity, dissolved oxygen, sea surface temperature,
water temperature

Collection dates:
West Hackberry

Collection dates:
Weeks Island

<u>Cruise</u>	<u>Start Date</u>	<u>Cruise</u>	<u>Start Date</u>
SPR 3	6/2/78	SPR 3	6/3/78
4	6/27/78	4	7/1/78
5	7/27/78	5	7/21/78
8	10/3/78	7	9/8/78
10	11/14/78	8	10/2/78
12	1/9/79	10	11/13/78
13	1/30/79	12	1/6/79
14	2/21/79	13	1/29/79
15	3/12/79	14	2/20/79
17	4/18/79	15	3/12/79
18	5/9/79	17	4/17/79
20	6/2/79	18	5/7/79
		20	6/2/79

ACKNOWLEDGMENTS

Captain Charles Burroughs, NOAA Brine Disposal Analysis Program Manager, and Mr. Hal Delaplane, DOE Technical Project Officer, provided management support and encouragement throughout the project. Rear Admiral Richard Houlder and Captain Wesley Hull, the responsible NOS officials, were especially supportive of the project team.

The timely evaluation of the Grundy Model 9021 current meter was made possible, prior to delivery of instruments to NOS, through the loan of three current meters by the U.S. Naval Oceanographic Office. Special thanks are offered to Dr. Kim Saunders of the Naval Ocean Research and Development Activity for the loan of three Neil Brown Instrument Systems acoustic current meters used in the Gulf At-Sea Performance (GASP) Experiment. Neil Brown Instrument Systems and Marsh McBirney, Incorporated, provided special assistance in preparing their current meters for the GASP Experiment.

Very special thanks are expressed to the officers and crew of the NOAA Ship FERREL for carrying out the field work with dedication to duty, particularly Commanders Dale North and John Callahan, Lieutenant Commander Michael Meyer, Lieutenant (jg) Robert King, Chief Boatswain David Brannon, and Boatswain Group Leader G. T. Cook. The NOAA Research Vessel VIRGINIA KEY carried out the field work during December 1978 and January 1979; thanks are offered to the Master, Mr. Birnham Neil, and crew and to those who volunteered to serve with the Project Manager in the field parties: Lieutenants (jg) Michael Sagalow and Timothy Roulon, Seaman Surveyor James Grant, AB Seaman Steven Bingham, and Messrs. James Bruce and David Crump.

Mrs. Su Lin Cheng and Ms. Cheryl Hughes, Optimum Systems, Incorporated, provided invaluable assistance in software development and data processing. Messrs. Bernard Gottholm and Michael Connolly, NOS Circulatory Surveys Branch, were particularly helpful in the processing and analysis of data. Messrs. Bruce Parker and Richard Patchen consulted on the adaptation of existing software and wrote new software for the project.

The development of the current measurement uncertainty analysis was supported by the NOAA Office of Ocean Engineering (OOE) which also provided partial support for the GASP Experiment; Mr. William Woodward of OOE is thanked for his valuable contributions to these tasks and for his belief in the merits of the program.

Many others, too numerous to mention here, contributed to the technical and operational progress of the project; their efforts are appreciated.

The efforts of Mr. Patrick McHugh as EDIS technical editor are acknowledged. Ms. Janet Springsteen of the NOS Editorial Section suggested many valuable clarifications to the text of sections 1 and 2. Mr. Thomas Allen of the NOS Office of Oceanography coordinated the layout and production of the final graphic artwork from original graphs and sketches. The final manuscript was typed with enthusiasm by Ms. Kathy McGrew (NOS) and Miss Pollie McKinney (EDIS).

The following reviewers provided valuable comments on the final draft: Captain Charles Burroughs and Messrs. Jack Foreman, Fred Everdale, and Leslie Scattergood of EDIS and Messrs. Eugene Russin, Dane Konop, and Charles Dinkel of NOS.

REFERENCES

- Appell, G. F., 1979: A summary of the Grundy Model 9021 recording current meter performance in a shallow water environment. Presented at the Fifth STD/Ocean Systems Conference and Workshop, San Diego, March 13-15, 1979.
- Appell, G. F., H. R. Frey, D. R. Crump, and W. E. Woodward, 1979: An at-sea current meter performance experiment in the Gulf of Mexico. Proceedings of the Fifteenth Annual Conference of the Marine Technology Society, October 10-12, 1979, New Orleans, La., 156-158.
- Beardsley, R. C., W. Boicourt, L. C. Huff, and J. Scott, 1977: A current meter intercomparison experiment conducted off Long Island in February-March 1976. WHOI Ref. 77-62, 123 pp. (unpublished manuscript).
- Carpenter, James H., 1965: The Chesapeake Bay Institute technique for the Winkler dissolved oxygen method. Limnology and Oceanography, vol. 10, no. 1, January 1965, 141-143.
- Der, C. Y. C., 1977: Some response characteristics of a fluid damped magnetic compass to dynamic azimuth inputs. Exposure Newsletter, vol. 5, no. 4, September 1977, p. 7.
- Fofonoff, N. P., 1958: Interpretation of oceanographic measurements --thermodynamics. In Physical and Chemical Properties of Sea Water, National Academy of Sciences/National Research Council Publication 600, 38-66.
- Frey, H. R., M. W. Szabados, and L. E. Hickman, 1981: NOS Strategic Petroleum Reserve Support Project, Final Report (vol. 1): Oceanography on the Louisiana Inner Continental Shelf. NOS Office of Oceanography, National Oceanic and Atmospheric Administration, Rockville, Md. (in preparation).
- Gill, G. C., L. E. Olsson, J. Sela, and M. Suda, 1967: Accuracy of wind measurements on towers or stacks. Bulletin of the American Meteorological Society, vol. 48, no. 9, 665-674.
- Groves, G. W. and B. D. Zetler, 1964: A program for detecting and correcting errors in long series of tidal heights. International Hydrographic Review, vol. 41, 103-107.
- Halpern, D., 1977: Review of intercomparisons of moored current measurements. Presented at MTS-IEEE Oceans 77 conference, 2, 46D-1, 6.
- Holmes, J. F., 1975: Investigation of meteorological sensors to maximize data quality of NDBO buoy systems. Proceedings of the World Meteorological Organization Technical Conference on Automated Meteorological Systems (TECAMS), February 18, 1975, Washington, D.C., preprint, 10 pp.
- Kalvaitis, A. N., 1978: The vertical planar motion mechanism: a dynamic test apparatus for evaluating current meters and other marine instrumentation. NOAA/EPA Interagency Energy/Environment

R&D Program Report EPA-6001 7-78-145, EPA Office of Energy, Minerals, and Industry, Washington, D.C., 37 pp.

- Kenny, B. C., 1977: Response characteristics affecting the design and use of current direction vanes. Deep-Sea Research, 24, 289.
- Koeppen, Stephen H., 1980: A current measurement uncertainty analysis for the Grundy Model 9021 current meter. Final Report, NOAA/NOS Contract No. NA-79-SAC-00726, MAR, Inc., Rockville, Md., 45 pp.
- Lindley, D., 1975: The design and performance of a 6-cup anemometer. Journal of Applied Meteorology, vol. 14, 1135-1145.
- MacCready, Jr., P. B., 1966: Mean wind speed measurements in turbulence. Journal of Applied Meteorology, vol. 5, 219-225.
- McTaggart-Cowan, J. D. and D. J. McKay, 1976: Radiation shields--an intercomparison. Atmospheric Environment Service, Canada, (unpublished manuscript), 18 pp.
- Mollo-Christensen, E., 1979: Upwind distortion due to probe support in boundary-layer observation. Journal of Applied Meteorology, vol. 18, no. 3, 367-370.
- Muir, L. R., 1978: Bernoulli effects on pressure-activated water level gages. International Hydrographic Review, Monaco, LV (2), 111-119.
- National Ocean Survey, 1978: NOS Strategic Petroleum Reserve Support Project, Integrated Logistics Support, (vol. 2 of 4 volumes): Operating Procedures and Field Check Procedures. NOS Office of Oceanography, National Oceanic and Atmospheric Administration, Rockville, Md., 200 pp. (unpublished report).
- Natrella, M. G., 1963: Experimental Statistics. NBS Handbook 91, National Bureau of Standards, Gaithersburg, Md., 504 pp.
- UNESCO, 1971: International oceanographic tables. Vol. 1, National Institutes of Oceanography of Great Britain and UNESCO.
- U.S. Department of Defense, 1975: Environmental Test Methods. MIL-STD-810C, Aeronautical Systems Division (ASD-ENYESA), Wright-Patterson AFB, Ohio, 200 pp.
- U.S. Department of Defense, 1974: Mechanical Vibrations of Shipboard Equipment (Type I, Environmental and Type II, Internally Excited). MIL-STD-167-1, Naval Ships System Command, Washington, D.C., 11 pp.
- U.S. Department of Energy, 1978: Final environmental impact statement, Strategic Petroleum Reserve--Texoma group salt domes. DOE/EIS-0029 (final statement to FEA-DES-77-8), vol. 5, Appendix U. 2, November 1978.
- U.S. Naval Oceanographic Office, 1968: Instruction Manual for Obtaining Oceanographic Data. Publication 607, third ed., 250 pp.

APPENDIX A. SUPPLEMENTAL DATA FOR CURRENT METER EVALUATION

This appendix provides additional information for readers interested in actual test data and details of the test procedure discussed in section 4. It also includes a summary of significant problems with the current meters that were identified and resolved during the T&EL evaluation and a history of common problems (failure mode analysis) experienced by other users prior to or during the T&EL evaluation.

A.1. TEST PROCEDURES

The test procedures were designed to determine (1) the performance of the speed, direction, temperature, and conductivity sensors of the Grundy Model 9021 current meter, (2) the recording system accuracy, and (3) the environmental capabilities of the system. Initial system checkout and instrument familiarization were completed using the manufacturer's manual. The test equipment, instrumentation, and major facilities used in the evaluation are listed in table A-1.

Table A-1.--Instrumentation used in current meter evaluation

<u>Instrument</u>	<u>Manufacturer</u>	<u>Model #</u>	<u>Serial #</u>	<u>Instrument/ facility accuracy</u>	<u>Calibration date prior to test</u>
Calculator	Hewlett-Packard	9825	1622A00927	N/A	N/A
Printer	" "	9866B	1547A00762	N/A	N/A
Universal counter	" "	5328A	164A02101	± 1 count	6/77 & 12/77
Universal counter	" "	5328A	1728A5249	± 1 count	6/77 & 12/77
Digital voltmeter	" "	3455A	1622A01683	$\pm 0.002\%$ of reading	Under warranty
Digital clock	" "	59309A	1600A00376	N/A	N/A
Mueller bridge	Leeds & Northrup	GS-8071	1723141	$\pm 0.003^\circ$	11/27/78
Platinum thermometer	" "	8163	1967810		5/17/76
Galvanometer	Guildline	9461			N/A
Autosal	"	8400	39,354	± 3 ppm	Weekly
Tow carriage	DT-NSRDC			± 0.02 cm/s	
Submerged jet	T&EL			± 1.0 cm/s	

N/A = Not Applicable

Grundy 9021 Rotor Evaluation

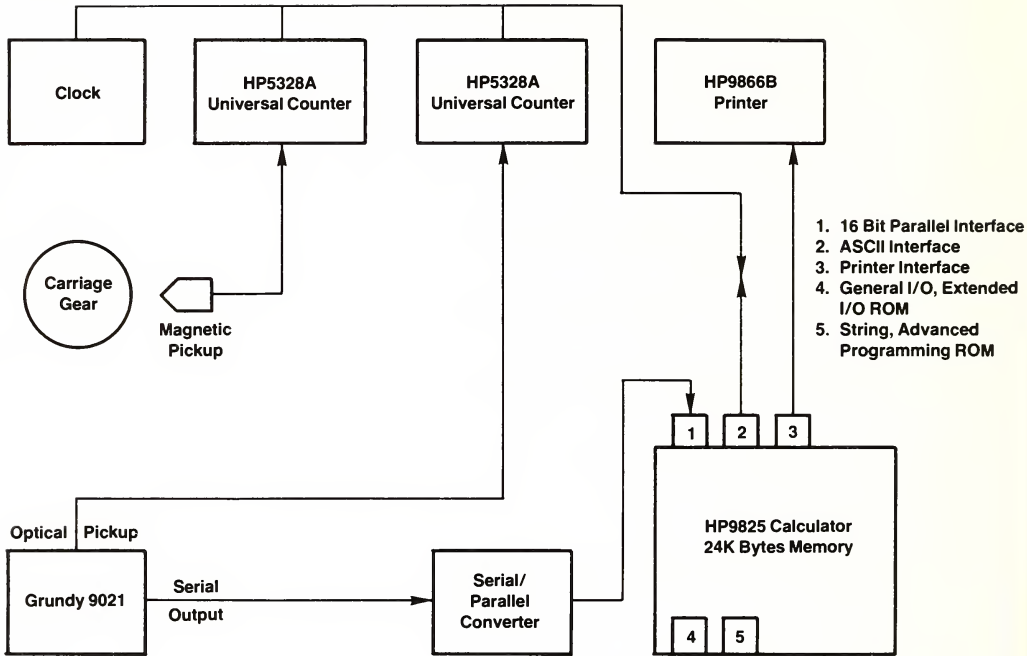


Figure A-1.--Block diagram of instrumentation used for rotor evaluation.

A.1.1. Rotor Speed Calibration

The instrument was mounted in its normal operating configuration, and rotor speed was monitored by an external optical pickup. Test speed measurement accuracies depended on the DT-NSRDC tow carriage as the primary standard (figure A-1).

A speed calibration was performed at the instrument threshold and at nominal speeds of 5, 10, 15, 20, 25, 30, 35, 40, 45, 50, 75, 100, 200, 250, and 350 cm/s. The recorded test data, at each speed, consisted of both the external digital samples of the carriage speed and rotor speed plus the internal measurements of the current meter during the 30-s sampling interval (table A-2). A statistical analysis, including the mean and standard error, was performed using the digital samples of carriage speed and rotor

Table A-2.--Rotor calibration data

DATA SUMMARY

Run #	Run Id.	Carriage Mean Cm/sec	9021Prop Mean RPM	Carriage 95% conf Cm/sec	9021Prop 95% conf RPM	Carriage Std.Dev. Cm/sec
1	1.000	5.688	9.126	0.083	0.792	0.092
2	1.000	11.433	19.614	0.094	0.336	0.174
3	1.000	21.386	37.740	0.054	0.374	0.139
4	1.000	26.982	47.410	0.045	0.186	0.138
5	1.000	32.044	56.214	0.036	0.182	0.121
6	1.000	37.031	64.648	0.029	0.172	0.103
7	1.000	41.974	73.456	0.027	0.164	0.103
8	-1.000	39.889	70.940	0.022	0.180	0.083
9	-1.000	36.506	63.440	0.018	0.192	0.065
10	-1.000	31.456	55.938	0.028	0.184	0.092
11	-1.000	26.499	47.162	0.025	0.210	0.077
12	-1.000	20.923	36.572	0.036	0.194	0.090
13	-1.000	15.978	27.674	0.036	0.256	0.083
14	-1.000	10.896	18.182	0.058	0.374	0.100
15	-1.000	5.239	7.256	0.157	1.240	0.149
16	1.000	46.962	83.280	0.040	0.192	0.162
17	1.000	52.044	92.178	0.031	0.186	0.134
18	1.000	78.148	138.486	0.021	0.198	0.110
19	-1.000	77.616	138.648	0.019	0.198	0.097
20	-1.000	51.699	91.974	0.029	0.200	0.125
21	-1.000	46.539	82.224	0.026	0.180	0.106
22	1.000	102.817	183.838	0.025	0.232	0.152
23	1.000	154.891	276.238	0.024	0.274	0.178
24	-1.000	154.645	276.816	0.023	0.284	0.167
25	-1.000	103.850	185.268	0.024	0.228	0.143
26	1.000	206.528	367.726	0.024	0.322	0.207
27	-1.000	206.455	368.552	0.022	0.346	0.190
28	-1.000	257.375	458.000	0.034	0.106	0.263
29	1.000	257.592	455.800	0.043	0.132	0.328
30	1.000	360.473	637.384	0.067	0.596	0.503
31	1.000	360.490	636.798	0.063	0.528	0.500

speed at each test speed. At least two cycles over the calibration range were performed.

Data reduction yielded one plot of rotor speed vs. carriage speed and two plots of the steady-flow accuracy presented as the error (cm/s) from (1) the manufacturer's calibration equation and (2) a computed calibration equation. The computer equation was generated from a polynomial regression of all calibration data (figure A-2 and table A-3).

A.1.2. Horizontal Directivity Tests

The horizontal, angular response characteristics of the rotor must be known to predict speed errors caused by a lagging vane

Grundy 9021 Rotor Evaluation

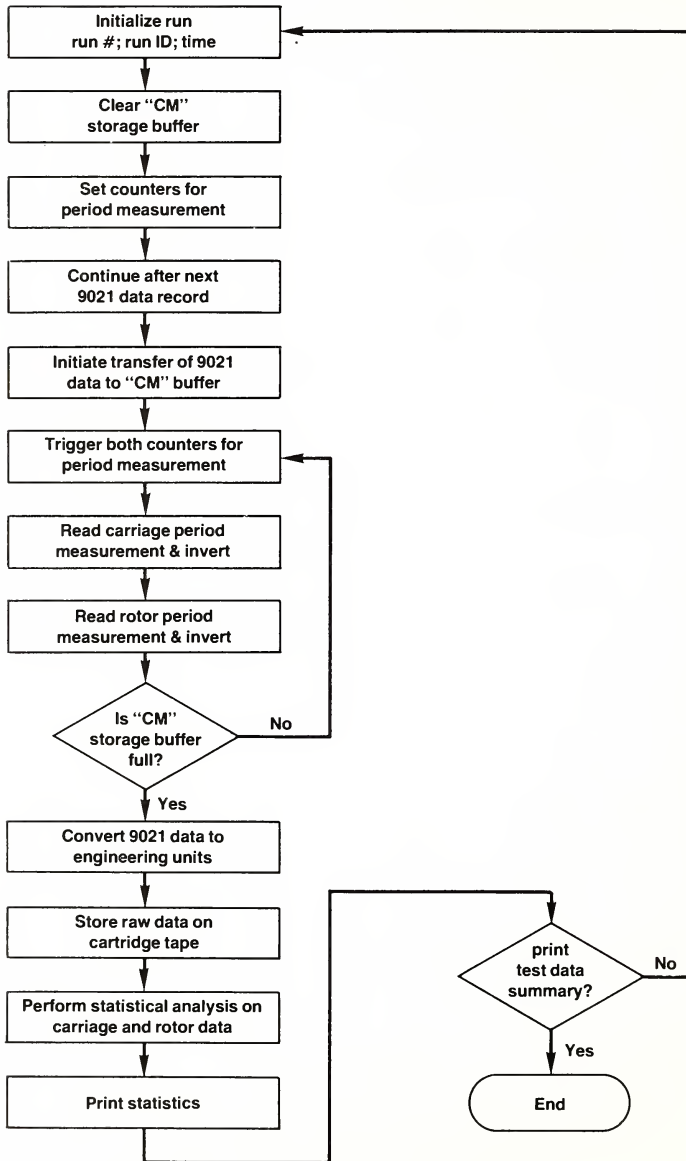


Figure A-2.--Data collection flow chart for regression analysis of rotor calibration data.

Table A-3.--Regression analysis of rotor calibration data

Polynomial Regression of Files 1 to 31

X is Rotor 52 Y is Carriage Degree Fit = 2

Term	Coefficient		
0	8.445E-01		
1	5.520E-01		
2	1.979E-05		
X Actual RPM	Y Actual Cm/Sec	Err Cm/Sec	%-Err Cm/Sec
9.126	5.688	0.196	3.3
19.614	11.433	0.246	2.1
37.740	21.386	0.318	1.5
47.410	26.982	0.075	0.3
56.214	32.044	-0.108	-0.3
64.648	37.031	-0.420	-1.1
73.456	41.974	-0.478	-1.2
70.940	39.889	0.212	0.5
63.440	36.506	-0.565	-1.6
55.938	31.456	0.326	1.0
47.162	26.499	0.421	1.6
36.572	20.923	0.134	0.6
27.674	15.978	0.157	1.0
18.182	10.896	-0.009	-0.1
7.256	5.239	-0.388	-8.0
83.280	46.962	-0.013	-0.0
92.178	52.044	-0.152	-0.3
138.486	78.148	-0.484	-0.6
138.648	77.616	0.138	0.2
91.974	51.699	0.079	0.2
82.224	46.539	-0.176	-0.4
183.838	102.817	0.169	0.2
276.238	154.891	-0.062	-0.0
276.816	154.645	0.510	0.3
185.268	103.850	-0.064	-0.1
367.726	206.528	-0.035	-0.0
368.552	206.455	0.506	0.2
458.000	257.375	0.421	0.2
455.800	257.592	-1.049	-0.4
637.384	360.473	0.226	0.1
636.798	360.490	-0.129	-0.0

Residual Standard Error is = 0.362 Cm/Sec

response in reversing-type flows. The DT-NSRDC tow carriage maintained a constant velocity to within an order of magnitude greater than the predicted accuracy of the test instrument. The fluid properties (temperature, salinity, turbulence, etc.) remained constant during the course of the test.

The instrument was mounted rigidly in the attitude normally used for measuring flow. The mounting fixture allowed the instrument to rotate about its vertical axis while minimizing induced vibrations, and a 0-degree reference was established with respect to the normal transducer attitude.

At nominal test speeds of 10 and 20 cm/s, data were recorded at 15-degree increments through 360 degrees. The recorded test data, at each speed and angle, consisted of the external digital samples of carriage speed, rotor speed, and the internal measurements of the meter during the sampling interval (table A-4). The mean and standard error were determined from the samples and represent one test point.

Data reduction should yield, via the rotor calibration equation, a plot of the rotor's response in cm/s vs. horizontal angle. The data should also be plotted as percent error from a true cosine response vs. angle.

A.1.3. Speed System Throughput Verification

This test was performed in the T&EL Submerged Jet Facility (figure A-3). The meter was positioned in the facility noting location for future reference. Rotor speed was monitored with an optical pickup and the facility speed turbine output, simultaneously. Verification of speed system throughput was performed at approximate flow speeds of 5, 10, 20, and 30 cm/s. Thirty digital samples of both the turbine output and rotor speed were recorded for 30 s while monitoring the meter output utilizing the HP9825 minicomputer (figure A-4). Finally, the internally recorded data were compared against the rotor's optical pickup for proper speed information.

A.1.4. Vane Alinement Accuracy

The instrument was mounted in its normal operating configuration, and an initial run was made at 12 cm/s to assure correct vane alinement; the meter was allowed to sample several times, and the compass measurement was recorded throughout the run. The vane was then held at 90 degrees to the towing direction, released, and allowed to aline at speeds of 3, 5, 10, and 25 cm/s in that order. The meter recorded the compass measurement at the final alinement position. The average of these angle measurements was then compared to that measured in the initial run.

Table A-4.--Horizontal cosine response of SN52 rotor

Run#	Actual Speed Cm/sec	Actual Angle Degrees	9021 Rotor RPM	Rotor Speed Cm/sec	Rotor Cos Error Cm/sec
1	10.8	0.0	17.7	10.6	-0.3
2	10.8	15.0	16.8	10.1	-0.3
3	10.8	30.0	13.1	8.0	-1.3
4	10.8	45.0	12.5	7.7	0.1
5	10.8	60.0	8.2	5.3	-0.1
6	10.8	105.0	6.7	4.5	1.7
7	10.8	120.0	9.7	6.2	0.8
8	11.3	135.0	11.9	7.4	-0.6
9	10.9	150.0	5.6	3.9	-5.5
10	10.7	175.0	5.1	3.6	-7.1
11	10.8	180.0	4.9	3.5	-7.3
12	10.8	195.0	6.4	4.3	-6.1
13	10.8	210.0	9.8	6.2	-3.1
14	10.8	225.0	10.7	6.7	-0.9
15	10.8	240.0	10.0	6.3	0.9
16	10.7	255.0	8.1	5.3	2.5
17	10.7	270.0	3.2	2.6	2.6
18	10.7	285.0	2.7	2.3	-0.5
19	10.5	300.0	7.8	5.1	-0.2
20	10.6	315.0	12.4	7.7	0.2
21	10.7	330.0	13.1	8.0	-1.2
22	10.9	345.0	17.8	10.7	0.2
23	11.3	360.0	19.0	11.3	0.1
24	20.4	0.0	35.8	20.6	0.2
25	20.4	15.0	33.5	19.3	-0.4
26	20.4	30.0	25.2	14.7	-2.9
27	20.4	45.0	25.1	14.7	0.2
28	20.5	60.0	15.3	9.3	-1.0
29	20.5	75.0	7.5	5.0	-0.3
30	20.4	105.0	12.7	7.8	2.5
31	20.5	120.0	19.2	11.4	1.2
32	20.4	135.0	22.6	13.3	-1.2
33	20.4	150.0	14.3	8.7	-9.0
34	20.4	165.0	13.6	8.3	-11.4
35	20.5	180.0	10.2	6.5	-14.1
36	20.5	195.0	15.2	9.2	-10.6
37	20.4	210.0	20.6	12.2	-5.5
38	20.4	225.0	21.2	12.5	-1.9
39	20.4	240.0	19.6	11.6	1.4
40	20.4	255.0	14.1	8.6	3.3
41	20.3	270.0	5.0	3.5	3.5
42	20.4	300.0	15.0	9.1	-1.1
43	20.4	315.0	25.1	14.7	0.3
44	20.4	330.0	26.3	15.4	-2.3
45	20.4	345.0	34.0	19.6	0.0
46	20.4	360.0	36.4	20.9	0.5

Grundy 9021 I&A Checkout

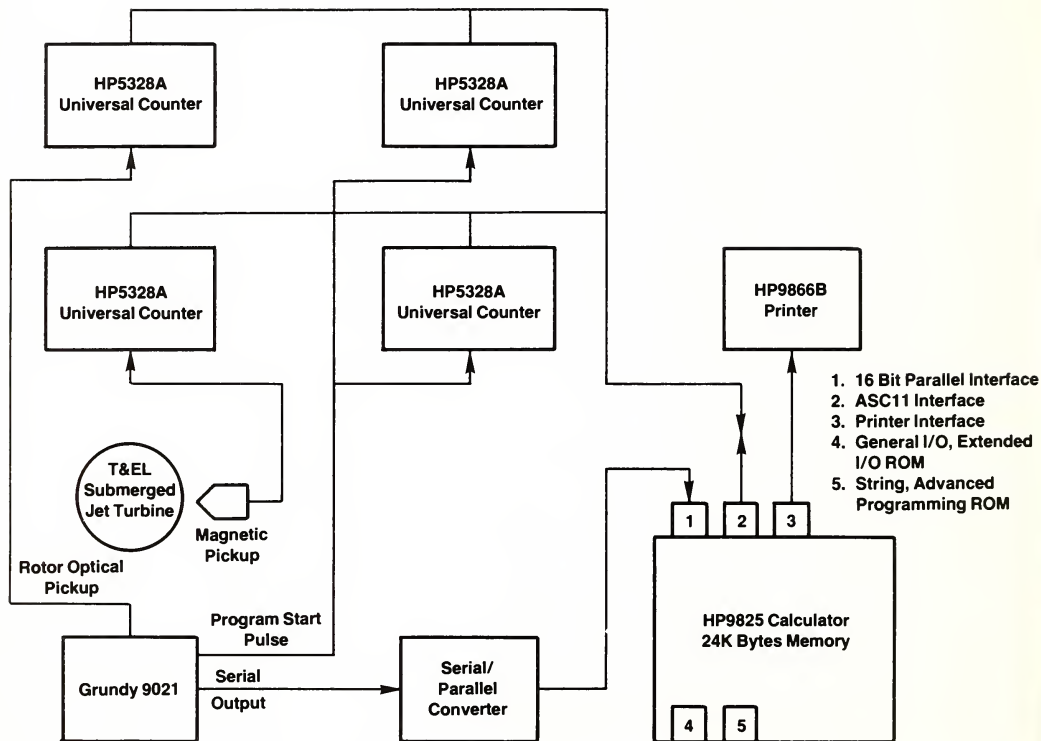


Figure A-3.--Block diagram of instrumentation used for speed system throughput verification.

Grundy 9021 I&A Checkout

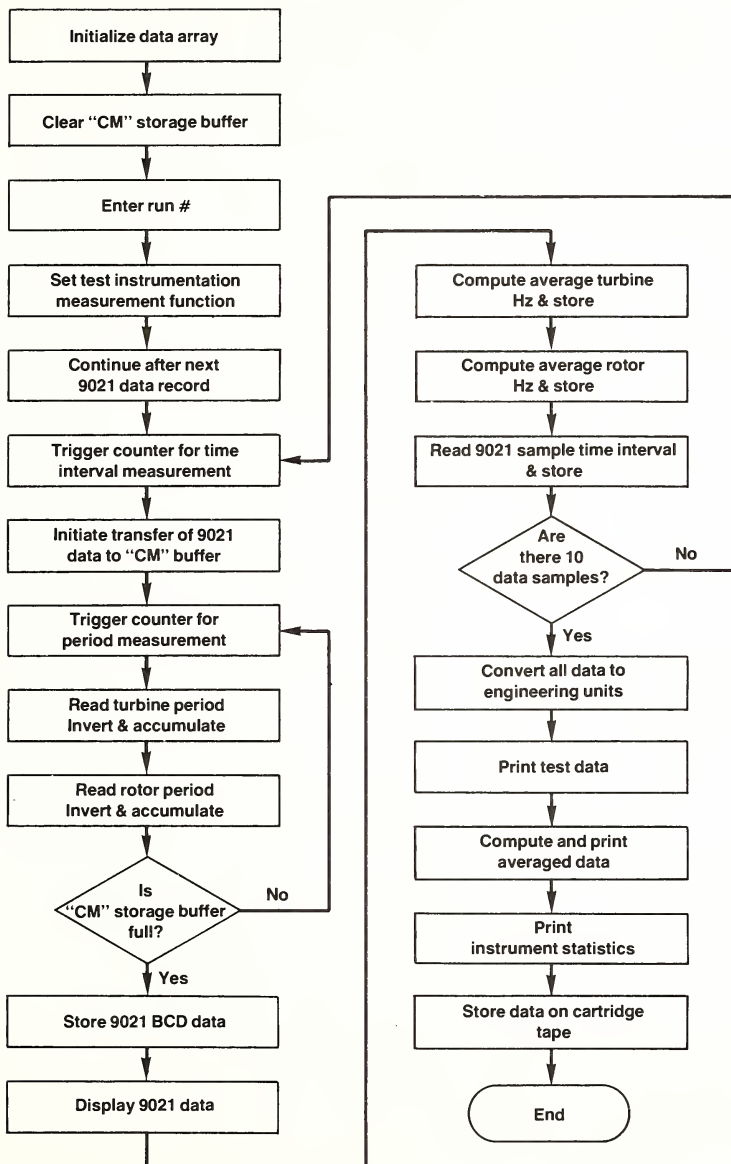


Figure A-4.--Data collection flow chart for speed system throughput verification.

Table A-5.--Compass calibration data

Plessey 9021 SN#51 Hyde Field

Heading Angle Deg.	Plessey 9021 BCD	Computed Angle Deg.	Angle Error Deg.
360	1016	357.23	-2.77
15	36	12.66	-2.34
30	80	28.13	-1.87
45	120	42.19	-2.81
60	164	57.66	-2.34
75	208	73.13	-1.87
90	252	88.60	-1.40
105	296	104.07	-0.93
120	340	119.54	-0.46
135	380	133.61	-1.39
150	424	149.08	-0.92
165	464	163.14	-1.86
180	508	178.61	-1.39
195	549	193.08	-1.92
210	592	208.15	-1.85
225	632	222.21	-2.79
240	676	237.68	-2.32
255	720	253.15	-1.85
270	760	267.22	-2.78
285	804	282.69	-2.31
300	848	298.16	-1.84
315	888	312.22	-2.78
330	932	327.69	-2.31
345	976	343.16	-1.84
360	1016	357.23	-2.77
15	36	12.66	-2.34
30	80	28.13	-1.87
45	120	42.19	-2.81
60	168	59.07	-0.93
75	208	73.13	-1.87
90	252	88.60	-1.40
105	296	104.07	-0.93
120	340	119.54	-0.46
135	380	133.61	-1.39
150	424	149.08	-0.92
165	468	164.55	-0.45
180	508	178.61	-1.39
195	552	194.08	-0.92
210	592	208.15	-1.85
225	632	222.21	-2.79
240	680	239.09	-0.91
255	720	253.15	-1.85
270	760	267.22	-2.78
285	808	284.09	-0.91
300	848	298.16	-1.84
315	888	312.22	-2.78
330	936	329.10	-0.90
345	976	343.16	-1.84
360	1016	357.23	-2.77

A.1.5. Vane Alinement Response Time

The vane was aligned 180 degrees to the towing direction and held until speeds of 5, 10, 20, and 25 cm/s were reached. The vane was then released, and the time required for it to aline to the towing direction at each speed was noted (visual observation). At each speed, the alinement time was multiplied by the speed to find the "distance constant."

A.1.6. Compass Calibration

This test was performed at a local (Hyde Field) airport to reduce the influence of nearby electromagnetic radiation. A Lutz magnetic compass was used as the reference standard. The current meter was set up without the vane and gimbal and alined to magnetic north. The meter was rotated cw then ccw in 15-degree increments through 360 degrees. The instrument was allowed to sample the compass so that at least two readings yielded the same digital number at each test angle. Both the instrument heading and the actual heading for each test angle were tabulated (table A-5). These procedures were repeated with a 25-degree instrument tilt and at 90-degree increments. The instrument compass error was plotted referenced to the actual heading.

A.1.7. Time Base, Recorder, and Power Supply Tests

The time between trigger pulses, using the 5-min timing plug supplied, was measured over the operating temperature range during the environmental temperature tests. The internally recorded data of all tests were compared to the verifier/printer printouts. The meter's battery pack was replaced with an external d.c. power supply and the 0.5-min time plug inserted for test duration. The 12-V supply was decreased to 6.0 V in 0.2-V increments, and the instrument output was recorded on the printer/verifier for each test condition. The output of each transducer was noted to determine the operation that malfunctioned first and the voltage at which the malfunction occurred.

A.1.8. Temperature Channel Tests

These tests were performed at T&EL using the Mallory Temperature/Salinity Facility. The meter was subjected to three temperature bath cycles at various salinities consisting of the following:

@35 <u>±</u> 1 ppt	@20 <u>±</u> 1 ppt	@5 <u>±</u> 1 ppt
35 [°] C	33 [°] C	34 [°] C
29	27	28
23	21	22
17	15	16
11	9	10
5	3	4
- 1	0	1
2	6	7
8	12	13
14	18	19
20	24	25
26	30	31
32		

At each temperature test point, the bath was stabilized (rate of temperature change, $\pm 0.005^{\circ}$ C per min) allowing a 20-min temperature equilibration period. After temperature stabilization, 30 data points were collected with an HP9825A calculator. Two sets of standard temperature measurements were taken with one set at the beginning and the second set at the end of data collection. Data for the conductivity channel were collected simultaneously during the temperature test points. (See procedure under conductivity data collection.) Uncertainty of the standard temperature measurements should be $\pm 0.003^{\circ}$ C.

The mean of the two sets of standard temperature measurements was computed. Then, at each test point, the sample mean and standard deviation(s) of the 30 temperature sensor samples were computed. The magnitude of the standard deviation indicates inherent noise in the temperature measurement channel. The temperature channel measurement errors (sensor mean - standard mean) were computed for each test point. NOTE: the manufacturer's transfer equation was used to convert the sensor sample mean output value to temperature in $^{\circ}$ C. Finally, the mean temperature measurement channel error at each temperature test point from data above was computed (table A-6).

Mean errors versus nominal applied bath temperatures were plotted; these error curves represent the systematic and random

Table A-6. Conductivity/temperature tests with SN24

Seq.#	Bath Temp. Deg.C	Bath Cond. mS/cm	Temp. Error Deg.C	Cond. Error mS/cm
1	34.52		0.04	
2	29.01	59.85	0.02	0.03
3	23.00	53.27	-0.01	0.02
4	16.99	46.90	-0.03	0.04
5	10.96	40.76	-0.06	-0.03
6	4.95	34.93	-0.04	-0.01
7	-1.04	29.44	-0.05	-0.07
8	1.93	32.11	-0.03	-0.06
9	7.95	37.80	-0.06	-0.01
10	13.95	43.78	-0.03	0.05
11	19.98	50.05	-0.03	0.05
12	26.00	56.53	0.01	0.07
13	32.01		0.02	
14	33.03	37.37	0.06	-0.05
15	27.01	33.44	0.01	-0.04
16	20.99	29.61	-0.02	-0.03
17	14.98	25.92	-0.03	0.00
18	8.95	22.38	-0.06	-0.06
19	2.94	19.01	-0.06	0.02
20	0.93	17.94	-0.04	-0.06
21	5.94	20.67	-0.04	-0.05
22	11.96	24.12	-0.05	0.05
23	17.96	27.73	-0.06	-0.01
24	23.99	31.50	-0.01	-0.04
25	29.99	35.36	-0.01	-0.03
26	34.03	12.86	0.06	-0.04
27	28.01	11.51	0.01	-0.07
28	22.00	10.19	-0.01	-0.05
29	15.98	8.91	-0.02	-0.06
30	9.96	7.70	-0.04	-0.02
31	3.95	6.54	-0.03	-0.03
32	0.95	5.99	-0.03	-0.05
33	6.95	7.11	-0.03	-0.02
34	12.96	8.30	-0.04	-0.04
35	18.97	9.54	-0.03	-0.04
36	24.99	10.84	-0.01	-0.06
37	31.01	12.18	0.03	-0.04

errors of the temperature measurement channel and were used as the baseline reference for other calibration comparisons.

A.1.9. Conductivity Channel Tests

These tests were performed using the same test equipment and facilities used to evaluate the temperature channel. Test baths for salinities of 35, 20, and 5 ppt \pm 1 ppt were prepared, and two water samples from each bath were collected and their conductivity ratio measured on the Guildline Autosol.

The mean of the two conductivity ratios from the dual samples taken at each test point was computed. From the mean conductivity ratio [R], bath temperature [T(°C)], and bath salinity [S(ppt)], the *in situ* bath conductivity [C_{S, T} (mS/cm)] was derived using

$$C_{S, T} = (C_{35, 15}) (C_{35, T}/C_{35, 15}) (C_{S, T}/C_{35, T})$$

where $(C_{35, 15}) = 42.896 \text{ mS/cm},$

$$(C_{35, T}/C_{35, 15}) = 0.676641 + 0.0200588 (T) + 1.09524 (10^{-4}) (T^2) - 6.417 (10^{-7}) (T^3),$$

and $(C_{S, T}/C_{35, T}) = R + A (T_1) - A(T).$

The temperature correction factors (A values) were computed by solving the following equation for $t = T_1$ and $t = T$:

$$A(t) = [(10^{-5}) (R) (R-1) (t-15)] [96.7 - 72R + 37.3 R^2 - (0.63 + 0.21R^2) (t-15)].$$

Output readings of the 30 conductivity sensor channels were reduced to mean and standard deviations using the method described for the temperature channel. The magnitude of the standard deviations indicates inherent noise in the conductivity measurement channel. The conductivity measurement channel errors (sensor mean - standard mean) were computed at each test point. NOTE: the mean output of each sensor sample was converted to conductivity in mS/cm. Finally, the mean conductivity error at each temperature/salinity test point from data above was computed (table A-6).

The mean error values vs. the *in situ* bath conductivity values were plotted; this error curve represents the systematic errors of the conductivity measurement channel over applied conditions of 0° C to 35° C at 35 ppt and were used as the baseline reference for other calibration comparisons.

A.1.10. Environmental Tests

The instrument was subjected to the sections of Mil-STD-810C (U.S. Department of Defense 1975) environmental temperature tests appropriate to manufacturer specifications and user requirements. The instrument's

output data were recorded externally through the printer/verifier, and variations in battery voltage and the 5-min sample pulse were monitored and recorded throughout the test.

In lieu of any other guidance, the instrument was subjected to vibration in accordance with the procedures of Mil-STD-167-1 (U.S. Department of Defense 1974). The instrument output data were monitored externally and recorded through the printer/verifier.

A.1.11. Dynamic Testing

Utilizing T&EL's Vertical Planar Motion Mechanism (VPMM) on DT-NSRDC's #1 tow carriage (figure A-5), orbital and horizontal dynamic motions in the presence of steady tow were simulated. The instrument was mounted in its normal configuration with the tow carriage as the primary speed standard. The dynamic tests were conducted at various carriage speeds, periods of oscillation, attack angles, and amplitudes expected to be encountered by the instrument during a field survey.

A reference heading for the instrument was established while towing in the east and then west direction by allowing the instrument to sample the compass while towing the length of the basin at 25 cm/s. The average of all compass readings per tow direction for the compass reference heading was then computed.

The test data collected under each test condition consisted of simultaneous digital measurements of carriage speed, dynamic fixture period, and the internal measurements of the current meter during the instrument sample interval (table A-7). The test data recorded during each run consisted of the computed average carriage speed and oscillator period over the instrument sampling interval plus the V_n and V_e components of \bar{V} computed from the instrument measured velocity. A minimum of 30 instrument readings were taken unless limited by the end of carriage travel.

A statistical analysis of the recorded test data (i.e., carriage speed, oscillator period, V_n , and V_e), including the mean and standard error, was determined from the digital samples (figure A-6). The instrument average vector magnitude \bar{V} was then reconstructed from the mean V_n and V_e component vectors and used to determine the velocity magnitude error $V - V_0$ in relation to the carriage speed. The velocity angle error was computed from the established reference heading.

Grundy 9021 Dynamics Evaluation

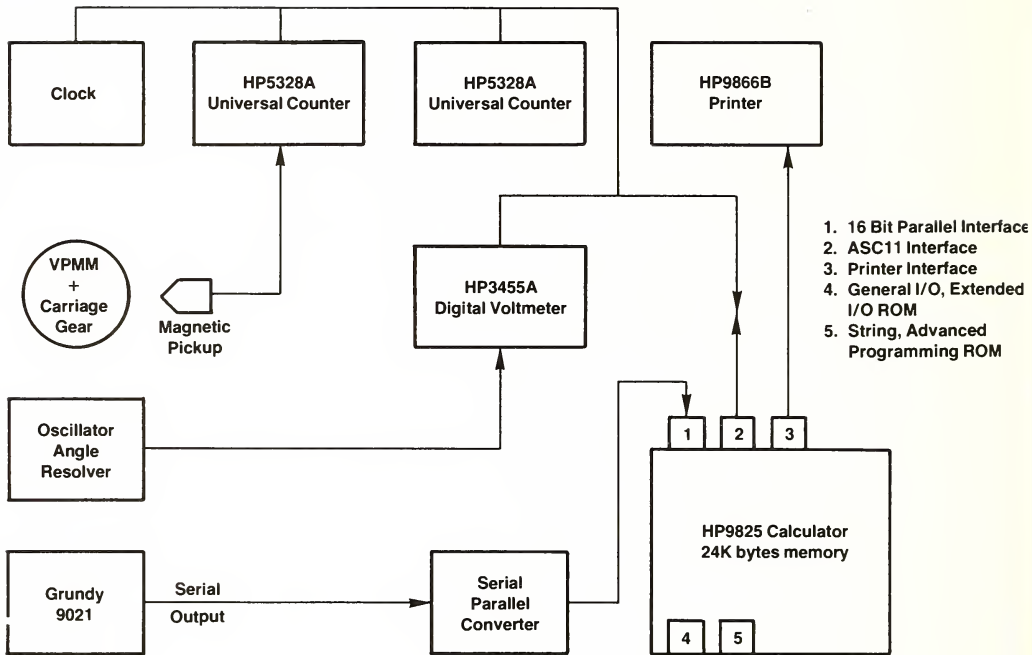


Figure A-5.--Block diagram of instrumentation used in the dynamics evaluation.

A.1.12. Acoustic Calibration

The current meter tested has an optional acoustic transducer that transmits a serial pulse train representing the current meter output during the time the data are recorded internally on magnetic tape. The system was calibrated by determining the source level and vertical directivity pattern of the acoustic transducer and the sensitivity of the acoustic receiver. An operational check of the acoustic telemetry link was made at the maximum detectable range specified by the manufacturer. These tests were conducted at the Naval Surface Weapons Center (NSWC) Acoustic Facility, White Oak, Md.

Table A-7. Dynamics test data

V_O = carriage speed (cm/s) T = period of dynamic motion (s)
 θ = angle between carriage heading and dynamic plane of motion (degrees) S/N = ratio of tow carriage speed to angular velocity of dynamic motion
 A = peak-to-peak amplitude of dynamic motion (m) \bar{V} = measured velocity magnitude of Grundy 9021 (cm/s)

ORBITAL DYNAMICS

V_O	θ	Test Conditions		S/N	\bar{V}	Test Results		
		A	T			$\bar{V}-V_O$	Heading Error	\bar{V}/V_O
13	0	1.2	5.6	0.2	16	3	-15	1.2
13	0	1.2	4.9	0.2	24	11	-32	1.8
12	0	0.6	4.5	0.3	12	0	- 2	1.0
26	0	1.2	5.0	0.3	34	8	24	1.3
26	0	1.2	5.6	0.4	29	3	- 7	1.1
36	0	1.2	4.8	0.4	33	-3	-17	0.9
37	0	1.2	5.6	0.6	36	-1	3	1.0
25	0	0.6	4.5	0.6	24	-1	0	1.0
27	0	1.2	8.3	0.6	27	0	0	1.0
36	0	0.6	12.7	0.8	31	-5	- 1	0.9
26	0	1.2	12.3	0.8	25	-1	- 1	1.0
36	0	1.2	12.7	1.2	37	1	- 1	1.0
14	45	1.2	4.9	0.2	12	-2	-48	0.9
13	45	1.2	4.8	0.2	20	7	35	1.5
13	45	1.2	9.2	0.3	17	4	- 8	1.3
13	45	0.6	4.5	0.3	9	-4	33	0.7
13	45	1.2	11.5	0.4	18	5	-13	1.4
36	45	1.2	4.8	0.5	39	3	-16	1.1
24	45	0.6	4.5	0.6	18	-6	-16	0.8
26	45	1.2	9.3	0.6	29	3	- 9	1.1
35	45	0.6	4.5	0.8	30	-5	49	0.9
26	45	1.2	11.5	0.8	29	3	-13	1.1
36	45	1.2	9.2	0.9	39	3	-10	1.1
36	45	1.2	11.5	1.1	39	3	- 7	1.1
51	45	1.2	12.4	1.7	52	1	- 5	1.0
12	90	1.2	5.6	0.2	5	-7	-63	0.4
13	90	1.2	6.3	0.2	18	5	-19	1.4
13	90	0.6	4.5	0.3	12	-1	3	0.9
13	90	1.2	9.4	0.3	21	8	- 5	1.6
25	90	1.2	5.6	0.4	29	4	- 3	1.2
13	90	1.2	12.0	0.4	19	6	- 1	1.5
26	90	1.2	7.7	0.5	30	4	- 3	1.1
36	90	1.2	5.4	0.5	36	0	18	1.0
37	90	1.2	5.6	0.6	40	3	10	1.1
25	90	0.6	4.5	0.6	25	0	8	1.0
36	90	0.6	4.5	0.8	35	-1	5	1.0
26	90	1.2	12.1	0.8	29	3	- 4	1.1
36	90	1.2	9.4	0.9	39	3	- 2	1.1
37	90	1.2	12.0	1.2	41	4	2	1.1

Table A-7. Dynamics test data (continued)

HORIZONTAL DYNAMICS								
V_O	θ	Test Conditions		S/N	\bar{V}	Test Results		
		A	T			$\bar{V}-V_O$	Heading Error	\bar{V}/V_O
13	0	1.2	5.6	0.2	9	-4	8	0.7
13	0	1.2	9.5	0.3	12	-1	18	0.9
13	0	0.6	4.9	0.3	13	0	3	1.0
13	0	1.2	11.9	0.4	12	-1	26	0.9
26	0	1.2	5.1	0.4	24	-2	16	0.9
26	0	1.2	7.0	0.4	26	0	3	1.0
36	0	1.2	5.0	0.5	34	-2	3	0.9
13	0	0.6	7.7	0.5	13	0	6	1.0
26	0	0.6	4.8	0.7	24	-2	1	0.9
36	0	1.2	8.5	0.8	35	-1	0	1.0
26	0	1.2	11.9	0.8	26	0	0	1.0
13	0	0.6	11.7	0.8	12	-1	1	0.9
36	0	0.6	4.8	0.9	35	-1	- 2	1.0
26	0	0.6	7.8	1.1	27	1	- 1	1.0
36	0	1.2	12.3	1.2	36	0	0	1.0
36	0	0.6	7.8	1.5	37	1	- 1	1.0
26	0	0.6	13.0	1.8	27	1	0	1.0
36	0	0.6	13.5	2.5	38	2	- 1	1.1
13	45	1.2	4.0	0.1	12	-1	21	0.9
12	45	1.2	7.8	0.2	9	-3	-19	0.8
13	45	0.6	4.9	0.3	11	-2	6	0.8
12	45	1.2	13.0	0.4	11	-1	-28	0.9
36	45	1.2	5.8	0.5	27	-9	- 6	0.8
13	45	0.6	8.5	0.6	12	-1	-11	0.9
35	45	0.6	4.0	0.7	31	-4	- 4	0.9
27	45	0.6	4.9	0.7	24	-3	0	0.9
35	45	1.2	8.4	0.8	35	0	- 9	1.0
13	45	0.6	11.3	0.8	12	-1	- 6	0.9
26	45	0.6	9.1	1.2	26	0	- 3	1.0
36	45	1.2	12.3	1.2	37	1	- 5	1.0
26	45	0.6	11.3	1.6	25	-1	- 2	1.0
36	45	0.6	9.0	1.7	36	0	- 1	1.0
36	45	0.6	11.3	2.1	37	1	1	1.0
14	90	1.2	7.7	0.3	7	-7	7	0.5
13	90	0.6	3.9	0.3	10	-3	0	0.8
14	90	1.2	9.8	0.4	15	1	0	1.1
13	90	0.6	6.9	0.4	11	-2	0	0.8
36	90	1.2	4.9	0.5	30	-6	5	0.8
26	90	0.6	4.3	0.6	21	-5	0	0.8
36	90	1.2	8.2	0.8	35	-1	4	1.0
13	90	0.6	11.8	0.8	12	-1	4	0.9
36	90	0.6	5.0	0.9	31	-5	- 3	0.9
36	90	1.2	11.9	1.1	37	1	3	1.0
26	90	0.6	8.4	1.1	25	-1	4	1.0
26	90	0.6	12.2	1.7	25	-1	2	1.0
36	90	0.6	11.9	2.2	36	0	0	1.0

Grundy 9021 Dynamics Evaluation

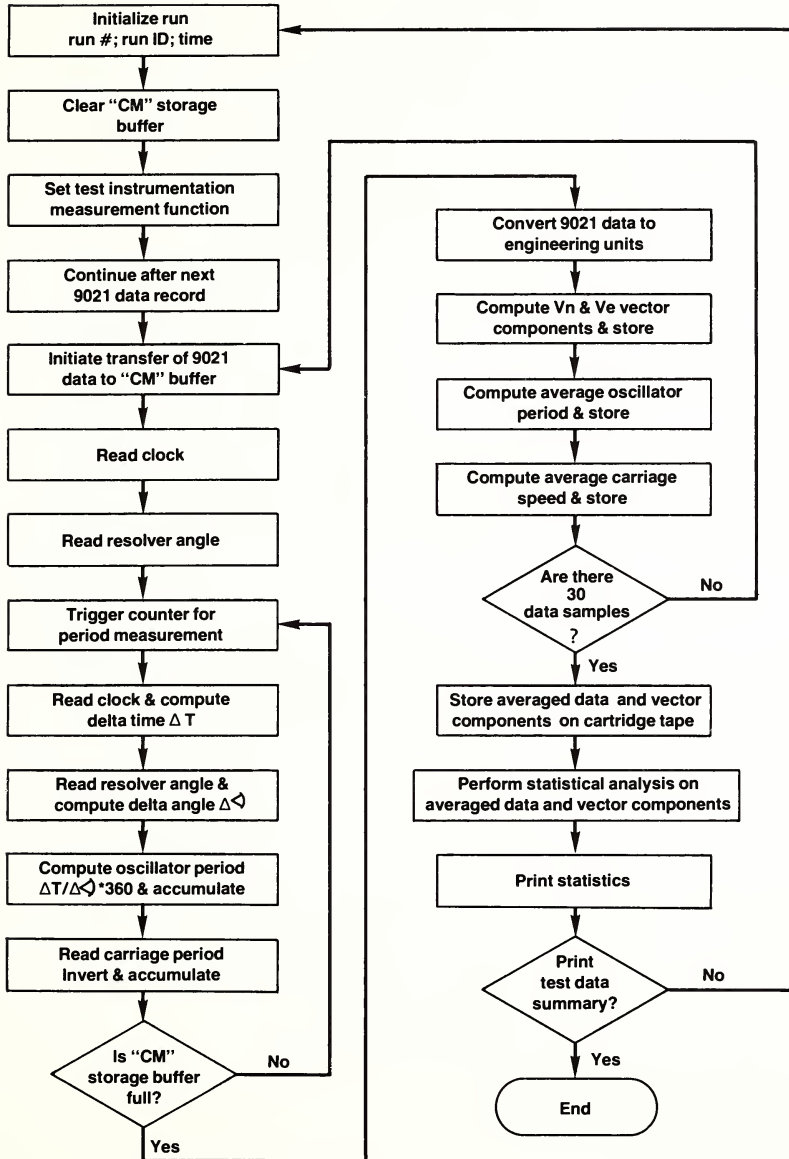


Figure A-6.--Data collection flow chart for dynamics tests.

A.2. SUMMARY OF IDENTIFIED PROBLEMS AND THEIR RESOLUTION

The evaluation phase and the inspection-acceptance phase of the T&EL program uncovered instrumentation problems that could have resulted in significant measurement errors and loss of information during the survey phase of the NOS program. The following summary highlights those problems:

A.2.1. Temperature

The semiconductor temperature sensor used on the Grundy 9021 exhibited unacceptable stability characteristics. The electronics exhibited a temperature dependency that affected the temperature measurement. The semiconductor sensor was replaced with a platinum-resistance sensor, and circuit components were replaced to reduce temperature dependency. Calibration errors in several units were traced to significant drift in the manufacturer's temperature standard.

A.2.2. Conductivity

The conductivity measurement was found to be dependent upon temperature. A temperature compensation circuit was installed by the manufacturer in each 9021, and electronic components were replaced.

A.2.3. Direction

The DIGICOURSE compass installed in the Grundy 9021 had an inadequate tilt latitude (+ 5 degrees) that caused the compass to stick. All NOS current meters were retrofitted with compass assemblies having a + 45-degree tilt latitude. During tilt tests, these compasses exhibited gimbal "hang-up" problems that required modification of all existing units. Following this modification, compass damage occurred during shipment, indicating that shock loading could result in gimbal failure; the manufacturer subsequently redesigned and rebuilt 19 compass assemblies. Eleven of the NOS Grundy 9021 current meters contain compass assemblies that have not received modifications to prevent shock damage.

T&EL compass tests were performed using a prototype steel platform designed for field deployment. After substantial distortion of the magnetic field was detected by the DIGICOURSE compass, the platforms were redesigned and fabricated using aluminum.

A.2.4. Speed

The manufacturer-derived calibration equations did not take into account the blockage created by the optional sensors. T&EL subsequently provided the proper calibration equations.

Reed switch bounce on several units resulted in lower than actual speeds being recorded internally. The manufacturer modified circuitry on all units to filter the bounce characteristics and replaced reed switch assemblies in several units.

A.2.5. Fouling

Following the initial survey, severe fouling of the meter resulted in degradation of the conductivity and speed measurements. Barnacles caused conductivity readings to be lower than the actual value and also caused rotors to stop turning. T&EL investigated several anti-foulants and recommended a compound to protect the meter and eliminate sensor measurement degradation.

A.2.6. Electronics

Six units were found to have defective integrated circuits, and three units required time-base adjustment. Various other electrical problems were detected and resolved. Calibration adjustments were performed on several units.

A.3. FAILURE MODE ANALYSIS

Plessey (now Grundy) Environmental Systems first marketed the Model 9021 Recording Current Meter in February 1977. The instrument is an electronically redesigned and updated version of the Plessey MO-21. A prototype/demonstration Plessey 9021 was lent by Plessey to several university scientists for intercomparisons on field deployments. Small quantities of these current meters were procured by government laboratories for experimental and evaluation purposes. The following descriptions of laboratory and field experiences represent the significant performance information available on the Plessey 9021 prior to the NOS procurement.

A.3.1. NAVOCEANO

The U.S. Naval Oceanographic Office (NAVOCEANO) was the first to purchase the Model 9021 in early 1977. Three current meters (SN 51,

52, and 53) were acceptance-tested at the National Space Technology Laboratories (NSTL) facilities in Mississippi in June 1977. The meters were returned to Plessey by NAVOCEANO because errors in all four sensors were outside the manufacturer's specifications. Plessey determined that the wrong conductivity cell and pressure transducers were installed on the meters (wrong pressure ratings). Plessey also discovered a wiring problem on the multiplexer circuit board (the input not being tied to ground) that caused erroneous sensor readings. After these problems were corrected, NAVOCEANO lent the three sensors to T&EL without conducting any further investigations. (NAVOCEANO tow tank tests conducted in Mississippi revealed errors larger than those discovered by T&EL; these errors could be attributable to residual flows in the smaller NSTL tow basin.)

A.3.2. Canada Centre for Inland Waters - (CCIW)

Early in 1977, the CCIW purchased three Plessey 9021 current meters with optional temperature transducers. Sensor errors, similar to those uncovered by NAVOCEANO, were discovered in initial acceptance tests. Plessey sent electrical schematics and instructions to CCIW for correcting the floating ground problem on the multiplexer board. The delay encountered in repair of the instruments did not allow sufficient time for laboratory calibrations prior to field deployment.

In July 1977, three units were deployed on subsurface moorings along with the older Plessey MO-21 current meters for an inter-comparison. They were recovered in September 1977, and data analysis is still underway at CCIW. The following comments and observations were offered by Jim Bull of CCIW:

- Good agreement was obtained between the Plessey MO-21 and 9021. Only 3 out of 1,500 temperature points were in disagreement.
- Two 9021 meters returned 100 percent data; the third returned only 50 percent because of apparent failure to charge the battery fully.
- The Ministry of Environment bought one Plessey 9021, and they experienced compass sticking during a field deployment.
- Laboratory tests, recently completed at CCIW, indicated a compass sticking problem during tow carriage runs and temperature errors of 0.2° C.

A.3.3. North Carolina State University

Plessey Environmental Systems lent N.C. State a demonstration instrument in the winter of 1977 for an intercomparison deployment with an Aanderaa meter. The mooring was subsurface at 45 m depth, with the first instruments within 17 to 18 m of the surface. There was little estimated dynamic force imparted to the mooring or instrumentation.

Data processing and analysis are underway at N.C. State. The following preliminary observations and comments were made by Len Pietrafesa and Jerry Sawyer:

- On moorings, the Plessey 9021 is more cumbersome to handle and deploy than the Aanderaa.
- There was less fouling on the Plessey rotor than on the Aanderaa rotor because of the antifoulant protection provided by Plessey.
- The Plessey unit had a complete data record, but the beginning of the tape had 3-hr periods of unexplained noise every 10 hr. Preliminary analysis suggests that the tape may have been binding in the recorder.
- Occasionally, data indicated continuous compass readings of the same value, suggesting that the compass may have been sticking.
- The demonstration 9021 current meter did not have any optional transducers.

A.3.4. Pacific Marine Environmental Laboratory (PMEL)

The PMEL borrowed a Plessey 9021 demonstration unit in the summer of 1977 for intercomparison with Aanderaa current meters. The instruments were deployed in the Strait of Juan de Fuca on a subsurface mooring 13 m below the surface. It was estimated that little dynamic force was imparted to the mooring or instrumentation. The 9021 was placed within 1 m of an Aanderaa unit for a period of 45 days from late June to early August 1977.

Data reduction and analysis are underway at PMEL, and the following comments and observations were offered by Pat Laird of PMEL:

- The 9021 is more difficult to deploy than the Aanderaa because of its mooring attachment arrangement.
- 100 percent data return on all instruments.

- No problems were observed with the operation of the Plessey 9021, and it "looked as good as the Aanderaa."
- The Plessey 9021 that PMEL used did not have optional sensors.

A.3.5. Summary

Based on the limited number of field deployments, the consensus of opinion is that the Plessey 9021 current meter operates reliably over 30- to 60-day periods. The compass sticking problem with the ± 5 -degree DIGICOURSE compass was experienced in the field by others, verified in our lab tests, and justified retrofit of the new ± 45 -degree compasses. The mooring attachment and handling problems are significant when compared to the Aanderaa. The data record noise experienced by N.C. State is the only unresolved problem.

No specific failure mode has been established, and the sample size of instruments that have been deployed in the field is much too small to perform a definitive failure mode analysis.

APPENDIX B. INSTRUMENT TRANSFER FUNCTIONS

The transfer functions described in this appendix were used to process data obtained during the NOS SPR Support Project.

B.1. GRUNDY MODEL 9021 CURRENT METER

The Grundy Model 9021 current meter data output contains six serially coded, 10-bit binary words for each sample sequence. The Grundy Model 8220 printer/verifier converts the six serial output words to their respective BCD equivalents. The order of output and the respective transfer functions, where N = BCD output, are listed below:

Word

1	Instrument serial number = serial number
2	Current direction = $0.3516N$ (degrees)
3	Current speed = $0.2 \text{ E-4 } N^2 + 0.552N + 0.8$ (cm/s)
4	Temperature = $0.03613 N - 2$ ($^{\circ}\text{C}$)
5	Sequence count = count
6	Conductivity = $0.05859N$ (mS/cm)

B.2. AANDERAA METEOROLOGICAL STATIONS

The Aanderaa Model DL-1 data logger, used to record meteorological data, can be set to record either 6 or 12 words serially. The data loggers recorded 12 words initially but were later modified to record 6 words during July 1978.

The transfer functions for the meteorological sensors, where N is the BCD output, are as follows:

$$\text{Wind speed} = 7.46 \text{ E-2 } N (\text{m/s})$$

(This equation applies to both maximum and average wind speed channels.)

$$\text{Wind direction} = 1.5 + 0.349 N (\text{degrees})$$

$$\text{Temperature} = 0.471 \text{ E-5 } N^2 + 0.04366 N - 8.164 (^{\circ}\text{C})$$

(N may require correction. If at 0°C , N is not equal to 183, correct it to that number. For example, if N = 184 at 0°C , then correct all data using $N = N \text{ actual} - 1$.)

Air pressure (Model 2056 sensor) = $A_0 + A_1 N + A_2 N^2 + B_1 \theta$ (mbar), where A_0 , A_1 , A_2 and B_1 are calibration coefficients and θ = instrument temperature.

Calibration coefficients:

SN 65

$A_0 = 0.6832817 \text{ E}+3 \text{ mbar}$
 $A_1 = 0.3205513 \text{ E}+0 \text{ mbar/count}$
 $A_2 = 0.5611417 \text{ E}-4 \text{ mbar/count}^2$
 $B_1 = 0.0$

SN 89

$A_0 = 0.6909884 \text{ E}+3 \text{ mbar}$
 $A_1 = 0.3109044 \text{ E}+0 \text{ mbar/count}$
 $A_2 = 0.6125455 \text{ E}-4 \text{ mbar/count}^2$
 $B_1 = -0.3088854 \text{ E}-1 \text{ mbar}/^\circ\text{C}$

SN 76

$A_0 = 0.6853384 \text{ E}+3 \text{ mbar}$
 $A_1 = 0.3129995 \text{ E}+0 \text{ mbar/count}$
 $A_2 = 0.6215505 \text{ E}-4 \text{ mbar/count}^2$
 $B_1 = 0.0$

SN 95

$A_0 = 0.6918387 \text{ E}+3 \text{ mbar}$
 $A_1 = 0.2972820 \text{ E}+0 \text{ mbar/count}$
 $A_2 = 0.7420589 \text{ E}-4 \text{ mbar/count}^2$
 $B_1 = -0.3239156 \text{ E}-1 \text{ mbar}/^\circ\text{C}$

SN 79

$A_0 = 0.6931317 \text{ E}+3 \text{ mbar}$
 $A_1 = 0.3105221 \text{ E}+0 \text{ mbar/count}$
 $A_2 = 0.6411008 \text{ E}-4 \text{ mbar/count}^2$
 $B_1 = -0.1903891 \text{ E}-1 \text{ mbar}/^\circ\text{C}$

SN 96

$A_0 = 0.6908134 \text{ E}+3 \text{ mbar}$
 $A_1 = 0.3102033 \text{ E}+0 \text{ mbar/count}$
 $A_2 = 0.6171853 \text{ E}-4 \text{ mbar/count}^2$
 $B_1 = -0.3206228 \text{ E}-1 \text{ mbar}/^\circ\text{C}$

B.3. AANDERAA MODEL WLR-5 WATER LEVEL RECORDER

The Aanderaa Model WLR-5 water level recorder has a four-word output. The first 10-bit word represents the instrument reference number. The second word is a block counter that increments one count for every 30 samples taken. The remaining two output words represent the pressure reading and are converted to engineering units by use of the equations below:

$T(\text{period average}) = [3 * 1024^2 + 1024 * \text{word 3} + \text{word 4}] * 10^{-5} \mu\text{s}$
 and

$\text{Pressure} = A_1 X + A_2 X^2 + B_1 \theta + C_1 X \theta \text{ decibar,}$

where

$X = 1 - (T_0/T),$

A_1, A_2, B_1, C_1 are equation coefficients given below,

and

θ is the instrument temperature ($^\circ\text{C}$).

Calibration coefficients:

WLR-5-SN 360 containing

Paroscientific SN-2370

$$T_O = 34.88115 \mu s$$

$$A_1 = 0.3153064 \text{ E+3 dbar}$$

$$A_2 = -0.1845324 \text{ E+3 dbar}$$

$$B_1 = 0.0$$

$$C_1 = -0.462361 \text{ E-2 dbar/}^{\circ}\text{C}$$

WLR-5-SN 361 containing

Paroscientific SN-2367

$$T_O = 34.28643 \mu s$$

$$A_1 = 0.3250349 \text{ E+3 dbar}$$

$$A_2 = -0.1911564 \text{ E+3 dbar}$$

$$B_1 = 0.0$$

$$C_1 = -0.1211763 \text{ E-1 dbar/}^{\circ}\text{C}$$

WLR-5-SN 362 containing

Paroscientific SN-2371

$$T_O = 34.78814 \mu s$$

$$A_1 = 0.3148490 \text{ E+3 dbar}$$

$$A_2 = -0.1858360 \text{ E+3 dbar}$$

$$B_1 = 0.0$$

$$C_1 = 0.0$$

B.4. APPLIED MICROSYSTEMS MODEL 750A WAVE HEIGHT RECORDER

The Applied Microsystems Model 750A wave height recorder generates 970 words during each sample sequence. The first two words combine to form a 20-bit time reference that can be converted to total elapsed time by using the equation given below. The third and fourth words combine to form a 20-bit mean water level that represents a 112.5-s average water level. The remaining 966 words indicate the 10 least significant digits (LSD's) from water level measurements sampled every 0.439 s. (Refer to the equations below for conversion to engineering units.)

Time Code:

$$\text{Total elapsed time (s)} = [\text{MSD } 1024 + \text{LSD}] 0.878,$$

where MSD = most significant digit (word 1) and

LSD = least significant digit (word 2).

Mean Water Level:

The 20-bit output must first be converted to period (seconds) by $T = 14.0625/C$,
where $C = 1024 \text{ MSD} + \text{LSD}$,
MSD = most significant digit (word 3), and
LSD = least significant digit (word 4).

Frequency can then be converted to pressure (in decibars) by

$$\text{Pressure} = A_1 x + A_2 x^2 + B_1 \theta + C_1 x \theta,$$

where

$$x = 1 - (T_0/T),$$

T_0 = sensor output at zero pressure (listed below for each sensor),

A_1, A_2, B_1, C_1 are equation coefficients (listed below for each sensor),

and

$$\theta = \text{sensor temperature } (^{\circ}\text{C}).$$

Calibration Coefficients:

AMI-SN 132 containing Paroscientific SN 1689

$$T_0 = 26.00667 \text{ } \mu\text{s}$$

$$A_1 = 0.6475401 \text{ E+3 dbar}$$

$$A_2 = -0.3572296 \text{ E+3 dbar}$$

$$B_1 = 0.2649731 \text{ E-3 dbar}/^{\circ}\text{C}$$

$$C_1 = -0.1242487 \text{ E-1 dbar}/^{\circ}\text{C}$$

AMI-SN 131 containing Paroscientific SN-1693

$$T_0 = 26.05597 \text{ } \mu\text{s}$$

$$A_1 = 0.6540478 \text{ E+3 dbar}$$

$$A_2 = -0.3634638 \text{ E+3 dbar}$$

$$B_1 = -0.4688728 \text{ E-3 dbar}/^{\circ}\text{C}$$

$$C_1 = -0.1400033 \text{ E-1 dbar}/^{\circ}\text{C}$$

AMI-SN 133 containing Paroscientific SN-1694

$$T_0 = 26.15483 \text{ } \mu\text{s}$$

$$A_1 = 0.6340035 \text{ E+3 dbar}$$

$$A_2 = -0.3473867 \text{ E+3 dbar}$$

$$B_1 = 0.0$$

$$C_1 = -0.1245184 \text{ E-1 dbar}/^{\circ}\text{C}$$

Wave Height:

The same equations are used as for mean water level. Output consists of only LSD; the required MSD is from the mean water level measurement. Care must be taken to observe zero crossings (and overranges) occurring in the LSD. In these cases, the MSD must be compensated for by subtracting (or adding) 1, respectively.

B.5. GRUNDY MODEL 9400 CTD SYSTEM

The Grundy 9400 CTD system, used in conjunction with a Grundy Model 8428 digital data logger, provides two simultaneous output formats. The data logger accepts FM output from the 9400 system and then digitizes and records the signals on a 9-track digital tape. The equations needed to reconvert the digital output to frequency, where N = digital output from tape, are listed below:

$$\text{Frequency (depth)} = (9.6191406 \text{ E}^{-2} N + 9712) \text{ Hz} = f_d$$

$$\text{Frequency (temperature)} = (6.8161011 \text{ E}^{-2} N + 1956.5) \text{ Hz} = f_t$$

$$\text{Frequency (conductivity)} = (1.182454 \text{ E}^{-2} N + 4995) \text{ Hz} = f_c$$

The transfer functions used to convert the frequency outputs to engineering units, where t = temperature ($^{\circ}\text{C}$), are as follows:

$$\text{Pressure} = (6.3785 \text{ E-2 } f_d - 619.48) \text{ dbar}$$

$$\text{Temperature} = (1.79031 \text{ E-2 } f_t - 40.023) \text{ }^{\circ}\text{C}$$

$$\text{Conductivity} = (2.06558 \text{ E-2 } f_c - 103.335 + 6.8 \text{ E-3 } t) \text{ mS/cm}$$

B.6. PAROSCIENTIFIC MODEL 2100A PRESSURE SENSOR

The Paroscientific pressure sensor was utilized as the shipboard pressure standard for the checkout and verification tests. The sensor output was obtained by engaging the button marked "T" on the Paroscientific pressure computer and displaying the sensor period in μs . This output can be converted to pressure via the equation below:

$$P \text{ (dbar)} = A_1 X + A_2 X^2 + A_3 X^3 + B_1 \theta + C_1 X \theta,$$

where

$$X = 1 - (T_O/T),$$

T_O = sensor output at 0 pressure,

A_1, A_2, A_3, B_1, C_1 are the equation coefficients given below,

and

θ = instrument temperature ($^{\circ}\text{C}$).

Calibration coefficients for SN 1698:

$$T_O = 26.11502 \text{ } \mu\text{s}$$

$$A_1 = 0.6566993 \text{ E+3 dbar}$$

$$A_2 = -0.3785600 \text{ E+3 dbar}$$

$$A_3 = 0.9011372 \text{ E+2 dbar}$$

$$B_1 = -0.3668448 \text{ E-3 dbar}/^{\circ}\text{C}$$

$$C_1 = -0.2773063 \text{ E-1 dbar}/^{\circ}\text{C}$$

APPENDIX C. A MODEL OF GRUNDY 9021 SPEED AND DIRECTION ERRORS FOR HORIZONTAL DYNAMICS

We want to determine the mean values and variances in speed and direction, as measured by the Grundy 9021, in the presence of dynamic wave particle currents. The differences in the mean measured values of the magnitude and direction from the true vector averages represent the bias errors introduced by the dynamic effects, while the variances are a measure of the sampling errors. The following assumptions are made:

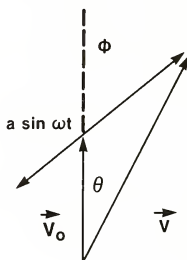
- Because the 9021 averages speed over an instrument sampling interval (and the 10-min sampling interval used in the survey contains a large number of current oscillations with periods ≈ 5 s), sampling errors in speed are neglected.
- The rotor performs a perfect speed average for speed variations faster than the rotor can respond.
- Length-scale effects are neglected; i.e., the current speed and direction are assumed to be the same at the rotor as at the vane. While length-scale effects can be accounted for, the small magnitude of the speed errors under the survey conditions did not justify its inclusion.

The approach taken consists of two parts. First, expressions for the mean speed and direction errors and the variance in direction will be calculated in terms of the signal-to-noise ratio, the angle between the mean and oscillating current components, the amplitude attenuation and phase lag of the current meter angular motion relative to that of the actual current vector, and the directivity response of the rotor (section 9.1.1). Second, the

amplitude attenuation and phase lag of the angular motion will be calculated using the angular differential equations of motion in the small-angle approximation.

C.1. ERROR EXPRESSIONS

Assume, for the moment, that the current meter vane follows the instantaneous current direction exactly. For a sinusoidally varying current component ($a \sin \omega t$) and a mean current of magnitude V_0 , we have the geometry shown below:



The instantaneous speed V and direction θ are given by

$$V = [(V_0 + a \cos \phi \sin \omega t)^2 + (a \sin \phi \sin \omega t)^2]^{1/2} \quad (C-1)$$

$$\text{and} \quad \tan \theta = (a \sin \phi \sin \omega t) / (V_0 + a \cos \phi \sin \omega t). \quad (C-2)$$

Using $\tan \theta \approx \theta$, expanding to second order in a/V_0 , and taking mean values, we get

$$\bar{V} = V_0 \{1 + [(a^2/V_0^2) \sin^2 \phi]/4\}$$

$$\text{and} \quad \bar{\theta} = - [(a^2/V_0^2) \sin 2\phi]/4.$$

Similarly, the variance in direction, $\sigma_\theta^2 = \overline{(\theta - \bar{\theta})^2}$, is found to be

$$\sigma_\theta^2 = (a^2/2V_0^2) \sin^2 \phi.$$

If we define the signal-to-noise ratio R as the ratio of V_o to the RMS value of the oscillating component, then

$$R = (\sqrt{2} V_o) / a, \quad (C-3)$$

$$\bar{V} = V_o (1 + \sin^2 \phi / 2R^2), \quad (C-4)$$

$$\bar{\theta} = - \sin 2\phi / 2R^2, \quad (C-5)$$

and $\sigma_{\theta} = \sin \phi / R. \quad (C-6)$

The speed and direction bias errors are seen to be of second order in the signal-to-noise ratio R , while the standard deviation in direction σ_{θ} is of first order.

While equation (C-4) predicts a positive speed bias, the lagging vane response of an actual current meter results in the meter not being aligned with the instantaneous current direction. This tends to produce a reading on the low side because of the lower off-axis response of most current meters. If we assume a linear response function for the motion of the current meter vane (amplitude attenuation and phase lag, but no distortion), we can calculate this effect. Taking the instantaneous time-varying current component to be $(a \sin \omega t)$ as above and the response of the vane to be $\{\alpha a \sin (\omega t - \beta)\}$, where α is the angular amplitude attenuation and β is the phase lag, we can calculate the mean-square value of the angle between the current meter and the instantaneous current vector from equation (C-2) just as in the calculation of σ^2_{θ} . We find

$$\sigma^2_{\theta'} - \theta = \sigma^2_{\theta} (1 + \alpha^2 - 2\alpha \cos \beta), \quad (C-7)$$

where θ' is the instantaneous direction of the current meter and θ is that of the actual current vector.

Let the off-axis response of the rotor be given by $f(\theta' - \theta)$. Because f is an even function of $\theta' - \theta$, for small off-axis angles then

$$f(\theta' - \theta) = 1 - \gamma[(\theta' - \theta)^2 / 2], \quad (C-8)$$

where $\gamma = 1$ for a perfect cosine response. The mean value of the measured speed, $V' = V f(\theta' - \theta)$, is thus given by

$$\bar{V}' = \bar{V} \{1 - \gamma [(\overline{(\theta' - \theta)^2})/2]\}. \quad (C-9)$$

Using \bar{V} from (C-4) and $\overline{(\theta' - \theta)^2} = \sigma_{\theta'}^2 - \theta^2$ from (C-7) and (C-6), we get

$$\bar{V}' = V_0 [(1 + \sin^2 \phi)/2R^2] [1 - (\gamma \sin^2 \phi/2R^2)(1 + \alpha^2 - 2\alpha \cos \beta)]$$

or

$$\Delta \bar{V}'/V_0 = (\bar{V}' - V_0)/V_0 \approx \sin^2 \phi/2R^2 [1 - \gamma(1 + \alpha^2 - 2\alpha \cos \beta)]. \quad (C-10)$$

For $\alpha = 0$, i.e., a stationary vane, we get the well known result that a meter with a perfect cosine response of $\gamma = 1$ gives the correct speed average. From the results of section 9.3.1, $\gamma \approx 1.29$ for the Grundy 9021.

From the derivations of $\bar{\theta}$ and σ_{θ} , it is seen that by replacing α with αa , the mean and standard deviation of θ' are given by

$$\bar{\theta}' = -\alpha^2 (\sin 2\phi/2R^2) \quad (C-11)$$

and

$$\sigma_{\theta'} = \alpha (\sin \phi/R). \quad (C-12)$$

C.2. ANGULAR AMPLITUDE ATTENUATION AND PHASE LAG CALCULATION

The amplitude attenuation α and phase lag β can be calculated from the differential equations for the angular motion of the current meter. For angles θ' which are not too large, this is a linear second-order equation (Kenny 1977) given by

$$J\ddot{\theta}' + P(L/V_0)\dot{\theta}' + P\theta' = P(a/V_0) \sin \omega t, \quad (C-13)$$

where J is the moment of inertia, L is the moment arm of the vane, V_0 and a are as defined above, and P is given by

$$P = \rho V_0^2 C_L^1 AL/2, \quad (C-14)$$

where ρ is the density of water, C'_ℓ the angular derivative of the vane's lift coefficient, and A the vane area. The solution to (C-13) is well known in terms of an amplitude attenuation α and phase lag β given by

$$\alpha = 1/[(1 - (f/f_0)^2)^2 + (2\zeta f/f_0)^2]^{1/2} \quad (C-15)$$

$$\text{and} \quad \beta = \tan^{-1} [2\zeta (f/f_0)] / [1 - (f/f_0)^2], \quad (C-16)$$

$$\text{where} \quad \zeta = [L/2V_0] [P/J]^{1/2} \quad \text{and} \quad f_0 = [1/2\pi] [P/J]^{1/2}$$

are the damping factor and natural frequency, respectively. For the values of the parameters for the Grundy 9021, we find

$$\zeta = 4.9, \quad (C-17a)$$

$$f_0 = 0.62 \text{ Hz}, \quad (C-17b)$$

$$\alpha \approx 1/[1 + (2\pi Lf/V_0)^2]^{1/2}, \quad (C-17c)$$

$$\text{and} \quad \beta \approx \tan^{-1} (2\pi Lf/V_0). \quad (C-17d)$$

The approximate expressions for α and β result from the fact that $\zeta^2 \gg 1$ and $(f/f_0)^2 \ll 1$ for typical values of $f \approx 0.2$ Hz. Because of this, α and β depend on only one current meter parameter, the vane moment arm L of about 64 cm for the 9021. From equations (C-15) and (C-16), one can show that, if any of the other current meter parameters were in error by even 100 percent, it would make a difference in α and β of only about 2 percent. Consequently, we needn't worry about the exact values of the current meter parameters other than L . Values of α and β also depend on only one environmental parameter, the quantity V_0/f , which is a length scale equal to the distance a water particle travels during one oscillation period. This is just what one would expect when hydrodynamic forces dominate inertial forces.

PENN STATE UNIVERSITY LIBRARIES



A000070941562

NOAA--S/T 80-39